Pre-processing of a CO_2 feedstream in a CCUS methanol microplant

Samir den Haan

Technische Universiteit Delft

TU Delft

Pre-processing of a CO_2 feedstream in a CCUS methanol microplant

by

Samir den Haan

to obtain the degree of Master of Science
at the Delft University of Technology,
to be defended publicly on Wednesday May 19, 2021 at 11:00 AM.

Student number:	4153936	
Project duration:	February 17, 2020 – May 19, 2021	
Thesis committee:	Prof. dr. ir. W. De Jong,	TU Delft, supervisor
	Prof. Dr. ir. E.L.V. Goetheer,	TU Delft
	Dr. R. Delfos,	TU Delft
	Ir. J. Van Kranendonk,	Zero Emission Fuels, daily supervisor

This thesis is confidential and cannot be made public until May 19, 2023.

TU Delft

Summary

When experimenting with the compression of a gas similar to the output of a CO2 Direct Air Capture unit using an off-the-shelf lubricated compressor, Zero Emission Fuels B.V.(ZEF) encountered severe condensation, damaging the compressor. This explorative study aims to identify the cause of this problem, create a concept solution, and test this concept based on model-supported experimentation.

Based on a literature study all theoretical concepts are divided into three solution classes. Two concepts are then created and theoretically compared. A concept is selected that is based on the adsorption of water into a solid desiccant.

As the concept solution is to operate in a closed system, regeneration of the desiccant needs to be faster than its utilization. For this, an experiment is made where a controlled quantity of inert gas is moisturized, dried, and used to regenerate a second column. From this it can be concluded that the gas can be dried adequately, and that regeneration can be done thoroughly.

A model is made to verify the experiment's workings, based on models from literature. This model is then validated using literature, and then fitted to experimental data. Combining experiment and literature data, three key performance indicators are calculated: Cyclic capacity, energy usage, and desorption rate. The design tools and models developed throughout this thesis are used to size the next iteration of the concept according to the needs of ZEF.

From this, it is concluded that the presented concept is indeed viable to prevent, rather than solve, the problem stated at the start of this thesis. Recommendations are done concerning further development of the prototype, experiments, model, and overall system.

Samir den Haan
Delft, May 2021

Acknowledgements

As this chapter of my life reaches its conclusion with the pages you are looking at, which I hope comprise the centerpiece to my work thus far, I would like to thank the people that made it all possible.

First, I'd like to thank you, the reader, for taking an interest in my work. We may be well acquainted or complete strangers, but I hope this thesis will enable you to contribute to something that is useful to the planet and its inhabitants, as I have sought to do.

I'd like to thank Wiebren de Jong and Jan van Kranendonk for taking on the role of supervisor and daily supervisor respectively. Wiebren's vast experience and view from the perspective of both scientist and educator, combined with Jan's incredible engineering skills across a huge number of topics and disciplines provided an excellent basis of support from which I was able to develop my own skills as an engineer. I always get the sense that you really value my work and ideas, and both of your thoughts and advice really allow me to make them even better.

A big thanks to my mother, sister, and grandmother, all of whom I did not visit enough during this project. Your love and support throughout the years are instrumental to keep me motivated to continue and you really enable me to reach my goals. I'm always excited to tell you about my newest feats and I hope this work makes you proud.

A huge and heartfelt thanks to all my friends: those based in Dordrecht, Delft and elsewhere, for tolerating my endless blabbering about this project and all other things that are on my mind. Being able to share my enthusiasm about science and technology is what allows it to continuously grow. I'd like to particularly show my appreciation to my fellow Daltons: Willem, Sam and Youri for each supporting me in your own way. I hope we'll continue our adventures and good times in years (decades!) to come. And of course I'd like to thank the lovely Suzanne who may be my greatest supporter of all during this project.

Thanks to the ZEF team which consists of Jan, Ulrich, Hessel and Mrigank. I admire the method with which you run your company, since your success almost fully depends on the success of the students you so skilfully coach. With just the four of you, you manage to realise iterations at the very cutting edge of technology faster than any other company could imagine, and we all look good and have fun doing so. The word "impossible" is simply unknown to you and I wish ZEF all the best.

Thanks to Michel, Jaap and all the other (lab) staff behind the scenes at TU Delft that make it possible to do any of this.

A word of appreciation for the D:DREAM community and Project MARCH. While not directly involved in this thesis, in retrospect they were the things to seriously trigger my interest in engineering as a boy visiting the TU Delft and as a bachelor student respectively. The experience has shaped how I perceive what it means to be an engineer and has shown me how to actually use my own potential. Without either of those, I would not have even started a project like this.

Finally, I'd like to express my thanks to my colleagues at ZEF considering the coronavirus pandemic including, but certainly not limited to Shawn, Tom, the Mulder brothers, Pieter, Bart, Jim, Thorsten, Mika, Kamal, Rahul, Andrea, Nelson and the ZEF team. Even when not physically around, you manage to create a positive and supportive working environment. I'm absolutely sure that if I had to face the writing of a thesis during a pandemic without your support, both this work and my own state of mind wouldn't even be able to hold a candle up to what it is now, and I thank you all for that.

List of Figures

List of Tables

Nomenclature

(A)DR	(Average) Desorption Rate
AEC	Alkaline Electrolysis Cell
CAPE	Computer-Aided Process Engineering
CCUS	Carbon Capture, Utilisation and Storage
CFD	Computational Fluid Dynamics
DAC	Direct Air Capture
DC (concept)	Delayed Condensation
DD (concept)	Desiccant Dehumidifier
DG-type	Degassing-type
DO-type	Deoiling-type
DW-type	Dewatering-type
FM	Fluid Machinery
GHG	Greenhouse Gases
GUI	Graphical User Interface
KPI	Key Performance Indicator
LDF	Linear Driving Force
MCS	Moisture Control System
MS	Methanol Synthesis
NTC	Negative Temperature Coefficient (resistor)
ODE	Ordinary Differential Equation
PCB	Printed Circuit Board
PFD	Process Flow Diagram
PSA	Pressure Swing Adsorption
PV	Photovoltaics
RH&T	Relative humidity and temperature
TSA	Temperature Swing Adsorption
ZEF	Zero Emission Fuels B.V.

Contents

1

Introduction

”Can’t you just make a machine that takes the CO_2 back out of the atmosphere?” is a question that might seem too straightforward to be relevant. Almost naive in a sense, as if asked by child. However, it is a more realistic question than one might expect. The answer can be found in Carbon Capture, Utilisation and Storage(CCUS) technology, and the answer increasingly appears to be ”Yes”.

The aim of this thesis is to create a part of just such a machine. Specifically, this thesis presents the process of creating a device that pre-processes the CO_2 that is captured from the air to ensure the captured gas is suitable for use in the required subsequent steps. These steps are the compression of the CO_2 to the conditions required for it to react with hydrogen to produce methanol, a valuable fuel and chemical commodity. The project is done within a company named Zero Emission Fuels(ZEF), a Delft-based startup company that attempts to create miniaturised, mass producible chemical plants that produces methanol from CO_2 and water vapour from that air at the scale of just a few solar panels.

The rest of this chapter will introduce the reader to the context of this thesis. Section 1.1 will quickly recap the global problem of global warming and greenhouse gases. Section 1.2 will then introduce the carbon cycle, and the concept of Carbon Capture, Utilisation and Storage. The company ZEF will be introduced in section 1.3. Sections 1.4 and 1.5 will then convey why this research is conducted and what this research will include respectively. The chapter will be concluded with section 1.6 where the rest of the report structure will be introduced.

1.1. The urgency of climate action

The problem involving greenhouse gas(GHG) emissions and global warming appears to have grown over the course of the 20th century, in relative silence, to enormous proportions and is likely one of the largest problems humanity is facing in the 21st century[1]. Over the past few decades, the problem was increasingly recognised by mass media and lawmakers across the globe. Several international agreements and goals were made in the past two decades. 2020, 2030 and 2050 are common milestone years mentioned in these goals. [21, 30]

This makes the timing of this thesis rather interesting as 2020, already a turbulent year at the time of writing, is a year in which many of these 2020 milestones need to be altered or forfeited. At the same time, the year 2030 seems tangible and feels like it approaches fast. This means that it is likely that the new decade will be one in which governments and other institutions will feel pressure to act rather than plan. This in turn, will likely lead to an unprecedented appreciation of projects and technologies that can (almost) be applied to make large scale contributions to these climate goals.

Time appears to be running out. The ”carbon budget”, the total amount of carbon that can still be emitted before severely damaging the planet, is running out fast [33]. Something must be done, that much can be agreed upon.

[1] It is assumed that the reader is familiar with the core concepts of the global warming problem due to its ubiquity in the past years

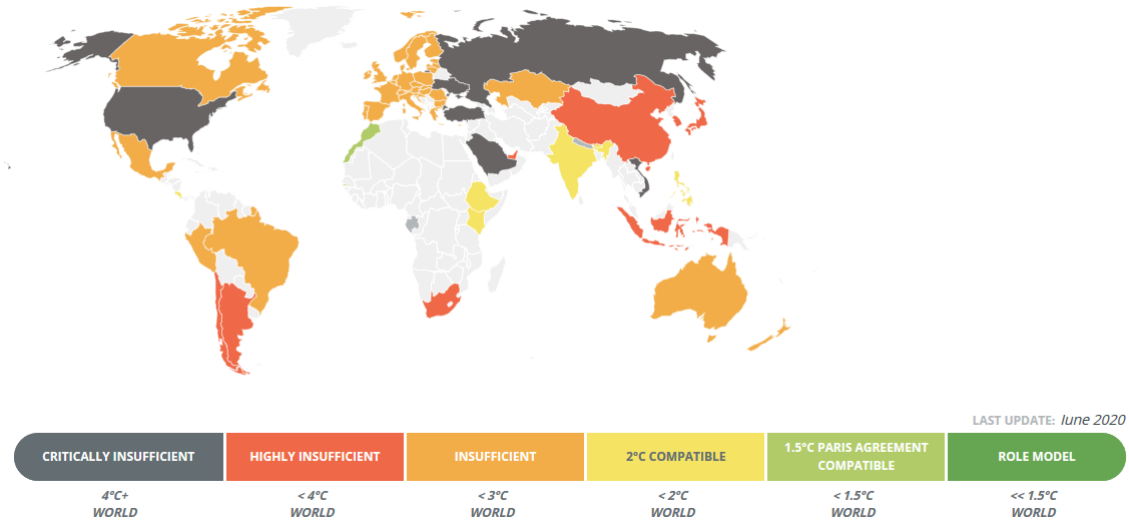

Figure 1.1: ”The Climate Action Tracker rates NDCs, 2020 pledges, and long-term targets against whether they are consistent with a country’s “fair share” effort to the Paris Agreement 1.5°C temperature goal.” Image adapted from [21]

1.2. The carbon cycle and CCUS

The earth can be considered a closed system. A wet rock floating in outer space. The only thing to enter and leave in significant quantities are energy via sunlight, and energy via radiative heat respectively. This also means that all carbon atoms, a moderately abundant element in this system, must remain in this system and can only change the form in which it does so. This results in a cyclical system, much like the better known water cycle, with many different loops and interactions. The traditional example is the one in which plants use CO_2 for photosynthesis, storing the carbon atom as hydrocarbon compounds such as glucose ($C_6H_{12}O_6$), which in turn are consumed by animals, burned inside their cells and exhaled in the form of CO_2, which can then be re-used by the plants. When all major connections in the network of carbon usage are drawn, it can be seen that this turns into a rather large and complex system as can be seen in figure 1.2.

While human action seen in 1.2 may appear small at first, the fact that our actions are depicted on the same scale as forces of nature is alarming. Human actions are also decisively one-sided, with a net accumulation of 4 gigatons of CO_2 per year in the atmosphere. This is caused by human behaviour exhibited throughout history, acting as if this cycle were nonexistent and a merely linear progression from biomass, soil and fossil carbon to the atmosphere via human consumption. Humanity was unaware of or unwilling to act upon the finite size of the planet and its nature as a closed system.

This becomes more clear when just the human related carbon-flows are observed, as was done in the Drawdown Reports for instance [71]. Here, a distinction is made between carbon sources and sinks, with sources being human actions that emit GHGs to the atmosphere, as well as carbon sinks, which are the mechanisms by which the carbon is sequestered (stored for long-term, often in other compounds or solutions). It is also readily observed from figure 1.3 that the majority of emissions are retained in the atmosphere. In order to reduce the effects humans have on the planet, there are effectively two options available: either reduce emissions to the atmosphere or increase carbon sinks. The latter can be done by either reinforcing natural carbon sinks, or by engineering new carbon sinks.

A technique to realise such carbon sinks is called ”Carbon Capture, Utilisation and Storage” (CCUS), which is a combination of ”Carbon Capture and Utilisation” (CCU) and ”Carbon Capture and Storage(CCS)”. The name of this family of techniques can be considered fairly descriptive of what they entail. It is the overarching term for the capture of carbon dioxide from a source(atmosphere, flue gases etc.), methods of storing it (i.e. empty natural gas fields), or utilisation as material for another molecule. An overview of these techniques can be seen in figure 1.4 and include, among others, formic acid, synthesis gas (a precursor to *many* products, including kerosene and diesel), or methanol, which is the application covered by this thesis.

The concept of drawing carbon dioxide from the atmosphere to turn into hydrocarbon fuel sources

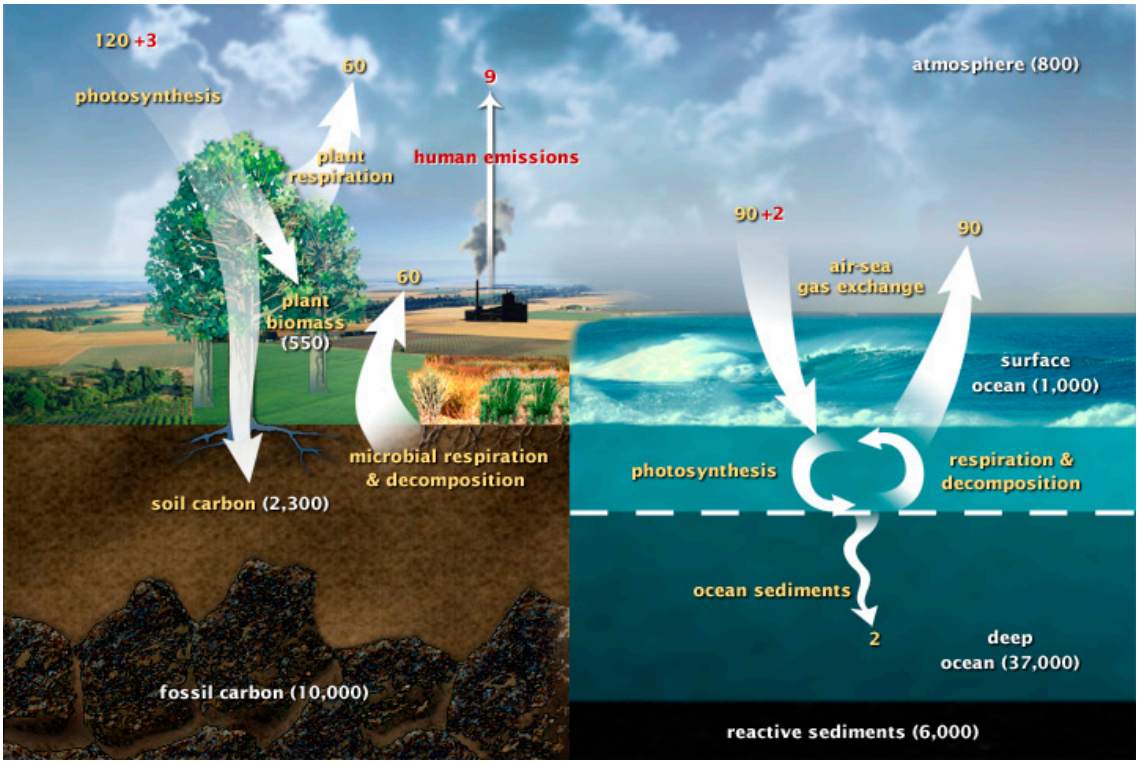

Figure 1.2: An overview of the carbon cycle. White numbers indicate stored carbon in gigatons, yellow and red numbers indicate the natural and man made flows respectively in gigatons/year. Adapted from [56]

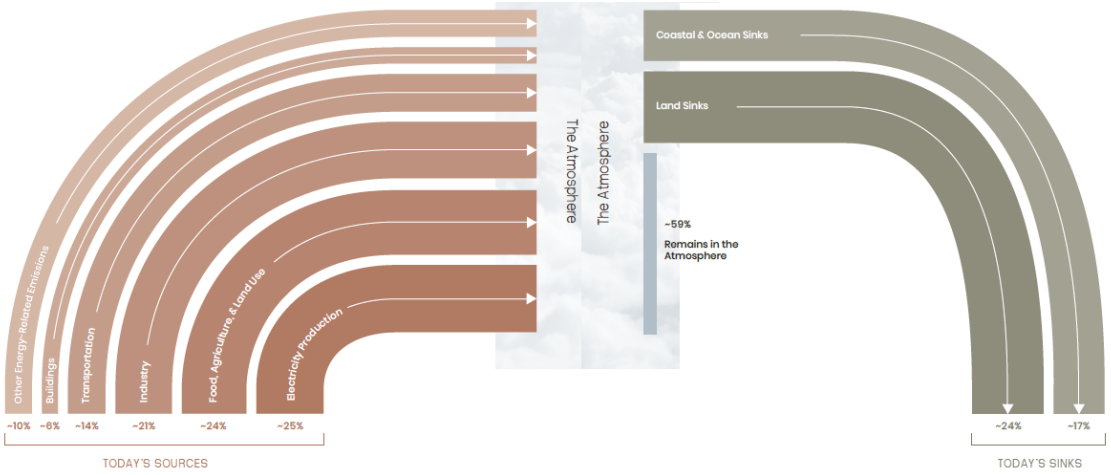

Figure 1.3: Carbon sources and sinks, broken down in categories. Adapted from [71]

is not new. In fact, it is a concept that predated human history. It is the same process that naturally occurs as photosynthesis! Thus, a CCUS system can be considered to take place in the carbon cycle right alongside natural plants. Artificial plants doing artificial ”photosynthesis”: truly a chemical ”plant” in multiple senses of the word.

> "Trees are like all of us, they need friends." - Bob Ross [1]

1.3. What is ZEF?

Zero Emission Fuels (ZEF) is a start-up company that operates from Delft, the Netherlands that focuses on the development of a CCUS technique. Their company structure is fairly unique, in the sense that the four employees' main task is to coach the 20 to 30 students that work on the project. The team

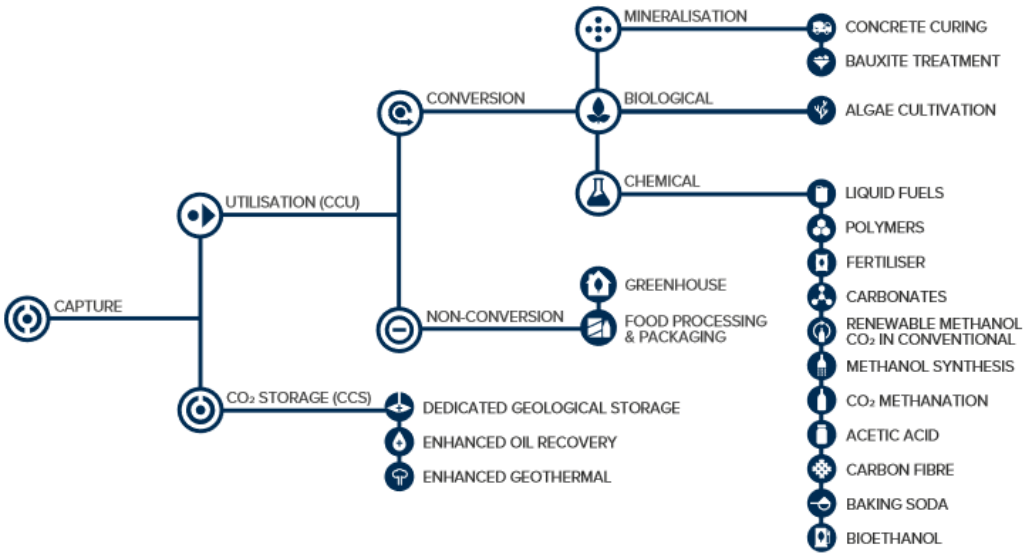

Figure 1.4: Overview of Carbon Capture, Utilization and Storage (CCUS) techniques. Reprinted from [34]

consists of students of various educational backgrounds and levels. Process engineers, industrial designers and instrument makers are but 3 of the many educational backgrounds that together form the balanced team of ZEF.

The technique ZEF uses is unique in two ways. First, it combines a Direct Air Capture (DAC) technique with the actual conversion of the CO_2 in one integrated process, whereas usually the capture and conversion of CO_2 are considered separately in order to take advantage of the higher CO_2 concentrations found in flue gases. However, the DAC technique can be applied anywhere on the globe, which is where the second unique aspect comes in.

The second unique aspect concerns the small-scale of the plants. Key to the ZEF concept is the miniaturisation of a methanol plant, enabling it to operate with the energy provided by just a few solar panels. The small scale enables the plant to heat up quickly, and operate dynamically to follow the varying supply of electricity provided by the solar panels. Whereas methanol plants are often very large complexes that take days or weeks to start, the ZEF system can start, operate and shut down, all within a day. The plant then awaits sunrise to continue operation.

1.3.1. The ZEF business model

This non-traditional method of operating requires a non-traditional business model in order to make it commercially viable. ZEF achieves their viability in multiple ways: first and foremost, the company believes in cost reduction via mass-production. Traditional chemical plants are almost fully custom-designed and custom-built. This is opposed to the ZEF system that features a modular design based upon the microplants. These microplants can easily be deployed virtually anywhere and in almost any number. This enables users to create a methanol plant of any size according to their needs and allows ZEF to produce many microplants. The quantity of identical microplants in turn, enable mass-production techniques to be used to unlock the benefits from economies of scale that are inherently absent in traditional chemical plant design, but are rather prevalent in the automotive industry for instance.

Secondly, methanol can be considered a highly versatile product in a market that has grown steadily in the past 20 years[4]. Its uses include production of other chemical intermediates such as formaldehyde and dimethyl ether, as well as fuel usage in biodiesel and blended gasoline[4] . More uses for methanol are conceived regularly. One local example is recent interest in the usage of methanol as maritime fuel by a consortium of major Dutch shipyards, research institutions, ports and other companies[52]. This very high diversity in methanol demand makes it relatively easy to connect with industry partners and consistently find the early buyers that are crucial for the development of a start-up company.

Thirdly, while methanol demand is highly diverse, methanol supply is not. With almost all methanol production based on natural gas and coal, it is important to consider the required feedstock and their

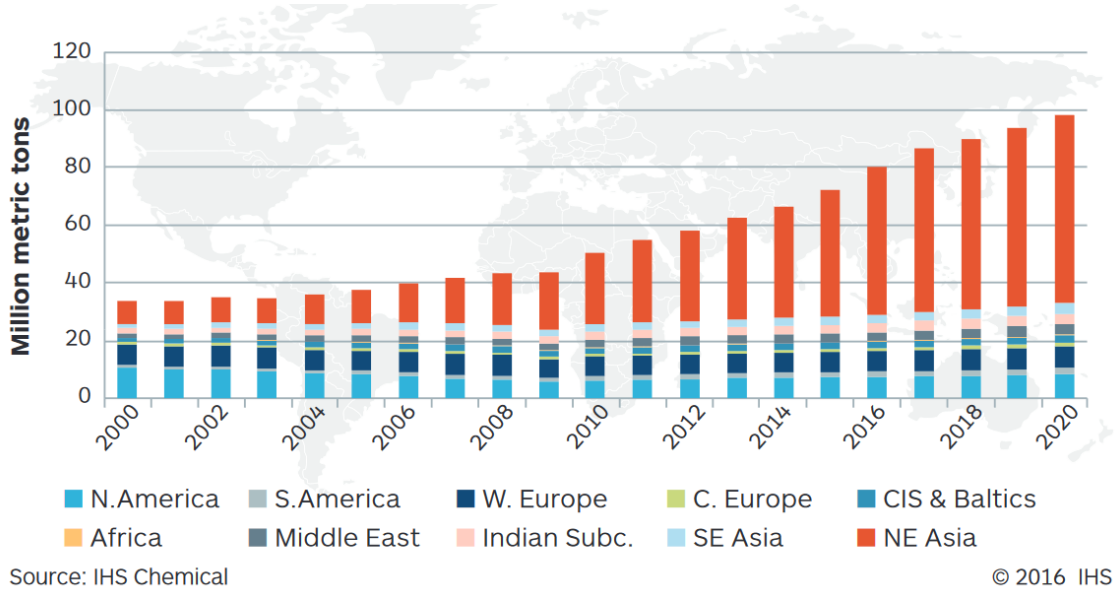

Figure 1.5: Global methanol demand per region, adapted from [4]

associated cost. This cost is stated to contribute as much as 90% of the operational costs by IHS Markit, who call it "The key to overall methanol economics" [4]. This enables regions with considerable coal and natural gas resources such as China and the Middle East respectively to be influential on the global methanol price.

An alternative to natural gas and coal is the process of catalytic hydrogenation of CO_2, in which carbon dioxide is combined with hydrogen to create methanol (this process is discussed in more detail in section 2.1.3) which has been received an increasing amount of interest since the turn of the century [24, 48]. As carbon capture techniques are being developed, their have dropped significantly and are expected to continue doing so throughout the decade at a faster rate than the 2010's[34]. Among these techniques is the Direct Air Capture technology, which is the technique used by ZEF due to its compatibility with the modular, scaling approach the company wants to take[34], and its synergy with the ever-falling price of solar photovoltaics (PV). [42]. When combined, methanol production based on CO_2, captured using solar energy, might provide incentive to other regions to explore alternatives for (geo)political and economic reasons next to the already established environmental reasons. This provides the basis for ZEF to present an alternative, fossil-free feedstock based on solar photovoltaics and Direct Air Capture.

1.4. Relevance of this research

While CO_2 might provide an attractive option as feedstock for methanol production, Direct Air Capture is still a fledgling technology [34]. In order to understand the need of this research, it is important to look at the scale at which ZEF intends to operate this technology, relative to other parties.

Companies that are currently involved in Direct Air Capture such as Climeworks or Carbon Engineering operate at the scale of a pilot-size traditional scale chemical plant [19, 22], which does not correspond with the vision of ZEF to operate at the scale of just a few solar panels. Companies that utilize solar electricity for their chemical plants operate at a much larger scale as well, harnessing the power of large solar arrays or concentrated solar energy as auxiliary power source in traditional plants [76, 81]. Even newly planned methanol plants that are considered to be "Small scale" operate at the megawatt level [17], while ZEF proposes to operate in the 1-10 kilowatt range, which better corresponds with lab-scale testing. However, this lab testing is often done in a non-continuous fashion, aimed to support research projects rather than as continuously as possible to optimise production for commercial purposes. While initiatives for lab research on a similar scale to ZEF are underway, their long development timeline only allows ZEF to take limited advantage from their results at best. [87]

This discrepancy in scale presents several barriers to the development of the ZEF system that are

technical in nature (in addition to economic barriers described in section 1.3.1). These barriers can be placed into three categories: first there is the scaling problem of the physical processes that scale differently. For instance, energy released in endo/exothermic processes may scale with volume, but heat exchange scales with area. Second, there is the discontinuous nature of solar energy availability. The plant must be dynamically operated in a way that is compatible with both the day/night cycle as well as cloudy days. Finally, there is the availability of equipment. While the ZEF system may be suited for mass-production, most parts that are available off-the-shelf are designed for much larger systems, introducing the requirement to custom engineer many parts in-house. This thesis will be concerned with tackling the last barrier mentioned: designing equipment of a suitable scale.

An overview of the ZEF process that is currently under development can be seen in figure 1.6, the process will be discussed in more detail in section 2.1 by the four core systems shown, as well as three auxiliary systems. First, the Direct Air Capture unit retrieves the feedstock from the ambient air, comprising of CO_2 and H_2O. A vapor-liquid equilibrium flash tank is used to separate the species into a gaseous CO_2-rich phase and a liquid water-rich phase. The water is then split in the Alkaline Electrolysis Cell (AEC), with high-pressure hydrogen (H_2) as product. Meanwhile, the carbon dioxide is compressed in multiple stages in the Fluid Machinery (FM) system to match the hydrogen pressure, which is required for the reaction in the Methanol Synthesis (MS) reactor, where the carbon dioxide reacts with the hydrogen in the catalytic hydrogenation reaction as shown in equation 1.1. [24]

$$CO_2 + 3\,H_2 \rightleftharpoons CH_3OH + H_2O \tag{1.1}$$

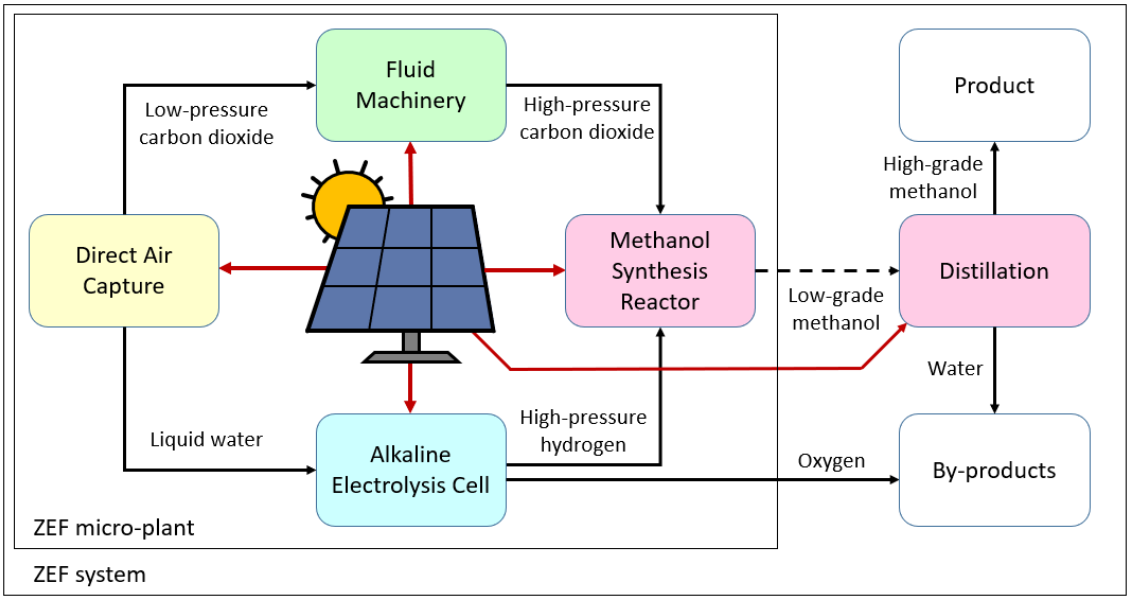

Figure 1.6: Simplified overview of the ZEF concept, powered by solar PV.

The assignment upon which the thesis is based originated from a problem the ZEF development team encountered in late 2019 while iterating upon the design of the FM subsystem. A custom-made dry reciprocating compressor was replaced with an off-the-shelf lubricated compressor. When running the first tests with this compressor, it was observed that the lubricant oil of the compressor formed an emulsion with the water in the compressor feed. A thesis assignment was drafted in which the problem was described as a problem in which the oil-water emulsion was to be separated. (The original assignment can be found in appendix F.1). The author was then asked to solve this problem.

1.5. Research scope

The goal of this research is to conceive and design a solution to the problem posed by liquid water in the FM system. This should include a model and prototype of the working principle of the system, and the solution should be developed to a state in which it can reasonably be implemented in integration tests in early 2021.

Research questions The main research question of this thesis can be stated as follows: How can the CO_2 & H_2O vapour output of a Direct Air Capture system be processed to prevent excessive water damage to a compression system and other downstream operations?

This main research question was broken down into the following sub-questions:

1. How does the interaction between the DAC and compression systems result in conditions that cause damage to downstream operations?
2. What techniques are available to process the DAC vapour, before or after compression, to prevent damaging conditions from occurring?
3. What is the most promising concept that be created which implements one or several of those techniques in the context of the ZEF micro-plant?
4. How can the characteristics and key performance indicators of a prototype of this concept be described and used, based on a model verified experiment?

1.6. Methodology & thesis outline

This thesis follows a system that is loosely based on the ”Double Diamond Design Process”, and is structured as such [26]. This structure is presented in figure 1.7. Research questions 1 and 2 are answered in chapters 2 through 4 by means of theoretical analysis of the ZEF system and relevant literature. Chapters 2 and 3 will focus on getting a broad understanding of the problem, and chapter 4 consolidates that understanding into a concept.

Research questions 3 and 4 are answered in chapters 5 through 8, with research question 3 being slightly emphasised in chapters 5 and 6 to investigate a broad range of modelling and experimental opportunities, and to gather the required data. Research question 4 is then slightly emphasised in chapters 7 and 8, where the the data is utilised to answer the main research question and to pinpoint the knowledge that will accelerate the development of the ZEF system and CCUS technology in general.

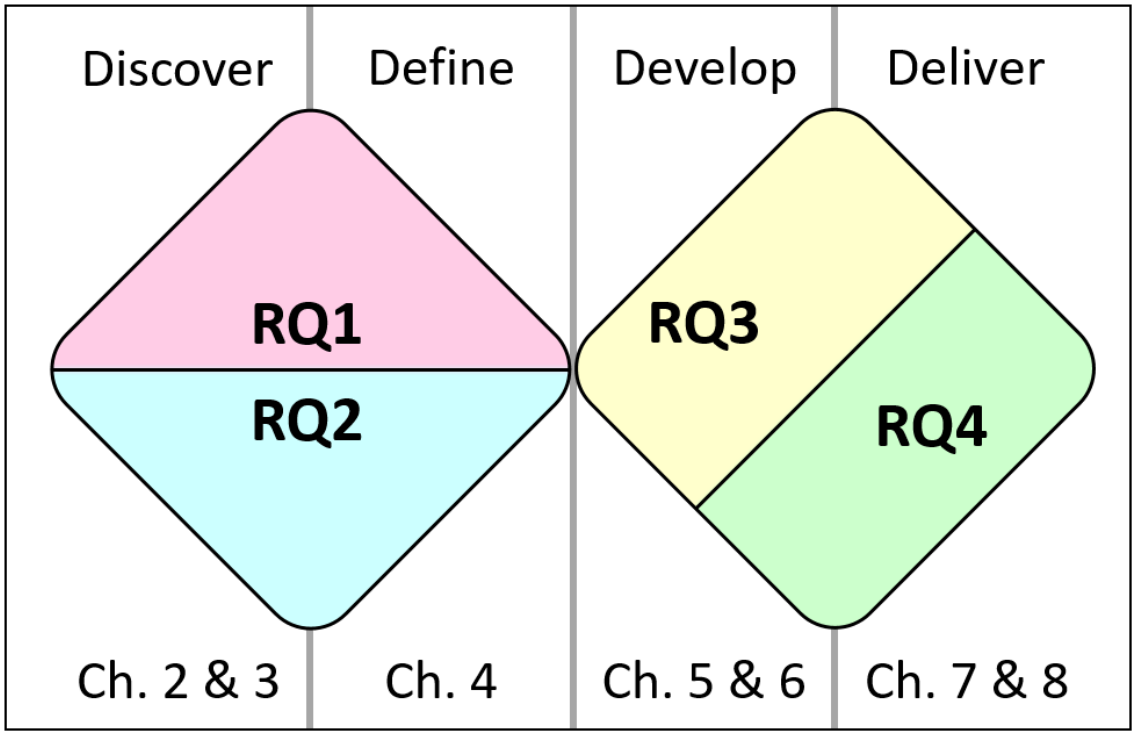

Figure 1.7: This report’s structure, based on the ”Double Diamond Design Process” [26]

2

Background

In this chapter, the ZEF system and some aspects of its development are described to present the reader with an image of a starting perspective from which this problem is approached. As this thesis is involved with the integration of two subsections, it is considered important to have a general understanding of all processes in the plant. Section 2.1 will briefly present all sections, their workings and interactions, with sections 2.1.2 and 2.1.1 providing a more in-depth description of the FM and DAC subsystems respectively. Section 2.1 will also provide an overview of the relevant work that has previously been done. Then, section 2.2 presents some basic parameters of the micro-plant that provide the context required to start the design process, with section 2.3 outlining the design process that will be used in this thesis.

2.1. Micro-plant overview

The ZEF micro-plant consists of four subsections that have already been presented in figure 2.1. Within the team, work is divided along these subsections, resulting in groups of students working on one of the following:

- The Direct Air Capture (DAC) subsystem that harvests CO_2 and H_2O from the atmosphere
- The Fluid Machinery (FM) subsystem that compresses the CO_2 to reaction pressure
- The Alkaline Electrolysis Cell (AEC) subsystem that splits liquid H_2O in order to create H_2 at reaction pressure
- The Methanol Synthesis (MS) where the reaction takes place to form methanol, with water as a byproduct as shown in equation 1.1

Additionally, several more peripheral groups can be identified, which will not be separately presented in section 2.1.3:

- The Distillation System (DS) team, that works on an optimal method to refine the product of the MS reactor to a high-grade product
- The Integration (INT) team, that works on the mechatronics aspect of the plant, creating an infrastructure for electronics and software that students from other groups can use to read sensors and actuate valves, heaters a.o.
- The Plant design (PLANT) team, that works on the layout of the various subsections into a single package

The rest of this section will cover the aspects of the microplant along the lines of these groups. First, extra background will be given on the FM and DAC systems, as they are most relevant to this thesis. Then, the work of the other groups and their role in the micro-plant is briefly presented.

2.1.1. ZEF DAC system

The ZEF DAC system which is currently under development is a continuous absorption and stripping process that uses a liquid sorbent. The sorbent flows inside the channels of the absorption column, where it is contacted with air with the use of a fan [80]. A heated stripping column is then used to

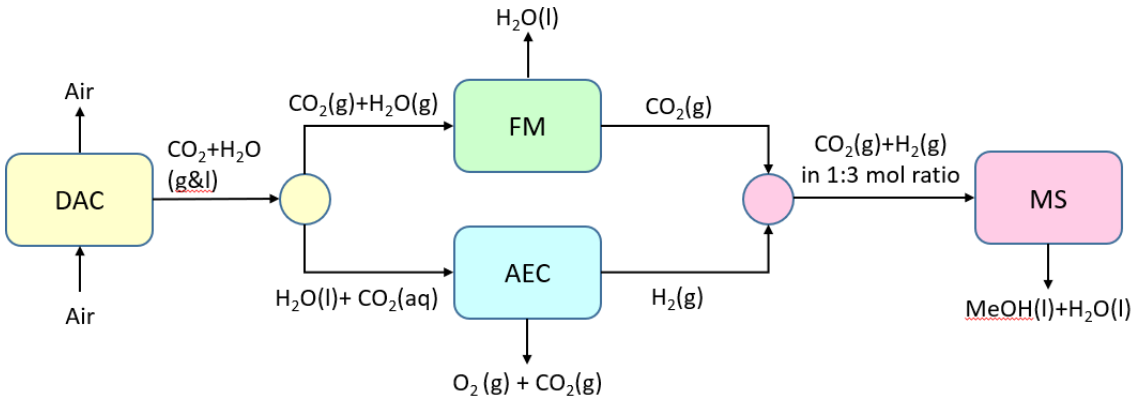

Figure 2.1: Simplified schematic of the ZEF micro-plant

desorb the water and CO_2 from this rich stream and to regenerate the sorbent. The gaseous product that emerges from the top of this stripping column consists of hot CO_2 and H_2O, which is cooled and allowed to settle into equilibrium in a flash tank, yielding both a liquid-phase and gas-phase product. The liquid is then used as a reflux as well as the main feedstock for the AEC system [27]. The gaseous phase is forwarded towards the FM system where it is compressed.

The ZEF 6 DAC prototype has been constructed and tested in the first half of 2020, yielding promising results.[90] The focus of these experiments have been on the absorption and stripping characterisation, and have not yet advanced to a point where a well-controlled composition of product can be produced. Thus, for this thesis, it is considered important to assume a range of possible DAC output conditions despite experimental results matching the theory fairly well. [27, 90]

2.1.2. ZEF FM system

The ZEF FM system which is currently under development is a multistage compression system that is supposed to compress the gaseous product of the DAC system to the pressure that is needed in the methanol reactor, which is between 50 and 60 bar. At the time of writing, the team is concentrating efforts on a two-stage system, each of which yielding roughly equal compression ratios. For utility reasons, this is usually rounded to the first stage operating at 8 bar, and the second stage at 50 when detailed calculations are not needed.

Prior to this project, this was already attempted several times with various methods to design a custom compressor for the ZEF system, which have resulted in failures despite theoretical studies suggesting that it should be possible [64]. The current iteration of the FM system is based upon off-the-shelf refrigerant compressors, which is also the first attempt made by ZEF to utilize lubricated compressors.

These lubricated compressors brought with them the need for an oil-reloop system. Unfortunately, first tests with these compressors indicated severe water contamination of the lubrication oil [14].

Another problem that is often mentioned is the heat management in the system. Overheating of the compressor is often stated to occur during experiments, specifically in situations where a high compression ratio is used [14, 44].

The current iteration is divided into short- and long-term projects, with this work being part of the long-term vision. The long term projects consist of a thorough evaluation of possible techniques to design a compressor for ZEF, as well as this work which is intended to be a thorough evaluation of the possible techniques to operate such a compressor within the ZEF context and design the required peripherals. The short-term projects consist of:

- The operation and analysis of a singular off-the-shelf compressor.
- Modelling of the performance of the off-the-shelf compressor.
- Disassembly, analysis and modification of such a compressor.
- The removal of the water contamination from the lubrication oil.

Table 2.1: Implications of the 600 g/day target based on equation 2.2

Reaction	CO_2	+	H_2	$\rightleftharpoons$	CH_3OH	+	H_2O
Stoichiometric Coefficients	1	+	3		1	+	1
Molar weight	44	+	2		32	+	18
$\dot{m}$ [Mol/(plant*day)]	18.75	+	56.25		18.75	+	18.75
$\dot{m}$ [g/(plant*day)]	825.0	+	112.5		600	+	337.5

2.1.3. Other micro-plant subsections

The Alkaline Electrolyzer Cell (AEC) system pressurizes the liquid H_2O captured from the DAC system, before decomposing it into H_2 and O_2 gases. The O_2 gas is purged into the environment after the alkaline electrolysis reaction. The H_2 is produced at high pressure (50 bar), which is the same pressure as the output of the FM system, and the required pressure to operate the methanol synthesis system.

$$\begin{aligned} &Anode: 4\,OH^-(aq) \rightleftharpoons O_2(g) + 2\,H_2O(l) + 4\,e^- \\ &Cathode: 4\,H_2O(l) + 4\,e^- \rightleftharpoons 4\,OH^-(aq) + 4\,H_2(g) \\ &Total: 4\,H_2O(l) \rightleftharpoons 4\,H_2(g) + 2\,O_2(g) \end{aligned} \tag{2.1}$$

The Methanol Synthesis (MS) system combines the CO_2 and H_2 gases at a pressure of 50 bar in the presence of a catalyst. The main reaction in the MS reactor is the following:

$$CO_2(g) + 3\,H_2(g) \rightleftharpoons CH_3OH(g) + H_2O(g) \qquad \Delta H^0_{298} = -42.9 kJ/mol \tag{2.2}$$

In order to succesfully operate the ZEF system, it is of prime importance to supply the MS reactor with the proper feedstock, in the correct ratios and under optimal conditions.

2.2. Basis of design

This section presents some initial calculations and assessment of the ZEF system in order to get acquainted with the context in which this problem occurs.

The overall target for the ZEF micro-plant is a methanol production of 600 grams per day, using 3 solar panels. This is deemed a highly ambitious, but theoretically possible goal. Based on equation 2.2, table 2.1 was made with some basic implications of this target.

This results in a total CO_2 mass flow that enters the FM system of **2.34** [mol/h], or **103.1** [g/h]. Note that this equation is aimed at the input quantities of the MS system. However, as seen in equation 2.1, H_2O and H_2 have a 1:1 molar ratio throughout the system. Thus, the H_2O target of the DAC system is also **56.25** [mol/(plant*day)] or **1012.5** [g/(plant*day)], which is a flow rate of **126.56** [g/h] that needs to enter the AEC system. It is assumed that the gaseous content of the flash tank is in equilibrium, and the temperature and pressure of this product are unknown. Temperatures from 40°C to 70°C are assumed in the design process, which is in accordance with studies of the desorption section of the DAC system. [90] As for the pressure of the gaseous DAC product, a range of 0.5 to 1 bar is assumed based on estimations in earlier explorative work. No further experimental or modelled information is available, partially due to this pressure varying widely between different stripping column design concepts, materials and operating conditions. This assumption is in concurrence with projects that are being run in parallel with this work, that are expected to yield more information on the topic.

Such a flash tank can be easily modelled in COCO simulator as shown in figure 2.2 in order to estimate the inlet conditions of the FM system under these circumstances. The input of this model is assumed to be the quantities of the output targets, being **103.1** [g/h] and **126.56** [g/h] of CO_2 and H_2O respectively, which is a 1:3 molar ratio. The model thus illustrates the non-idealities of the chosen input temperatures and pressures, which are shown in table 2.2.

The contents of table 2.2 can be used to gain the following insights:

- Lower temperatures and higher pressures promote favourable distribution of the captured species.
- The distribution of the water content is a lot more sensitive to the DAC output temperature and pressure than the CO_2 content.
- It can be assumed that the DAC team will aim to increase the operating pressure as development continues.

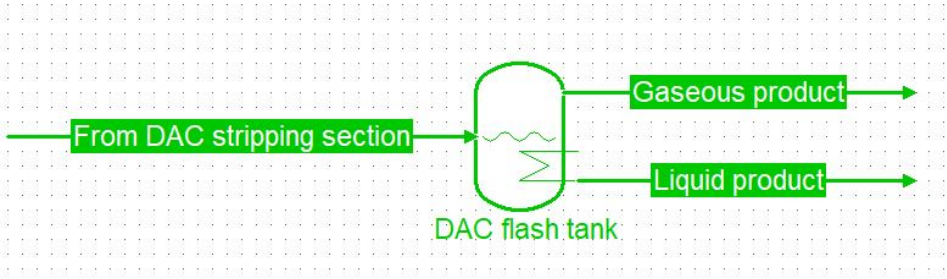

Figure 2.2: The COCO simulator model of the DAC flash tank

Table 2.2: The contents of the gaseous and liquid products of the DAC flash tank at selected conditions.

	Gaseous product			Liquid product		
	CO_2, [g/h]	H_2O, [g/h]	H_2O content, [g/100g]	CO_2, [g/h]	H_2O, [g/h]	CO_2 content, [g/100g]
40°C, 0.5 bar	103,07	6,29	5,75	0,001	120,29	0,001
40°C, 0.8 bar	103,06	3,73	3,49	0,017	122,84	0,014
40°C, 1 bar	103,05	2,94	2,77	0,022	123,63	0,018
70°C, 0.5 bar	103,07	56,82	35,54	0,003	69,75	0,004
70°C, 0.8 bar	103,06	23,70	18,70	0,012	102,87	0,012
70°C, 1 bar	103,06	17,10	14,23	0,018	109,48	0,016

- In order to run integration tests of DAC and FM systems, early prototypes can be additionally cooled in order to manipulate the distribution of captured species to more resemble field conditions.
- During development of this work, it is therefore reasonable to assume that the contents of the gaseous content range between the estimation of high pressure, high temperature, and low pressure, low temperature. This results in an assumed water content of the gaseous product ranging between approximately 5% and 15% of the total gaseous product mass.

Problems with tests of lubricated refrigeration compressor In the tests conducted in earlier work, a lubricated refrigeration compressor was used. In the current ZEF development plans, these compressors are used due to their low cost and mature development. However, the usage of these compressors introduce their lubrication oil as a third species into the mixture. This oil must be separated and recycled back to the compressor in order to ensure continuous operation. Furthermore, the gas mixture must also be cooled to be suitable for use in subsequent compression stages or the MS reactor which results in condensation of the water content of the mixture.

This liquid water then combines with the liquid oil and appears to form an emulsion that remains stable and cloudy at room temperatures for more than a day. An observation in earlier work [14] is made in which it was seen that the material leaving the exhaust port of the compressor resembled a fine oil mist. The datasheet of the compressor states that no liquids other than the specified lubrication oil are to be present inside the compressor in order to ensure proper lubrication and prevent damage [72].

These observations are what made the ZEF team formulate the original assignment as seen in appendix F.1 from the perspective of separating the oil-water emulsion. However, this emulsion might just be a symptom rather than the cause of the problem. In order to get a more complete view of the problem, one might better approach this problem from the perspective of the three-species flow, with the goal of not damaging the compressor and further downstream operations. This is the perspective that will be used in this work to guide the literature research (chapter 3) and conceptualisation (chapter 4). As the solution space should not be unnecessarily limited during the diverging phase of design [13], this system can be considered to be more than the ”oil-water separation” that was mentioned in the original assignment, and will be referred to ”Moisture control system” (MCS)

Summarising, ZEF FM inlet conditions are estimated to be as portrayed in figure 2.3. Under previously tested circumstances, the compression of this mixture introduced lubrication oil into the system, creating a three-phase mixture that contaminated the oil with the water content of the stream that

condenses at the cooling step that is required after compression. This contamination in turn quickly damages the compressor, which explicitly prohibits any liquids from being present, with the exception of the specified lubrication oil. The device that will be conceived in this work is a ”Moisture Control System”(MCS) that is tasked with handling the FM input flow and conditions in a method that ensures the water content does not inhibit proper operation of the compression system.

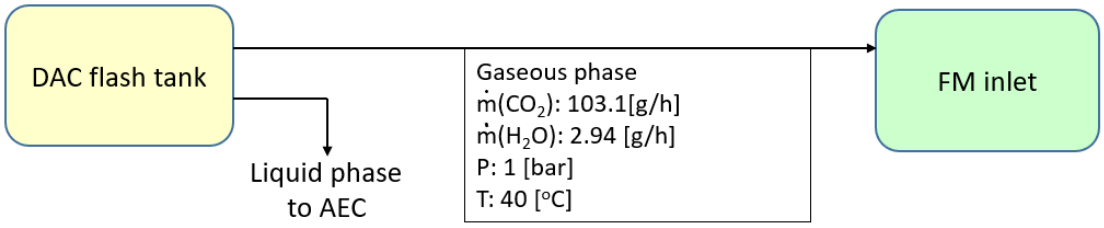

Figure 2.3: Overview of the imlet conditions of the FM section

2.3. Design approach and criteria

In the previous section, it has been established that the device that is conceived in this work is a ”Moisture control system” (MCS). This section will present the general approach to conceiving such a device, as well as the properties such a device might have using a MoSCoW model.

It is considered a standard element of a thesis project to start with a literature research. This will be detailed in chapter 3 and will be based upon the insights into the problem gained in this chapter. The results of this will be used to get a good overview on the available techniques, from which concepts are made that can be prototyped. It should enable the creation of a model as well. From this, a proof-of-concept prototype is to be made, and validated with the model, which can then serve as basis to create further prototypes.

During this process, several design methodologies will be used to assist in the creation of the concept. The first one of this which will be applied is an adaptation of the MoSCoW method [3]. This method is fairly common in software development, and can be adapted to be applicable to hardware prototyping as well. The method works by placing criteria in 4 categories: Must, Should, Could and Would.

The ”Must” category contains features that are critical. If any of the ”Must” features are not implemented, the product is considered invalid. The ”Should” category contains features that have a high priority to be implemented, but it should be possible to make a valid product in which one or several of these features are omitted or worked around. The ”Could” category includes features that are not essential for the operation of the product, but significantly improve operation and/or functionality. It should be attempted to implement as many ”Could” features as reasonably possible. Finally, the ”Would” category consists of features that are of minor improvement to the product. ”Would” features are never leading in the design, but should prove to be a worthwhile addition if easily implemented into an existing design.[1]

MoSCoW model Description: This device will be the ”Moisture Control System” section of the ”Fluid Machinery” subsystem. The device will handle the processing of material input, which is (are) the output stream(s) of the compressor stages and/or the direct air capture subsystem. Its criteria are listed in table 2.3.

Concluding, the ”Moisture Control System” project will focus on one or several experimental prototypes, supported by a digital model. This is preceded with a literature study to take inventory of the possible solutions. The literature study will take the viewpoint of the main functionalities of the MCS which is the handling of CO_2 & H_2O stream as it runs through a compressor that introduces oil into that mixture. Note that this differs from the originally stated project description. The goal is to ensure that

[1] The original MoSCoW method uses W for ”Won’t”. As this work is on hardware development, it is deemed fit to use ”Would”, due to the more ambiguous nature of hardware over software, facilitating (positive) side effects of and multi-functionality of design elements.

Table 2.3: Full list of MoSCoW model criteria

The product must	The product Should
• Allow for a compressor oil-recycle system to operate with an amount of water contamination at which it does not significantly damage the compressor. • Transfer the carbon dioxide of the input stream to the next compression stage, or to the reactor if the input stream is of adequate pressure. The CO2 output stream must not contain components that significantly damage downstream operations. • Handle the water content of the input stream in a safe and adequate manner. • Be equipped with adequate sensing capabilities to provide safe operation. • Be able to process the volume of material corresponding to the ZEF microplant process.	• Be designed to have a minimal pressure drop between input and CO2-rich output. • Comply with (temperature) criteria at interfaces with other components such as the compressor and reactor. • Provide a method of adequately handling the water stream. • Allow for easy maintenance in the development phase. • Include an analysis of recommended usage in the operational phase of the device. • Be equipped with adequate sensing capabilities to provide a supporting role in the operation and maintenance of the device. • Have a design and development cycle that is compatible with other developments within the company.
The product could	**The product would**
• Purify the water stream to an extent that it can be safely purged to the environment. • Have a minimal consumption of electrical power. • Not make the fluid machinery subsystem significantly larger than a typical ZEF subsystem. • Be designed to be easily mass-produced. • Be equipped with adequate sensing capabilities to provide information of flow compositions during	• Be designed to minimize cost. • Allow for easy maintenance in an operational setup. • Be designed in a way that malfunctions in the operational phase do not damage the rest of the plant and/or the environment. • Include an analysis on longevity and failure modes of the device. • Include a risk analysis for the operational phase for the device.

each of the three mixture components arrive at their appropriate locations in a purity where it does not damage the rest of the machine or the environment.

3

Theory and Literature

This chapter will explicate the theoretical background of the thesis. The main problem as observed in section 2.2 concerned the existence of a three-phase mixture consisting of carbon dioxide, liquid water and lubrication oil. Thus, the starting point of this literature research concerns devices that are intended to separate these three phases.

These three-phase separation devices are explored in section 3.1. Some basics on the interaction of compressors with their surroundings are presented in section 3.2.

In section 3.3 come properties of water, carbon dioxide and lubrication oil. Sections 3.3.1, 3.3.2 and 3.3.3 explore the interactions between these compounds and their surroundings.

Section 3.4 presents many possible separation techniques that can be used. They are loosely split into mechanical, chemical, filtration and adsorption based techniques, which will be presented in sections 3.4.1, 3.4.2, 3.4.3 respectively. The chapter is then concluded in section 3.5 by linking the found techniques to the design approach outlined in section 2.3, and providing a solid basis for conceptualisation.

3.1. Three-phase separation

Three-phase separation is not a new problem, nor is it specific to a single application. Starting from the 1970's, quite a few patents can be found for continuously operated three-phase or multi-phase separators.[15, 40, 67] Many of these devices are aimed to improve crude-oil extraction, but also examples from the medical [60] and water treatment [89] field can be found.

It must be noted that besides those patents, very few scientific papers regarding three-phase separators have been found, and that those that were found mainly focus on modelling and understanding the flow of devices that already existed at the time of writing [43]. This implies that "Three-phase separation" is likely an application of separation technology in general, and cannot be seen independently. In order to understand how a three-phase separator for the ZEF system might be created, it is required to understand the underlying mechanisms at work.

When looking at the cross-sections of the examples in figures 3.1 and 3.2, one can see that the approach that was taken varies between the two designs. The Peters design appears to be based on settling tanks, whereas the Brown and Erickson design appears to be based on a centrifuge. Both of these approaches use the difference in density between the three phases to separate them [86]. The densities of each separated phase needs to be sufficiently dissimilar from the most similar other component in order for them to separate properly. Thus, the density difference between individual phases, and not the overall density disparity, is leading in this separation, enabling one to look at just two of the three phases at once. From this perspective, it is visible that these three-phase separation devices really consist of two separators in series, each removing one component from the mixture.

The example presented in figure 3.3 is a lot simpler than the ones presented earlier which makes it a easier to see that it is, in fact, two separation stages in series. First, the mixture is spread across a plate that is referred to as the "primary separator" in the patent. This inceased surface area reduces flow velocity and promotes the separation of the gas into the gas phase. The remaining liquid, a combination of a light and heavy phase, is then returned to the inlet-side of the separator to avoid zones with no net

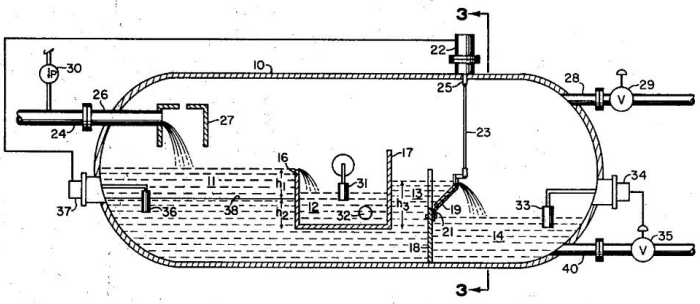

Figure 3.1: Peters' three-phase separator from 1976 takes a settling-based approach, using many components to control fluid levels in the various compartments of the system. Reprint from [67]

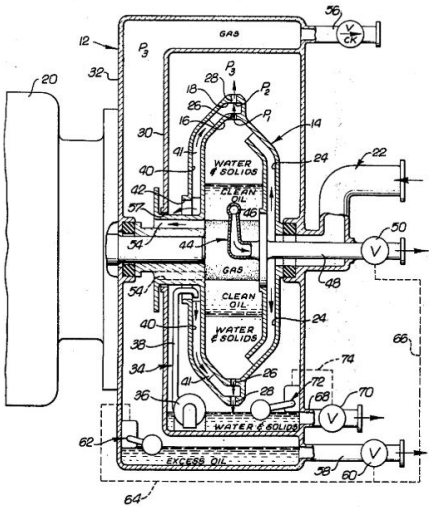

Figure 3.2: Brown and Erickson, also in 1976, utilise a centrifugal approach, with an elaborate internal design to extract the various components from the rotating barrel. Reprint from [15]

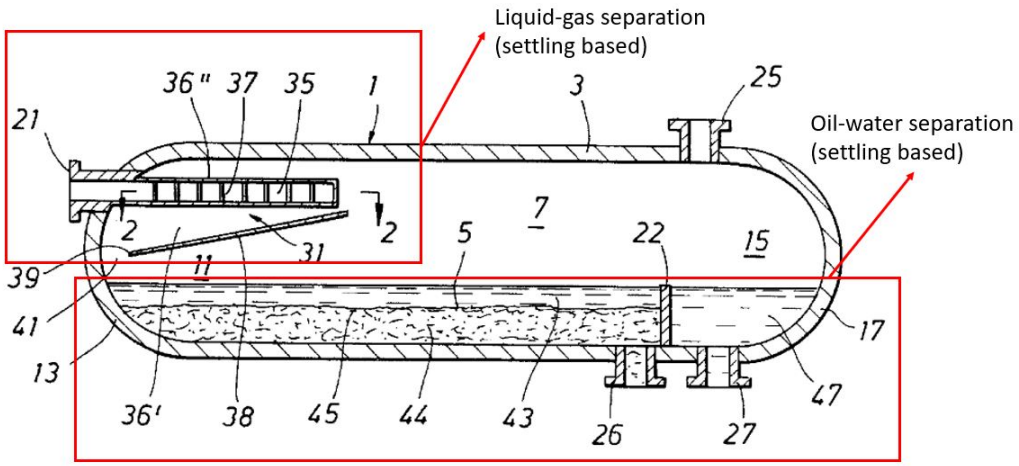

Figure 3.3: Polderman's 2003 design is simpler than the earlier examples, making it easier to see that this three-phase separator consists of two sepators in series. Adapted from [70]

flow, and make maximum use of the separator's footprint. This allows maximum separation of the oil and water in the settling tank, that finally uses a simple weir to allow the lighter flow to pass over the top, and send both phases to their own outlet.

Polderman states in his patent, that the design as presented is but one embodiment of the concept, and that the design of the separators is not fixed. In fact, both separators have several variations proposed in the patent, allowing the user to mix and match according to their needs. Thus, Polderman's design is an excellent example that shows that a three-phase separator can be designed by treating it as two separators in series.

Treating the three-phase separator as two separators in series, enables one to have a new perspective on all other examples found earlier. For instance, Brown and Erickson's design [15] can be seen as two centrifugal stages in the same barrel. Perhaps this is most clear in Hays' design of the "Multi-phase separator" from 1978[40], which quite literally uses multiple centrifuges in series, each scooping out one of the components.

This approach to three-phase separation can also be taken in the context of the ZEF micro-plant to get the most broad view possible. The separation of either oil, water or CO_2 as as a first step presents three[1] theoretically possible permutations. The three main-types of separators will be named “Dewatering-type”, “Deoiling-type” and “Degassing-type”, for devices that remove water, oil and carbon dioxide respectively in the first separation. An overview of these device types can be found in figure 3.4. They will be referred to in this work as DW-, DO- or DG-type devices, consisting of separator 1 and 2. For instance, the second separator of the deoiling-type device is a DO-2 type separator.

It must be noted that in this overview, the dewatering-type varies from the others in the sense that the first separation stage happens before the compressor. This is due to the fact that after compression, the hot water vapour and gasesous CO_2 do not form separate phases until condensation and emulsification with the oil occurs. As it can be seen further in this chapter, no solutions were found that removes water first, just as the mixture leaves the compressor. On the other hand, degassing and deoiling types cannot have their first separation before the compressor, due to the oil being introduced at the compression, and the carbon dioxide being required to pass through the compressor.

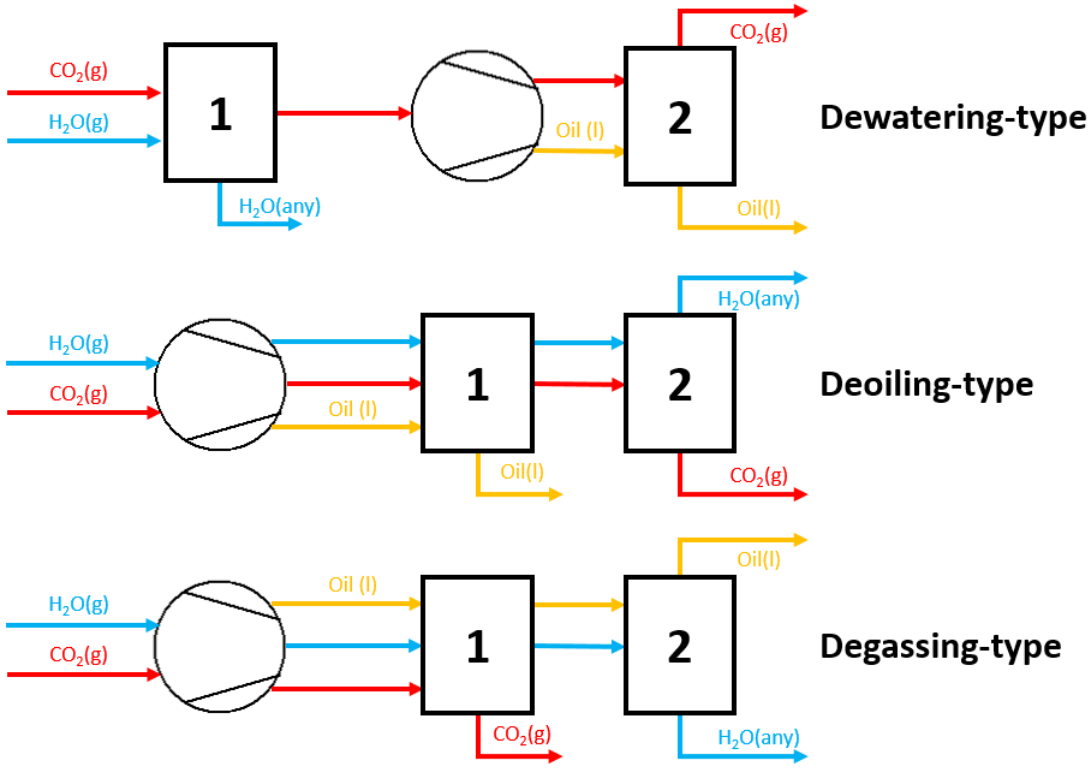

Figure 3.4: The three possible configuration types of the moisture control system: dewatering (DW), deoiling(DO) and degassing(DG).

3.2. Gas compressors in system context

While the compressor development is not in the scope of this work[2], a brief introduction to the compressors used at ZEF appears to be in place due to the large role the compressor has to play in the FM system and micro-plant in general. The compressor currently in use for testing at ZEF is a repurposed Purswave LT35DC refrigeration compressor. This compressor falls into the rotary piston compressor type, which traps a pocket of air, that is then reduced in volume by the rotating roller to increase pressure. Rotary piston compressors are known for their low cost, robust control, and a good range of

[1] The total amount of permutations is six, but three of these are considered invalid which are the situations explained in the next paragraph

[2] For more information on the (current) developments of the compressor, please refer to the work of other ZEF team members.

suitable operating pressures[11].

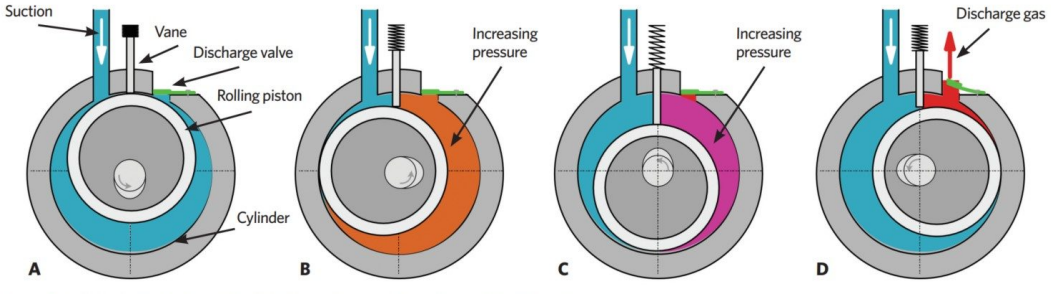

Figure 3.5: Schematic view of a rotary piston compressor at various stages of the compression cycle, reprint from [28].

Regarding the performance of the compressor, adiabatic compression is assumed. An equation to describe this compression is based upon the equation of work in a polytropic process (pv^n = constant) for an ideal gas and presented in equation 3.1 [54]

$$\frac{\dot{W}_{cv}}{\dot{m}} = -RTln(p2/p1) \qquad \text{, only when } pV = nRT, \text{ with } n = 1 \tag{3.1}$$

The main takeaways of this equation that are relevant for the MCS are that under (approximately) adiabatic compression, a high outlet temperature is unavoidable. This introduces a requirement to cool the compressed mixture in order to make the gas suitable for use in further compression stages. This cooling functionality can be included in, but must not be mutually exclusive to the MCS separation stages that are situated after the compressor. It must also be assumed that the CO_2 buffer before the MS system can col down to ambient temperature during the night.

As will be further explored in section 3.3.2 gas under higher pressures has an increased dewpoint. It is likely that this increased dewpoint makes it that the output has a very high risk of condensation. This might occur in steady-state, but will almost certainly occur during startup after a cold night.

3.3. Relevant compounds and interactions

This section will provide some more details on the compounds involved in the MCS and their interaction. It is assumed that the reader is already familiar with water and carbon dioxide. While these materials sit at the core of this work, they are also incredibly common, so this section will focus on the lubrication oil and interaction between compounds.

Lubrication oil While oil might sound like a single thing, it is actually an umbrella term of a wide range of organic chemicals. Oil in the contect of the MCS refers to the lubrication oil of the compressor. While it is beyond the scope of this thesis to go into the various lubrication types and their properties, it must be stated that the required lubricant type varies per compressor design and is always stated by the supplier of the equipment.

Refrigeration compressors like the Purswave LT35DC commonly use silicate ester oil such as the RL32-H oil stated in the compressor datasheet[72]. However, this lubricant is specifically intended for use in closed systems, such as refrigerators. For open systems such as the ZEF FM system, it is unlikely to be fit for use, at least during the testing and development stages, due to its poor stability in (humid)air [53]. During testing, various types of hydrophobic mineral oils were used. At the time of writing, it is yet unknown what compressor-lubricant combination will be used in the long run. Based on work of other ZEF teammembers that was not yet published at the time of writing, it can be stated that the selection of lubricants is not a trivial question.

When considering the required simplicity of the ZEF micro-plant does not allow for sophisticated collection and filtering of any emissions, used lubricant that travels away from the FM system might end up in other sections of the micro-plant (such as the MS reactor), the product or one of the purge streams where it might cause significant damage [7]. Whatever the choice, it should always be considered where the used lubricant ends up, however small the quantities.

3.3.1. Oil-water mixtures

Mayonnaise and vinaigrette are two non-engineering examples of situations in which oil and water do mix. The formation of these emulsions are common in industry too, with crude oil extraction, food processing and contaminated machine lubrication as examples [20, 25]. In short, water is a lot more of a polar compound than oils and fats are. This causes water to mostly hold together using hydrogen bonds. As oils are unable to form these, the water molecules are inclined to group together, squeezing out the oil molecules, forcing them to group together too.

The groups of minority molecules then form droplets in the majority compound's continuous phase. These droplets are subject to a difference in density with the continuous phase, causing a force to be exerted on them. However, to move a droplet through a continuous phase, viscous forces are applied to it as well. Quite a few variations on hydrodynamic-based models exist, and are described in chapter 19 of Seader, Henley and Roper's 2011 book [78]. One of the better known of these settling equations for laminar flows (Re < 2100) is based on Stokes' law and is presented in equation 3.2.

$$u_f = \frac{g d_p^2 (\rho_p - \rho_f)}{18\mu} \quad \text{, only for laminar flow with} Re < 2100 \tag{3.2}$$

It can be seen that the settling velocity u_f strongly depends on the droplet diameter d_p. Droplet diameter appears to also be leading in determining the proper settling equation to pick [78]. While this work will not extensively cover all available modelling methods, it must be noted that the emulsion observed in the initial testing described in section 2.2 is likely to consist of very fine droplets, due to its low settling speed. From this, the assumption is made that the Stokes' law settling equation is a good starting point for further investigation, and can be backed up by the Stokes-Cunningham law or Brownian movement equations if needed [78].

3.3.2. Gas-water mixtures

State of the art models are available to estimate the behaviour of many different mixtures, including CO_2 and H_2O [2] to a much higher detail than is likely required for the purposes of this work.

For the design of the MCS, it will be assumed that all gases involved behave as ideal gases, meaning that the Dalton model applies and the ideal gas equation of state can be used for each component.

The humidity ratio ω is defined as the ratio of the mass of water vapour to the mass of dry air(component a)[54] ($\omega = m_v/m_a$). Using the property $n = m/M$, with n, m, and M being the amount of moles, mass and molecular weight of these components, the definition of the water vapour component as component v, and the humidity ratio, the ideal gas equation of state can be rewritten to equation 3.3 [54].

$$\omega = \frac{m_v}{m_a} = \frac{M_v p_v V/\bar{R}T}{M_a p_a V/\bar{R}T} = \frac{M_v p_v}{M_a p_a} \tag{3.3}$$

Another common measure of air humidity is the relative humidity (equation3.4), which differs from the humidity ratio in the sense that the relative humidity does not compare the amount of water vapour to the other gaseous component, but rather to a mixture at the same temperature and pressure at which the gas is saturated with water vapour.

$$\phi = \frac{y_v}{y_{v,sat}} \text{with T, p constant} \tag{3.4}$$

Relative humidity is easy to measure. This was traditionally done with a psychrometer: a device that measures both wet-bulb and dry-bulb temperatures, using the difference in temperature caused by evaporation in the wet-bulb thermometer to calculate relative humidity. The earliest mention of a psychrometer was attributed to Ernst August in the early 19th century, although not much has been found from that era [6]. The devices have steadily evolved throughout history, eventually resulting in electrical and digital versions as well, and the adaptation of the name hygrometer. Scott et al. [49] published a guide to measuring relative humidity in 1996 that was considered useful by the author for a broader understanding of these measurements, although its contents were not directly used in this work.

As stated by equation 3.4, the relative humidity can be used to measure the quantity of water in the gas, provided temperature and pressure are known. Another useful quantity that can be determined is the dew point. The dew point is the temperature and pressure associated with saturated water: it

Figure 3.6: Replica of August's psychrometer made in 1876. Currently in the collection of the Science Museum Group in the UK. Overall height: 69cm. [93]

Figure 3.7: Variations of Honeywell's HIH6100 series digital humidity/temperature sensors, released in 2015. Overall height excluding connectors: 3.90mm.[41]

Table 3.1: Partial pressures and dewpoints under various FM input conditions. Made using the COCO simulator model shown in figure 3.8

T_{in}, P_{in}	p_{CO_2} [bar] uncompressed	p_{H_2O} [bar] uncompressed	p_{CO_2} [bar] P = 50 [bar]	p_{H_2O} [bar] P = 50 [bar]	Dewpoint [°C]
40 C, 0.5 bar	0.435515	0.064485	43.5515	6.4485	152.13
40 C, 1 bar	0.934734	0.065266	46.7367	3.2633	126.23
70 C, 0.5 bar	0.213057	0.286943	21.3057	28.6943	225.37
70 C, 1 bar	0.711624	0.288375	35.5812	14.4186	187.81

can be found using thermodynamic tables of varying temperatures or pressures that can be found in various literature sources [49, 54]. This can also be done using psychrometric charts [31], or Computer Aided Process Engineering (CAPE) software such as COCO Simulator [88].

Using the assumptions made in section 2.2 that the feed is at or near 100% relative humidity, 0,5 to 1 bar, and 40 to 70 °C, equation 3.3 can be used to find the partial pressure of water vapour and the corresponding dew points using COCO simulator. The model used is the model presented in section 2.2, extended with a compressor as can be seen in figure 3.8.

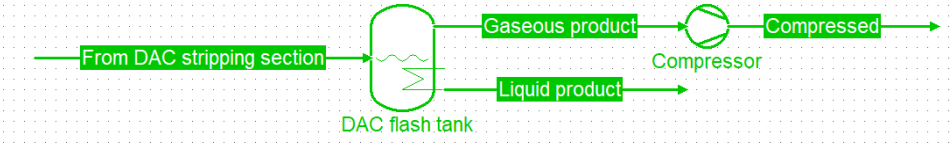

Figure 3.8: The COCO simulator model used to find the dewpoints of various compressed CO_2 and H_2O mixtures.

From this table, it can be seen that throughout the compression process, the dew point significantly rises and is determined by the DAC output conditions. This makes sense, as the partial pressure of water in the inlet, is also compressed by the same compression factor of the overall gas. As a worst-case scenario, this means that as the CO_2 and H_2O mixture is compressed by a factor 100 from 0.5 to 50 bar, the partial pressure of water increases hundredfold too, resulting in a dewpoint running into hundreds of degrees celsius. This means that in order to be used in further compression or reaction

steps or while sitting in the pressurized CO_2 buffer after the compressors(at night), the mixture is to be cooled to a point that is almost certainly beyond the dewpoint of the mixture. This leaves the conclusion that the requirement to deal with condensation is inherent from the gas composition.

3.3.3. Other interactions

Other relevant interactions that were found throughout this investigation concern CO_2 with lubrication oil, and (acidic) water with compressors.

CO_2-oil interaction Beerbower's 1961 paper "The behavior of lubricating oils in inert gas atmospheres" [9] is a comprehensive starting point to explore the behaviour of oil in gas. From this paper, it can be concluded that the effects of the viscosity effects on the oil are well predicted by theory. This theory has steadily evolved over the last century or so [8, 46] and is considered to not pose a problem. One thing that should be noted is that CO_2 is stated by Beerbower[9] to cause "Heavy fogging" (the entrainment of oil in a gas stream), and appeared to not be strongly dependent on oil type. This contributes to the explanation of the observations in early testing and adds reason to believe that the expelling of fine oil droplets is not a trivial problem and when left unchecked, could cause high lubricant consumption, as well as contamination in the MS reactor or even the final product.

Compressor-(acidic) water interaction The corrosion of compressors due to the presence of CO_2 is a well known and documented problem in the fossil fuel industry where, especially in offshore environments, can lead to the failure of equipment via various mechanisms.

While water vapour and carbon dioxide by themselves do not appear to have very corrosive effects, problems are reported to start once the water concentration in oil exceeds the limited amount that can be dissolved, and starts to form a separate phase. This "free water" can already impact the performance of a compressor by changing the viscosity [84] of the oil, which often requires a prescribed value from the equipment manufacturer [72]. Free water also increases surface corrosion and wear, as well as affect lubricity and lubricant stability [25].

Free water in the presence of CO_2 has an even worse effect on corrosion and wear, due to the dissolved CO_2 forming carbonic acid (H_2CO_3), which lowers the pH of the water and causes serious damage to the steel components that are found in many compressors.[37] Guedes et al. specifically warn potential developers of CO_2 compression systems to be mindful of the dewpoint of the compressed mixture as it is associated with the onset of CO_2 corrosion [37].

Even when all water is in solution with the oil, adverse effects can occur. Cantley for instance, reports that even at fairly low concentrations of water, bearing life is significantly affected [18]. Cantley's work reported that no additive or oil type was used that sufficiently reduced this effect. While this 1977 paper is fairly old, no documentation was found that rendered Cantley's work obsolete.

While the design of the compressor and selection of lubricant is not in the scope of this thesis, it is considered relevant to consider the in- and output conditions of the MCS and its interaction with other sections of the machine.

3.4. Separation methods

This section will present the various methods found to create the separation mechanisms as presented in figure 3.4. They are roughly split into three categories, which will be presented in the sections 3.4.1 to 3.4.3.

3.4.1. Mechanical separation

The "mechanical separation" category is a fairly broad term, that mainly revolves around mechanical movement and forces of the two species that are being separated to achieve separation.

Settling tanks Settling tanks or decanters are a classic example of a separation technique and have been used for a very long time to separate immiscible species based on density and can be operated both in batch and continuous fashion. They are usable for many of the separators of figure 3.4. The tank provides the feed with enough residence time for the lighter phase to move up and the heavier phase to move down. This is driven by a buoyancy force imposed by the density difference between the two phases, and counteracted by the viscous forces of fluids moving along one another.

In order to design a settling tank, the (terminal) settling velocity is needed. This can be done using Stokes' law as presented in equation 3.2. It makes sense that the droplet size is the most important variable in settling tank design, due to the terminal settling velocity scales with the square of droplet size. Towler and Sinnott claim that settling tanks are usually used to separate droplets larger than 150 [μm] and that typical residence times are in the range of minutes.

This makes settling tanks quite unsuitable for use in the ZEF context, since the emulsions that were sampled from early compressor testing remained stable for several days. Assuming that a clear band at the top and bottom of the sample would be clearly visible if the droplets had moved 5mm in 24 hours a settling velocity of $5.78 * 10^{-8}$ [m/s] can be found. Applying stokes law for droplets with this velocity of 900 [kg/m³] oil in 1000 [kg/m³] water with a 1 [Ns/m²] viscosity gives a maximum droplet size of of 32.5[μm], which is already a factor 5 smaller than what Towler and Sinnott describe as "well below the droplet sizes normally found in decanter feeds" [86]. This hypothesis is reinforced when looking at the sample through a simple lab microscope, in which large droplets visible in the sample were measured to be in the order of 10 [μm], with many droplets being beyond the microscope's capabilities to accurately measure.

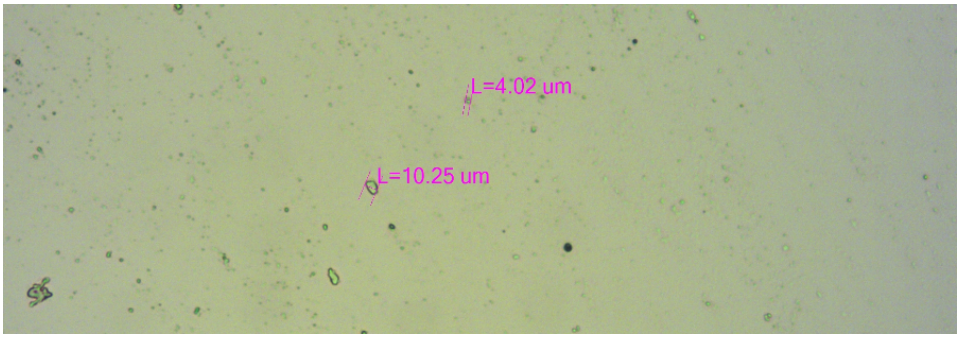

Figure 3.9: Emulsion formed from compressor exhaust during early testing at ZEF, as seen under a basic lab microscope.

Mechanical coalescers As seen in the previous paragraph, small droplet sizes are somewhat of a dealbreaker in the use of settling tank. One way to circumvent this problem is to increase the droplet size. The process of merging together droplets to increase their size is called coalescence. A commonly used strategy is the usage of packs of inclined plates or packed fibrous materials. These plates/fibres are coated with a thin film of material, allowing droplets of light-phase material to easily adhere to a light-phase film and ascend to the continuous light phase, the same effect applies with a heavy-phase film to sink heavy-phase material. Work presented in the early 90's did describe the phenomenon, but failed to reach a sufficient modelling method, as the hydrodynamic modelling of single droplets resulted in higher coalescence times than those measured in experiment [51], from which it was concluded that the coalescence process itself required further investigation [75].

New interest in the technology was sparked due to its low energy consumption. However, a literature review made by Han et al. in 2017 [39] stated problems that are fairly similar to those stated by Rommel, Blass and Meon more than 2 decades prior. More empirical data was available, as well as more research on various coalescence mechanisms, (biomimetic) materials and material modifications. However, there was still no satisfactory model or understanding of the process. More importantly for this work, a lower limit on droplet size of 100-150 [μm] was still reported [39]. Smaller droplet sizes in the range of the large droplets seen in figure 3.9 have been reported by Li & Gu in fibrous and granular beds, but their performance did not match the requirements of the ZEF MCS [47]. Mechanical coalescers may be of interest for the degassing-2 and deoiling-1 type separator of figure 3.4.

Electrostatic coalescers Electrostatic coalescence is another method to combine small droplets into larger ones, allowing the forces induced by the density difference be dominant. This is achieved by introducing electrostatic forces alongside the gravitational and viscous forces. The first patent for an electrostatic separator was issued as far back as 1911 [23], but while Cottrell's device seems fairly straightforward, the exact mechanism at work required more investigation to be understood. Even in modern times, reports show that while electrostatic coalescers are commercially used, their scientific

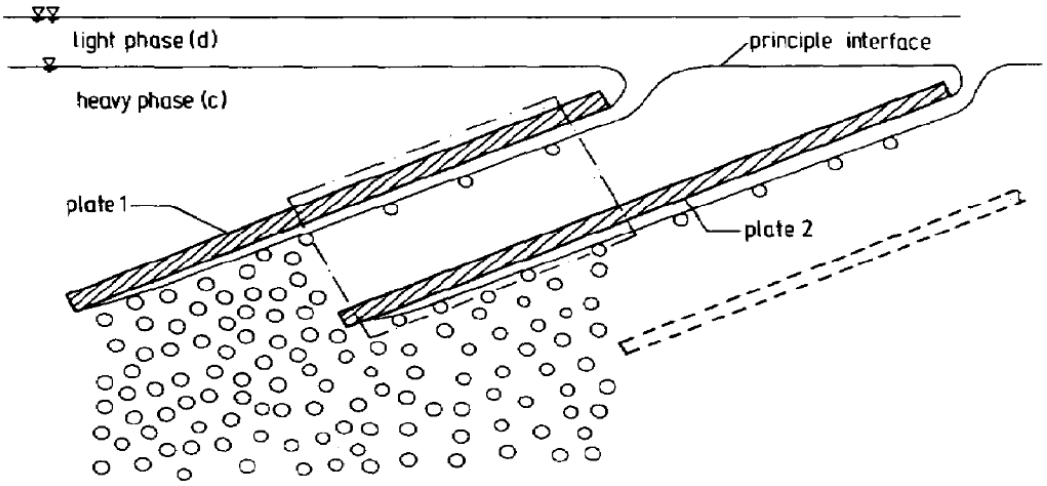

Figure 3.10: Illustration of the principle of plate coalescence. Reprint from [74]

understanding differs significantly from their engineering applications [59]. This reduced understanding of the theory is assumed to significantly increase development risk, particularly when combined with the non-fully understood setting that is the ZEF system. It can also be expected that the effectiveness of electrostatic coalescers is limited. This is due to the fact that the (di)electrophoretic force that moves droplets through a liquid to an interface also scales with the second and third power of the droplet size, similar to Stokes' law. This implies that increasingly high voltages are needed to generate a strong enough electric field to have any effect. Electrostatic coalescence may be of interest for the degassing-2 type separator of figure 3.4.

$$F_{ele} = \frac{2}{3}\pi^3 d_p^2 \epsilon_c E^2 \quad [59] \tag{3.5a}$$

$$F_{diele} = 2\pi d_p^3 \epsilon_c \beta \nabla |\vec{E}|^2 \quad [59] \tag{3.5b}$$

Refrigeration dehumidification Removing water from a wet gas by cooling it beyond the point of condensation is known as refigeration dehumidification. It may be of interest for a dewatering-1 or deoiling-2 type separator of figure 3.4 By running refrigerant through a compressor, via a hot heat exchanger(condenser) to an expanding valve, the gas cools down and allows the creation of a heat exchanger that is colder than ambient(evaporator). By running the humid gas through the evaporator, the temperature is dropped to beyond the dew point, causing water to condense out. The gas is then used to cool the condenser and return to approximately its original temperature, but with a reduced water content. Brundrett states that this method can achieve a water content as low as a 0°C dewpoint. Any lower than that would introduce freezing issues.

The refrigeration dehumidifier might be interesting in the ZEF context considering that some development of compressor-based systems is already being done. It is important to state that the heat exchangers mentioned by Brundrett [16] may not even be mandatory as the key concept is not the creation of a refrigeration cycle, but lowering the temperature of the gas beyond the dewpoint by whatever means.

This insight might enable the development team to creatively apply the dehumidification concept. For instance, it may be possible to utilise the increasing dew points at increased pressures to drop the temperature of the gas beyond the, now increased, dew point. This is similar to what Brundett describes as "Vapour compression drying". [16]

Should this method be chosen, more research is required on the many different permutations of such a concept, as well as the integration with the rest of the FM system, for which this technique lends itself splendidly.

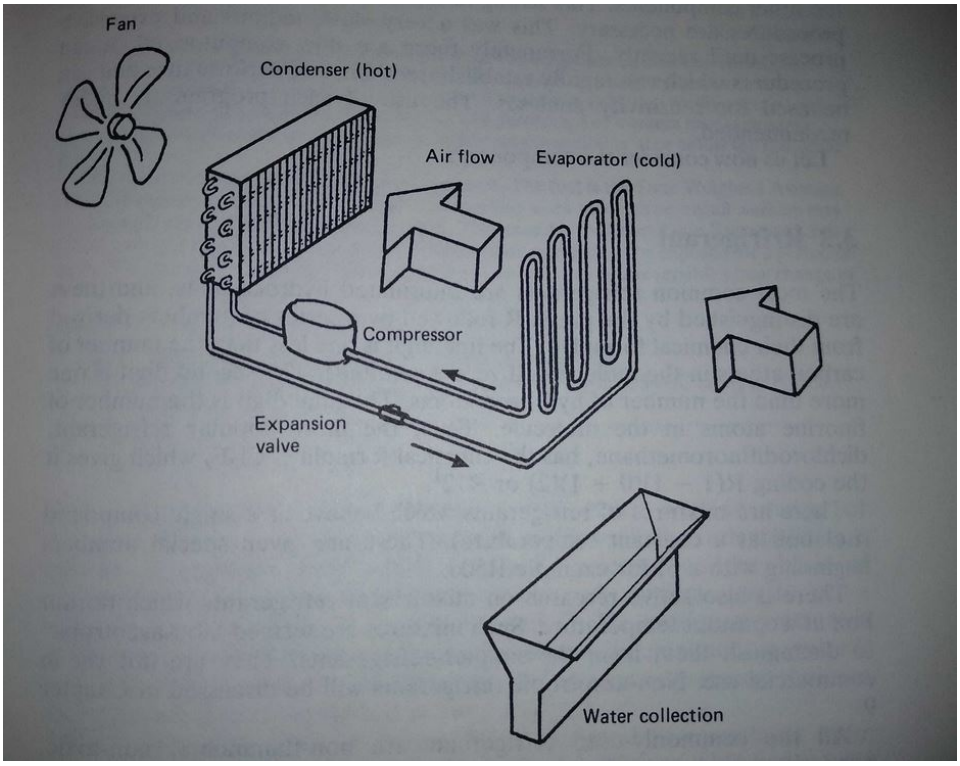

Figure 3.11: Schematic of a refrigeration dehumidifier. Reprinted from [16]

Hydrocyclones These devices use the momentum of the incoming fluid to realise a centrifuge-like action. Often used for the separation of particles, it can be equally applied to fluid-fluid separation where the phases have a density difference, as is the case in the ZEF system [86]. This can be the case for the DW-1 DW-2, DO-2 and DG-2 separator types indicated in figure 3.4.

The fluid enters the cyclone, and is drawn down to the conical section where the decreasing radius of the fluid's path increases its centripetal acceleration, and thus the force the fluid experiences. This forces the denser fluids to the outside of the cyclone, and subsequently out through the underflow connection. The lighter materials near the axis of the cyclone are eventually forced upward through the overflow connection.

Hydrocyclones are fairly well studied, both in experiment and (CFD-) modelling. Gomez et al., for instance, provide a comprehensive overview of many relevant aspects, particularly for separation of (crude) oil and water. However, the hydrocyclones studied by Gomez et al. dealt with a lot higher flowrate (18 to 26 GPM $\approx$ 4 to 6 m^3/h [35]), as well as larger droplets (30 to 160 microns[35]). It was reported that the separation efficiency held an "S" shape, implying that the separation efficiency increases sharply once a certain threshold droplet size d_{50} is reached, which is the droplet diameter at which 50% of droplets are separated.

Zhu, Liow and Neely published papers in 2010 and 2012 on the topic of hydrocyclone miniaturization[96, 97]. The studies, based on CFD simulations of miniaturized hydrocyclones, claimed that the working principle of the hydrocyclones appeared to remain intact, there were some considerations to be made regarding the separation efficiency and centrifugal stability. The 2012 study used laminar regime Reynolds numbers (Re = 300), and found that particularly at low inlet velocities, the flow stability reduced and the d_{50} droplet size significantly increased. The smallest droplet size reported as d_{50} in the 2012 paper was approximately 20 microns. This must be taken into account when investigating the applicability of hydrocyclones within the ZEF system. Since the flowrates in the system are very low, it must be investigated how high the flow velocity can be, without reducing the pipe diameter to the point where manufacture difficulty and cost becomes a major issue. This consideration is to be weighed against the relative ease with which small hydrocyclones can be produced using modern (powder-based) additive manufacturing techniques.

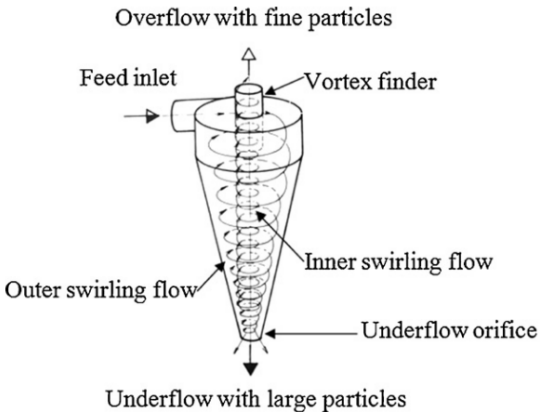

Figure 3.12: Schematic of a typical hydrocyclone. Reprint from [83].

3.4.2. Filtration-based separation

The filtration principle is quite familiar to most, as the filtration of coffee grounds from a fresh brew is a quintessential part of the morning for many, including the author. While the filtration of solids seems more intuitive, filtration in a liquid-liquid system such as a DG-2 type separator is also possible, as shown in the overview in figure 3.13 from Cheryan's 1998 book. From this, it can be seen that the filtration of lubrication oils in water fairly clearly falls into the "Ultrafiltration" class, which is generally done with specifically made ultrafiltration membranes. [20].

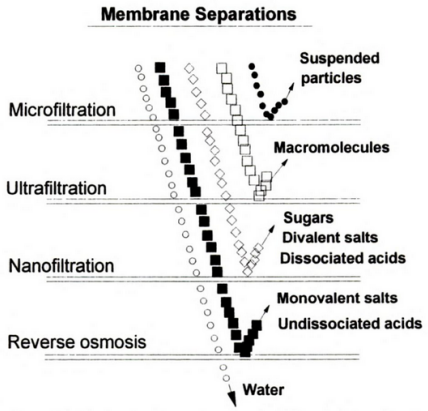

Figure 3.13: Various types of filtration processes. Reprint from [20]

The coffee is an example of filtration in a dead-end configuration, which is one of two main configurations in which non-adsorbing filters operate, the other being the cross-flow configuration. The main difference is that in dead-end operation, the particles that do not cross the filter are packed against the filter, resulting in cake filtration and the need to deal with this cake. While cake filtration is well understood and modelled [45], it might not be a very likely candidate for the MCS, since both phases are to be recovered in a fairly pure state in order to both purge the water and recycle the oil in a safe manner. Cross-flow filtration thus seems more suitable for the ZEF system. It is based on a feed flow past the filter, with the permeate (water) passing through the membrane, reducing its concentration in the retentate (oil).

Cheryan also provides an example of a process to treat oily wastewater based on ultrafiltration, specifically tailored to a situation in which an oil-water emulsion is dispersed too finely to be separated with conventional means such as settling tanks. A "Nominal Molecular Weight Cut-off" or nominal rating of 50000 to 200000 is recommended, which is the molecule size at which 90% of particles are retained as shown in figure 3.17. It should be noted that if this process is to be used, more investigation is needed toward the material of the membrane, as Cheryan warns for a situation in which a continuous

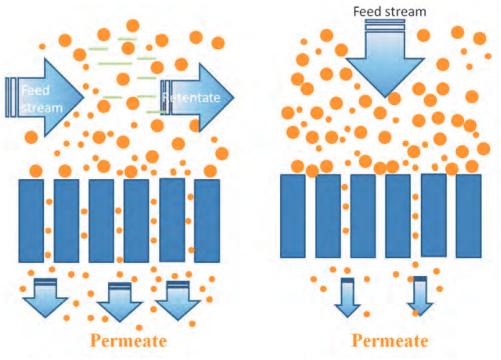

Figure 3.14: Schematic of cross-flow and dead-end filtration configurations. Reprint from [29]

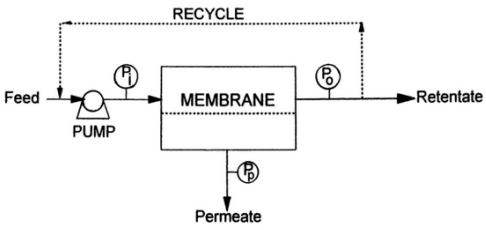

Figure 3.15: Overview of a cross-flow filtration system. Reprint from [20].

phase of oil can foul the membrane by blocking small water droplets from reaching the hydrophilic membrane, since the oil cannot pass through.

Separation of gases using membranes appears to be possible [10], although very few examples of this application are found and membrane units do not appear to be readily available, which might introduce an extra barrier to implementation for this work.

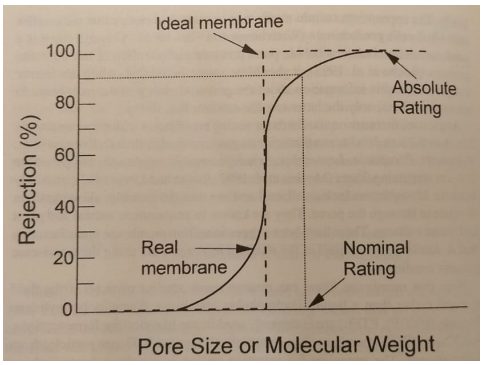

Figure 3.16: Illustration of non-idealities and nominal ratings of ultrafiltration membranes. Reprint from [20]

Coalescing filters While the coalescing of droplets has been discussed in section 3.4.1, it must be noted that filters exist with similar functionalities. These are commonly used in air compression systems [63] and tailor-made to filter out both small solids and small (aerosolized) liquid droplets, which can be useful in DW-2 and DO-1 type separators of figure 3.4. This is usually done by passing the flow through specifically engineered filter materials, presenting a large surface area where a continuous phase can be formed, that allows the roplets to easily adhere in a similar fashion as (plate) coalescers as shown in figure 3.10. As these filters are commercially available, it is considered trivial to discuss them in-depth in this work.

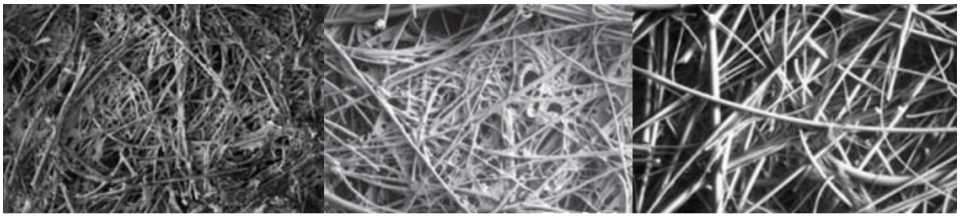

Figure 3.17: Materials for Parker Hannifin Corporation coalescing filters, 500x magnification. Left: grade 2, middle: grade 4, right: grade 8. Adapted from [63]

3.4.3. Sorption-based separation

Desiccant dehumidification Brundrett's book [16] states some advantages of dehumidification in the context of compressed air. Particularly the precipitation of water throughout the system is stated to be detrimental due to a reduction in lubricant quality, equipment lifetime and product purity. This closely corresponds to the problems observed at ZEF. The refrigeration dehumidification method presented in section 3.4.1 is stated by Brundrett to regularly be used to combat this problem. Particularly when used in tandem with a solid desiccant system, very low water content can be achieved with dewpoints reaching as low as -40 to -70 °C. This can be very useful to the ZEF system, as the final stage of the DAC subsystem, cooling the stripped gas beyond its dewpoint to condense the water for the AEC system, essentially is the same working principle as the refrigeration dehumidifier. As stated in section 3.3.2 the partial pressure of water is expected to increase 50- to 100-fold, resulting in fairly high requirements of any pre-processing steps that remove water.

The process of desiccant dryers use the adsorption capabilities of materials such as silica gel and zeolite that the water can adhere to, to be released again at a later time as the material is regenerated. This implies that any of such devices must be able to operate in two modes for both drying and regeneration. Two main categories of desiccant dryers can be identified: first are heated dryers, based on Temperature Swing Adsorption (TSA) which utilise the diminishing capability of the solid desiccant to retain moisture at higher temperatures . The second type are heatless dryers, based on Pressure Swing Adsorption(PSA) which leverage the heat of adsorption remaining in the desiccant after drying, as well as the diminishing capability of the desiccant to retain moisture under lower pressures.

Various setups can be identified, although it seems to be most common for a basic system to operate using 2 vessels that can either be heated (TSA) or depressurized (PSA). TSA systems can also operate using a slowly rotating desiccant wheel, exposing channels to either hot, dry air for regeneration or cold, wet air for drying. Desiccant wheels appear to have gained in popularity in recent years [94], but are not a new concept, as Brundrett already mentions commercially available desiccant wheels in 1987 [16].

Desiccant materials Various materials can be used in desiccant dryer systems, but the materials that are most common for this purpose are silica gel and zeolites or "molecular sieves" [16]. Zeolite is known for its thermal stability, but is also fairly selective towards carbon dioxide, and can thus be excluded from application for the MCS. This appears to be less the case for silica gel, which is more selective towards water [92].

Whereas zeolites tend to show a consistent adsorptive capacity at equilibrium with all but the lowest of ambient relative humidities, the capacity of silica gel scales greatly and consistently with ambient humidity [16] and can reach up to around 35% of sorbent weight [32, 58]. The equilibrium of desiccants and their environment has been described in various ways, starting with Polanyi in 1932. His theory proposes an analytical expression for the relation between the adsorbed amount of gas and the adsorption potential, which depended on the temperature and partial pressure of the adsorbed gas [69]. To the modern day this approach is used to model adsorption processes. For instance, Ambrozek and Nastaj use the Dubinin-Radushkevich equation, which is based on Polanyi's work, as recently as 2020 [5]. It is presented in equation 3.6a, where the two terms indicate the 2 types of adsorption sites, which is the most common approach [58].

$$X_w^* = X_{0,1} exp\left[-\left(\frac{A}{E_{0,1}}\right)^2\right] + X_{0,2} exp\left[-\left(\frac{A}{E_{0,2}}\right)^2\right] \tag{3.6a}$$

$$A = RTln\left(\frac{p}{p_s}\right) \tag{3.6b}$$

where

X^*_w = Equilibrium water content in the solid phase [kg/kg]
$X_{0,n}$ = Parameter related to the total micropore capacity of sites of type n [kg/kg]
$E_{0,n}$ = Characteristic energy of adsorption [J/mol]
A = adsorption potential as shown in equation C.6b

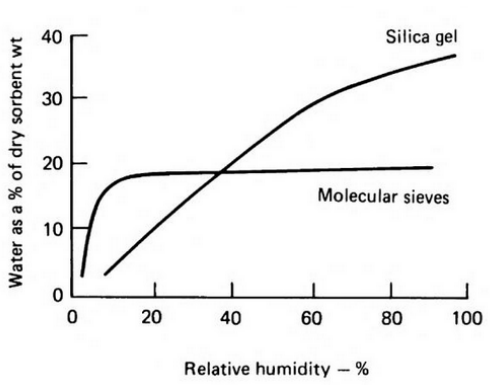

Figure 3.18: "Illustrative equilibrium characteristics for two common sorbents", reprint from [16]

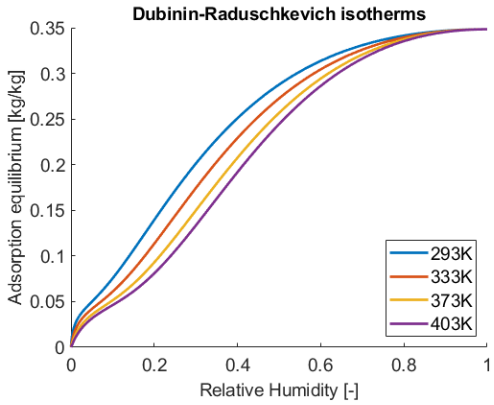

Figure 3.19: Several isotherms for silica gel using the Dubinin-Radushkevich equation and parameters from [58]

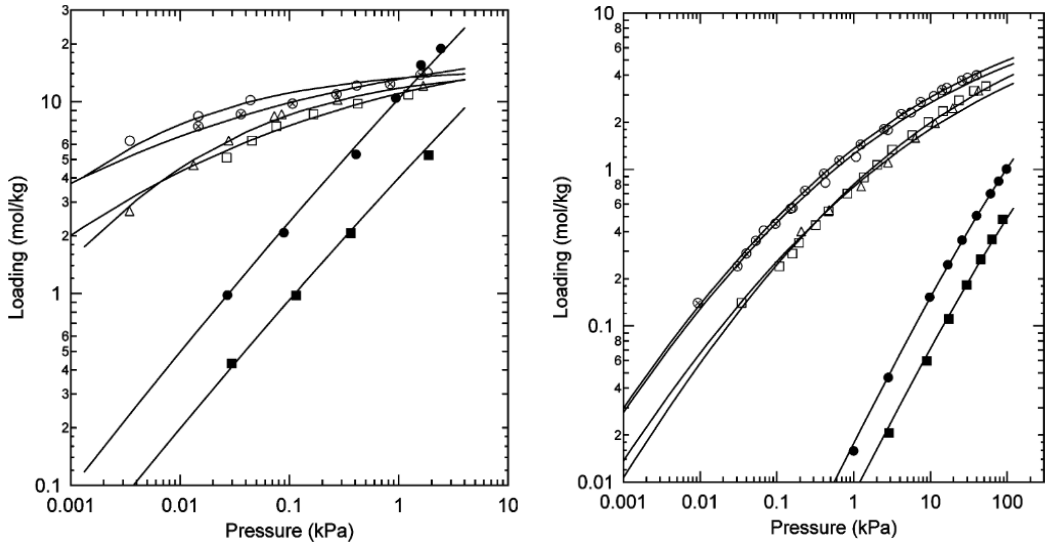

Figure 3.20: Toth isotherms of H_2O (left) and CO_2 (right) for zeolite 13X(○ at 25 °C, △ at 50 °C), zeolite 5A(⊗ at 25 °C, □ at 50 °C) and silica gel (• at 25 °C, ■ at 50 °C). Reprinted from [92]

Oil adsorption In order to clean a water stream from any residual oil, as may be the case in the DG-2 type separators, adsorption can also be considered. Research on the topic shows a fair range of materials that are up for the task, including activated carbon and relatively simple bio-based materials [61, 73, 82]. However, no way to regenerate these materials for re-use has been presented. This greatly limits the applicability of this principle, residing almost fully in the shadow of filtration based systems presented in section 3.4.2.

3.5. Conclusion

This chapter presents a more in-depth look at the theoretical background upon which the development of the ZEF Moisture Control System is based. First and foremost: it is shown that the problem involving three-phase separation, as stated in 2.2, can be viewed as two two-phase separators in series. This realisation leads to the conclusion that all possible solutions to the problem are of either one of three archetypes: the dewatering-type(DW-type) which removes water first, the deoiling-type(DO-type) which removes oil first, and the degassing-type(DG-type) that removes the gas first. Figure 3.4 is a schematic overview of these types and can be reviewed in section 3.1.

The rolling piston compressor employed by ZEF compresses its input, increasing both the temperature and total pressure. As the Dalton model is assumed to apply, this means that the partial pressure

of water is also increased, which increases the dewpoint of the compressed mixture. This increased dewpoint combined with the cooling that is needed between compressor steps or occurs in the CO_2 buffer at night makes it unavoidable to deal with condensation in one way or another.

Should condensation be left unchecked, the compressor will be severely damaged. Droplets of free water compromise the critical functionality of the lubricant, and should this free water contain significant amounts of CO_2, which is nearly a certainty in a H_2O-CO_2 system, carbonic acid(H_2CO_3) is formed, lowering the pH of the water and causing severe damage to the mostly steel components.

When left unchecked, condensed water combines with the fine oil mist expelled by the compressor to form an emulsion that remains stable for several days, as was observed in section 2.1.2. The behaviour of this emulsion can be described by various settling equations such as Stokes' law or the Stokes-Cunningham law and is mostly determined by the droplet size of this emulsion.

Many different separation techniques are available to be applied in any of the six separator types proposed in figure 3.4. Table 3.2 provides an overview of the available techniques, based on these separator types.

DW-1	**DW-2**	**DO-1**	**DO-2**	**DG-1**	**DG-2**
Refigeration dehumidifier	Coalescing filter	Coalescing filter	Coalescing filter	Coalescing filter	Coalescing filter
Desiccant dehumidifier	Cyclone	Cyclone	Cyclone	Cyclone	Ultrafiltration membrane
Gas separation membrane	Basic settling tank	Structure packed coalescer	Basic settling tank	Basic settling tank	Structure packed coalescer
	Ultrafiltration membrane	Packed bed coalescer	Refrigeration dehumidifier		Packed bed coalescer
					Electrostatic coalescer

Table 3.2: Separation techniques available for each separator type

4

Conceptualisation

This chapter will present the process that has been performed in order to find a suitable concept for the MCS. For conciseness, the process will be somewhat shortened, stating only the most relevant developments in the process. Full documentation will be given in appendix B. 4.1 presents the two most promising principal solutions that were made by combining the methods presented in the end of the previous chapter. Two more that were deemed less promising can be found in appendix B.3.

Section 4.2 then presents a brief analysis to roughly estimate the system properties, with section 4.2.1 specifically focussing on a rough estimation of the energy consumption. Finally, a choice between concepts is made in section 4.3 by means of a list of criteria and a Harris profile [13]. The elaboration on the decisions made in the Harris profile can be found in appendix B.4 to prevent this chapter from becoming overly long.

4.1. Principal solutions

This section presents the two most promising principal solutions: combinations of partial solutions that together can form a coherent solutions to the problem [13]. They are based on the knowledge gained in chapters 2 and 3. These principal solutions should not be taken as a definitive analysis, but rather as an early step in the design synthesis process.

Concept 1: delayed condensation (deoiling-type)

- Separator 1: coalescing filter (backup: packed bed coalescer)
- Separator 2: settling tank (backup: cyclone and/or coalescing filter)
- Oil recycling: distributed
- Operation: synchronous with plant
- Cooling configuration: between separator 1 and 2

Short description: this concept prevents an emulsion from forming, relying on the ability of the water to change phase during the transfer from the first compression stage to the subsequent stages. All condensation is to be prevented in the first separator, allowing coalescence of the fine oil droplets that emerge from the compressor, with minimal water contamination present. The second separator then collects the condensed water, removing it as much as possible to ensure maximum purity of the CO2 stream.

Concept 2: Desiccant dehumidifier (dewatering-type)

- Separator 1: heated desiccant dryer
- Separator 2: settling tank (backup: coalescing filter)
- Oil recycling: distributed
- Operation: based on peak power availability
- Cooling configuration: after compressor

Short description: this concept prevents the emulsion from forming by removing the water from the input stream at the very start of the compression system. As the air leaves the DAC system at a

Table 4.1: Pros and cons of the delayed condensation concept

Pros •Prevent emulsion from forming •Low capital costs	Cons •Pressure drop of CO2 •Potential of condensation in and around the compressor and separator 1 •Sensitive to day/night heating/cooling cycle due to reliance on thermal control •Potential degradation of hot oil
Opportunities: •Form integration •Heat exchanger optimisation •Similarity to current developments at ZEF	Dependencies: •Availability of coalescence filters suitable for required operating conditions

relative humidity of 100%, meaning that the dewpoint is equal to this DAC output temperature. When compressed, such a mixture would reach dewpoints that are rather hard to work with as explored in section 3.3.2. Thus, it could be helpful to remove the water before compression, utilising the cooling of the DAC output and desiccant dryer systems in tandem as described by Brundrett [16] and explored in section 3.4.3.

Table 4.2: Pros and cons of the desiccant dehumidifier concept

Pros •Low operating pressure of separator 1 •Potential for heat integration •Reduction of water corrosion potential of hardware •Prevention of water contamination of lubricant (free & dissolved)	Cons •Potentially high energy consumption without heat integration •Potentially requires many components
Opportunities: •Incremental/iterative development •Heat integration, operational optimisation •Take advantage of low mechanical/pressure requirements to design for manufacture.	Dependencies: •Availability of desiccant with correct properties. •Effect on day/night cycle on desiccant •Availability of waste heat

4.2. Concept analysis

In this section, the two concepts presented in section 4.1 will be compared, and one concept will be chosen to continue investigation. A sketch version of a process diagram is made as a first layer of scrutiny and provides a basis for the comparisons. Then, a list of criteria is drafted. Of this list only a rough estimation for the energy usage, as well as any major differences in criteria compliance is presented in this section. The elaborate analysis of the criteria can be found in appendix B.4

This list of criteria is an application of the MoSCoW model presented in section 2.3 and is aimed at uncovering the conceptual difference between the two principle solutions presented in the previous section. The criteria are:

- **Low energy consumption.**
- Reasonably solvable dependencies
- Make-able within thesis time constraints
- Compatible with likely development of the ZEF system and design methodology in the coming years
- Maximise water removal from critical components
- Operation should be compatible with plant operation

- Failure risks should be predictable and allow for mitigation
- Cost should be minimised and enable further reduction in future iterations

The first of these criteria, involving energy consumption, is deemed to be of the highest impact, and is weighed heaviest. It is presented in more detail in the next section.

Assessment of the other criteria can be found in appendix B.4. Most did not yield any major discrepancies, but two differences must be noted. First, the quantity of water that is removed. The desiccant dehumidifier concept is stated to yield mixtures with dewpoints easily reaching -40 °C [16], ensuring hardly any water enters the compression system. In a situation using the delayed condensation concept where both before and after compression, the mixture reaches the same (ambient) temperature, the amount of water remaining in the compressed mixture is one divided by the compression ratio. This also implies that the need to deal with water comes with every compression stage, while the desiccant dehumidifier concept deals with all water up-front in one go.

The other major discrepancy is the one of redundancy as part of the failure risks criterion. A desiccant dehumidifier concept mostly operates passive. So long as the bed is in place and not full, the device works. This provides time to repair or replace any faulty active components in case of malfunction with little to no interruption in operation. The delayed condensation concept does not share this advantage, as any misplaced condensation caused by a malfunctioning component or control system can quickly contaminate lubrication oil and damage components. This requires a shutdown and depressurisation of the system to repair.

Concluding, the minor selection criteria set the desiccant dehumidifier concept up to be favourable, provided no significant discrepancy in energy consumption.

4.2.1. Energy consumption

This section will present a rough estimation of the energy usage of both concepts with some significant simplifications and assumptions and simple formulae. Ideal situations are assumed wherever applicable. Goal of this exercise is not to accurately predict energy usage, but rather to provide an indication of the concepts fall within expectations, and to uncover any major differences between the two.

It is assumed that the main contributors of the energy usage of the delayed condensation (DC) concept are the heating of the filter and heat loss through the walls. The desiccant dehumidifier(DD) concept adds the heat of adsorption to this calculation and replaces the heating of the filter with heating of the desiccant.

It is assumed that both concepts operate at the same ambient temperature of **40** °C, have a CO_2 and H_2O flow of **825** [g/day] and **80** [g/day] respectively. The plant is assumed to operate 8 hours, and since both concepts rely on insulation, it is assumed that both have the same cylinder height, use a **20** [mm] layer of rockwool insulation and cool down to the ambient **40** °C before operation.The diameter of the silica gel cylinder is increased to accommodate the required amount of sorbent. Details on the assumptions can be found in appendix B.5

The formulae used are presented in equation 4.4. Finally, the results are shown in table 4.3.

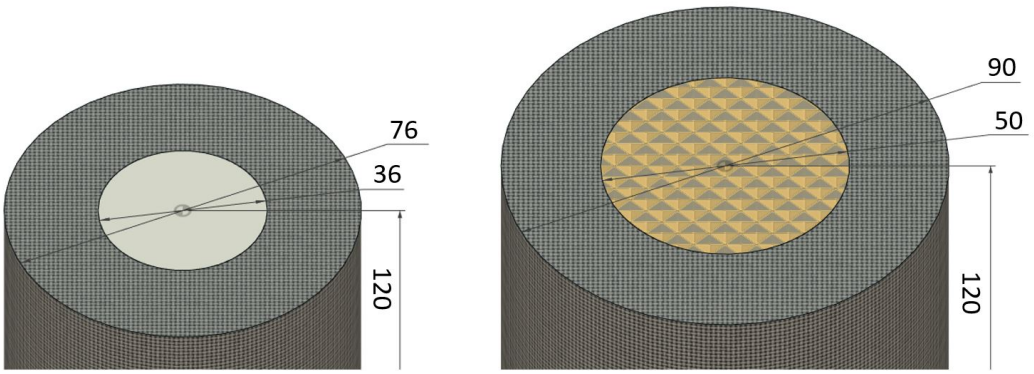

Figure 4.1: Sketch of the DC(left) and DD(right) concept thermal model

$$E_{warmup} = c_p * m * (T_{op} - T_{amb}) \tag{4.1}$$

$$\dot{Q}_{walls} = 2 * \pi * L / \left(ln \left(\frac{(D + t_{ins})/2}{D/2} \right) / k_{ins} \right) \tag{4.2}$$

$$E_{walls} = \dot{Q}_{walls} * (8 * 3600)[s/8h] \tag{4.3}$$

$$E_{ads} = \Delta H * m_{CO_2,daily} \tag{4.4}$$

Table 4.3: Energy consumption of both concepts, per category, in [kJ/day].

Category	DC	DD
Heatup	15.68	36.18
Heat loss	25	30
Heat of adsorption	0	260

It can be seen from table 4.3 that the desiccant dehumidifier scores worse on all categories, but particularly the heat of adsorption is close to an order of magnitude larger than the other expenses. While it may seem obvious to toss out this concept, several things must be noted. First, the energy consumption of the DD concept scales with the water content of the processed mixture, while the DC concept does not, which implies that the DC concept can deal with the water ”for free”. In reality, hardly anything is truly free and neither is this as the heat of condensation increases the duty of any heat exchangers in the compression system. Second, the scope of this analysis is only focused on the system itself, and not with other areas in the plant. It should also be noted that energy consumption due to pressure drop is not included here. As the pressure drop for a filter for the DC concept is provided by the manufacturer, the pressure drop for the DD concept is calculated using the Ergun equation, and the flow rate is known, it is possible to conclude that this quantity is negligible (appendix B.6).

Several factors can be identified that affect the energy usage elsewhere in the plant that might induce a penalty or bonus to this energy consumption:

- The compressor system power scales with the amount of material processed. The volume percentage of water removed from the mixture using either concept should also be subtracted from compressor power. A theoretical estimate was made by ZEF of 2 compressors using 50W each. Tests performed by the FM team during this project indicate that the setup that is currently under development is likely to use significantly more energy.
- In the DC system, the heat of condensation that is released as the mixture is cooled must be dealt with. The consequences of this depend on the system configuration used and might need to be considered.
- The DD system enables the recycling of the water content of the gaseous flow, which might be a valuable resource. While early work at ZEF estimated that the quantity of water coming from the DAC unit would never be a limiting factor, recent work shows that this is not always the case with a poorly performing DAC stripping unit and/or very low moisture content in the air[27]. A possible energy usage penalty for the DC concept must be stated for reducing the overall productivity of the entire DAC system if a situation is encountered where water is, in fact, the limiting factor.

The calculations for these extra factors will not be presented in-depth in this section. They are based on the ZEF flow inventory (appendix A, not included in this work) and calculations in appendix B.4. Energy of condensation is calculated similarly to the energy of adsorption in equation 4.4, replacing heat of adsorption with heat of condensation. Table 4.4 presents these findings.

The main takeaway from this table is that the externalities that come with this system largely dictate its influence on the entire machine. This means that based on these calculations, no concept is clearly more efficient than the other. The quantity of these externalities are subject to change as well, as the compression system energy use is a theoretical estimate of a purpose-built compressor, which differs significantly from the current state of development. The energy use of the DAC is estimated from both theory and experimental work and the method of cooling (and associated energy use) has not yet been thoroughly investigated within ZEF. All of these systems are still in full development, meaning that it must be expected that these numbers can and will vary significantly. Regardless of the concept that is

Table 4.4: Energy consumption of both concepts and their externalities, in [kJ/day]. Optional factors indicated with *

Category	DC	Description	DD	Description
Heatup	15.68		36.18	
Heat loss	25		30	
Heat of adsorption	0		260.8	
Total, device scope	40.68		327.0	
Compressor 1	-0	No material removed	-115.2	8% energy savings, 50W compressor
Compressor 2	-100.8	7% energy savings, 50W compressor	-115.2	8% energy savings, 50W compressor
Total, FM system scope	-60.8		96.6	
Heat of condensation*	180.8		0	
Purge penalty*	216.8	2% of daily DAC energy total	0	
Total with optional factors	433.8		96.6	

chosen, engineering quality and interaction with other systems will likely dictate which system has the lowest energy cost.

4.3. Concept choice

In this section, the findings from the previous sections are combined to form a Harris profile based upon the criteria stated in section 4.2 [13]. This is done to help make the decision on which concept to develop further, alongside several other arguments presented here. Please refer to B.4 for details.

	DC	DD
Energy consumption	**+**	**+**
Dependencies	+	+
Makeability	++	++
Compatible with ZEF development	+	++
Water removal	+/-	++
Compatible with plant operation	+	+
Failure risks	+/-	+
Cost minimisation potential	++	+

Table 4.5: Harris profile based on criteria presented in section 4.2

It can be seen that both concepts score equally in 4 out of 8 criteria, and both appear to receive positive ratings for their criteria. Scoring each + as adding a point, and each - as removing one, the final score is **8** points for the delayed condensation and **11** points for the desiccant dehumidifier concept.[1]

While it was expected that energy consumption would be the leading factor in choosing the concept, the analysis of the energy consumption done in section 4.2.1 implied that that criterium indicated no clear best choice, and indicated that the conditions in which the device operates and interacts with other parts of the factory are the key to designing an optimal Moisture Control System. The question of the optimal choice of concept is still unanswered, as all knowledge gained indicates that both concepts can lead to successful devices.

This leads to the final argument in this decision process: the ZEF company as a whole. ZEF is a company that revolves around quick iterations, and adjusting the overall plant as they go. As this machine evolves over time, so do the components with which the MCS interacts and with it, potentially the optimal technique to design the MCS for that generation of the plant. In order to effectively accomplish this, it is considered very useful to have a broad range of knowledge of various techniques within the company. The short-term project within the FM team of ZEF mentioned in section 2.1.2 that is involved with removing water contamination from lubrication oil is similar to the device proposed in the DC con-

[1] The author considers himself to be a curious and optimistic person. This means that the ratings in this comparison are likely to have somewhat of a positive bias, which should not matter in a head-to-head comparison.

cept, which is a deoiling-type system. Additionally, at the time of writing, the other long-term project includes an analysis of utilising a non-lubricated compressor as a first stage compressor which would open up an avenue into a degassing-type system. Thus, it is considered more useful to the team as a whole to have a good understanding of all three system types of figure 3.4 (deoiling, degassing and dewatering) to add to the toolbox of future ZEF designers. This means that in the coming chapters, the desiccant dehumidifier concept will be investigated further.

To conclude, the rest of this work will involve the investigation of a sorption-based Moisture Control System, rather than a filtration-based concept. The investigation of this chapter indicates that both concepts could be viable. It was expected that the energy consumption of the concepts would be leading in the choice, investigation was inconclusive and instead indicated that the interaction of the device with other components would be leading in determining the energy usage. The desiccant dehumidifier concept is deemed a better fit within the company in order to have knowledge of a broader range of techniques. It is expected that in a rapidly iterating environment such as ZEF, the most value can be gained by adding another tool to the ”Swiss army knife” of its engineers, leading to the choice of a desiccant dehumidifier concept.

5

Modelling

This chapter presents the development of the model used to describe a column of desiccant, such as that which would be used in the ”Desiccant dehumidifier” concept presented in chapter 4. This model is used to verify the experiments performed in chapter 6 and is then used in conjunction with said experiments to design the MCS in chapter 7.

Section 5.1 describes the goals of the modelling efforts and the selection of modelling method. Section 5.2 then presents the details of the selected model that is to be re-created from literature. This is followed by section 5.3 that elaborates the problems, and their solutions, that were encountered during the development of this model. Finally, section 5.4 presents the workings of the model, and compares it to literature. Note that the work in this chapter is done simultaneously with the work in chapter 6 and encompasses a shorter time span.

5.1. Modelling goals and methods

This section presents the modelling methods found that are found to be most suitable for this project, the similarities and differences between these models, as well as the goals in using said models.

As desiccant-based sorption was explored in section 3.4.3, papers were found that describe processes that are very similar to the desiccant dehumidifier concept that concludes chapter 4. Works such as that by Pesaran & Mills [65, 66], Schork & Fair [77] and Park & Knaebel all attempt to devise a mathematical description of this silica gel-based thermal swing adsorption system, and compare it to experimental data.

Further investigation yielded work by Nastaj & Ambrozek[58], supported by the aforementioned paper by Park & Knaebel as prime candidate models to reproduce, and then adjust to accommodate the ZEF MCS concept. Both of these models describe the adsorption and regeneration of water into columns of silica gel. Hot gas is then used to regenerate the column. Several arguments can be made why this particular model is suitable for the job:

- First and foremost, the striking similarity of the process in the 2009 Nastaj & Ambrozek paper to the MCS concept make this a good match. The primary difference between the two appears to be the method for supplying heat, which is considered feasible to adjust.
- The Nastaj & Ambrozek model appears to be relatively easy to implement[1], since their system of spatially discretized ODEs appear suitable for implementation in MATLAB which is the preferred scripting language within ZEF, and is within the author’s experience.
- Nastaj & Ambrozek’s further work in temperature swing adsorption with various materials [57] and pressure-temperature swing adsorption [5] provides an indication that the model’s application is not limited to a narrow set of conditions and can be expanded for further conceptual development.

The following goals are determined for the use of this model:

- Replicate the adsorption process as seen in literature models
- Replicate the desorption process using hot gas as seen in literature models.

[1] As shown throughout this and following chapters, this assumption is incorrect.

- Adjust the desorption using a heater as applied in the experiments outlined in chapter 6
- Re-create one of the experiments outlined in chapter 6 to verify the working of both the model and experiments, and to assess their adequacy as design tools for the next MCS prototype, as described in chapter 7.

5.2. Nastaj & Ambrozek model equations

This section presents the equations that make up model devised by Nastaj & Ambrozek in their 2009 paper [58], their variations and several auxiliary equations necessary to implement the model.

The model is a one-dimensional approximation of a column of desiccant, through which an ideal gas mixture flows. This mixture is assumed to consist of an inert gas and a water component which is considered to be the only component that is adsorbed. The model uses the Dubinin-Raduschkevich equation to describe the equilibrium state, and uses a linear driving force (LDF) model to represent the change towards said equilibrium state. Several other assumptions are listed in the paper.

Three states are central to the model: water content of the sorbent (X_w), water content of the gas (Y_w), and the temperature (T), these will be summarised as "Main states". In order to calculate these states, the Dubinin-Raduschkevich equation as described in equation 3.6a is first used to determine the equilibrium state at a given point. Then, the change in X_w is calculated using the LDF model described in equation 5.1. This value is then used to calculate the changes in Y_w and T as described in equations 5.2 and 5.3 respectively. Equation 5.2 shows that the rate of change of the water content of the gas phase is determined by (from left to right) diffusion, convection and adsorption terms. Equation 5.3 shows that the rate of change of the temperature is determined by (from left to right) thermal conduction, convection, adsorption and environmental heat exchange terms. These values are then used to proceed whatever numerical solver is utilised to solve the system of equations involving these three main states. Calculating peripheral values and auxiliary states are calculated each step where possible.

$$\frac{\partial X_w}{\partial t} = K_w(X_w^* - X_w) \tag{5.1}$$

$$\frac{\partial Y_w}{\partial t} = D_l\frac{\partial^2 Y_w}{\partial z^2} - \frac{J_i}{\epsilon\rho_i}\frac{\partial Y_w}{\partial z} - \frac{\rho_b}{\epsilon\rho_i}\frac{\partial X_w}{\partial t} \tag{5.2}$$

$$\frac{\partial T}{\partial t} = \frac{k_e}{c_\Sigma}\frac{\partial^2 T}{\partial z^2} - \frac{J_i c_{p_g}}{c_\Sigma}\frac{\partial T_w}{\partial z} + \frac{\rho_b \Delta H_w}{c_\Sigma}\frac{\partial X_w}{\partial t} - \frac{4k_w}{Dc_\Sigma}(T - T_\infty) \tag{5.3}$$

X_w = Water content of the solid phase [kg/kg]
X_w^* = Equilibrium water content of the solid phase [kg/kg]
Y_w = Water content of the gas phase [kg/kg]
T = Temperature [K]
K_w = Mass transfer coefficient [1/s]
D_l = Gas diffusion coefficient [m^2/s]
J_i = Mass flux density [kg/(m^2 s)]
ϵ = Void fraction of the bed [-]
ρ_i = Density of the inert gas [kg/m^3]
ρ_b = Bulk density of the solid phase [kg/m^3]
k_e = Thermal conductivity of adsorbent bed [W/(m K)]
c_Σ = Overall volumetric heat capacity[J/(m^3K)]
c_{p_g} = Specific heat of gas phase [J/(kg K)]
ΔH_w = Heat of adsorption of water vapor [J/kg] [2]
k_w = Overall heat transfer coefficient [W/m^2K]
D = Diameter of adsorbent bed [m]
T_∞ = Ambient temperature [K]

The system described by equations 5.1, 5.2 and 5.3 is fairly similar to those used by Park & Knaebel, and primarily differ in their introduction of second order terms in equations governing Y_w and T that represent gas diffusion and thermal conduction respectively. Nastaj & Ambrozek then proceed to change

[2] Note that the paper stated this variable to be in [J/mol], however unit analysis determined that the unit of [J/kg] makes more sense in this context. This is confirmed by prof. Nastaj as presented in appendix C.3

these equations to a dimensionless form by introducing dimensionless variables for space and time: Z and τ respectively.

Then, a spatial discretization is applied to obtain equations found in appendix C.1. This is done in order to divide the bed into N sections, reducing the system of partial differential equations to ordinary differential equations in order to solve them using well-known tools. Note that in the 2009 paper, N = 50 and the dimensionless equations are valid for $2 \leq n \leq N+1$. Equations for input conditions, boundary conditions and additional variables such as heat capacity and gas density are taken from the 2009 paper and can be found in appendix C.1.

While the necessity of calculating the heat of adsorption is made clear from the 2009 paper, the method of obtaining the value is deemed non-trivial and is done in a different fashion with respect to the paper[3]. A variation of the Clausius-Clapeyron equation is used as described in equation 5.4, and assumes an ideal gas. This was first implemented into a MATLAB lookup table using pre-calculated values. Later, this was adjusted to a continuous method by calculating P1 and P2 using the Tetens equation (equation 5.5) at T±0.01 as T1 and T2.

$$\Delta H = \frac{-ln\left(\frac{P2}{P1}\right) R}{(1/T2) - (1/T1)} \tag{5.4}$$

$$P = 0.61078 exp\left(\frac{17.27T}{T + 237.3}\right) \tag{5.5}$$

The method of obtaining some variables is described neither by Nastaj & Ambrozek nor Park & Knaebel. The following methods are used in this work to obtain said values: the gas water content is calculated as the partial pressure of water at a certain temperature and relative humidity. Initially, steam tables [54] were used to calculate these values, but the discontinuities introduced by such a method were found to be detrimental to the model. The Tetens equation as stated in equation 5.5 is chosen as it provides a good approximation in the domain used in this work (10-150 °C).

The calculation of gas water content Y_w is done by means of the ideal gas equation of state as described in equation 3.3. The values are verified using the method described by Pesaran & Mills [65], which yields identical values.

5.3. Model implementation

When building of this model in MATLAB, several difficulties and/or inconsistencies are encountered. This section presents these situations, and deliberates upon the thought process involved in solving and/or circumventing the problem.

Model structure In order to create a script that can be used to solve the system described by section 5.2, it is deemed useful to sketch an algorithm in order to map the dependencies in the equations, which is depicted in 5.1.

The solution will be approached in two stages. First, the spatial solver calculates all states for a specific τ, starting with the auxiliary states that can directly be calculated from the previous main states. Then, the derivative of X_w is calculated by means of the Dubinin-Raduschkevich equation to resolve the dependency in the equations to calculate the derivatives of Y_w and T. The time step is then resolved by the temporal solver, and the process is repeated for the duration of the run. More information on the selection and implementation of the solver, the discretization and calculation times can be found in appendix C.1.

Interim results & gas water content discrepancy When running the model as described thus far, the obtained curves have roughly the same shape as those in the paper, indicating that the model works to some extent. However, the goal is to replicate the models described in literature, which is not yet the case at this point as some discrepancies are found. The overall workings of the model are seen in figure 5.2, showing that wet gas quickly comes into equilibrium and imparts the moisture of the gas to the desiccant in increasingly small quantities before passing through most of the column towards the

[3] Upon further inspection near completion of this work, it is found that Park & Knaebel use a slightly different equation, usually resulting in a 0 to 20% higher heat of adsorption depending on X_w. This is briefly discussed in appendix C.1

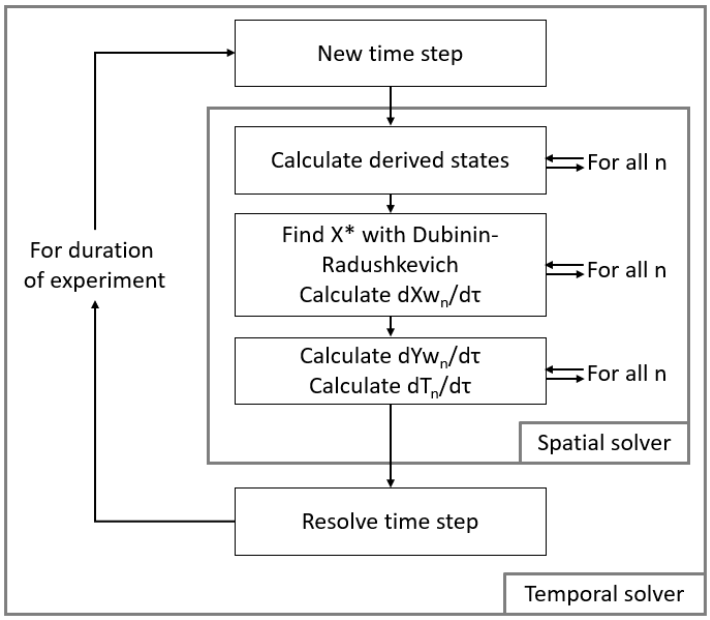

Figure 5.1: Sketch of an algorithm that depicts the interrelation of the model equations.

end in a dry state. As the sections of desiccant begin to saturate, the location where most moisture is adsorbed can be seen to slowly move forward. This also reflects into the temperature-space curves, as their peaks migrate along with the location of the most severe change in gas water content and solid water content, indicating maximum rate of adsorption.

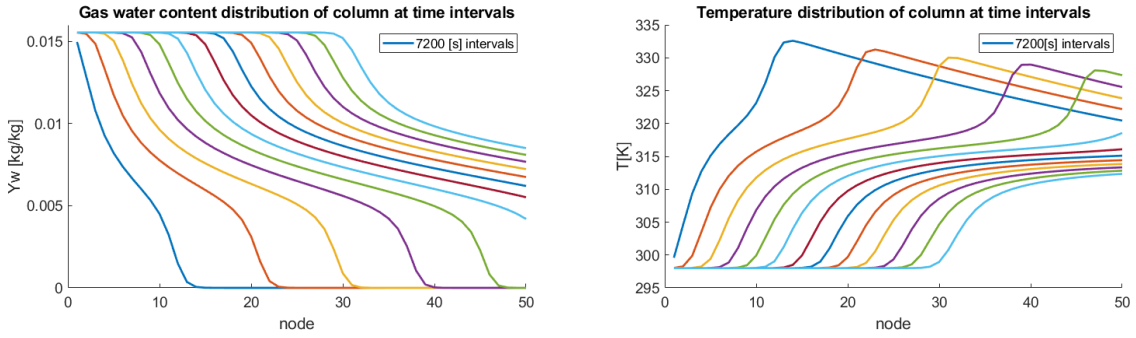

Figure 5.2: Gas water content and temperature distributions within the column at identical time intervals of 7200 [s]

As described by literature, the shapes of the curves show a ”double shockwave” behaviour, and in the temperature curves the effects of convection are clearly seen, as the heat at the peaks is seen to be smoothly ”swept along” the remainder of the column.

However, three discrepancies are still found, which should not be the case, since the values are taken from Nastaj & Ambrozek (2009) [58] as much as possible and should therefore yield very similar results. The first discrepancy is seen in the gas water content as illustrated in figure 5.3 Here, the breakthrough curve is observed, which is the relative humidity and temperature at the last node of the column over time. It is seen that at matching relative humidity, the model in this work breaks through at approximately t = 80000[s] earlier than the model in literature. It is seen that the steady-state gas water content at the end of the experiment, which is considered to be equal to the inlet, is also lower than seen in this work. As the steady-state breakthrough temperature is seen to be 298 [K] in both cases, it is concluded that although temperature, relative humidity and sorbent are equal, the gas water content is still significantly different. Neither paper describes their methods for obtaining these values, but Park & Knaebel’s work cannot be used for verification as they almost exclusively use relative humidity values. Other papers were not found to have describe similar enough situations to make a good comparison. Lowering the relative humidity to a point where Y_w is equal to the value in literature, does appear to

yield a matching result for the time required to reach steady-state, but reveals somewhat of a change in curve shape. However, as seen in literature, some variation in breakthrough curve shape is to be expected for various experimental conditions such as relative humidity.

For now, it is assumed that the method used in this work to obtain the gas water content (Tetens equation), or the method used to convert this to the [kg/kg] unit (based on ideal gas law, verified with [66]) is not identical to that used in the paper. An e-mail is sent to prof. Nastaj, asking what method was used to determine these values in his paper, this correspondence, as well as questions on other topics are presented at the end of this section. Full correspondence can be found in appendix C.3.

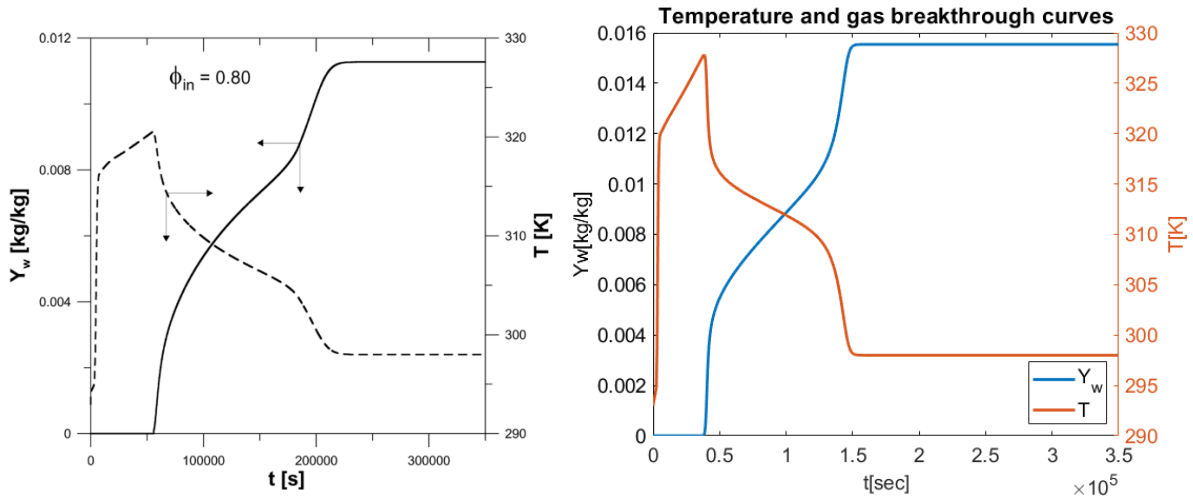

Figure 5.3: Temperature and breakthrough curves, with all known parameters identical. Left: Nastaj & Ambrozek, 2009 [58]. Right: This work.

Thermal conductivity discrepancies The second discrepancy between this work and literature are found in the shape of the X_w-Z, Y_w-Z and T-Z curves. It is seen that this work, while attempting to emulate Nastaj & Ambrozek(2009), the shapes obtained are more similar to those seen in Park & Knaebel (1992), being most pronounced in the T-Z curves. While Park & Knaebel and this work have a characteristic plateau preceding the migrating peak, Nastaj & Ambrozek have a much more smooth-looking approach to this summit. This is consistent with figure 5.3, where the plot from this work also shows sharper curves than the smoother plot from the paper. While investigating what might cause this smooth shape, it was deemed useful to emphasise the difference between the two models. As stated in section 5.2, the new terms introduced in the equations of the 2009 paper are gas diffusion and thermal conductivity. In an attempt to better understand these models and their difference, a test was performed where the differences between the two were amplified beyond reasonable levels to create a clear illustration. Initially, an assumed constant thermal conductivity value of **0.15** [W/(m K)] obtained from literature is used [12, 38], since no values for this parameter are given. This value is then increased hundredfold to illustrate the differences, shown in figure 5.4. A larger version of this image can be found in appendix C.1.

Figure 5.4 shows that whereas the temperature curve with the thermal conductivity from literature is similar to Park & Knaebel, the curves with the exaggerated conductivity are a lot more similar to Nastaj & Ambrozek's. The known dimensions and conditions in figure 5.4 are adjusted to be identical of the respective papers they emulate. This then yields the question how these discrepancies came to be, to which three hypotheses exist. Either a completely wrong value was used in this work, an error was made in creating plots (either in this report or literature), or another unknown difference in modelling method caused these results.

Unit analysis discrepancies Finally, the third discrepancy is uncovered while attempting to more thoroughly understand the models as stated in the previous paragraph. A unit analysis of the models in the papers is done in order to find any errors in building the models for this work. While most equations did yield the expected units, some equations shown in figure 5.5 is found to yield answers for most

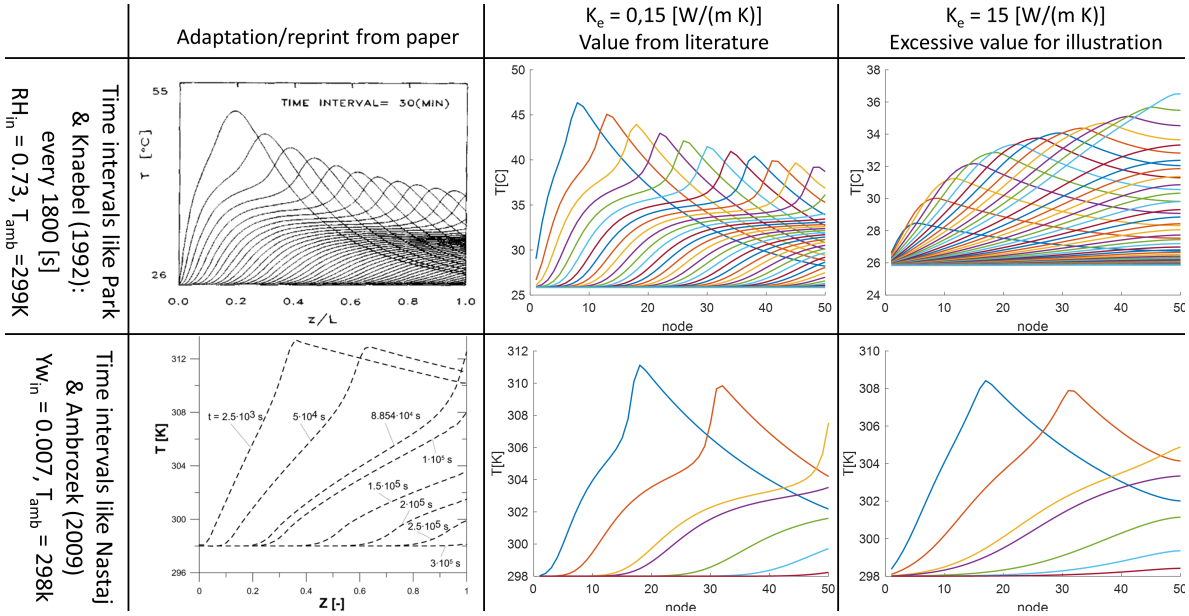

Figure 5.4: Emulation of temperature-space curves at specific intervals from Nastaj & Ambrozek (2009) and Park & Knaebel (1992), as well as a purposeful exaggeration to illustrate the difference between the model, and to highlight the thermal conductivity discrepancy.

terms in [(K m^3)/kg] instead of the expected [K]. The unit analysis done for other equations from the Nastaj & Ambrozek 2009 paper are found in appendix C.2, as the equations governing temperature are the only ones where inconsistencies are found.

$$\frac{\partial T}{\partial t} = \frac{k_e}{c_\Sigma}\frac{\partial^2 T}{\partial z^2} - J_i\frac{c_{p_g}}{c_\Sigma}\frac{\partial T}{\partial z} + \frac{\rho_b \Delta H_w}{c_\Sigma}\frac{\partial X_w}{\partial t} - \frac{4k_w}{Dc_\Sigma}(T - T_\infty)$$

K/s

$$\frac{\partial T}{\partial \tau} = k_e\frac{\rho_{i0}}{J_i\rho_b L c_\Sigma}\frac{\partial^2 T}{\partial Z^2} - \frac{\rho_{i0}c_{p_g}}{\rho_b c_\Sigma}\frac{\partial T}{\partial Z} - \frac{\Delta H_w}{c_\Sigma}\frac{\partial X_w}{\partial \tau} - \frac{\rho_{i0}L}{J_i\rho_b c_\Sigma}\frac{4k_w(T - T_\infty)}{D}$$

K

(K m^3)/kg

$$\frac{dT_n}{\partial \tau} = k_e\frac{\rho_{i0}}{J_i\rho_b L c_\Sigma}\frac{T_{n+1} - 2T_n + T_{n-1}}{\Delta Z^2} - \frac{\rho_{i0}c_{p_g}}{c_\Sigma}\frac{T_{n+1} - T_n}{\Delta Z} + \frac{\Delta H_w}{c_\Sigma}\frac{dX_{w_n}}{\partial \tau} - \frac{\rho_{i0}L}{J_i\rho_b c_\Sigma}\frac{4k_w}{D}(T_i - T_\infty)$$

K

(K m^3)/kg

Figure 5.5: Unit analysis on the equations as found in Nastaj & Ambrozek (2009), with the expected units depicted in green boxes, and other units in red boxes. Note that the middle equation is a dimensionless & non-discretized intermediate form used in the paper, but not presented in this work.

While failing to uncover the source of the other discrepancies, the unit analysis did reveal what

looks like an introduction of the ρ_b (which is not stated in equation C.1a) into most other terms during the step to create the dimensionless equations.

In order to identify any differences between the equations dimensioned & discretized equations are created by combining the dimensioned & non-discretized equations (5.1 through 5.3) with the dimensionless & discretized equations (C.2 through C.4). These equations, depicted in equations 5.6, 5.7 and 5.8 are then implemented. To the author's surprise, no clearly visible differences were identified. Since the cause of the inconsistency is thus unknown, and no obvious cons are found to oppose the dimensioned & discretized version, these equations are used moving forward.

$$\frac{\partial X_w}{\partial t} = K_w(X_w^* - X_w) \tag{5.6}$$

$$\frac{\partial Y_w}{\partial t} = D_l \frac{Y_{n+1} - 2Y_n + Y_{n-1}}{\Delta Z^2} - \frac{J_i}{\epsilon \rho_i} \frac{Y_{n+1} - Y_n}{\Delta Z} - \frac{\rho_b}{\epsilon \rho_i} \frac{\partial X_w}{\partial t} \tag{5.7}$$

$$\frac{\partial T}{\partial t} = \frac{k_e}{c_\Sigma} \frac{T_{n+1} - 2T_n + T_{n-1}}{\Delta Z^2} - \frac{J_i c_{p_g}}{c_\Sigma} \frac{T_{n+1} - T_n}{\Delta Z} + \frac{\rho_b \Delta H_w}{c_\Sigma} \frac{\partial X_w}{\partial t} - \frac{4k_w}{D c_\Sigma}(T - T_\infty) \tag{5.8}$$

Correspondence and conclusion As stated throughout this section, prof. Nastaj and dr. Ambrozek have been contacted concerning the discrepancies between the model and the papers, which can be summarised in the following questions:

- What method was used in the papers to determine Y_w, and can this explain the difference from the Tetens equation-based method used in this work?
- What value was used in the papers for the thermal conductivity? And does this cover the difference with the Park & Knaebel paper?
- What caused the discrepancy in units between different forms of the equations of the 2009 paper? Why do both versions still look identical? What might have gone wrong during implementation of the model in this work? And what might be a correct way forward?

The full correspondence is included in appendix C.3. The answers to the questions and the processing of these comments are as follows:

- In order to determine Y_w, Nastaj & Ambrozek used the Riedel or Antoine equations. Since the Antoine and Tetens equations are both reported to be accurate to within 1% for the used temperatures, it is assumed that the methods used in this work thusfar are correct, despite the numbers not matching up with the paper.
- Thermal conductivity k_e is stated to be calculated using the thermal analogy of the Edwards and Richardson correlation, which is also used to calculate the D_l gas diffusion coefficient. This correlation is displayed in 5.9 and is implemented into the model without much adaptation. As this is an empirical correlation, it is assumed that thermal conductivity values as taken from literature are at least as reliable, and these are continued to be applied.
- The remark on the heat exchange with the environment being the cause of the difference in thermal distribution along the bed has been tested as part of fitting the model's heat exchange to literature data as portrayed in section 5.4
- Finally, several typos have been introduced to the paper during editing. These have been fairly straightforward to implement, and some were already circumvented through the unit analysis and the implementation of equations 5.6, 5.7 and 5.8.

$$D_L = 0.73 D_M + \frac{0.5 u d_p}{(1 + 9.7 D_M)/(u d_p)} \qquad \begin{matrix}(0.008 < Re < 50) \\ (0.377 < d_p < 6mm)\end{matrix} \tag{5.9}$$

5.4. Model results and discussion

With the model being developed to the point of satisfaction, using the ode15s solver and equations 5.6 through 5.8, the experiments described in chapter 6 can be emulated. This section is not intended to compare the model and the experiment, as that will be done in chapter 7, but is rather intended to demonstrate and understand the principles that are expected to be at work during the experiments described in section 6.2 for which several points of interest can be identified.

- Adsorption process, to compare to literature
- Desorption process via hot air, to compare to literature
- Desorption process via external heater, to compare to experiment
- Generic design principles, to implement in experiment and design

Depicted in figure 5.6 is what can be considered to be a typical run in the conditions given in literature. Figure 5.7 then compares the breakthrough curves of this model with those given by Nastaj & Ambrozek and Park & Knaebel.

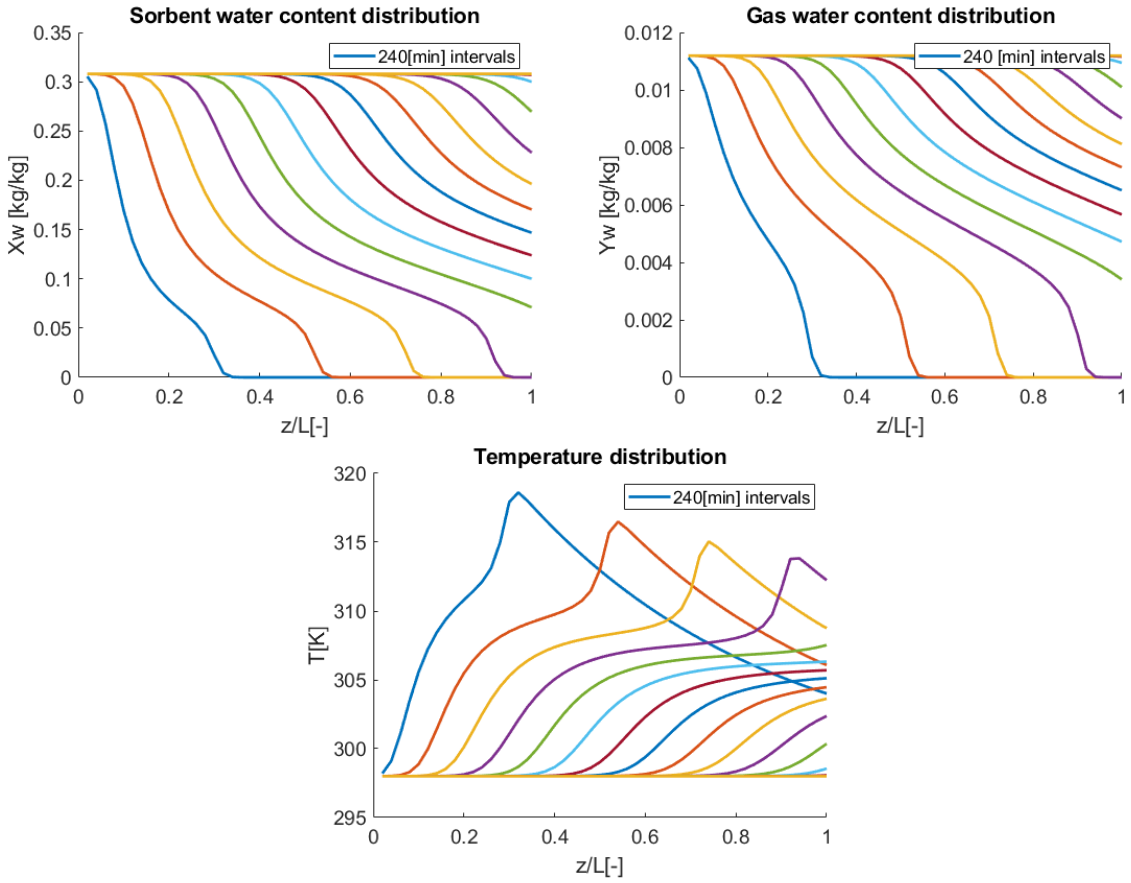

Figure 5.6: The three main states at intervals of 240[min]. Conditions identical to the right side of figure 5.7

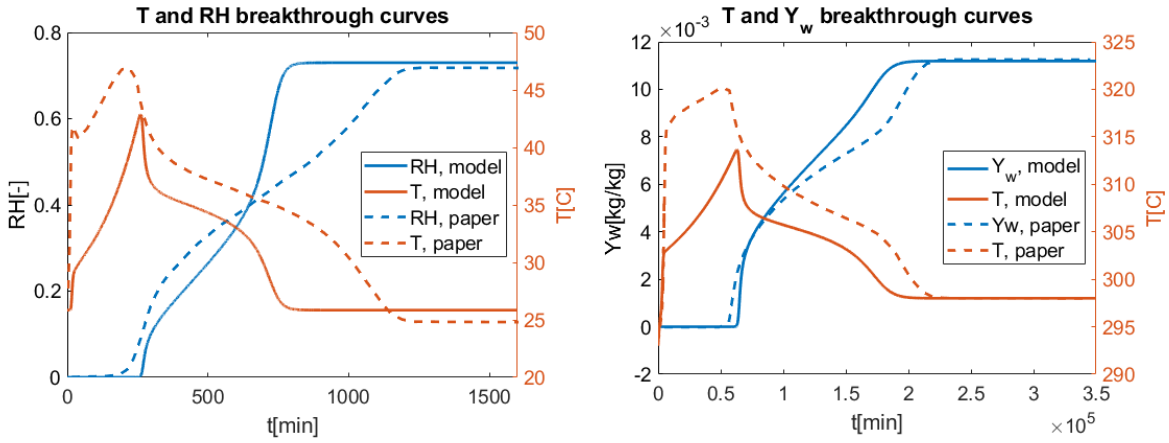

Figure 5.7: Temperature and gas breakthrough curves compared to literature scenarios. Left: this work and Park & Knaebel [62]. Right: this work and Nastaj & Ambrozek [58].

It can be seen from figure 5.6 and 5.7 that the process depicted is quite similar to that in literature [58, 62]. The ”double shock” effect that is thoroughly described in literature is clearly visible in all three images in figure 5.6 and is associated with the locations where the most adsorption takes place. It can also be seen from figure 5.7 that this work, while using equations based upon Nastaj & Ambrozek, yields results that are also similar to Park & Knaebel. The largest difference with literature is the temperature distribution along the column. As the investigation in section 5.3 regarding the thermal conductivity concluded, it is assumed that this work is correct, and that a seemingly sharper profile is to be expected in this work. It can also be noted that in the gas breakthrough curves, the inflections somewhat vary in both location and intensity. In literature, this is associated with both input gas conditions as well as thermal effects [62]. It is therefore concluded that the model in this work adequately describes adsorption.

The process of desorption via hot air also serves as a comparison between this work and literature, and should help to illustrate differences between desorption by hot gas as done in literature, and desorption by means of an external heater as proposed in chapter 6.

The equations used in the model also govern desorption, as hysteresis is not considered in this work [62]. Desorption is modelled by first running the adsorption run, and then a desorption run at **393**[K] as described by Nastaj & Ambrozek, of which the temperature and sorbent water content (T and X_w) are saved, to be then re-loaded in the model in reverse order as to emulate the gas flowing towards the other direction. Figure 5.8b then depicts the temperature distribution curves at identical times to the figure from the paper, shown in figure 5.8a.

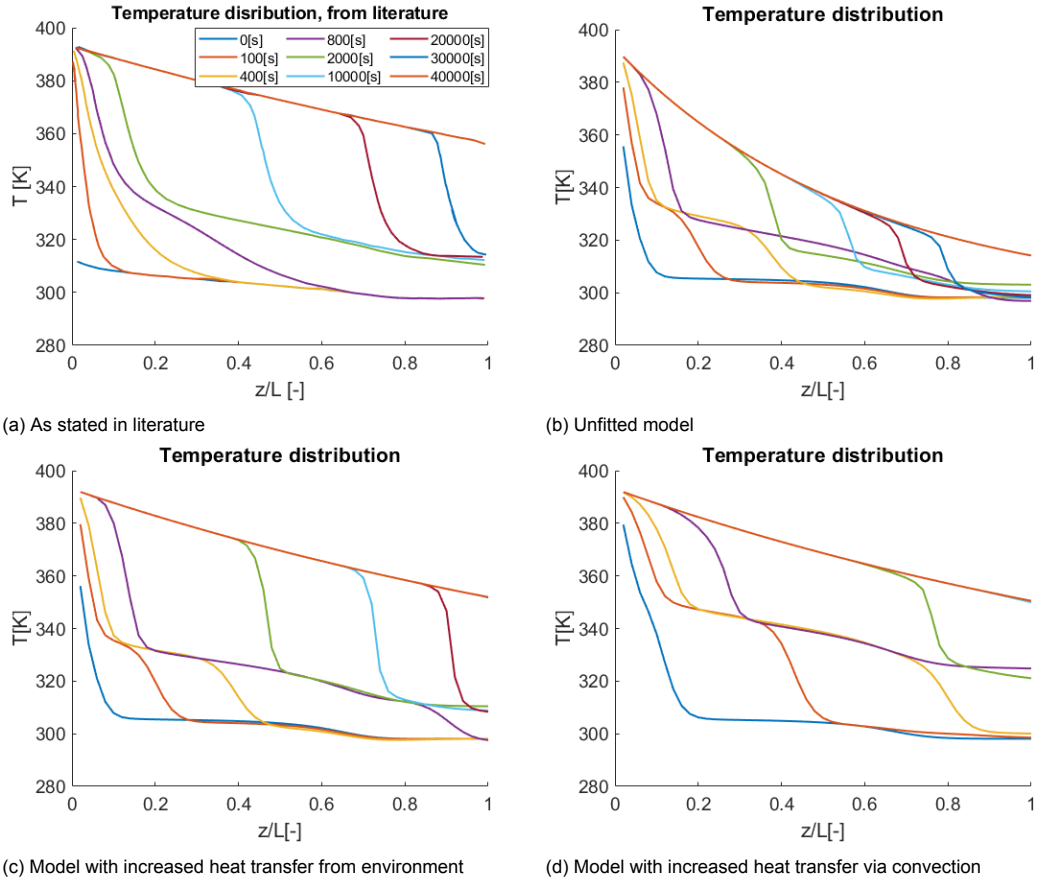

(a) As stated in literature

(b) Unfitted model

(c) Model with increased heat transfer from environment

(d) Model with increased heat transfer via convection

Figure 5.8: Heat distribution curves at specific times comparing literature (a) with an unfitted model (b) and 2 variations (c and d)

It is seen from figure 5.8a and 5.8b that in this work, the temperature drop over the entire column is higher, as seen from the temperature difference between the first and last nodes. Two hypotheses are then tested to identify the parameter that can best be adjusted in order to fit the model to literature. First, the convection term is increased, to allow more heat to move from one node to the next. Second, the ambient heat exchange is reduced, in order to improve heat retention. The results are shown in

figures 5.8c and 5.8d. It can be clearly seen that the adjusting of the ambient heat exchange brings the distribution curves more closely to those from the paper. The ambient heat exchange is subsequently manually fitted to match literature values.

The correspondence from section 5.3 and appendix C.3 state that the diameter is of significant importance for the heat transfer with the environment, which would be of subsequent importance to the operation of the desorption process. In order to test this, the model with ambient heat transfer fitted to literature data is carried out for two adsorption-desorption cycles under the same conditions as the previous paragraph. The first one with a bed diameter of **0.1** [m], the second with only the diameter adjusted to **0.023** [m], which is one of the values Park & Knaebel used [62].

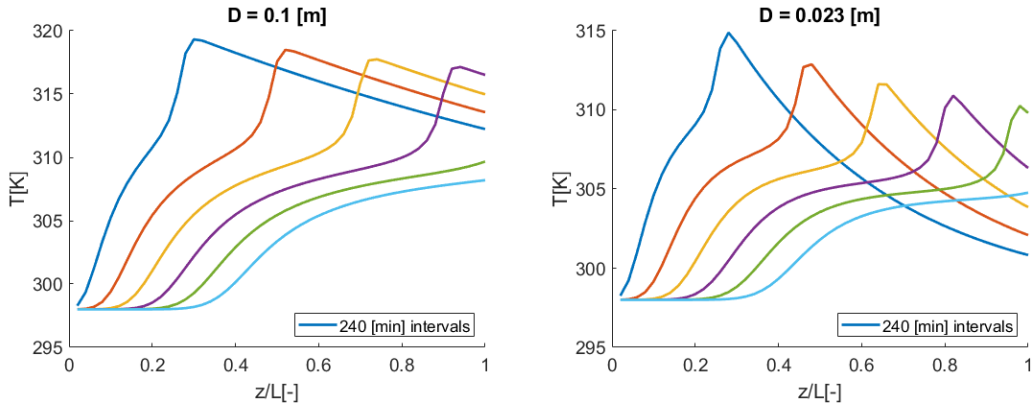

(a) Wide column, as used by Nastaj & Ambrozek

(b) Thin column, as used by Park & Knaebel

Figure 5.9: Temperature distributions at intervals of t = 240[min] to illustrate effect of column diameter. Modelling conditions like 5.8c.

It can be seen from figure 5.9 that the thinner tube, as expected, has an increased temperature drop due to the shifting ratio between column volume (where heat is generated through adsorption) and column area (where heat is ceded to the environment). This relatively faster heat exchange with the environment narrows the characteristic peaks in the Temperature-space diagram. It does not, however, explain why Nastaj & Ambrozek obtain their smooth approaches to the temperature peaks. It is therefore concluded that this model is more similar to Park & Knaebel's results. This strongly reinforces the hypothesis made in section 5.3 that the temperature distributions in this model are indeed, correct. This conclusion is taken as explanation for situations in which the model from this work shows sharper temperature transitions, such as figure 5.8c compared to 5.8a, or figure 5.7.

When combined, these analyses suggest it may be good practice to fit model data to the experiments done in chapter 6, similarly to how Park & Knaebel, as well as Schork & Fair have done [62, 77].

Finally, these results are used to compare heating via hot air as done in literature to heating by means of an external heater as proposed in the concept concluding chapter 4 and the embodiment of that concept in chapter 6 In order to simulate heating via an external heater, the ambient temperature in the model is increased to **393** [K], with the ambient and inlet temperatures being **298** [K], which is a reversal from the hot air desorption model. It can be seen from figure E.1d that the thinner column requires a lot less column length to adopt the higher outside temperature due to the more favourable area to volume ratio. This observation synergizes well with the expected small column size that is expected from the small quantities of water involved in the gas flows of this project. When also observing the sorbent water content in figure 5.11 it is clearly seen that the hot air desorption created a moving front in a similar fashion to the adsorption process, while the desorption with the external heater warms up and desorbs from the entire length of the column. This means that both hot air and external heaters can be used in this desorption process, so long as proper design choices are made.

Conclusion The model used is found to adequately describe the adsorption and desorption processes, both for gas-heated and externally-heated columns, which is the functionality required to emulate the experiments described in chapter 6. These experiments are not yet performed using this model, as it is considered to be good practice to fit the heat exchange with actual experimental data, as was done by some authors in literature. The analysis from this section did provide a better understanding

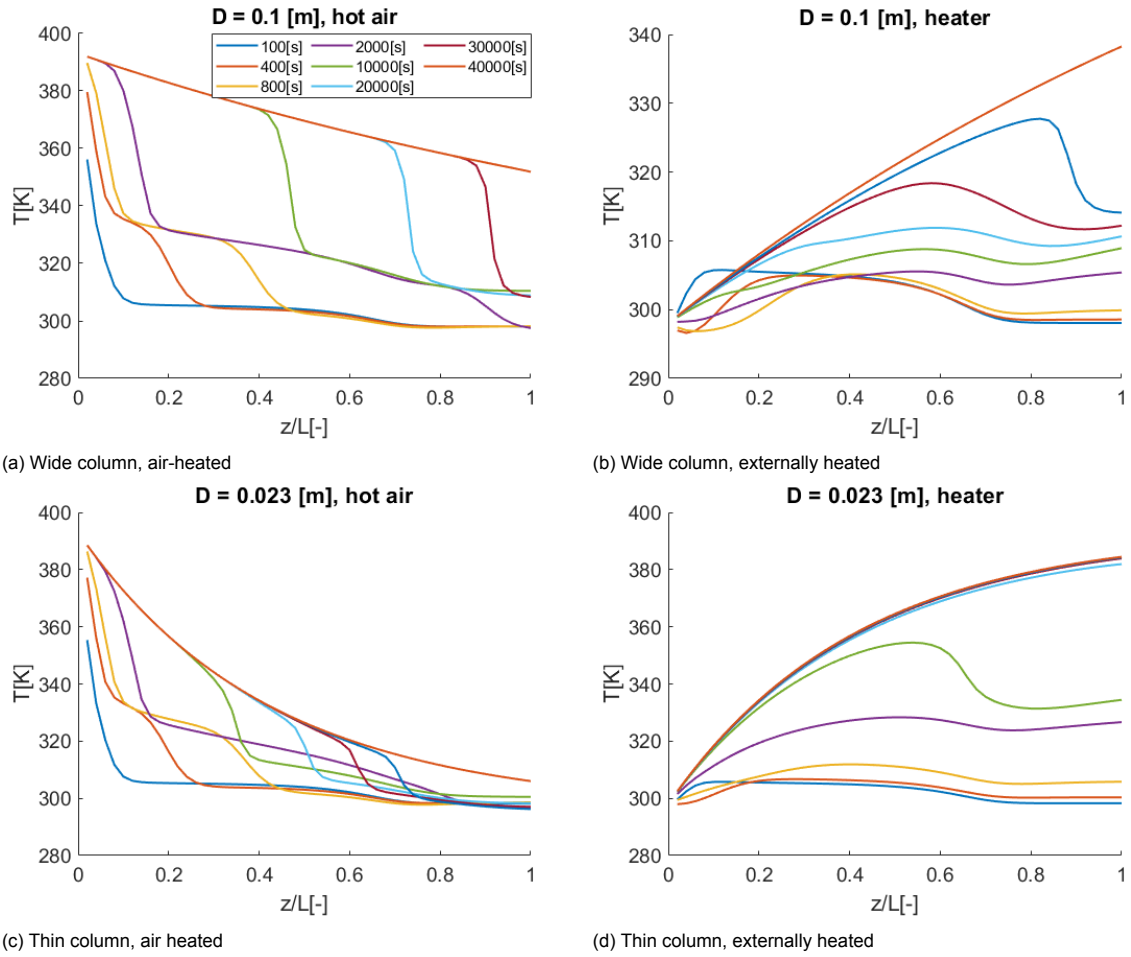

(a) Wide column, air-heated

(b) Wide column, externally heated

(c) Thin column, air heated

(d) Thin column, externally heated

Figure 5.10: Heat distribution curves at selected times during desorption by varying heat sources and diameters. Note how the hot air creates a moving front, similar to the adsorption, while the external heater desorbs along the length of the column.

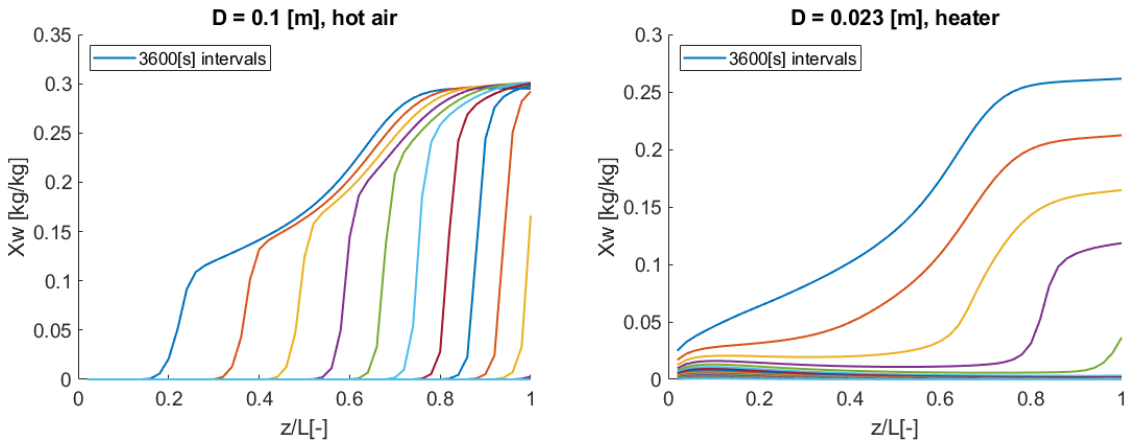

Figure 5.11: Sorbent water content distributions at intervals of t = 3600[s], figures are made from the same model runs as E.1a and E.1d respectively.

of how the model compares to literature and by extension, the experimental data used in literature. However, it is also shown that results such as the location and shape of breakthrough curves, as well as the distributions of heat and mass in the sorbent vary, based on inputs such as relative humidity, ambient temperature and heat exchange both within the column as well as with the environment.

It is also shown that, given the correct design choices, it is possible to use an external heater to regenerate the column, similarly to how this is done with hot air in literature. Given the concentrations and gas quantity involved in this project, using a relatively thin column with an external heater is therefore considered to be a good design choice for the MCS.

6

Experimentation

This chapter presents the development of the ”Dessicant dehumidifier” principle that concludes chapter 4 into an experiment to verify its workings and enables the design of the MCS that will be used in integration testing. Note that the work in this chapter is done in a window of time that encompasses the work done in chapter 5.

Section 6.1 presents the steps made to develop the working principle into a comprehensive concept design. Section 6.2 then presents the steps made to develop the concept design into an experiment. Efforts have been made to create a relatively simple experiment to illustrate the working principle. It is presented in section D.1. The proof of concept experiment, while insufficient, did provide valuable insights into the design of the proper experiment which is documented in section 6.3, further detailing the experiments on desorption and adsorption breakthrough characteristics in sections 6.3.2 and 6.3.2 respectively. This is then followed by the results and discussion in sections 6.4 and 6.5 to conclude the chapter.

6.1. Device concept development

As the previous chapter left off with just the selection of the working principle, additional work is needed to create a complete device concept out of this working principle.

The nature of adsorption processes imply that an adsorption and regeneration step need to take place. If the device is to be operate continuously, this can occur either by redirecting the gas, such as done in a multi-vessel setup, or by redirecting the desiccant itself, as is the case in a desiccant wheel setup.

- The utilisation of a setup in which a single bed is operated discontinuously, as sketched in appendix A.1, was briefly considered. It was rejected as regeneration would have to take place at night to not disturb plant-operations which is a time at which no (solar) energy is available. Utilising the remaining heat in the plant at the end of the day via thermal integration is considered to be beyond the scope of this thesis and is also considered to be incompatible with the current developments of the ZEF system.

- A dessicant wheel-type setup was considered to not yield significant benefits while being considerably more difficult to build in a closed system, which resulted in a preference for a double-column setup. A sketch PFD for this can be seen in appendix A.1 and is similar in layout to ubiquitous examples given by various industry companies, as well as Brundrett’s book [16].

- The double-column setup operates by decoupling the regenerating column from the rest of the machine via the use of two 4-way valves. The isolated regenerating column is then heated as ambient air is blown through by means of a fan. The heating both increases the saturation pressure of water in the air to reduce relative humidity, as well as shifting the adsorption isotherm of figure 3.19, both of which reduce the equilibrium water content of the desiccant and provide a driving force for the drying process.

Upon review, the main issue presented with this double-column concept is the introduction of ambient air into the system. This effectively introduces nitrogen and oxygen in the MS reactor, which is deemed a detriment to its operation and thus introduces the need to purge this air from a regenerated column before switching to active operation. However, utilising the valuable CO_2 to purge the system of air is not desirable either.

This has led to the idea to utilise the CO_2 as a drying gas to regenerate the column. A sketch of this "looped-column" working principle is presented in figure 6.1. A PFD of this concept can be found in appendix A. Similar to the double-column setup, the switching of the columns initiates the regeneration. The concept yet again relies on the double effect of heating: increased saturation pressure and a shifted isotherm caused to improve regeneration speed. A newly introduced constraint is that the water content of the gas leaving the regenerating dryer needs to be higher than that of the gas entering the active dryer in order for this concept to work.

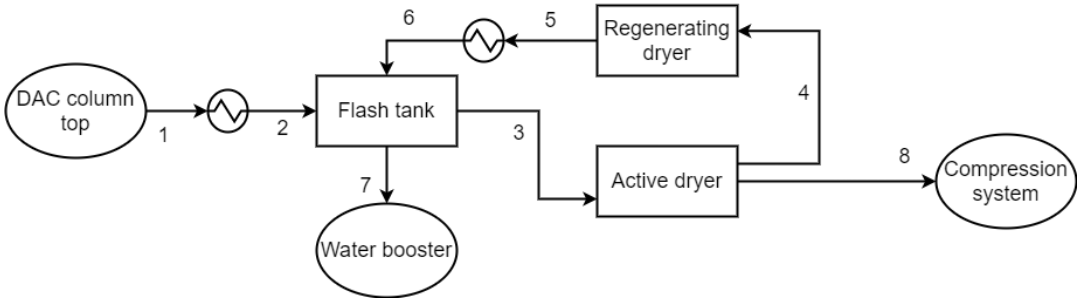

Figure 6.1: Illustration of the working principle of the looped-column setup. A PFD of this concept can be found in appendix A.1

The hot gas that is used for regeneration is then cooled on the way back to the DAC flash tank, condensing the water content into a liquid form. This process of cooling a hot mixture of CO_2 and H_2O is the very same as the one that occurs between the top of the DAC stripper and the DAC flash tank. The cooled gas is then ready to take another pass through the active dryer. The optimal method of operating such a device in terms of gas flow and temperature is not obvious from the literature, and requires further investigation.

A rough estimation for the quantity of gas used to regenerate a column can be made. Figure 6.2 shows an illustration of the water content in a cycle with table 6.1 showing a representative range of input and output conditions. The streams are labelled according to figure 6.1. Figure 6.3 then compares these example scenarios.

Table 6.1: Partial pressure [bar] of water at a selection of potential input and regeneration conditions.

Input conditions [°C]	$p_w = p_{sat}$, 100% RH [bar]		
40 °C	0.07384		
70 °C	0.3119		
Regeneration conditions [°C]	**p_w, 10% RH**	**p_w, 20% RH**	**p_w, 30% RH**
120 °C	0.1985	0.397	0.5955
140 °C	0.3613	0.7226	1.0839

From figure 6.2 and table 6.1, taking into account the Dubinin-Radushkevich isotherms of figure 3.19, some conclusions can be made. While water contents vary significantly depending on assumed conditions, it can be reasonably expected that MCS output water content can be significantly higher than the input water content if in- and output conditions are selected correctly as shown in figure 6.3. Note how regeneration temperature may play a large role in desorption rate. Energy usage of various temperatures should be investigated further by either modelling or experimentation to weigh the benefits of faster regeneration to the costs of more intense heating. Experimentation should thoroughly investigate the desorption rate and desorption gas conditions in order to accurately estimate the performance of this concept.

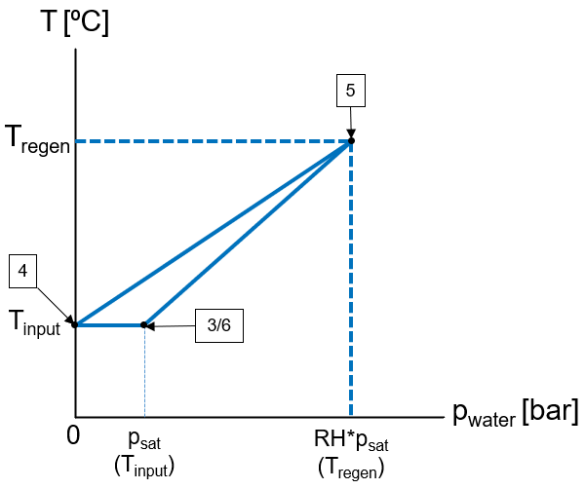

Figure 6.2: Illustration of possible water content in MCS cycle. Values for potential in- and output conditions in table 6.1. Flow labels according to figure 6.1

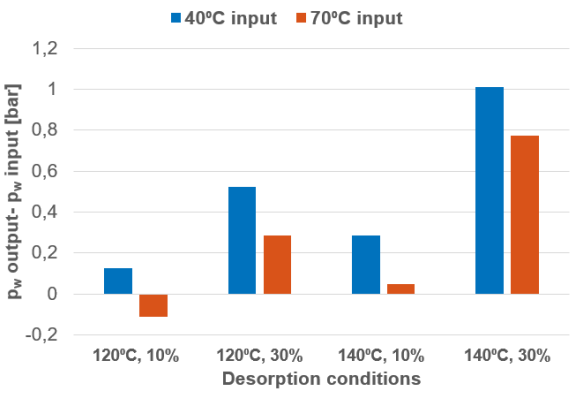

Figure 6.3: Drying potential at a selection of potential input and regeneration conditions (table 6.1

6.2. Experimental concept

As concluded in the previous section, determining the desorption characteristics of the looped dryer concept is vital to its performance. As a rule of thumb, the concept only works if the desorption process happens at a faster rate then the adsorption process. If it does, one might choose whether to utilise all dried gas to regenerate the column as fast as possible, or to utilise a fraction of the gas to regenerate the column over a longer period of time.

Figure 6.4 shows the PFD for the experiment. It can be seen that this experiment is conducted in two phases, the adsorption phase and the desorption phase. The working principle is to dry a known quantity of gas with a known (high) water content. Then, the same gas is used to regenerate a previously loaded column. After loading the first column, the columns can be swapped for each experimental run to perform adsorption and desorption simultaneously. The regenerating column is equipped with a heater to create the required regeneration conditions. The water content is measured at various points throughout the process using relative humidity sensors.

The experiment uses all dried gas for regeneration, this is done to improve control over experimental conditions. If it is assumed that equilibrium between the gas and desiccant forms quickly the gas composition should be unaffected by flow rate, meaning that this choice does not influence the outcome of the experiment. Similar techniques are used in literature such as Nastaj & Ambrozek's use of dimensionless time in their models [58].

6.3. Experiment design and experimental method

This section will present the design of the experiment and methods used to conduct the experiment. The proof of concept experiment as described in appendix D.1 has been performed prior to this design, and experience gained from that design process is used in this design as well. Several requirements that are introduced with the experiment design, on top of those already in place in the proof of concept experiment(appendix D.1), are as follows:

- Temperature-controlled chamber in order to equalise ambient conditions across experiments and to increase partial pressure of water entering the adsorbing column, thus improving experiment speed and similarity to ZEF use case.
- Reduce or eliminate the effect of condensation on sensor readings to accurately determine gas water content throughout the system.
- Addition of a mass-based redundant measurement method to verify relative humidity data.

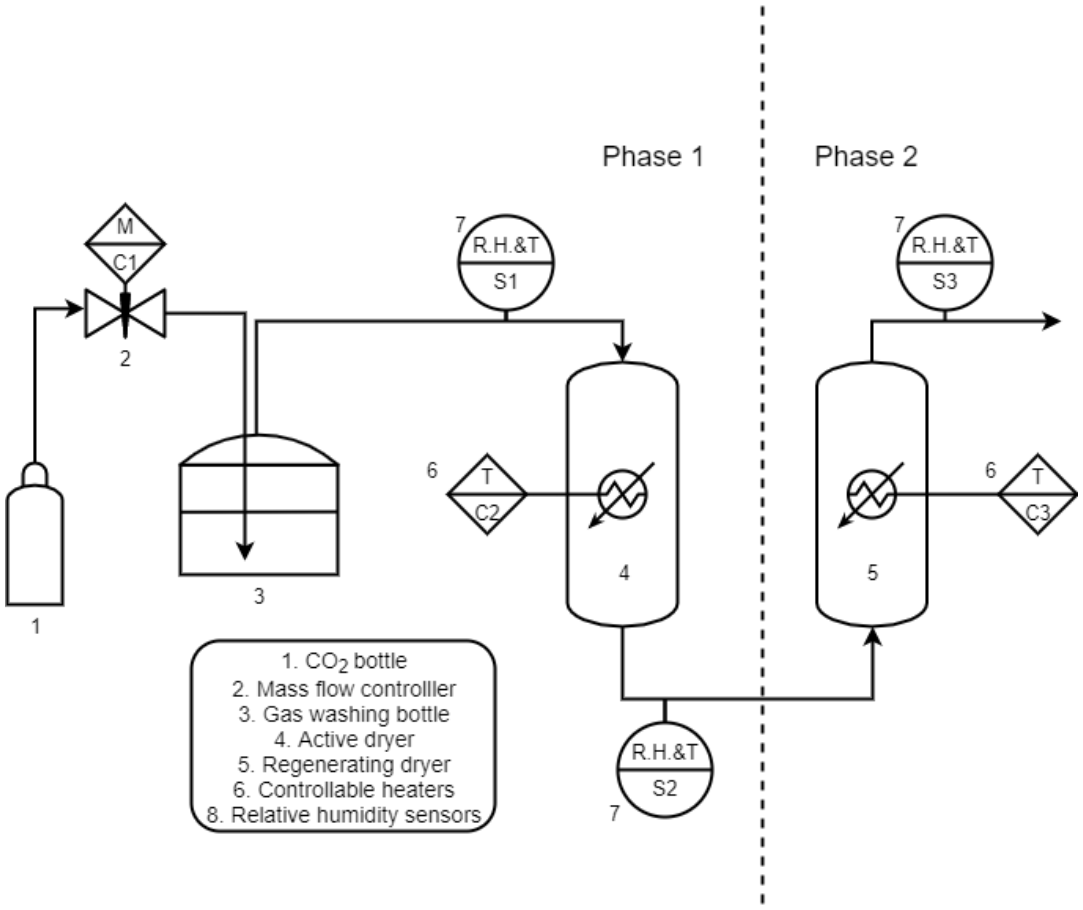

Figure 6.4: PFD of the experimental concept

6.3.1. Redesign of test setup

The new design of the experiment starts with the design of the columns. A heated chamber can more easily be realised in a more cubic aspect ratio, compared to the relatively tall proof of concept setup. As glass tubes are only available in certain sizes, the inner diameter of the column was increased from **24** [mm] to **35** [mm], with a length of **250** [mm]. This comfortably accommodates **50** to **150** [g] of sorbent while still maintaining a sufficient aspect ratio to develop the flow [78] and enables some flexibility in the placement of sensors and cables. The primary material for this casing is chosen to be **9** [mm] plywood due to its availability, good thermal properties and ease of processing with laser cutters. The flat panels are combined into a structure by use of connecting components[1], made by use of 3D printed PETG. This method is also used to create interface parts for the equipment and enables versatility in the machine by means of iterative design. PETG(PolyEthylene Terephthalate Glycol) was chosen as it is more temperature-resistant than the more commonly used PLA (PolyLactic Acid), being able to withstand temperatures of **70** [°C], whereas PLA should operate below **40** [°C]. Plexiglass windows are added to the design, made of 3mm double-pane panel in order to both reduce material use (and thus cost) and to improve isolating capabilities. Appendix D.2 presents a rough estimation of the sizing of the columns and casing.

A CAD design of all components is made in Fusion 360. The main casing is divided into three parts: the heated chamber, the base upon which it sits and the hood that can be placed over the chamber. First, a sketch of all equipment that should fit into the heated chamber is placed inside in order to confirm the sizing. Then, a detailed design of all parts is made and placed in suitable places. Interfaces in and out of the heated chamber are made to connect hoses to and lead cables through. Equipment that needs to be accessible during operation, or does not require an elevated operation temperature such as the mass flow controller or power supply are placed in the base. The

[1] Inspiration for the method of joining laser-cut panels and other components is taken from flat-packed furniture.

main electronics board is the same ZEF prototyping PCB as used in section D.1 which accommodates relays, serial/I²C communication, NTCs and more and is controlled by an Arduino Nano. It is placed on the outside of the chamber to reduce cable length to the sensors, which reduces the probability of glitches in the I²C communication. The software used for communication with the sensors is mostly based on open-source libraries, specific for those sensors. Arduino's "Wire" library is used to facilitate the I²C protocol, which has been modified to introduce a time-out functionality. The time-out enables the control board to re-try to open communications with the sensor in case no reply from the sensor is received. It is hypothesised that one source of software freezes in section D.1 and other ZEF setups is a glitch in communication, causing both the sensor and the Arduino to indefinitely wait for the other to start sending data. Observations on both this setup and other setups at ZEF report a (near) elimination of these seemingly random software freezes.

The ZEF PCB software utilises a 2-stage control scheme: a fixed-duration control stage, and a variable-duration data exchange stage. During the data exchange stage, data from all sensors is gathered and reported to the Arduino, which calculates the duty cycle for both heaters(D_a and D_b) for the next control cycle based on a PD-controller (proportional-derivative controller). Then, during the control stage, heaters are switched on for the duration of the duty cycle, multiplied by the control stage duration, which is chosen to be 2 seconds. A schematic overview is given in figure 6.5.

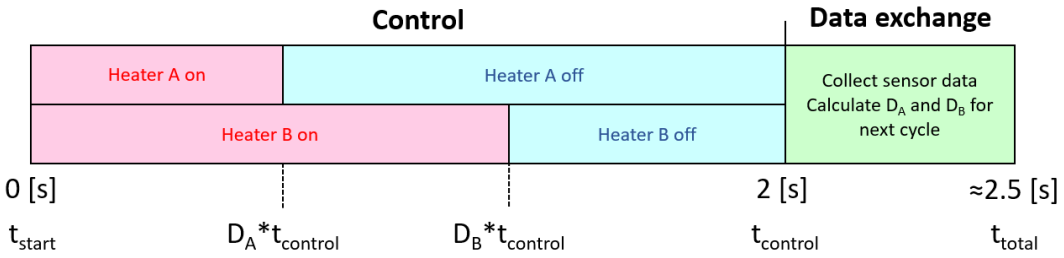

Figure 6.5: Illustration of the control scheme of the ZEF PCB

The Honeywell HIH6100 series sensors are included in the design and housed in the casing shown in figure 6.6. This sensor is chosen due to its similar price and availability as the Telaire ChipCap 2 sensors used in appendix D.1, but trades the ChipCap's high max operating temperature for the capability to operate in condensing environments[2]. Both sensors have a similar ease of use in being factory-calibrated and utilising I²C communication. The sensor placement at first was relatively similar to the previous experiment with the first sensor just after the gas washing bottle, the second on the dry side in between columns, and the third at the exit. A fourth sensor is added to monitor the ambient conditions within the chamber. It is placed in an opened housing to accommodate air flow. In a later stage, both columns were also equipped with a ChipCap sensor on the bottom of the column, by means of placing a fiberglass-mesh covered piece of stainless steel tube over the sensor to support the sorbent. This is done to measure the humidity very close to the sorbent, before interaction with the ambient environment occurs, to get an undisturbed image of the gas going in and out of the system.

As the hot gas leaves the regenerating column, it is quickly led out of the chamber, where it passes through a simple condenser, composed of an aluminium tube to facilitate heat exchange with the environment and a bottle where the condensed water is caught. This bottle will then contain most of the condensed water, and could be weighed and combined with the gas water content of the output to verify the mass balance of the system.

Attention is given to the redundancy of measurement methods. As the previous experiment exposed the vulnerability of only relying on one type of measurement, both mass and gas water content is measured in the system. This is done both at the start and end of an experimental run, but also live, as the regenerating column is to be placed on top of a PCE-BSK 1100 weight scale. This scale also reports its values to the Arduino, passing through an RS-232 to TTL converter to reduce the voltage of the signal to acceptable levels for the Arduino.

The chamber's ambient heater is made out of a repurposed 12V heater, intended for use as a buildplate heater in a generic 3D printer.This aluminium heater is combined with a 120x20mm 12V PC fan which is mounted on a bracket in front of the heater, circulating the air inside the chamber to

[2]The Honeywell HIH8100 series can do both, but was unavailable at the time of ordering

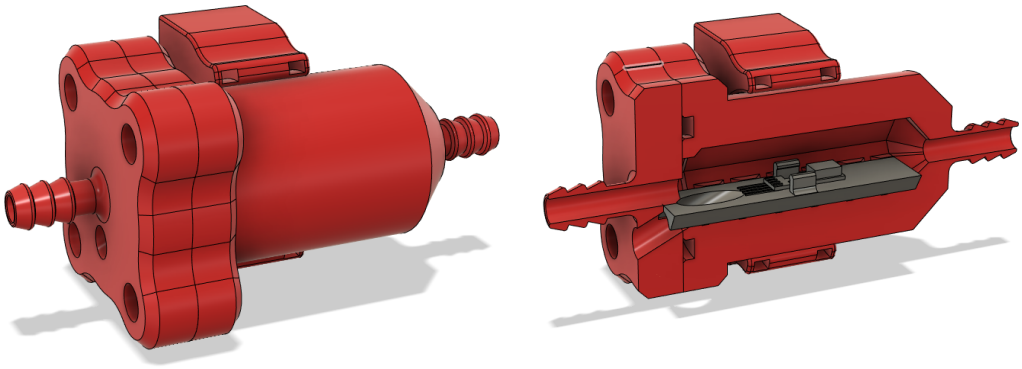

Figure 6.6: Casing for relative humidity and temperature sensors, including a section view. A Telaire ChipCap 2 sensor is depicted inside. Both images do not include cables and connectors.

homogenise the temperature. This hardware is chosen due to its low cost, high availability and ease of use. Unit testing the heater assembly shows that both power and heat transfer requirements are met.

The column heater is made of an aluminium tube with a generic ribbon-shaped silicone pad heater wrapped around. The inside of the tube is spray-painted black to improve radiative heat transfer to the column, as the larger diameter of the caps of the column introduced a small air-gap between the heater and the glass body of the column. The column then rests upon an interface part that seats it on the weight scale, which is shown in figure 6.8

Figure 6.7: Assembly that is used to house the regenerating column. The column can be placed by removing the lid. The assembly is fitted with a silicone heater ribbon and rockwool isolation sleeve that is not depicted on this image.

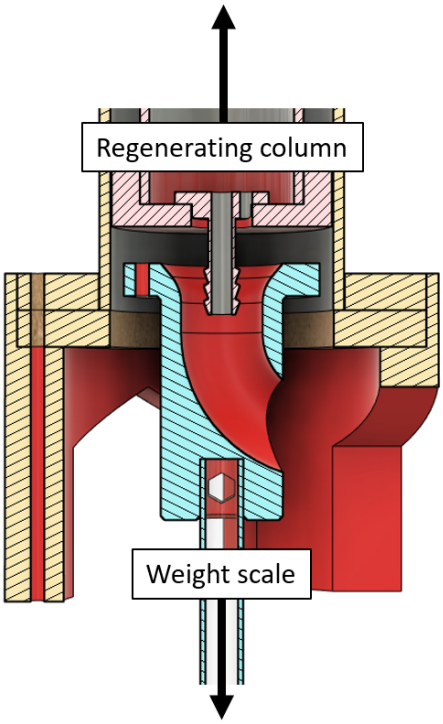

Figure 6.8: Cross-section of the interface part of the regenerating column, enabling it to be seated within the heater, fully resting on the weight scale, while providing connectivity and stress-relief options for connecting hoses and cables.

During tests of this feature, it was found that the weight scale continuously drifted at an unacceptably high rate as the column experiences any radial forces introduced by leaning the assembly against

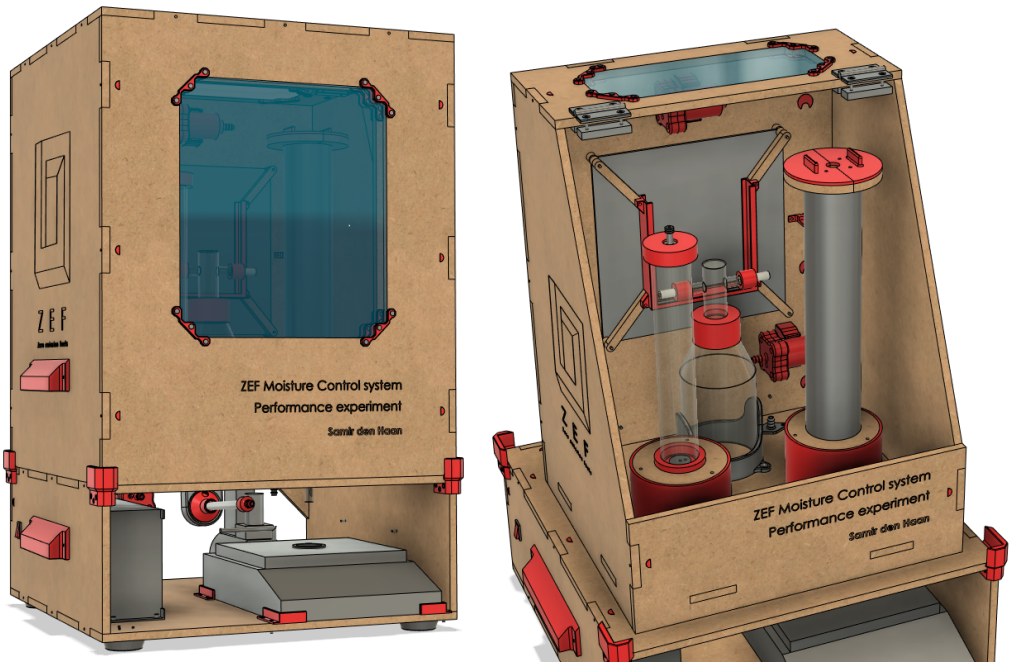

Figure 6.9: Left: CAD model of the machine's assembly. Right: The equipment inside the chamber is displayed by hiding the hood and top-hinging door of the CAD model.

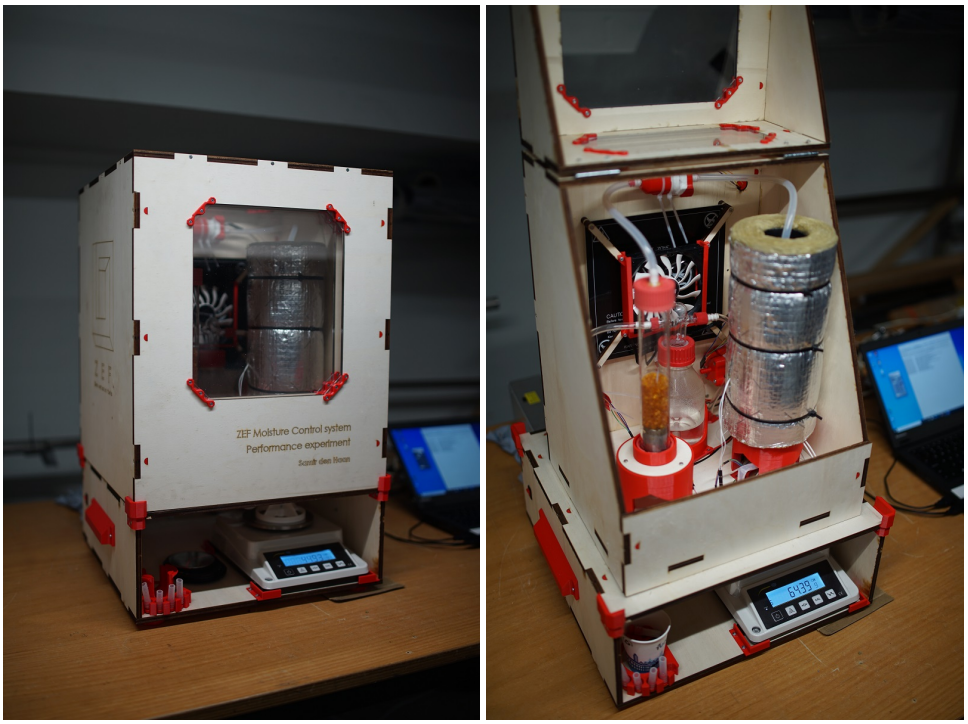

Figure 6.10: The fully assembled machine as depicted in the model of figure 6.9

the heater tube, while it was expected to quickly reach static equilibrium and stabe scale values. Therefore, rather than separating axial and radial forces as done with the earlier interface part, it is deemed necessary to adjust this interface to be more of a standalone platform. This allows the entire column to remain balanced on the interface, without introducing any other forces. The adjustment included reducing the diameter of the column caps on a lathe in order to allow the full column assembly to stand

detached from the heater tube. This introduced an even larger air-gap in the heater, increasing expected heater losses. Tests of this part have indicated that the nominal temperature of **120** [°C] could still be attained within reasonable times. Therefore this setup is considered to be adequate. The setup is placed on a stable table on a stable floor in order to reduce vibrations of passers-by, which would otherwise be picked up by the scale.

Finally, several aspects concerning usability and ergonomics are considered. This includes, but is not limited to a column idler that is designed to hold an entire column upright, including cables, in order to easily and consistently weigh it before and after runs. Handles are included to the hood to easily place it on top of the setup, as well as to the base, enabling a single person to carry it to a new position such as a fume hood, should that be required. A laser engraving with the company logo and experiment title is added as a finishing touch.

6.3.2. Desorption experiment method

The first experiment can be considered an improved version of the proof of concept experiment described in section D.1. The adsorption/desorption is run for fixed periods of time before switching the columns and repeating the process. This experiment has the following goals:

- Develop an overall insight in the performance of the system, confirm consistent system behaviour and gather preliminary data on the KPIs stated in section 6.1.
- Quantitatively determine the gas composition at the adsorption input, the section in between columns containing the dried gas, and at the desorption output.
- Determine the state of the desiccant from observation.
- Determine the degree to which the wet input gas can be dried.
- Determine the degree to which the desiccant can be regenerated, as well as determine any significant changes in characteristics during the first few cycles.
- Both qualitatively and quantitatively compare the weight scale and relative humidity sensor methods to continuously measure the desorption rate.

Before starting the experiment series, both columns are weighed on a VOLTCRAFT PS-750 letter weighing scale. This scale was used for all weight measurements outside of the machine. Then, both columns are filled with **100** [g] of generic silica gel with indicator of **3 - 5** [mm] particle size. The indicator changes color from orange to blue as the loading increases. The gas used for the experiment is nitrogen, for the same reasons explained in section D.1. The mass flow rate is set to **1** [ln/min] The PFD for this experiment is shown in figure 6.11.

The procedure for an experimental run is as follows:

1. The gas washing bottle, condenser assembly and both columns are weighed. Then, they are placed in position and connected to the appropriate hoses and cables.
2. The chamber is closed and the hood is placed over the chamber.
3. The ZEF GUI, FlowDDE and FlowView software is started. The ZEF GUI is used to check if the sensors are responsive and send nominal values.
4. The fan is switched on, and the ambient temperature is set to the desired value, which is chosen to be **40** [°C] to mimic the ZEF use-case. Then, the experiment is left to pre-heat for **30** minutes.
5. FlowView is used to switch the gas flow on at the desired rate. This is chosen as t=0. The column heater is set to the desired temperature. The experiment is left to run for **120** minutes.
6. The flow is stopped, both heaters and the fan are switched off, the hood is removed and the chamber is opened. The columns, gas washing bottle and condenser are weighed.
7. The setup is then left to cool at least until all temperature sensors indicate room-temperature values.

6.3.3. Breakthrough experiment method

The second experiment is intended to observe desiccant behaviour across a wide range of sorbent loadings, as well as to observe the device's behaviour when a column is full. It is also intended to serve as a link between models developed in chapter 5, experiments from literature, and this work. The following goals for this experiment can be determined:

- Observe breakthrough behaviour of the column to determine the duration of a sufficient level of operation.

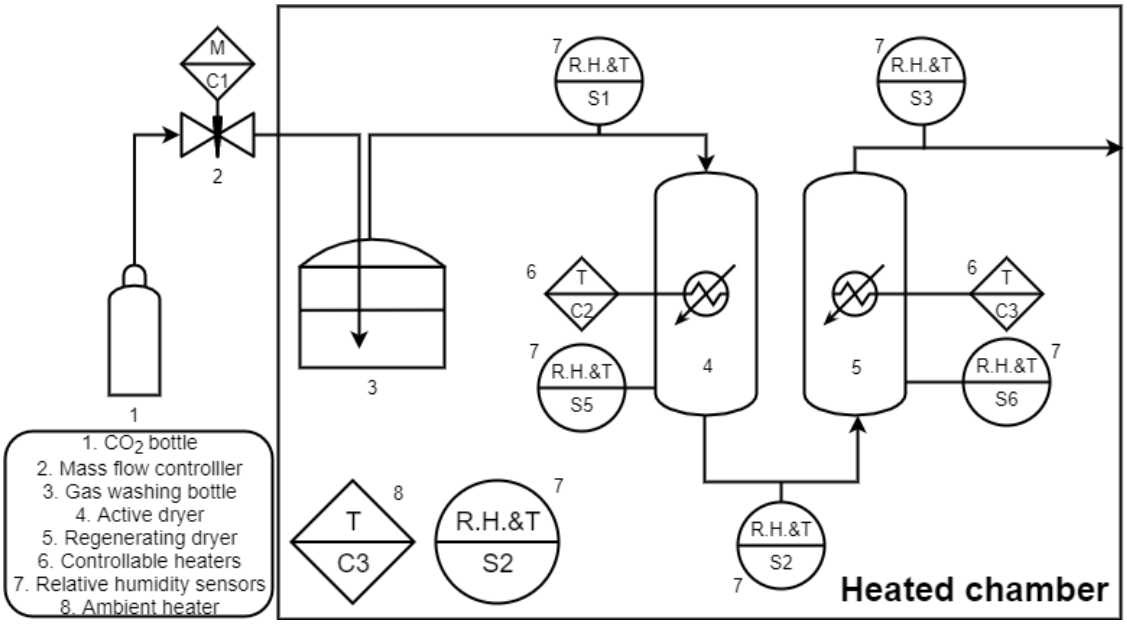

Figure 6.11: PFD for the desorption experiment

- Create breakthrough data such as seen in figure 3 of Nastaj & Ambrozek(2009) [58] and figure 5 or figure 6c of Park & Knaebel (1992) [62], in order to compare this system to those in literature.
- Gather additional data to determine the KPIs stated in section 6.1.

The same equipment is used as in the experiment in section 6.3.2. The quantity of sorbent is reduced to 50g in order to enable the completion of a run within reasonable time. The 3-5mm material with indicator which is used in the desorption experiment is also used in this experiment. However, as elaborated upon in section 6.5 it has been decided during analysis of the data of this experiment to also use a generic silica gel without indicator and a 0.5-1.5mm diameter particle size as this material is more similar to the sorbent used in literature [58, 62]. The mass flow rate is set to 0.6 [ln/min], which is the minimum rate attainable with this mass flow controller. The PFD for this experiment is shown in figure D.4.

The procedure for an experimental run is as follows:

1. The gas washing bottle and adsorbing column are both weighed. Then, they are placed in position and connected to the appropriate hoses and cables.
2. The chamber is closed and the hood is placed over the chamber
3. The ZEF GUI, FlowDDE and FlowView software is started. The ZEF GUI is used to check if the sensors are responsive and send nominal values
4. The fan is switched on, and the ambient temperature is set to the desired value, which is chosen as **25** [°C] to mimic the papers upon which the model is based [58, 62]. Then, the experiment is left to pre-heat for **30** minutes.
5. FlowView is used to switch the gas flow on at the desired rate. The experiment is left to run until the relative humidity of the dry side appears to no longer change significantly.
6. The flow is stopped, the heater and the fan are switched off, the hood is removed and the chamber is opened. The column and gas washing bottle are weighed.

6.4. Desorption experiment results & discussion

The experimental data is gathered approximately every **2.5** seconds via the ZEF GUI. The types of data gathered from sensors is presented in table 6.2. The power consumption of the column heater and ambient heater are estimated by using the duty cycle data as described in section 6.3.1 and can be seen in appendix E.3.

The repeatability of the VOLTCRAFT letter weighing scale is tested by taking 20 pairs measurements found in the test results that weigh the same object. The error averages at μ = **0.025** [g] with

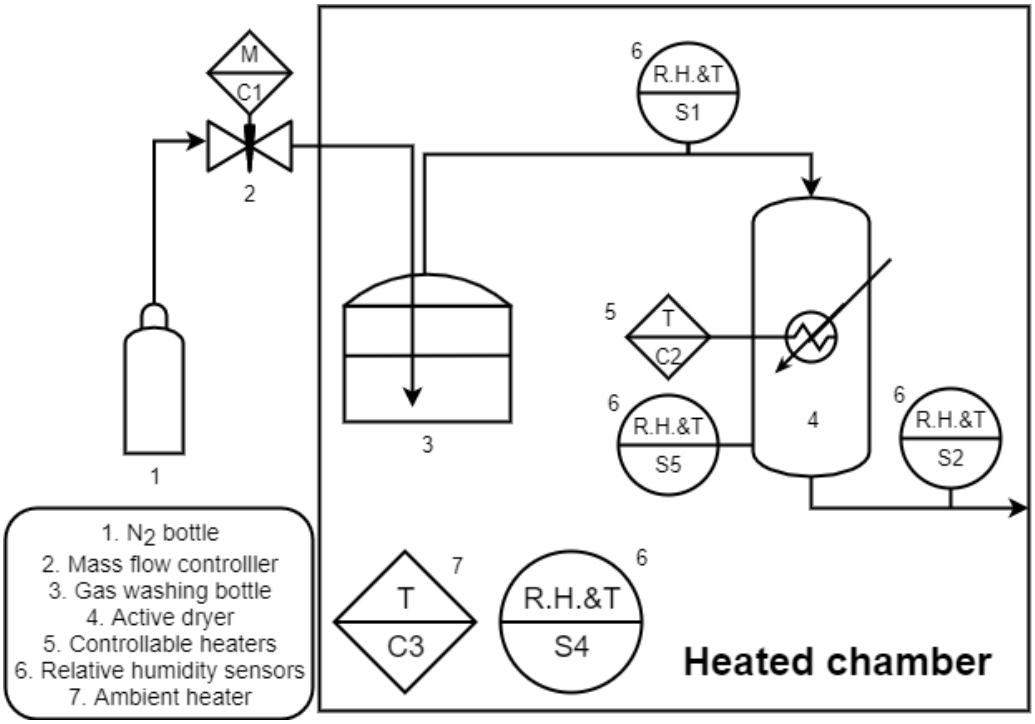

Figure 6.12: PFD for the breakthrough experiment

standard deviation σ = **0.088** [g]. This is considered to be adequate.

Table 6.2: Overview of sensor data gathered: D = desorption experiment, B = Breakthrough experiment

	T	RH		Weight Start & end	Weight Continuous
After GWB	D B	D B	Gas wash bottle	D B	
Active column, base	D B	D B	Active column	D B	
Active column, center	D B		Regenerating column	D	D
Dry side (between columns)	D B	D B	Condenser assembly	D	
Regenerating column, base	D				
Regenerating column, center	D	D			

Desorption experiment sorbent loading To start the first cycle, column B is pre-loaded by reducing the experiment to the adsorption step only, using only column B. Then, the desorption experiment is performed 8 times, with an active and regenerating column in each run. This results in both desiccants completing 4 cycles of loading, followed by regeneration, with an additional loading done for column B. The RH, temperature and weight data of all runs is shown in appendix D.3. The loading before and after each adsorption and desorption step is depicted in figure 6.13.

In order to calculate the loading from the weight measured before and after each run, it is assumed that the lowest weight observed in a column is equal to a lean loading of **0**.

Several topics of interest can be discerned in figure 6.13. First: It appears that the desiccant, as shipped from the factory, already contains an amount of water. This causes the gas in the first cycle to be dried to an insufficient degree, as the gas leaving the column is assumed to be in equilibrium with a significantly nonzero loaded desiccant resulting in a significantly nonzero relative humidity at the dry side as dictated by the Dubinin-Raduschkevich equation. Second: It is also seen that given the opportunity, the change in loading is larger during the desorption step, then during the adsorption step. This can both be seen from the loading in image 6.13, as well as the relative humidity at the output of the regenerating column, which hits 0 before the end of the experiment. Third: No significant reduction is seen in the performance of the desiccant over the first few cycles. On the contrary, it appears that

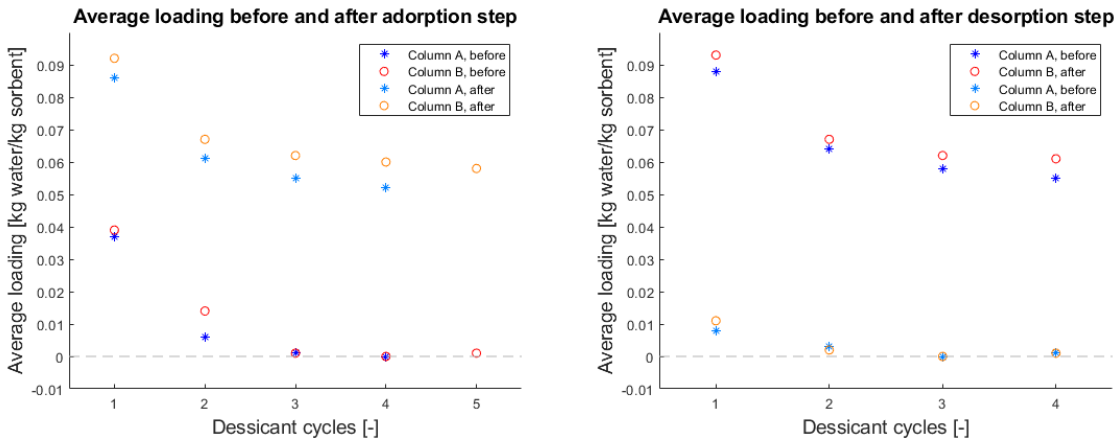

Figure 6.13: Average loading of the columns before and after adsorption and desorption steps.

the material can be dried even further than the ”virgin” state, improving the degree to which the gas can be dried once the material has been thoroughly regenerated.

Gas composition The gas water content can be determined from the relative humidity and temperature, by means of the Tetens equation. This is also done in the model and is described in section 5.2. The gas water content at the inlet of the active column, at the dry side and at the outlet of the regenerating column is shown in figure 6.14, with the thicker line indicating the average.

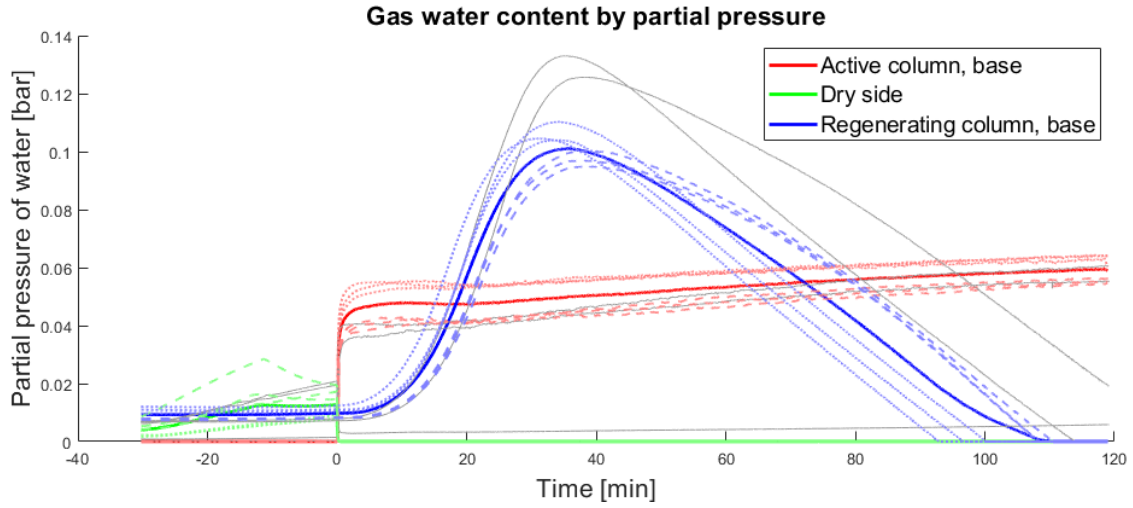

Figure 6.14: Gas water content at various points in the experiment. Note that the gas flow is switched on at t=0.

This figure clearly depicts the runs in three distinct groups. The first group is indicated in grey lines and consists of the first two runs. They are not included in the average and are characterized by their increased loading of the regenerated column at the start of the experiment. This results in an increased regeneration time, but also a higher maximum regeneration rate. However, finding the regeneration rate under varying loading was no goal of this experiment and thus, no conclusion can be taken from this observation alone.

The second group, indicated in dotted lines, are experiments done as a second run of the day. While a cooldown period is included in the test procedure, it seems that the water in the gas washing bottle did not fully cool down to ambient temperatures during the time, resulting in a slightly increased temperature for the gas leaving the gas washing bottle, resulting in a slightly increased water content entering the active dryer. This appears to be backed up by temperature readings after the gas washing bottle shown in appendix D.3. It appears that this slightly higher input did not alter the experiment by a lot, but does explain why figure 6.13 suggests that column B consistently has higher loadings, since

all three times that 2 experiments were conducted in 1 day, column B served as the active dryer in the second experiment.

The remaining three experimental runs are part of the third group, indicated in dashed lines, which are experiments done as the first run of the day. The lower water temperature corresponds with a lower adsorption rate for the active dryers. Since the columns that are to be regenerated in this group have a higher loading before regeneration, they appear to take a bit longer. It might be suggested that the reduced maximum regeneration rate is caused by the column fully cooling down overnight, the higher loading might explain the increased regeneration time as well. Temperature data taken at the centre of the regenerating column during the start of the experiment does not show a distinct grouping like the gas water content does. This means that no conclusion can be made for this hypothesis. Like the second group, the lines in the third group are closely stacked together. This indicates a fairly repeatable process once the initial drying is completed, so long as initial conditions are identical.

Continuous weight data verification In order to determine the desorption rate, one of two methods can be chosen. Both a direct measurement method by means of the weight scale, as well as an indirect measurement method via the measured gas water content can be used. While plotting the weight scale data is fairly straightforward, some work is needed to convert the gas water content to a mass flow rate, as desribed in equation 6.1a. Equations 6.1b present the method used to calculate the effective volumetric flow rate of the gas, as well as the molar volume at that temperature.

$$\Delta m = \int_{t1}^{t2} Q_{eff} p_w V_m^{-1} M_w \tag{6.1a}$$

$$Q_{eff} = Q_{stp}(T/Tstp)(P/P_{stp}) \qquad V_m = \frac{RT}{P} \tag{6.1b}$$

where

Subscript $_{stp}$ indicates gas at 0 [°C], and 1 [bar]
Q_{stp} = Volumetric flow rate as set on the mass flow controller [l/min]
Q_{eff} = Effective volumetric flow rate at actual conditions [l/min]
V_m = Molar volume in [l/mol]
M_w = Molecular weight of water = 18.015 [g/mol]

Then, the pressure drop is estimated. As shown in sppendix B.6, the pressure drop of the packed bed is estimated with the Ergun equation to be small. A very rough estimation of pipe flow pressure drop estimates the pressure drop in the system to be dominated by minor losses such as the in and outlets of the column. This is estimated in the kPa range, and then manually adjusted to fit the data, resulting in an assumed pressure drop of **4.5**[kPa] per column. Note that this is a simplification, as actual pressure drop is not measured and leakages are assumed to be negligible.

The difference between the discontinuously measured mass before and after the experiments relative to the two methods of continuous measurement are found in table 6.3. Inspecting the representative example given in figure 6.15, one can easily identify that the weight scale mostly reports the correct trends, but fails to report the correct values. The weight scale also reports some change in mass in situations where this should be found. Examples include the time before t = **0** when no gas is running and the time after completion of the desorption. In some suns such as run 6, the data is seen as more noisy, and in other runs such as run 7, a vulnerability to (user-induced) disturbances can be seen.

From this it can be concluded that measurement of the desorption rate by placing the column onto a weight scale is not possible in this context, and that the measurement via the relative humidity sensors is adequate, although this could be improved by measuring pressure drop.

Summarised, the desorption experiment can be seen as a success. While the continuous weight measurement of the scale did not provide much insight, the RH& T sensors provide a good view of the processes that occur in the setup. This enables analysis of gas composition at any non-condensing point in the system, which makes the assessment of sorbent condition possible. It is verified that the gas is dried to an appropriate degree, and that the desiccant can and should be properly regenerated to a state even dryer than the virgin material.

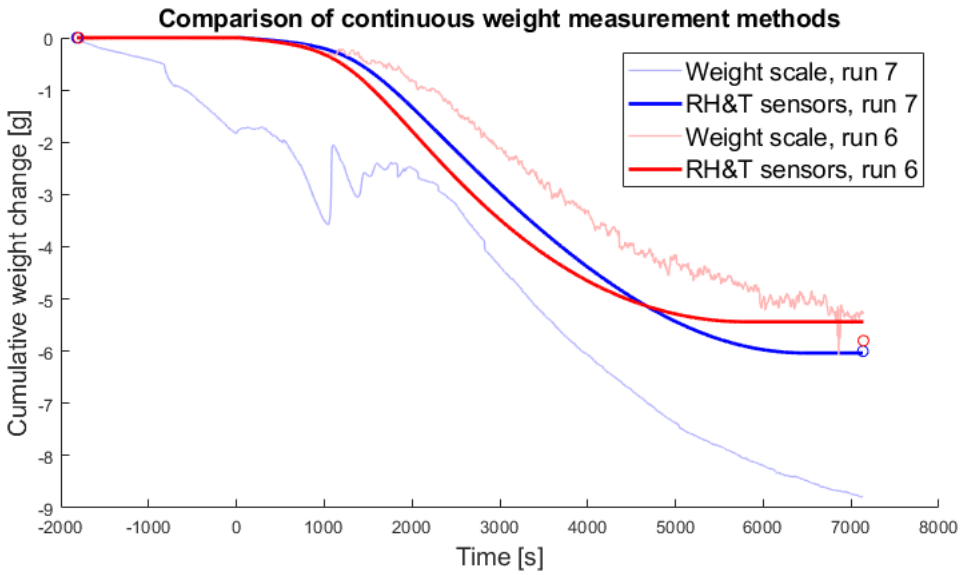

Figure 6.15: Illustrative examples of the two weight measurement methods.

Table 6.3: Values for adsorption and desorption weight changes as measured before and after each run, as well as compared to various continuous measurement methods. All units in [g]. Note that the average quantity of desorbed water appears to be higher due to the initial loading of the virgin desiccant.

Weight change measured before and after experiment	Mean	Standard deviation
Adsorption	5.51	0.42
Desorption	-6.52	1.02
Error relative to discontinuous measurements	Mean	Standard deviation
Adsorption (RH&T sensors)	0.18	0.39
Desorption (RH&T sensors)	$4.45*10^{-5}$	0.36
Adsorption & Desorption (RH&T sensors)	0.09	0.37
Desorption (Continuous weight measurement)	-2.77	3.58

6.5. Breakthrough experiment results & discussion

The data of this experiment is gathered using the same method as the desorption experiment in section 6.3.2. Relevant data is described in table 6.2, and primarily concerns gas conditions before and after the adsorbing column.

The parameters used for the modelled data in figure 6.16 can be found in appendix E.1, and are chosen to match experimental conditions. It can be seen from figure 6.16 that both lines share a certain similarity, but are not at all identical. Note that the sudden drop of measured relative humidity marks the end of the experiment. It can be seen that the measured data breaks through earlier and slower than its modelled counterpart. In order to find what may have caused this discrepancy, some parameters are changed one at a time in order to get a comparison. Figure 6.17 shows these variations.

- First, initial loading is increased to **0.04** [kg/kg], to investigate whether the assumption made in section 6.4, that the lowest seen loading is a loading of **0** [kg/kg], could cause this discrepancy if incorrect.
- Second, ambient temperature is increased to determine whether a mismatch in ambient temperature could cause such a change in behaviour
- Third, the input relative humdity is lowered to **85**%, which more closely resembles the final measured breakthrough value, in order to determine if the reported data from the sensors may have been too high.
- Finally, the mass transfer coefficient is dropped drastically, as a lower mass transfer would result in slower equilibrium and larger out-flow effects.

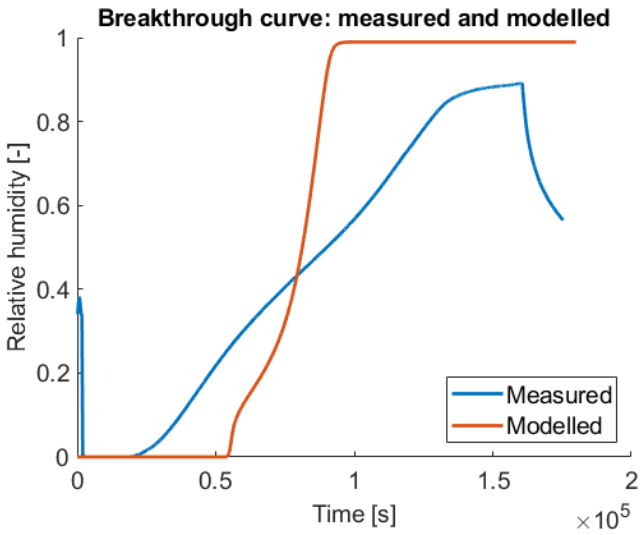

Figure 6.16: Breakthrough data as measured and modelled.

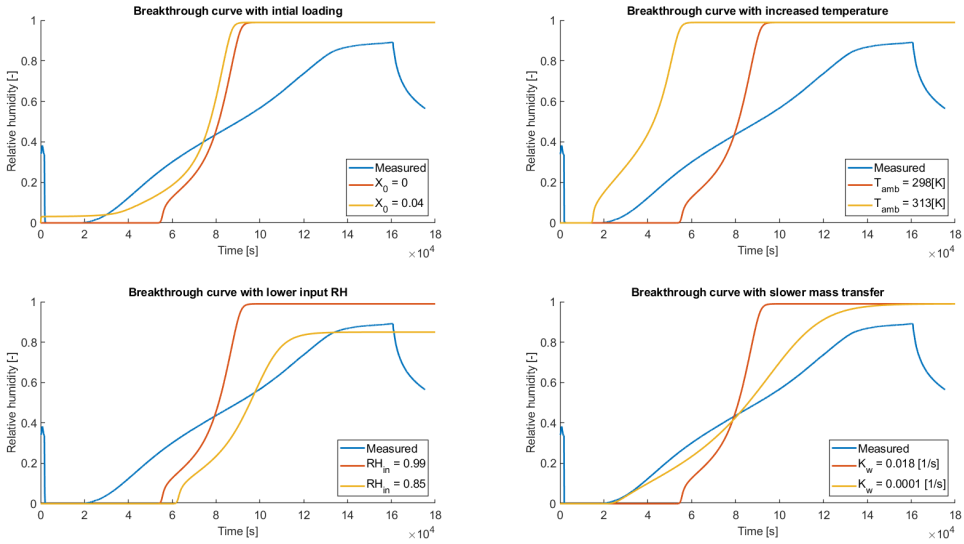

Figure 6.17: Variations of breakthrough data modelled in figure 6.16 and compared to measured data.

The following observations are made from figure 6.17

- The increased initial loading mainly appears to affect the lowest measured value that is dominant in the pre-breakthrough stage. This is highly consistent with observations in the first runs of the desorption experiment (section 6.4), and does not cause significantly closer values to the measured breakthrough curve.
- The increased ambient temperature appears to not cause significantly different sorbent behaviour. It does seem to advance the onset of breakthrough as the warmer ambient causes the input gas to have a higher gas water content at higher temperatures.
- The reduced relative humidity does look like a better match near the end of the experiment, but has a much later, rather than earlier onset of breakthrough. Another hypothesis should be formed to explain this discrepancy at higher relative humidities.
- The radical lowering of the mass transfer coefficient does appear to be a much better match to the measured data. However, hypotheses should still be found to determine why this value can be so far apart, and to determine the different behaviour at higher RH.

Upon closer inspection of the work of Park & Knaebel [62] and Nastaj & Ambrozek [58], it can be seen that both use the mass transfer coefficient that Park & Knaebel obtained by parameter estimation to match their experimental data to the model. However, one major discrepancy between those papers and this work can be found in the material used. Park & Knaebel state to use ”Silica gel (Davison PA-400) 12-28 mesh”.

The obvious choice here would be to purchase identical material and re-run the test, but is not possible as the material is no longer available as Davison Chemical Co. has merged with another company, and no longer make this product. Second: the indicated size of ”12-28 mesh” creates some ambiguity when compared to conversion tables such as found at Sigma-Aldrich [79], and no way exist to check this figure against a catalog. However, the material used is a lot smaller than what was used in this work thusfar. It is also unknown what the performance characteristics of the ”PA-400” grade has been like, as no data sheets are available anymore.

It can be reasonably expected that a material with a finer particle size would have an increased mass transfer coefficient due to the increased surface area per volume. The Petrovich & Thodos correlation is used to estimate this effect as is discussed in appendix C.1. Should this indeed be the case, the effects should be quite visible if the test is re-run using another generic silica gel with a finer particle size. This removes the need to acquire an identical material if the mass transfer coefficient is estimated afterwards, similar to Park & Knaebel’s work. A 0.5-1.5mm particle size generic silica gel is chosen as it is likely the most similar readily available material.

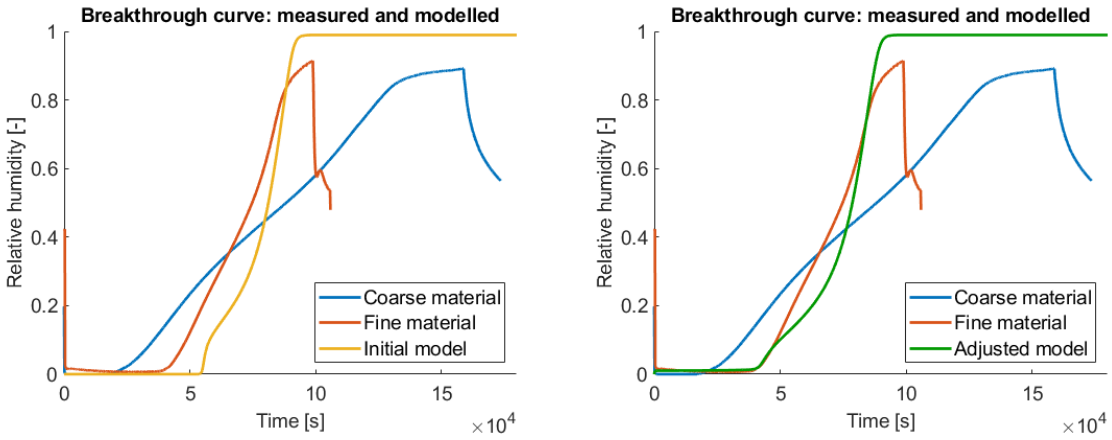

Figure 6.18: left: Breakthrough data of fine material, compared to coarse material and model. Left: model such as presented in figure 6.16 Right: model with X_0 = 0.025[kg/kg] and K_w = 0.0036 [1/s]

The breakthrough curve for the finer material does indeed appear to closer match the model. In order to determine the degree to which this occurs, some model parameters are adjusted by eye to roughly fit the model. First, the model is given an initial loading of **0.025** [kg/kg] in order to match the pre-breakthrough humidity readings, since virgin material is used, which is found in section 6.4 to contain some moisture. Second, the mass transfer coefficient was chosen as **0.0036** [1/s], which is a factor 5 smaller than the value given in literature [58]. These values appear to provide a fairly close match overall, but are particularly close at values where breakthrough just begins to occur. This is a relevant region since one of the performance criteria of the MCS is to dry the gas to under 2% relative humidity. Determining when the breakthrough starts supersedes the determination of the exact development of the breakthrough itself.

Figure 6.18 presents the result of the model with adjusted parameters. From this figure, some observations can be made.

While the mass transfer coefficient is still lower than literature values, this can be considered a massive improvement, considering how 6.17 used an even lower value to reach similar results. Since the average particle diameter has only been reduced by a factor 4 (**3-5** [mm] to **0.5-1.5** [mm]) it is assumed that the remaining difference in coefficients can be allocated to the undetermined specifics in material size, grade and unknown other performance indicators that characterize the ”Davison PA-400, 12-28 mesh” material. A closer look at a theoretical approach to the mass transfer coefficient can be found in appendix C.1.

The performance difference between model and experiment at higher RH was not seen in Park & Knaebel's experiment. However, they used a lower RH during their experiments. It is hypothesised that the model is no longer valid at very high RH, where the availability of adsorption sites might play a role that is not described by the model. Another hypothesis is that the isotherm described by the Dubinin-Raduschkevich equation may not be fully applicable to the material used in the experiment. Particularly the assumption that the mass transfer coefficient is constant in all conditions might be less than infallible, given the apparent sensitivity of this parameter as a material property. Either way, it is deemed beyond the scope of this thesis, as high RH breakthrough behaviour is not considered relevant for the MCS design.

Finally, the exact shape of the middle-RH region of the curves appear to differ, with the measured data appearing more linear. This experiment did not yield enough data to explain that particular difference and would require a closer look to determine. Data from Park & Knaebel appears to imply some variation in the breakthrough curve, depending on the experiment conditions [62], which has also been seen in the modelling in section 5.4. For the purposes of this work, the approximation made in this experiment is deemed more than sufficient.

Figure 6.19: Davison silica gel as used in by Park & Knaebel in 1992 [62], which is no longer in production. Note the year 1946 mentioned on the packaging.

Conclusion The breakthrough experiment can be considered a success. The process of comparing the measured values to the ones found in literature revealed a discrepancy in material used. Using the correct material is seen to have a profound impact on results, revealing a close similarity between experiment, literature and model. Due to the apparent sensitivity of both model-based and experimental results to the used material and conditions, the variation is considered to be in line with the observed variation in experiments and models described in literature. While it seems prudent to prototype and test any future design based on the model, it is deemed suitable as a design tool for the MCS as defined in chapter 7.

7

Design of the MCS

This chapter presents the combining and application of the efforts done in chapters 5 and 6 in order to provide a theoretical design for the MCS prototype that can be further developed by ZEF.

Section 7.1 presents the fitting of the model with experimental data, and describes the applicability of the model as a design tool. Section 7.2 presents the evaluation of the ”Key performance indicators” (KPI’s), which are the cyclic capacity, energy consumption and desorption rate. Section 7.3 contains the case study for the MCS prototype that is to be used for integration testing at ZEF. The chapter is then concluded with recommendations for further work.

7.1. Model-experiment validation

This section presents the steps taken in order to combine model and experimental efforts. In order to validate the model with experimental data, as is suggested in the conclusion of chapter 5, several steps are to be taken. As first and second step, the two degrees of freedom that are the heat and mass transfer coefficients of the model respectively should be fitted using experimental data.

Section 5.4 suggests that the model adequately describes the process, but requires experimental data to verify the heat and mass transfer coefficients and rates. In order to perform the fitting, paramters from the desorption experiment(section 6.3.2) are mimiced as much as possible in a two-step process. A set of adsorption data is obtained using parameters found in appendix E.1. From this data, only the sorbent loading as shown in figure 7.1 with a constant temperature, in order to mimic the step from the desorption experiment (section 6.3.2) where a column used for adsorption cools down between runs. The column heater is then imitated by linearly increasing the ambient temperature from **293** [K] to **393** [K] over the course of **1200** [s]. The total run time of the model is **7200** [s], just like the experiment. The adsorbing column is not fitted in this way, as the assumption made by Park & Knaebel that natural convection dominates heat transfer is readily seen to be invalid due to the fan in the chamber.

The temperatures of the RH&T and NTC temperature sensors inside the column are modelled using the temperature of the final node and a node in the middle[1] respectively.

Figure 7.2 shows a variation in heat transfer coefficient k_w. Values of **2.66** [W/(m^2 K)] (found to match the Nastaj & Ambrozek model) and **8.37** [W/(m^2 K)] (given by Park & Knaebel) are attempted first. Of particular interest is the temperature response just after the heater is switched on, since the change in desorption based on the shifting isotherm is expected to be minimal there. It is clearly seen from the figure that the value found by Park & Knaebel actually closely resembles the temperature response of the experiment. Therefore, this value is taken to be valid for the experiment. It should be noted however, that this is a fairly rough thermal model and does not take into account the heating of the isolation material, the thermal resistance of the wall and air gap, or the change of air flow through the heater as conditions change. Nonetheless, this constant value is deemed adequate for the purposes of this work.

Next, the mass transfer coefficient is fitted by eye. As higher mass transfer coefficients mean the equilibrium is more closely followed, it can be expected that as temperature increases and the isotherm

[1] The exact location of the NTC is difficult to determine, so some room for manual selection of the node is deliberately left open.

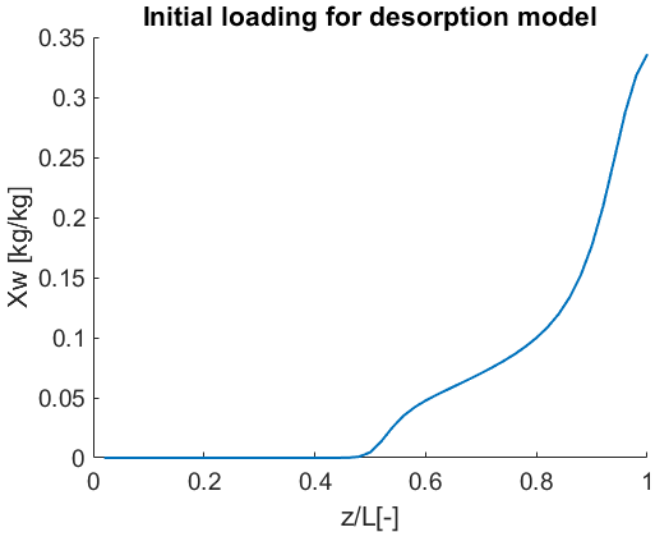

Figure 7.1: Example of sorbent loading distribution after the adsorption step.

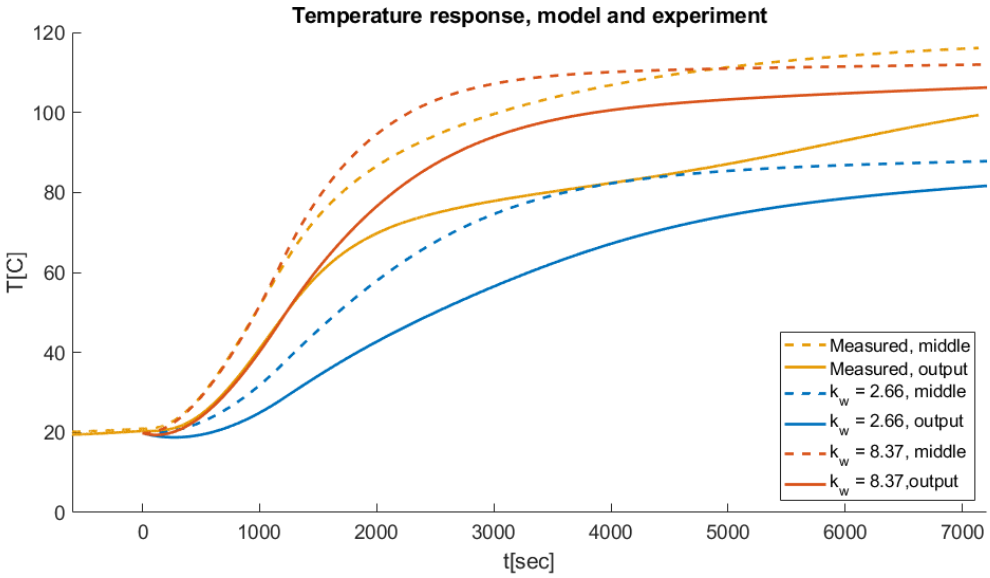

Figure 7.2: Temperature response of the experiment and model with two heat transfer coefficients.

shifts, most energy is used for desorption rather than temperature increase. This would result in a more clearly pronounced ”Double-shock” effect in the temperature response at the end of the column.

Figure 7.3 shows the temperature response with varying mass transfer coefficient, with the heat transfer coefficient remaining at the established **8.37** [W/(m^2 K)]. Values taken are from literature (**0.018** [-/s]) and lower, as suggested from the breakthrough experiment in section 6.5. In order to view the effect of the mass transfer coefficient, a factor 10 and 100 smaller are taken in figure 7.3. The effect of the mass transfer coefficient starts to show as the column heats up and the isotherm shifts. It can be seen that the inflection points are situated in roughly the same location across the models and experimental data which implies that the model does indeed describe the experimental situation. High mass-transfer coefficients clearly show the double-shock effect described in literature. It is hypothesised that this plateau at a given temperature is characteristic of the energy entering the column being mostly used for desorption, rather than heating as implied by the model's equation of temperature (equation 5.8) Lower mass-transfer coefficients on the other hand imply a slower response time to a hypothetical change in equilibrium loading X_w^* as described by the model in equation 5.6, which allows the diversion of time and energy from desorbing to warming up the column, inducing an even larger

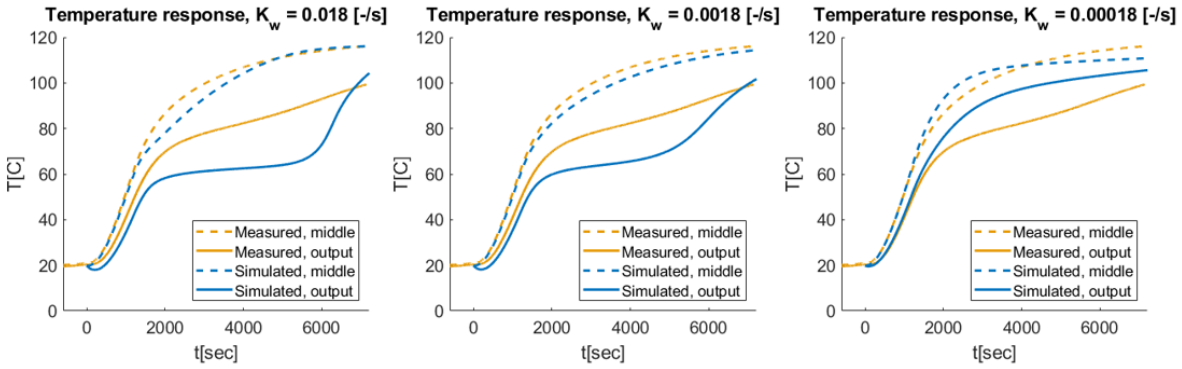

Figure 7.3: Temperature response of the experiment and model with varying mass transfer coefficients.

shift in equilibrium loading, which creates a balance that results in a smoother curve.

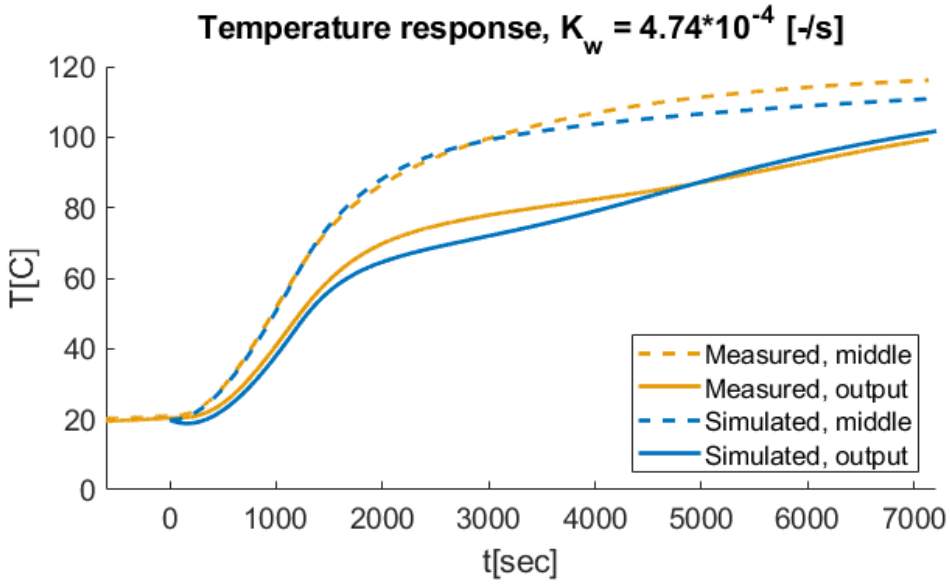

Figure 7.4: Temperature response of the experiment with the fitted mass transfer coefficient

Figure 7.4 shows the fit of the chosen coefficient of **4.74*10**$^{-4}$ which appears to be valid for the desorption experiment using the coarse material. As described in section 6.5, the fine material can then be estimated using the Petrovich & Thodos correlation (equation C.10 of appendix C.1) to have a mass transfer coefficient of (4.74*10^{-4})*4$^{1.36}$ = **3.12*10**$^{-3}$, which is reasonably close to the estimation made from the breakthrough experiment in section 6.5.

Figure 7.5 then shows the desorption breakthrough curves of the model and the experiment. It can be seen that at very low loadings, the output humidity of the model does not quite reach 0 while the experiment does. It is hypothesised that this difference can have a multitude of causes.

- First, it may be possible that the linear driving force model no longer adequately describes adsorption in situations close to equilibrium. However, both modelled and experimental findings of Schork & Fair also show the reduced desorption rate as the water content of the column approaches 0, just like the model from this work.
- Second, it may also be possible that the adsorption isotherm is material-specific and/or no longer adequately described by the Dubinin-Raduschkevich equation at very high or very low loadings. Both of these explanations would also explain the breakthrough curves of the breakthrough experiment flattening near the end of the experimental runs for both materials(Figure 6.18. It should be noted that none of the authors in literature use such high relative humidity values in their breakthrough experiment.

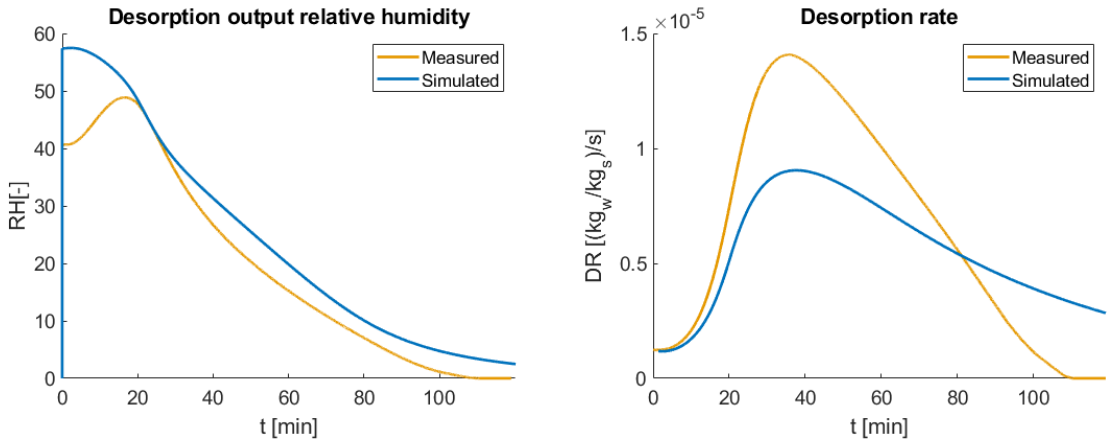

Figure 7.5: Desorption breakthrough curves, relative humidity and gas water content.

- A third explanation could be that the sensors no longer accurately measure at such high and low RH values, as their specified **±4%** RH accuracy only applies to the **10-90%** range [41]. This means that the desorption experiments attempt to measure not only within the sensor's tolerance, but also out of specified operational conditions.

Before and after desorbing, the modelled column is estimated to have an average loading of **0.0563** [kg/kg] and **0.0114** [kg/kg] respectively, with a distribution shown in figure 7.6. Note that while this is not identical to the experimental sorbent loading depicted in figure 6.13, within the scope of this thesis it is considered to be an adequate estimation of the process, but it does introduce some limitations to the model's applicability as a design tool in its current form.

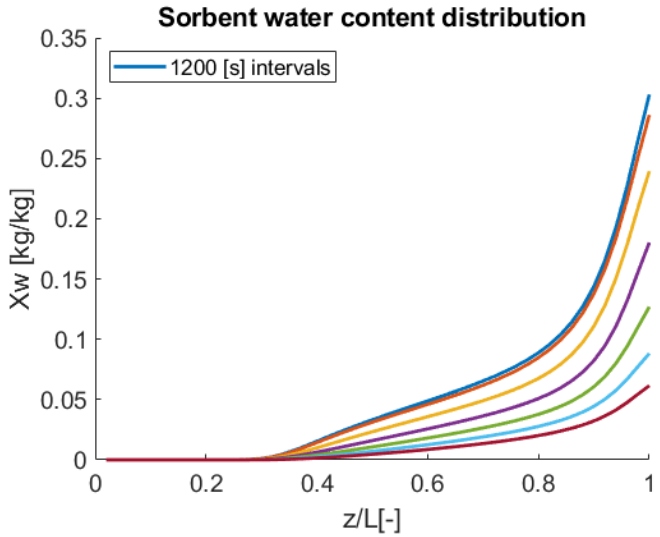

Figure 7.6: Sorbent water distribution during simulated desorption experiment, with intervals of 1200[s]

Conclusion It is concluded that the heat and mass transfer coefficients are two degrees of freedom that are not accounted for via this theoretical approach. For the desorbing column, the heat transfer value found is identical to Park & Knaebel which is likely not valid for the adsorbing column due to the forced convection introduced by the chamber fan. The coarse material mass transfer coefficient is fitted by eye using the data from the desorption experiment, yielding a value of **4.74*10**$^{-4}$. From this value, the fine material mass transfer coefficient is estimated as **3.12*10**$^{-4}$. It is recommended to repeat this process to find the particular heat transfer coefficient for a certain setup, and the particular mass transfer coefficient for a certain material. It should also be noted that the model starts to significantly

deviate from the experimental data at very low loadings.

7.2. Key performance indicators

This section presents three key performance indicators: Cyclic capacity, energy consumption and desorption rate. They are determined for the desorption experiment, as well as evaluated for improvement in order to estimate the design parameters of the MCS prototype presented in section 7.3

7.2.1. Cyclic capacity

The cyclic capacity can be defined as the difference in loading between a column that is fully loaded within operational context (rich loading) and a column that is fully regenerated (Lean loading). This metric is useful to estimate the required system size and is determined via modelling. It is then verified using experimental data from the breakthrough experiment of section 6.

The model as described in chapter 5 and validated in section 7.1 is used to fill up a the same column as section 7.1, under similar conditions as the desorption experiment of chapter 6 (model parameters in appendix E.1) The column is considered full when the measured breakthrough is at **0.5%** relative humidity, which appears to be high enough to detect using the sensors used in the experiments, but low enough to allow some clearance from the **2%** RH threshold. It is assumed that a properly regenerated column can be completely dry, as suggested by experimental data from section 6.4.

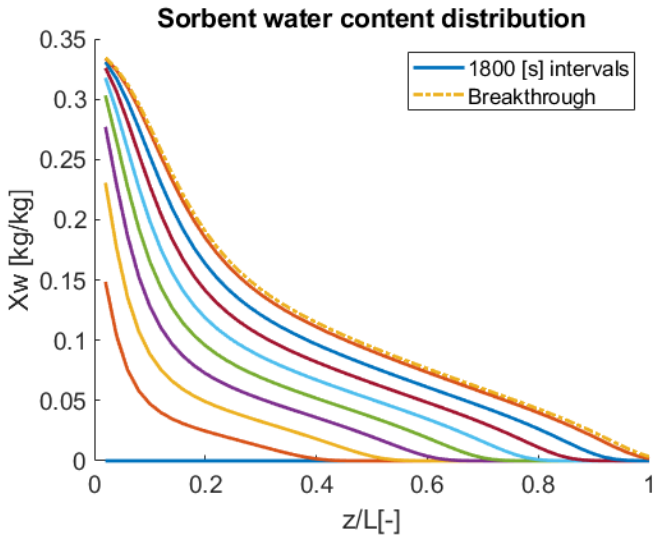

Figure 7.7: Sorbent water distribution during alternative simulated adsorption until breakthrough, with intervals of 1800[s], and an extra line at the point of breakthrough at t = 14870[s]

Figure 7.7 shows the loading distribution of the simulation, which shows an average rich loading at breakthrough of **0.116** [kg/kg] at t = **14870** [s]. Some attempts are made to improve average rich loading at breakthrough, which are plotted in figures 7.8 and 7.9, with breakthrough times and average loadings stated in table 7.1, and parameters stated in appendix E.1, and can be described as follows:

(a) A slimmer column, using the same amount of sorbent and gas flow.
(b) Lower ambient temperature, using the same gas input conditions.
(c) Higher mass transfer coefficient using the fine material used in the breakthrough experiment

From these tables and figures, it can be seen that a very significant possibility for improvement exists, which may be quite easy to enact. First of which is the operation at a lower temperature. As suggested by the Dubinin-Radushkevich equation, the equilibrium loading increases at lower temperatures. This is not very significant at very high relative humidities, but the sorbent water distribution in figure 7.8 indicate very nicely that the internals of the columns operate at lower loadings which do benefit from a lower temperature. This can be achieved both by a more effective dissipation of the heat released from adsorption as seen in the slimmer column, but can also be achieved with lower ambient temperatures. Note that using the column itself to cool down the gas is not advised, as this might cause

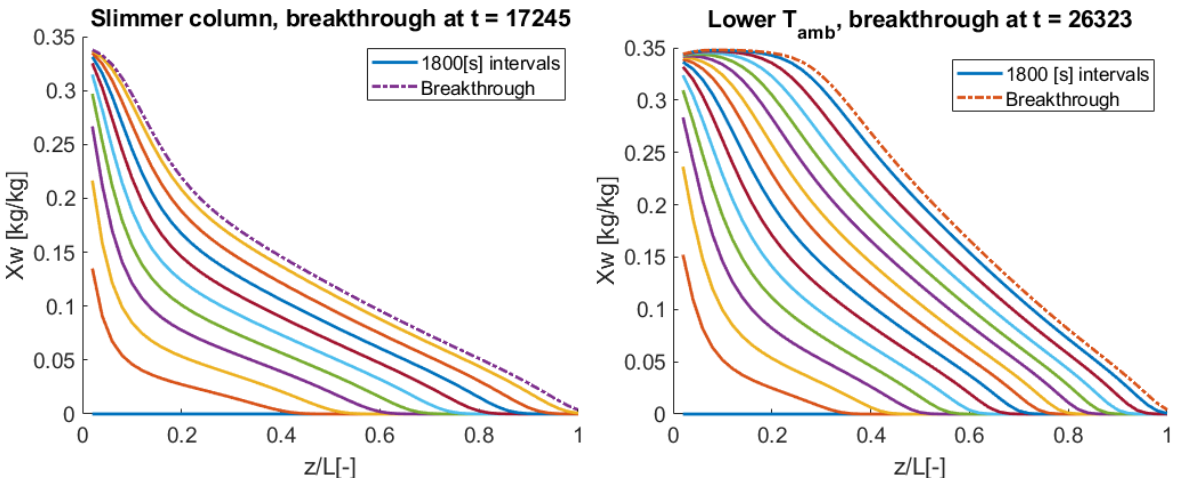

Figure 7.8: Sorbent water distribution during simulated adsorption until breakthrough, with intervals of t=1800[s], with an extra line at the moment of breakthrough.

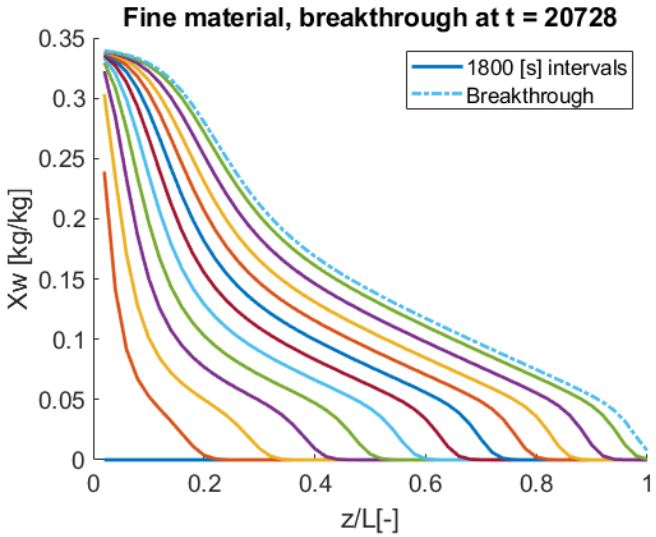

Figure 7.9: Sorbent water distribution during alternative simulated adsorption until breakthrough, with intervals of t=1800[s], and an extra line at the moment of breakthrough

condensation within the column. This means that in reality, a lower ambient temperature would also reduce the quantity of water entering a column. This was omitted in order to make a fair comparison. The second effect that can be seen is that of a clearly increased performance of a fine material. When comparing figures 7.7 with 7.9, it can be seen that as the wet gas contacts the sorbent, the fine material uses a much shorter space until the gas is very near equilibrium with the sorbent. Particularly in both the high- and low-loading regions where driving forces tend to be low, the fine material is clearly more effective at removing the remaining bit of moisture in the low-loading region, simultaneously enabling a larger portion of the column at higher loading to continue adsorption. This definitively confirms the fine material as the superior choice in this situation.

Conclusion A silica gel column at breakthrough tends to have adsorbed between **0.1** and **0.2** [kg water/kg sorbent] and is subject to both design choices and operating conditions. This loading is also assumed to be the cyclic capacity, as experimental data suggests a lean loading of 0 can be achieved. Model data suggests this process to be slower in the low-loading regions than measured, for which several hypotheses are made that could be tested in subsequent projects. Model data from chapter6 already concluded that model data can be used to simulate adsorption breakthrough.

Some attempts are made to improve the average rich loading at breakthrough. It is seen that lower

Table 7.1: Time and average loading at breakthrough in various scenarios

Columns loaded until breakthrough		
Case	Average loading [kg/kg]	Time [s]
Base	0.1160	14870
Slimmer column	0.1346	17245
Lower ambient	0.2054	26323
Finer material	0.1618	20728

sorbent temperatures have a beneficial effect. Finer material with a higher mass transfer coefficient appears to have a beneficial effect as well and is particularly relevant as the choice of sorbent does not depend on external conditions and can be considered purely a design choice.

7.2.2. Energy consumption

The energy consumption of the process can be defined in various methods. The overall energy usage of the experiment can be measured, and broken down into its components, or the energy usage of the relevant components themselves can be indirectly measured.

The first approach does not appear to be valid, due to the inability to estimate the heat exchange between the various components of the experiment chamber, the chamber itself and the environment, particularly as they are not in steady-state. A more detailed description can be found in appendix E.3. Seven components can be identified, the first three of which (desorption, gas warmup, sorbent warmup) can be determined from both experimental and simulated values. The remaining three are only identified via experimental values, as they are the product of design rather than the physical process. Finally, the total energy use of the experiment's column heater is known as well. The properties and equations governing the components of the energy usage can be found in appendix E.3. In short, they are the following:

- Desorption energy, from the heat of desorption found with the clausius-clapeyron equation as described in equation 5.4.
- Gas heating, based on the inlet and outlet temperatures, combined with the methods to calculate the specific heat as done in chapter 5.
- Sorbent heating, based on the (simulated) NTC sensor in the middle of the bed and sorbent specific heat. Note that by the time of writing, the model implies that the temperature at roughly the middle of the bed as measured in the experiment does not have to be representative of the average bed temperature, but since the experiment does not provide temperature distribution data, this approximation is used to provide a fair comparison between experimental and simulated data.
- Hardware heating, from the estimated specific heat of the column itself by means of weighing the significant compontents, and the (simulated) NTC sensor in the middle of the bed.
- Heater heating, from the simplified estimation that the specific heat of the heater can be estimated by the aluminium tube and the inner part of the rockwool isolation sleeve, all operating at the same temperature, indicated by the NTC of the heater.
- Losses, which is the remainder of the energy consumed by the column heater and entails the warmup of the chamber, the losses to the environment and other non-modelled components.

These components can be taken together to form the energy balance stated in equation 7.1. Note that details on E_{heater} can be found in appendixE.3.

$$\int_{t1}^{t2} (E_{heater} - E_{desorption} - E_{GH} - E_{SH} - E_{HWH} - E_{HH} - E_{losses})dt = 0 \tag{7.1}$$

Figure 7.10 shows the five categories identified above during the average of all 6 desorption experiment runs after the first cycle. From it, it can be seen that by far the most energy is used to warm up the equipment at the early stages of the experiment. Since these are the consequence of design choices and not inherent to the process itself, it will suffice for this work to mention that the design of a column-heater pair should not only consider heat transfer, but also specific heat. It is also observed that the combined energy use shown in the figure follows the trend of the heater's power consumption which is displayed in appendix E.3.

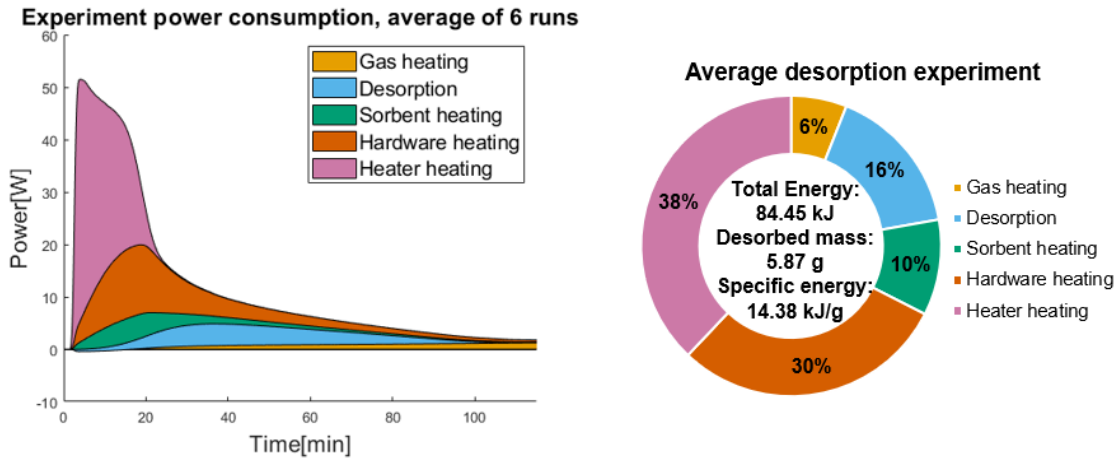

Figure 7.10: Total energy usage of the 5 most relevant categories of the averaged data from all desorption experiment runs.

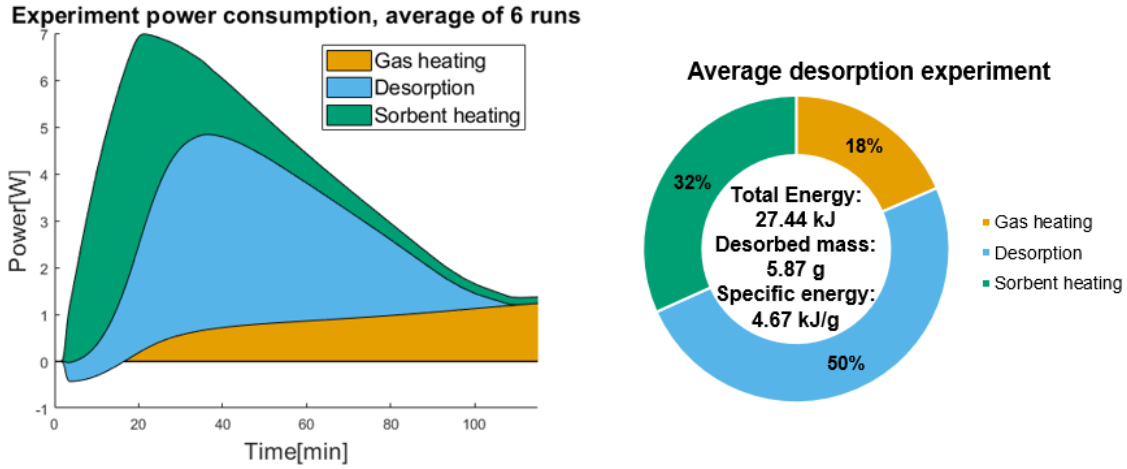

Figure 7.11: Total energy usage of the 3 most relevant categories of the averaged data from all desorption experiment runs.

Figure 7.11 repeats figure 7.10, but only for the three most relevant categories. These categories are considered to be part of the desorption process and are governed by the operational strategy rather than design choices. They represent a practical minimum energy requirement for the desorption process, based upon the averaged data from all 6 desorption experiment runs after the first cycle.

Some observations can be made from 7.11.

- First, it can be seen that the desorption energy starts below the **0** [W] line. This is caused by the gas at elevated ambient temperature entering the column that is still near environment temperature due to its thermally isolated position in the chamber.
- Second, it can be seen that the energy usage from desorption lags behind energy usage for sorbent heating which appears to confirm that the desorption rate's significant increase around t = **30** [min] is caused by the shifting isotherm at higher temperatures.
- Third: note that after approximately t = **90** [min], gas heating actually becomes the dominant energy use. This implies that a more energy efficient strategy might exist where the column is not fully regenerated, aiming to push the adsorption front back enough to practically use the column in the next cycle, rather than aiming to remove as much water as possible as was done in the experiments in this work.

Desorption strategies have not had a prominent role in this work thus far, although the figures in this section do imply that this can be of importance for efficient operation. It is deemed beyond the scope of this thesis to optimise this strategy, as this work is more on the topic of "What can work?" rather than "How can it work best?", but might be interesting for later research. In order to explore some of

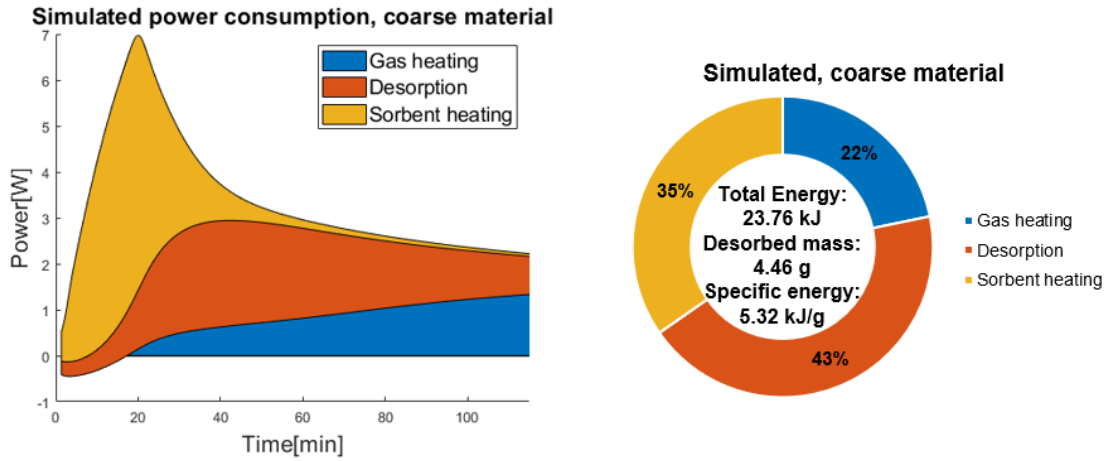

Figure 7.12: Total energy usage of the 3 most relevant categories of simulated data using the coarse desiccant.

the routes that can be taken, the energy usage calculations were done for simulated data using the model for both coarse and fine material as achieved in section 7.1, the parameters for which are found in appendix E.1. Figure 7.12 depicts the energy usage of a simulated desorption experiment such as seen in figure 7.5. Note that the simulation's energy consumption results are not identical to those from the experiment, but do provide a representative image given the differences between experimental and model desorption stated in section 7.1. Further early exploration of desorption strategy is done in section 7.2.3.

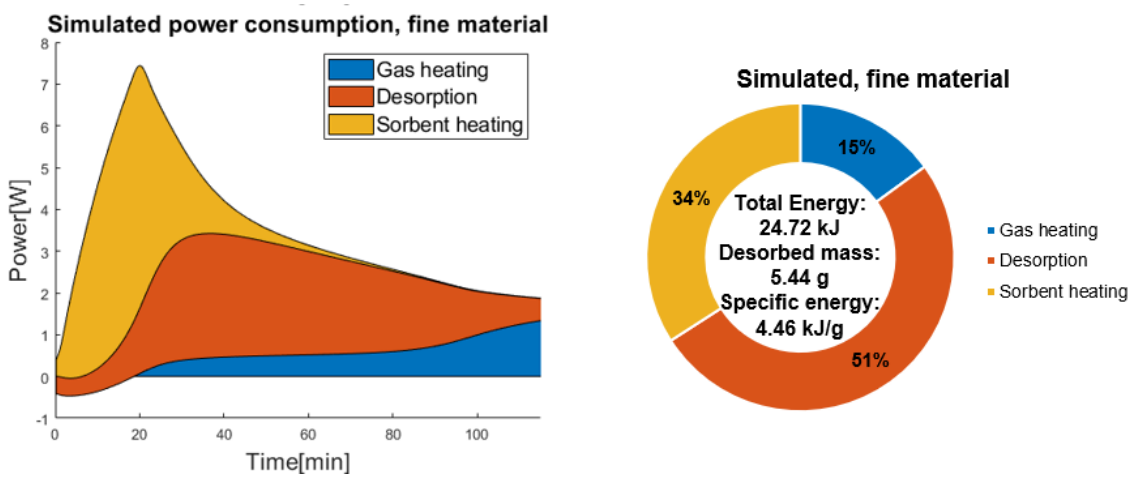

Figure 7.13: Total energy usage of the 3 most relevant categories of simulated data using the fine desiccant.

From figure 7.13 it can be seen that the transitions between the dominant energy use are more pronounced. As the double-shock effect as shown in figure 7.3 among others is more pronounced at higher mass transfer coefficients, figure 7.13 confirms the shift of energy use from sorbent heating to desorption, causing the "Platform" in output gas temperature. Note that as the output gas is at a lower quantity for longer, the energy used to heat the gas is lower. It should also be stated that when the average temperature for the sorbent is taken, the power for sorbent heating is more consistent throughout the run, and results in a slightly lower energy use overall. The figure for which can be seen in appendix E.2.

The specific energy (energy per desorbed gram of water), in both experimental and simulated approaches is in the order of **4** to **6** [kJ/g], with approximately half of this quantity being accounted for as energy used for desorption. As the experiment uses **1** ln/min of gas, this quantity translates to approximately **0.15** to **0.22**[kJ/g dried N_2]. Should an equal volume of CO_2 be used, this results in approximately **0.1** to **0.15** [kJ/dried CO_2]. However, while it appears to be a better metric, it should be

noted that the energy per unit of dried gas metric does not neccessarily reflect the performance of the MCS, but also the conditions of the input gas. This is due to the fact that differing DAC output compositions bring different water quantities to the MCS. Therefore, the energy per unit dried gas metric is recommended for use when observing the entire system, but the energy per unit desorbed water is recommended when observing the desorption process itself.

Conclusion During these experiments, most energy is used for material heating with around **75%** going to hardware and heater. These energy expenditures should be designed for in future iterations. The energy use for the gas heating, sorbent heating and desorption are considered inherent to the process, and appeared to be in the **5** [kJ/g] range. Some attempts are made to improve the energy usage by means of simulated data, resulting in yet another category in which a finer material performs better. While not part of this work, it is implied that a strategy might exist for optimal desorption, since the losses via gas heating become the dominant energy usage after some time, both in experimental and simulated data.

7.2.3. Desorption rate

The third and final KPI that will be analysed is the desorption rate and some factors associated with it. For this work, the scope of the desorption rate is limited to the quantity of water that is desorbed from the column. In a later stage, this KPI can be improved by comparing this desorption rate to the adsorption rate on a system scale in order to find the material flows in the closed system described in section 6.1. However, due to the difference between experimental and simulated desorption rate shown in figure 7.5, it is considered good practice to focus on getting a good enough quality on more elemental aspects such as this desorption rate before introducing it into more convoluted calculations such as system-scale analysis. This column-scale data is therefore more suited to get an insight on what aspects might influence the desorption rate based on simulated data.

The desorption rate can be defined as the amount of water desorbed from the column per unit sorbent, resulting in a unit of [kg_{water}/($kg_{sorbent}$s)]. This can be calculated via the value of Y_w at the end of the column by means of the RH&T sensor for experimental data as seen in eqauation 7.2. While applicable for simulated data, a more direct approach is to take the average of $\partial X_w/\partial t$ as seen in equation 5.6 for all nodes for simulated data as shown in equation 7.3.

$$DR = \frac{Y_{w,desorption}\, A J_i}{A\, L\, \rho_b} \tag{7.2}$$

$$DR = \frac{d\overline{X_w}}{dt} \tag{7.3}$$

In order to get an overview of desorption performance in just a few numbers, the average desorption rate is calculated from the start of the experiment, to the point where a selected share of initial loading has been desorbed as shown in equation. The selected values for desorption are **50%**, **80%** and **95%** of the adsorbed water mass. The average desorption rate (ADR) is then calculated as shown in equation 7.4.

$$\frac{1}{t_{(n\%)}} \int_0^{t_{(n\%)}} DR\, dt \tag{7.4}$$

A comparison of various simulations is done in figure 7.14,where the DR_{max} is plotted per scenario for both coarse and fine material, as well as figure 7.15, which depicts the average desorption rate at selected values of **50%**, **80%** and **95%**. In order to maintain a consistent comparison, experimental data is not included in this analysis. The base scenario parameters used can be found in appendix 7.15. In short, these scenarios are all consist of an adsorption step, followed by a desorption step for an equal duration. All scenarios have equal RH and T input (and therefore equal water input), and are tested with both coarse and fine material and can be described as follows:

1. Timed: Adsorption for **7200** [s], followed by desorption at **120** [°C].
2. Breakthrough: Adsorption until **0.5%** RH at adsorption output, followed by desorption at **120** [°C] for the same amount of time as needed to reach adsorption breakthrough.

3. Cooler ambient: Like breakthrough, but with an adsorption column ambient temperature of **298** [K][2].
4. Lower desorption mass flow: Like breakthrough, but with inert gas flow during cut in half during the desorption step only.
5. Higher desorption temperature: Like breakthrough, but with a desorption temperature of **433** [K].
6. Fast warmup: like breakthrough, but with the heater reaching desorption temperature instantly.
7. Slimmer column: Like breakthrough, but with a smaller diameter column. Mass flux and column length compensated to provide the same sorbent mass and inert gas mass flow, as was done in section 7.2.1.

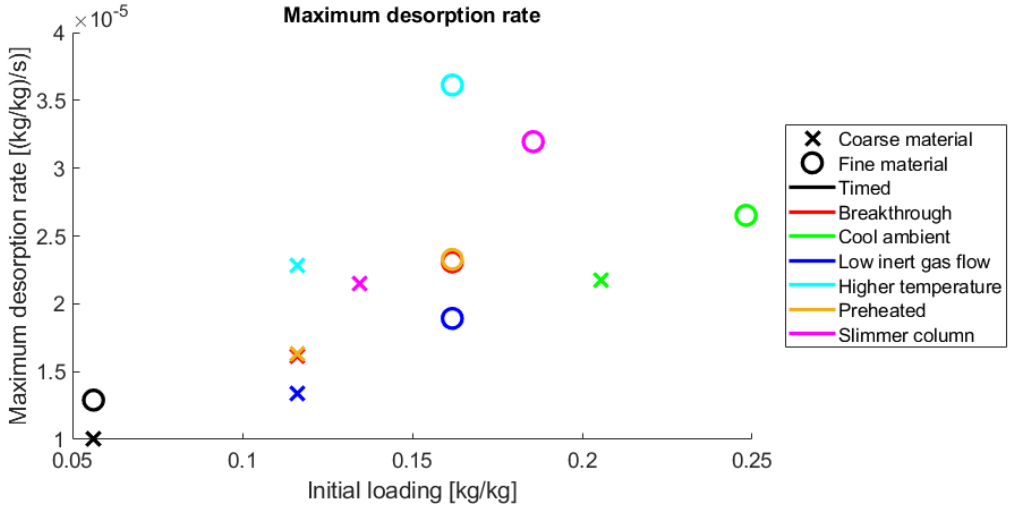

Figure 7.14: Maximum desorption observed and average breakthrough column loading in the simulated data from the described scenarios.

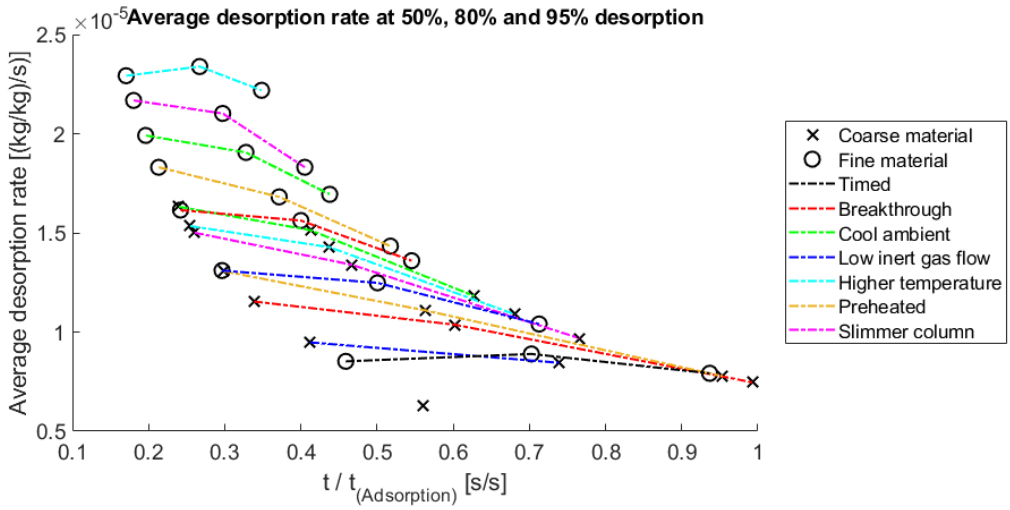

Figure 7.15: Average desorption rate at selected desorption shares. Simulated data from the described scenarios.

From figure 7.14, several observations can be made. Figure 7.14 also shows the effects seen in section 7.2.1. It is seen that the fine material has higher desorption rates than the coarse materials, and has a higher average loading at breaktrough than the coarse material, with the exception of the timed scenario. This is consistent with the observation that the different water distribution in the columns of different materials is irrelevant at significantly low loadings. When comparing scenarios with a single

[2]Note that the RH and T input are still the same, similar to section 7.2.1, resulting in the gas cooling once it enters the column, wich may cause condensation when applied in an experiment.

material, it is seen that a higher loading at breakthrough does not imply a higher maximum desorption rate. One interesting result is the slimmer column, which appears to have both a better desorption rate and loading at breakthrough than base conditions. This implies that it might not be the overall heat transfer, rather than temperature alone, that improves desorption rate there. It is also shown that both adjusting adsorption conditions (timed, breakthrough, slimmer column, cool ambient) and desorption conditions(breakthrough, low inert gas flow, preheating and higher temperature) have effect on the desorption rate, but only adjusting the adsorption conditions affects the average loading at breakthrough. This implies a designer can exert control over a wide array of performance characteristics.

Figure 7.15 shows the time taken to desorb to selected percentages in the scenarios. The data points for **50%**, **80%** and **95%** are all positioned on a set of hyperboles as is expected, since desorption rate is inversely proportional with desorption time. The positioning of the simulation runs on these hyperboles however, can and do vary and are an indication of how the scenario performs in that domain from which several observations are made.

- First, the fine material appears to desorb much faster than the coarse material in all scenarios. This implies that in a closed system in particular, having a finer material works better since the difference between desorption and adsorption (the water that condenses and ends up in the AEC system), rather than desorption itself is what matters most on a system-scale.
- Second, the cooler ambient conditions appear to perform very well, while the timed scenario performs rather poorly. This implies that if more water is available for desorption, the desorption rate is higher.
- Third, both the higher temperature and slimmer material have the highest desorption rates. However, it can be noted that the slimmer column significantly slows down near complete desorption, which is much less the case for the higher temperature. This might be caused by the property of the slimmer column which adopts the ambient temperature more easily. However, the higher temperature shifts the isotherm further which may be a reason why the higher temperature scenario can maintain a high desorption rate for longer: the slimmer column may move faster towards the equilibrium, but the higher temperature places the equalibrium farther away.
- Fourth, preheating the heater appears to mostly be of impact at lower desorption percentages due to the thermal headstart, but appears to lose its impact over time.
- Fifth and last, the lower gas flow appears to have a lower average desorption rate, but while the gas flow is reduced by half, the desorption rate is reduced by much less. This implies that when a closed system is considered, there would likely be a tradeoff to be made between fast desorption with all the dried gas, and slow desorption with a limited quantity of gas. The fast desorption has the advantage of supplying heat to the system for a shorter amount of time, reducing thermal losses, while performing a slower desorption process with a reduced requirement of gas would reintroduce less gas into a closed system, and therefore less water, reducing column sizing requirements and by extension, energy required to heat the system during desorption. This might form a very interesting optimisation problem and it is highly recommended by the author to investigate this further once system-scale analysis is performed, in order to design for the appropriate desorption rate for the selected operational strategy of the MCS and the ZEF micro-plant as a whole.

Conclusion The desorption rate is observed by means of simulated data on a column-scale, rather than system scale in order to explore the factors that affect it. In simulated scenarios where a column is in adsorption mode, and then in desorption mode for an equal amount of time, it is seen that for most configurations, it is possible to desorb well over **95%** of the water in the column after adsorption, within the time taken for the adsorption step. Both the desorption rate and average loading of an adsorption column at breakthrough can be influenced by several changes to adsorption and desorption conditions. The fine material selected earlier yields better results than the coarse material. It is likely a tradeoff can be made to optimise the adsorption rate for the selected operational strategy.

7.3. Case study: ZEF integration MCS prototype

This section presents two case studies using the knowledge and design tools developed during this project. For each of the two scenarios, the relevant parameters are gathered and used to find a proper column sizing. Then, the KPIs from section 7.2 are determined by means of simulation.

Two cases are defined. The ”3X, field setting”, which has been presented in chapter 2 and has served as a guideline throughout this work. It is based on a microplant using 3 solar panels in a warm environment. The ”10X, lab setting” case is a setting that has been added during the course of this project and is intended to test the integration of the direct air capture and compression systems. It utilises a hypothetical plant using 10 solar panels, as this would theoretically yield material flows that most closely resemble the operating regime of the compressors that are currently being tested and developed at ZEF.

In order to get recommend adequate sizing parameters, the adsorption model is used. This is deemed viable as the breakthrough experiment (section 6.5) implied that the point of breakthrough can reasonably be predicted by the model. It is then assumed that full regeneration is possible, as was suggested by the desorption experiment of 6.4. Energy consumption and desorption rate are both KPIs that involve desorption and therefore the mismatch between model and experiment described in section 7.1. However, they can provide a measure to compare new experimental data to.

Table 7.2: Adsorption model parameters for column sizing

	3X, field setting		10X, lab setting	
CO_2 massflow	101.3	[g/h]	343.75	[g/h]
RH_{in}	100	%	100	%
T_{in}	313	[K]	298	[K]
$T_{ambient}$	313	[K]	298	[K]
Material	Generic fine silica gel		Generic fine silica gel	
Particle size	1	[mm]	1	[mm]
Carrier gas	Carbon dioxide		Nitrogen	

Column sizing The parameters required for the model are presented in table 7.2. These parameters are then used as inputs for the adsorption model in the following steps:

1. A diameter is selected of the glass tubes that are available from ZEF’s preferred glassware supplier.
2. Column length is then adjusted to achieve breakthrough at a time 1.5 times later than the specified time in the parameters as a safety factor to accommodate variations in temperature, experimentation and unexpected events.
3. For the 10X, it is also important that the columns are relatively easy to handle in a lab. A maximum length of **600** [mm] is therefore suggested as maximum. Should the pressure drop as suggested by the Ergun equation be too large or the length of the tube exceed reasonable sizes, a larger diameter column is used.
4. The breakthrough time and additional sizing results are recorded. Then, the model is run in desorption mode for a time equal to the breakthrough time in order to calculate desorption rate and energy usage. Note that, since differences exist between simulation and experiment, these figures should be interpreted with care.

Results for the column sizing are presented in table 7.3, with the KPIs in table 7.3. Recommendations for the practical implementation of these protoypes can be found in section 8.2.

Simulated KPI’s The systems are simulated to determine the KPI’s as developed on section 7.2. The results of this are shown in table 7.4.

Table 7.3: Adsorption model results for column sizing

	3X, field setting		10X, lab setting	
L	0.73	[m]	0.51	[m]
D	0.024	[m]	0.035	[m]
$t_{breakthrough}$	43407	[s]	44165	[s]
Xw,avg	0.244	[kg/kg]	0.233	[kg/kg]
DeltaP	380	[Pa]	804	[Pa]
Re	6.56	[-]	8.42	[-]
$m_{sorbent}$	0.238	[kg]	0.353	[kg]

Table 7.4: Simulated desorption time, average desorption rate and specific energy of the two case study scenarios at **50%**, **80%** and **95%** desorption

	3X, lab setting		10X, field setting	
$t_{50\%}$	0,130048	[$s_{desorption}/s_{adsorption}$]	0,128427	[$s_{desorption}/s_{adsorption}$]
$t_{80\%}$	0,219204	[$s_{desorption}/s_{adsorption}$]	0,21474	[$s_{desorption}/s_{adsorption}$]
$t_{95\%}$	0,302831	[$s_{desorption}/s_{adsorption}$]	0,285611	[$s_{desorption}/s_{adsorption}$]
$ADR_{50\%}$	2,17E-05	[(kg/kg)/s]	2,06E-05	[(kg/kg)/s]
$ADR_{80\%}$	2,05E-05	[(kg/kg)/s]	1,97E-05	[(kg/kg)/s]
$ADR_{95\%}$	1,77E-05	[(kg/kg)/s]	1,76E-05	[(kg/kg)/s]
$SE_{50\%}$	3,043083	[kJ/g water]	3,260658	[kJ/g water]
$SE_{80\%}$	3,008186	[kJ/g water]	3,368222	[kJ/g water]
$SE_{95\%}$	3,006783	[kJ/g water]	3,384349	[kJ/g water]

8

Recommendations & Conclusion

8.1. Conclusions

The purpose of this work is to explore how the vapour output of a Direct Air Capture (DAC) system, containing CO_2 and H_2O can be processed to prevent excessive water damage to a compression system and other downstream operations. In order to do this, four subquestions are stated.

How does the interaction between the DAC and compression systems result in conditions that cause damage to downstream operations? As the DAC unit cools its output mixture in order to condense most of the water into a liquid state, it remains at or near the saturation pressure of water for that temperature. If this near-saturated mixture is then compressed and cooled back to the initial temperature, the partial pressure of water will always be higher than the saturation pressure, making condensation unavoidable without further processing.

What techniques are available to process the DAC vapour, before or after compression, to prevent damaging conditions from occurring? Many different separation techniques exist that could be relevant to solve the problem. In order to organise them, the central problem is redefined as a three-phase separation, where CO_2, H_2O and lubrication oil are all to be separated. What is known in literature as three-phase separation is done by integrating two consecutive two-phase separation systems into one. In the context of this work, this can be done by removing either the CO_2, water or oil first. All three possibilities to do so are portrayed in figure 8.1.

What is the most promising concept that be created which implements one or several of those techniques in the context of the ZEF micro-plant? As several concepts are analysed, it is concluded that the choice for the most promising one mainly depends on the interaction with the rest of the plant and is therefore inconclusive. The concept that entails the removal of water vapour before it reaches the compressor by means of a solid desiccant is chosen, as this offers the most opportunity for diversification of knowledge within the company. Two columns filled with the solid desiccant are used, one to adsorb the water vapour from the gas, and one that is heated in order to regenerate the column. The columns are integrated into a closed system which both preserves the process gas (CO_2) and prevents ambient air from entering the system. A simplified sketch of the concept is shown in figure 8.2. Integral to the working of the concept is the cooling of the desorption gas, which then deposits the water back in the flash tank in liquid form. If this desorption process can be done faster than the re-uptake of water as the desorption gas goes back to the active dryer, water is effectively removed from the system.

How can the characteristics and key performance indicators of a prototype of this concept be described and used, based on a model verified experiment? A model is built based on literature. This model primarily describes three states: Water content of the gas phase, water content of the solid phase and temperature. The adsorption process is modelled with a linear driving force model, an isotherm based on the Dubinin-Radushkevich equation, and mass and energy balances. The model is then verified against literature, uncovering some differences between sources. While based on the equations of Nastaj & Ambrozek [58], the results are more akin to Park & Knaebel [62]. The model does seem to adequately describe the situation. An experimental setup is designed and built that enables testing of the concept. This is done by drying a wet gas flow, checking for adequate dryness, and then

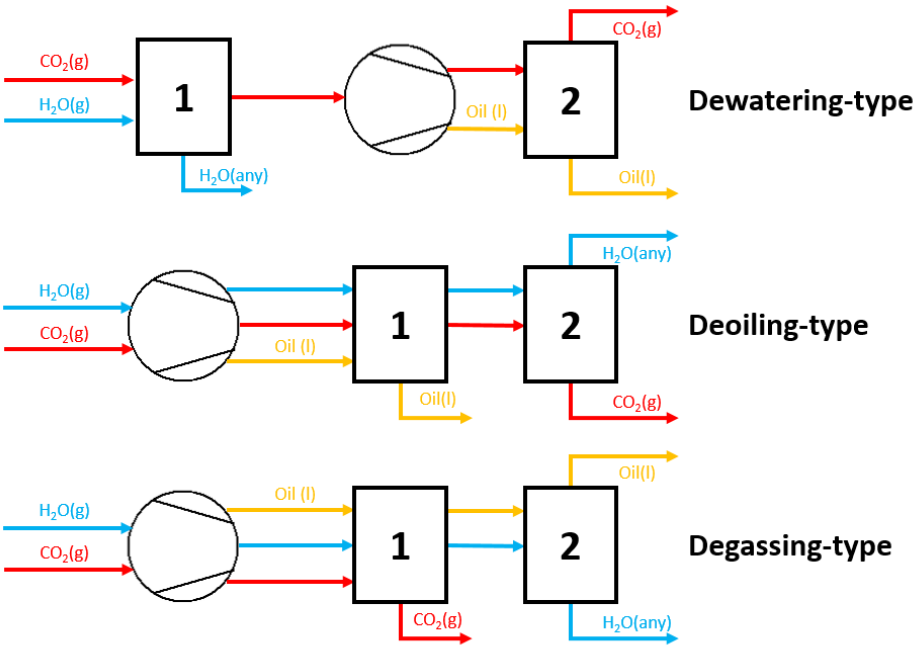

Figure 8.1: The three device types as identified in chapter 3

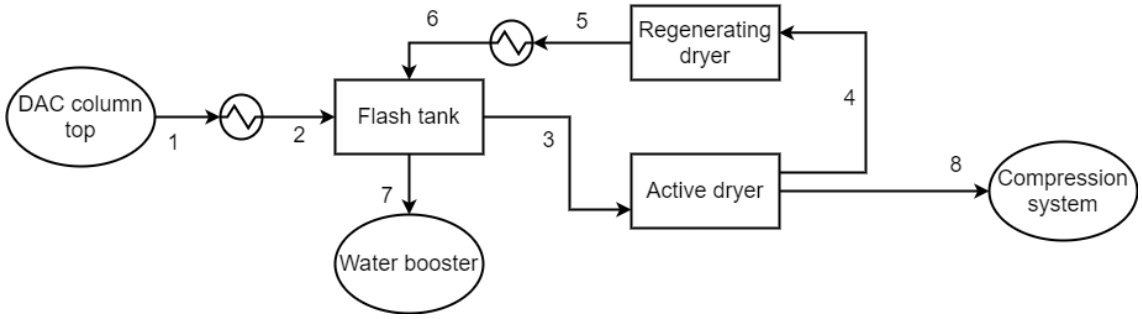

Figure 8.2: Simplified schematic of the closed loop concept.

using that quantity of dried gas to regenerate the column. This should be a faster process, and it is shown that this can be the case.

The same test setup is used to see how long adequate dryness of the gas can be maintained before the water breaks through, which can then be compared to the model. This revealed that the particular sorbent used is of importance for the model, as most literature sources used material with a smaller particle size. A larger mass-transfer coefficient allows a faster establishment of equilibrium, and thus a smaller section of the column that actively engages in adsorption, allowing a larger share of the column to retain water before breakthrough.

The heat and mass transfer coefficients can be fitted to model data, resulting in adequate predictions of adsorption behaviour, but in different desorption behaviours, with the model desorbing slower than the experiment and slowing down even more when a loading of 0 is almost reached.

Three key performance indicators are identified:

- Cyclic capacity: The average loading of the rich sorbent at breakthrough minus the average loading of the lean sorbent after regeneration (which is considered to be 0 based on the desorption experiment). This was simulated to be between 0.1 and 0.2 [kg water/kg sorbent] depending on adsorption conditions.
- Energy consumption: Several categories of energy use are defined, with the energy used for desorption, sorbent heating and has heating being considered inherent to the process itself. Fig-

ure 8.3 shows the energy consumption of the desorption experiment, averaged over 6 runs. The specific energy when excluding energy required to heat the heater and hardware varied between **4** and **6** [kJ/g].

- Desorption rate: the rate of water removal in [(kg water/kg sorbent)/s]. Several simulated scenarios are attempted to get an impression of the desorption process, how it progresses over time, and how it progresses relative to the time taken to adsorb that quantity of water. Typical values are between **1*10**$^{-5}$ and **2*10**$^{-5}$ [(kg/kg)/s]. No correlation is found between average rich loading and maximum desorption rate. The fine material simulations did appear to consistently have both a higher rich loading and desorption rate when compared to their coarse counterparts.

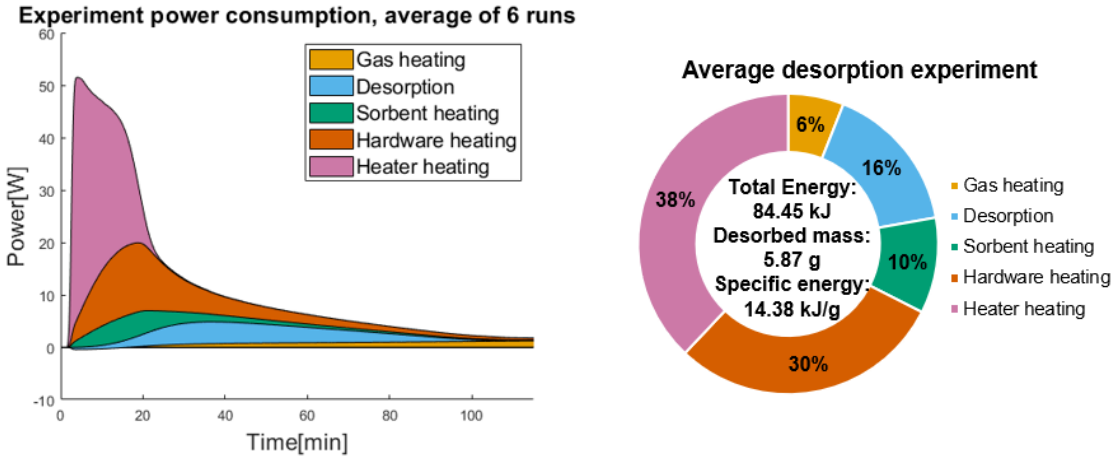

Figure 8.3: Overview of the energy consumption of the desorption experiment.

Finally, the main research question of this thesis: **"How can the CO_2 & H_2O vapour output of a Direct Air Capture system be processed to prevent excessive water damage to a compression system and other downstream operations?"** can be answered as follows:

The vapour output of a Direct Air Capture unit can be dried using a system based on a solid desiccant in a closed system, relying on the dried gas to regenerate previously used sorbent. This system can adequately dry the gas before the compression required for the methanol synthesis reaction. This can be done to the point where the partial pressure of water at the end of the compression system no longer exceeds the saturation pressure of water at the same temperature as the start of the compression system.

The first generation prototype of this system with supporting model provides ZEF with the tools and knowledge needed to further develop and optimise this Moisture Control System to play an integral role in their quest for a sustainable future.

8.2. Recommendations

This section presents the recommendations to continue development of a Moisture Control System for the ZEF micro-plant. This work is considered an explorative study to solve a problem that has not had any prior research done. As such, the aspects studied in this work can be considered to be the first generation of MCS prototypes, particularly in an environment such as ZEF where iterative design is the norm. An overview is presented in figure 8.4 on how particular lessons learned can be applied in the second and even third generation of MCS prototypes. They will be presented as four categories that can be summarised as follows:

- Prototyping recommendations: Practical suggestions for the implementation of the column sized in the case study of section 7.3.
- Experimental recommendations: As experimentation has been limited, particularly due to the COVID-19 pandemic lockdowns, the experimental setup as built in chapter 6 still has unused potential. These recommendations mainly describe additional useful knowledge that can be gained through experimentation.

- Model recommendations: Suggestions for the improvements on the adsorption/desorption model made in chapter 5, which primarily concern matching the experimental results in simulation.
- Strategy recommendations: These recommendations concern system-scale modelling, and the operational strategy of the MCS as an integrated part of the dynamically operated micro-plant as a whole.

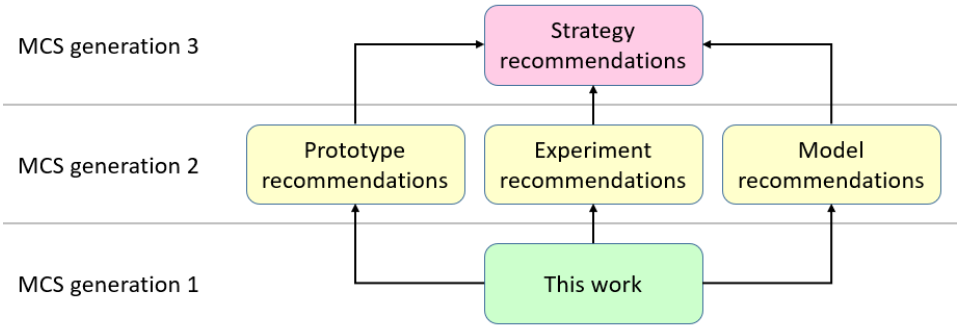

Figure 8.4: Categories of recommendations to further develop the MCS.

Prototyping recommendations

1. **Column aspect ratio:** Modelling from this work implies that a slim and long column has superior adsorption characteristics, due to an improved ability to release the heat of adsorption to the environment. It also improves the ability of the column to take up heat from said enviroment, which improves desorption characteristics. Note that limits will likely be encountered in either the practical implementation of the bed size, the ratio of particle diameter to column diameter, or pressure drop [86]. This should provide a designer with a minimum diameter.
2. **Material use:** It is recommended to use a silica gel with a fine particle size. Between the two materials tested in this work which had an average particle size of **1** and **4** [mm], the **1** [mm] material (often referred to as ”fine material” in this work) consistently performed better than its coarse counterpart. Note that the fine material does not have a higher capacity to retain water, but does introduce a higher mass-transfer coefficient, allowing it to move to equilibrium much faster. This creates a smaller active zone in the column where water is being adsorbed, allowing a much higher average loading at breakthrough. While the increase in pressure drop may appear severe, the low flow rate and small columns make it so that energy use for pressure drop is very small compared to other energy uses.
3. **Variable isolation:** It has been seen that during adsorption, it is beneficial to promote heat exchange with the enviroment, while during desorption when the column is heated, heat exchange with the environment is considered a loss. In order to circumvent this problem, it might be beneficial to isolate the column using a layer of stagnant air. A valve or hatch might then be opened to allow this air to freely flow again, allowing natural or forced convection of air very close to the column. A sketch of this concept is shown in figure 8.5. The concept of a convection oven might also be applied, using the air around the column for heating which, by opening the closed system and introducing ambient air, can be changed into cooling at will.
4. **RH&T sensors:** It is recommended to switch to Honeywell **HIH8121** sensors, as they are capable of performing the tasks of both types of sensors used in this work, and also have a better sensing ability at low humidity. It is recommended to create a clean, well documented implementation of this sensor type in the standard ZEF software library. This should make the low-cost sensor almost universally usable in future projects of ZEF with a very high ease of use for students who may be unfamiliar with electronics. It is also recommended to create a new iteration of the sensor setup tool which is used to assign the correct I²C addresses to the sensors, in order to also have this process streamlined and easy to use. It is recommended to place a pair of these sensors within the column, near both sides of the desiccant bed in order to accurately determine inlet and outlet conditions of the gas, as any changes occurring between the dry side sensor and the top

of the columns is unaccounted for. The dry side sensor can then be used for quality control of the gas that proceeds to the compressor and should be placed near the compressor inlet.

5. **Lab desorption:** It is recommended to include a small fan or air pump so that ambient air can be used for desorption in a lab setting. This may reduce the need for bottled gases and reduce the risk of having to wait for a column to regenerate as the bottleneck in integration testing.
6. **Heater design:** It is shown in section 4.2.1 that quite a large share of energy is used to warm up the equipment and heater, which is not considered ”useful” energy. As the goal is not to maintain a certain temperature, but rather to ”push” the energy into the adsorbed water, it is useful to place the heater as close to the column as possible or maybe even within the column itself. If the heater is placed on the outside of the column, it is considered useful to construct the column itself from a light, thin material with a low overall thermal capacity in order to take advantage of the near-atmospheric pressure environment and its associated low strength requirements on column material.

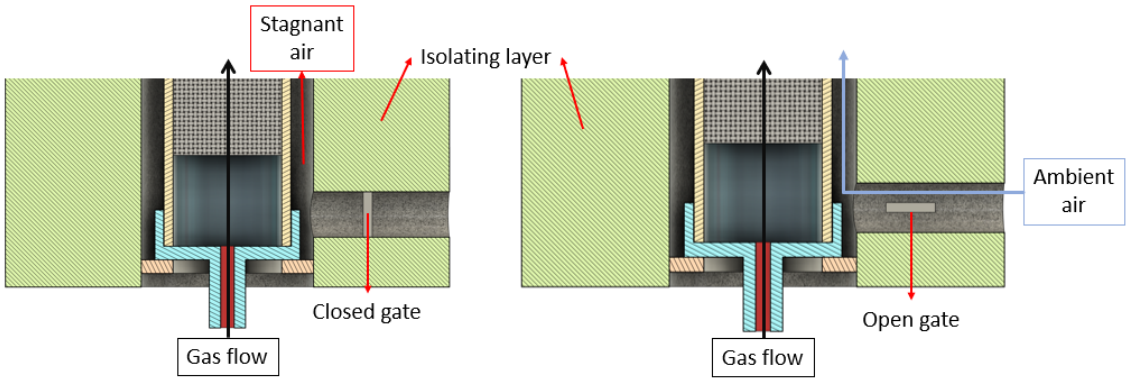

Figure 8.5: Sketch of the variable isolation concept.

Experimental recommendations

1. **Desorption experiment fine material:** First of all, it is recommended to repeat the desorption experiment with a fine material. It is expected that this material would show a higher desorption rate and a more readily visible ”plateau” in desorption output temperature as seen in section 7.1. This is associated with energy being used for desorption as a dominant factor, which implies more efficient operation. This should also provide valuable data on the last part of the desorption process, where average loading is very low.
2. **Variation of desorption temperature:** As implied by section 7.2.3, a higher desorption temperature would result in a higher desorption rate. This could occur both by an increased saturation pressure at higher temperatures, as well as the isotherm shifting further. As higher temperatures also imply higher energy requirements, it is considered beneficial to test this higher desorption temperature and determine the specific energy requirement to determine whether this extra energy is actually used for desorption(section 4.2.1. After all, it is not the temperature, but a change in equilibrium that drives the desorption process.
3. **Variation of inert gas flow rate:** similarly to how the variation in desorption temperature could uncover the interaction between desorption rate and energy consumption, the variation of flow rate could provide insight in desorption rate compared to the gas requirements. This is considered useful due to the fact that in a closed system, gas used for desorption will pass through the adsorbing column as well after reducing its water content by cooling down to the temperature of the DAC flash tank. A low flow rate may reduce this re-uptake of water in the system, but a high flow rate may reduce the time required for desorption, both of which could reduce energy consumption. A test such as this might provide a good starting point for the development of a third generation prototype.
4. **Variation of material:** It is implied in various situations in both chapter 6 and 7 that not all desiccant is created equal, and that is only with two variations being tested. It is recommended to

get an overview of properties of various grades of silica gel and their differences, as well as the properties of other desiccants such as various zeolites, activated carbon and composites [95].

5. **Improve low humidity sensing capability:** It is considered that the most prominent roadblock in the development of the MCS is the discrepancy between simulated and experimental desorption rates near the end of the desorption experiment when the column is nearly dry. One cause of this problem may be the HIH6100 series sensor's capability to accurately measure at low humidity. The datasheet of the sensor shows a **±4%** accuracy for RH measurements. This means that the desorption experiments involve measuring well into the uncertainty range of the sensors. While this does not explain the difference in peak desorption rate, it will provide the opportunity of consolidating the confidence in the observations done by removing one more potential for error. It should also be noted that, since the MCS as a whole is to produce CO_2 at a RH of under **2%**, accurately measuring low relative humidity would be required anyway.

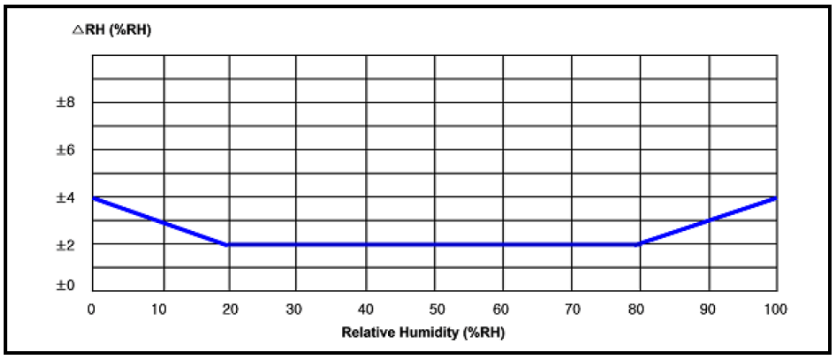

Figure 8.6: Telaire's ChipCap2 datasheet report a lower RH accuracy at very high and very low RH, which is common for these type of sensors [85].

Model recommendations

1. **Validity of isotherm and other parameters:** It is recommended to investigate what the limits are of the applicability of the the isotherm described by the Dubinin-Radushkevich equation, which is beyond the scope of this work. It is suggested from section 7.1 that even after fitting mass and heat transfer coefficients, a difference could be seen in measured and modelled desorption rates. This leaves the isotherm as the largest uninvestigated assumption that could cause both a lower peak desorption rate and slower approach to the point where loading is 0. As shown in appendix C.1, improvements can be made to the estimation of the heat of adsorption (equation C.9b) and mass transfer coefficients(equation C.10).
2. **Linear driving force:** It is recommended to develop a better understanding of the linear driving force adsorption model. While this model appears to be the used fairly commonly in literature, it does imply asymptotic behaviour of the desorption rate when the difference between the current state and equilibrium is low, which might introduce a problem when the equilibrium state cannot be shifted anymore, which is what happens when a loading of 0 is almost reached. An improved understanding of the linear driving force model in conjunction with the low RH sensing capability eperimental recommendation, should provide proper insight to why Schork & Fair[77], for instance, manage to very closely match their model and experimental data while this work did not.
3. **Fitting of material properties:** Another set of desorption experiment data using the fine silica gel as suggested in the experimental recommendations can enable the verification of the method used to fit heat and mass transfer data as done in section 7.1. This should enable improved analysis of desiccant materials in the future while also uncovering any wrong assumptions in the fitting process of this work that may have unintentionally created the model-experiment discrepancy.
4. **Simulate multiple cycles:** The model of this work concerned only a single cycle of adsorption and desorption. As of yet, it is undetermined whether the desorption process quickly reduces the column loading to 0 as implied by the experiment, or whether it lingers near 0 for some time

as implied by the model. It is assumed that this uncertainty would be amplified when running the simulation each cycle. However, as the MCS should be able to operate autonomously for many cycles, simulating this behaviour is deemed essential. Simulation of multiple cycles could be used to view the desorption process not in terms of water removed from the column, but rather in terms of time gained during which the regenerated column can operate without breakthrough. As the desorption process progresses, section 7.2 implies that desorption rate drops and section 4.4 implies that the near-unavoidable losses of gas heating become the dominant energy use. This should open up the way to progress toward selecting the most efficient desorption strategy, which might involve partially rather than full regeneration of the column.

5. Matching model and experimental data: While all other recommendations in this category imply that successfully and accurately replicating desorption in simulation should be a goal, this recommendations serves to reinforce that implication. In fact, the difference between model and experiment is seen by the author as the largest roadblock to the development of the MCS and should be resolved before creating system-scale models which are essential for the further development of the MCS concept.

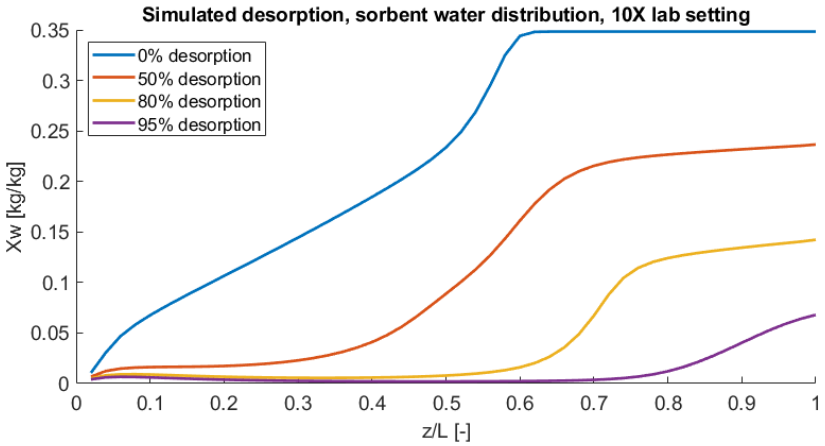

Figure 8.7: Water distribution at various stages of desorption for 10X lab setting. See E.2 for 3X data.

Strategy recommendations

1. **Create system model:** In order to find a good operational strategy for the MCS, it is essential to make a system-scale model, simulating all flows between the DAC top, AEC inlet and first compressor (Example: appendix A). By including the re-uptake of water by the gas used for desorption in the closed system, the desorption rate and specific desorption energy can be redefined with a more realistic definition, as the goal of the MCS is not to regenerate a column, but to remove water from a gas flow. This can be used to determine performance in terms of **[(g dry CO_2)/h]**, which is a better representation of the actual goals of the MCS when replacing the current desorption rate KPI.
2. **Relate desorption specific energy, desorption rate and adsorption rate:** As described in the experimental recommendations, variation of the flow rate in the regenerating column can have both beneficial and detrimental consequences. Using a system-scale model, it should be possible to add the (energy) costs of higher desorption rates and the (energy) benefits of lower water re-uptake to the model. Note that this type of model could also effectively accommodate energy externalities(section 4.3) such as reduced compressor power. This allows the utilisation of **[(g dry CO_2)/h]** as a boundary condition of which a minimum is to be met, with the KPI changing to a unit of **[kJ/g dry CO_2]**.
3. **CapEx/OpEx analysis and concept augmentation:** the optimisation of energy consumption as suggested by the previous recommendation should provide a good stepping stone for an improved level of analysis by weighing capital expenditure (CapEx) and operational expenditure (OpEx). This allows a designer to change the KPI to a unit of [€/g dry CO_2], which should help to

provide a fair comparison to potential augmentations to the MCS. Examples of these augmentations can include:

- A fan for active cooling(higher CapEx and OpEx), which allows a higher average loading at breakthrough and therefore a smaller column which requires less energy to heat (lower CapEx and OpEx).
- A more elaborate column design with a heater on the inside to heat the columns from the inside out (higher CapEx, lower OpEx)
- A heat pump (higher CapEx and OpEx) to cool the MCS inlet gas and/or an improved heat exchanger(higher CapEx) to cool the DAC outlet gas to (sub-)ambient while simultaneously providing heat to another area of the plant (lower OpEx).
- A more thorough drying of the gas (higher OpEx and/or CapEx), to improve compressor lifetime(lower CapEx) and flow rate (lower OpEx).

4. **Investigate multi-stage/multi-material adsorption:** As the average desorption rate drops near the end of the desorption process, it might be useful to split the operation in two stages. The first stage could focus on removing the bulk of the water, resulting in frequent regenerations that are optimized for efficient water removal. The second stage would then focus on removing the last bit of water from the flow, requiring a less frequent, but more thorough regeneration. This can be done by selecting appropriate desorption strategies for each stage, but could also include using a different desiccant. Several papers are found investigating the benefits of combining desiccants for a more efficient dehumidification device. This literature is considered well beyond the scope of this thesis, but can prove to be interesting nonetheless. A future researcher can investigate to determine the applicability of using a multi-stage or multi-material approach in order to more efficiently get to the very low humidity required by the compressor.
5. **Link MCS models to DAC models:** Throughout this work, a set of assumptions are used on the output of the DAC subsystem. However, as development of the DAC subsystem progresses, the iterations should include the knowledge gained from the MCS development to determine desired DAC output and vice versa. Recent efforts have started to show the effect of external conditions on the DAC output [27, 55], with this work showing that both the DAC output conditions and ambient conditions play a significant role for the MCS. As the scenarios in section 7.2.3 suggest, the MCS may be more or less effective depending on ambient conditions, which may correlate to more or less ubiquitous availability of solar energy. This creates an interesting tradeoff for future designers to mix and match features of the ZEF micro-plant corresponding to the climate where the system is to be deployed and/or the wishes of the user.

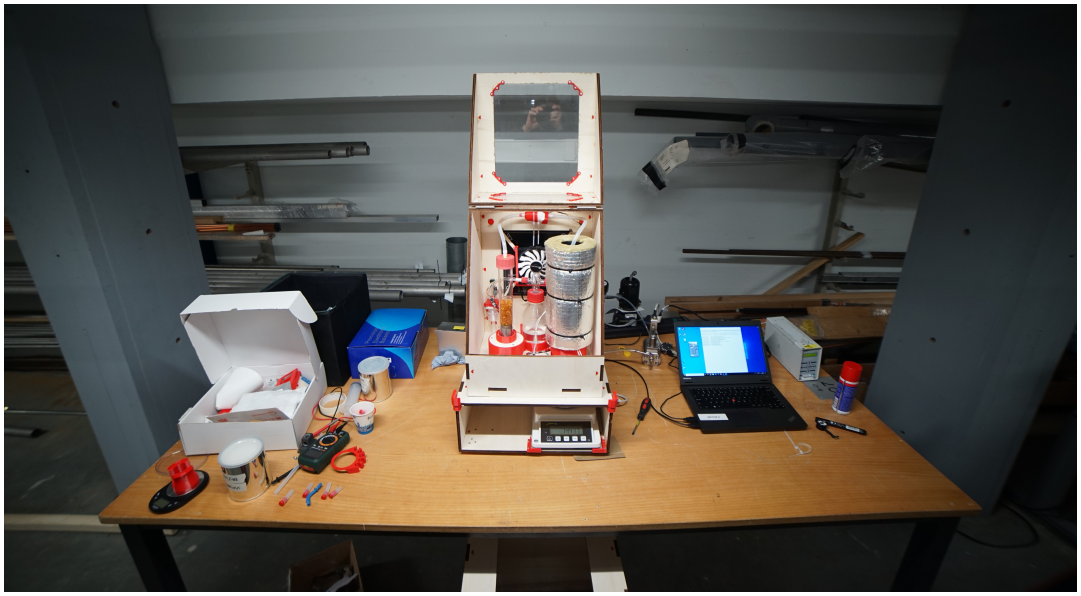

Figure 8.8: Work in progress on the experimental setup.

A

Process Flow Diagrams

Various versions of the PFD and flow inventory of the ZEF micro-plant that are used throughout this work are considered company property and are not disclosed here. Should the reader require these PFDs anyway, please inquire with ZEF B.V. The background and conceptualisation (chapters 2 and 4) are based upon version 18. Section 7.3 designs the columns for use in PFD version 27.

A.1. Concept PFDs

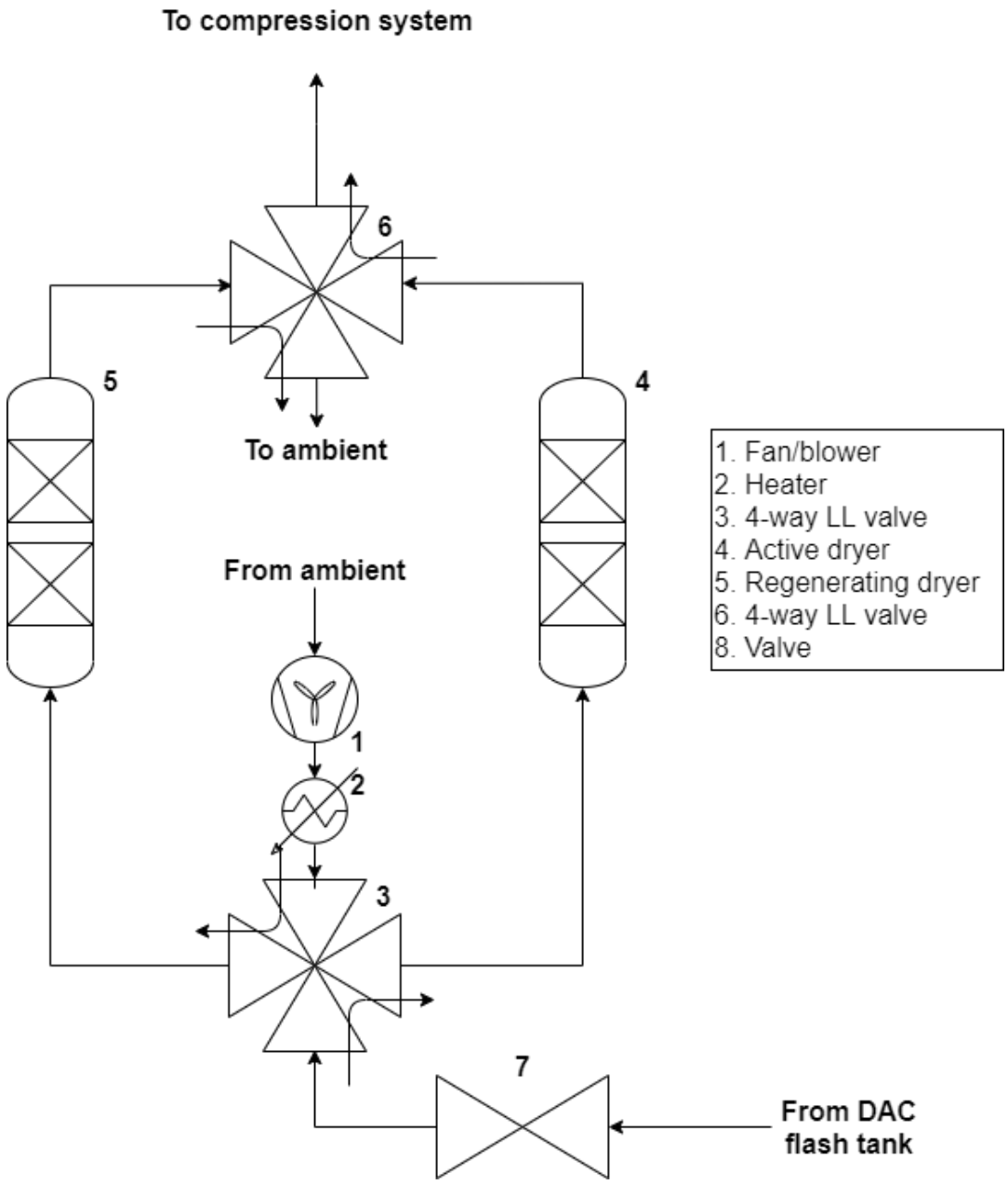

Figure A.1: PFD of the double-column concept setup

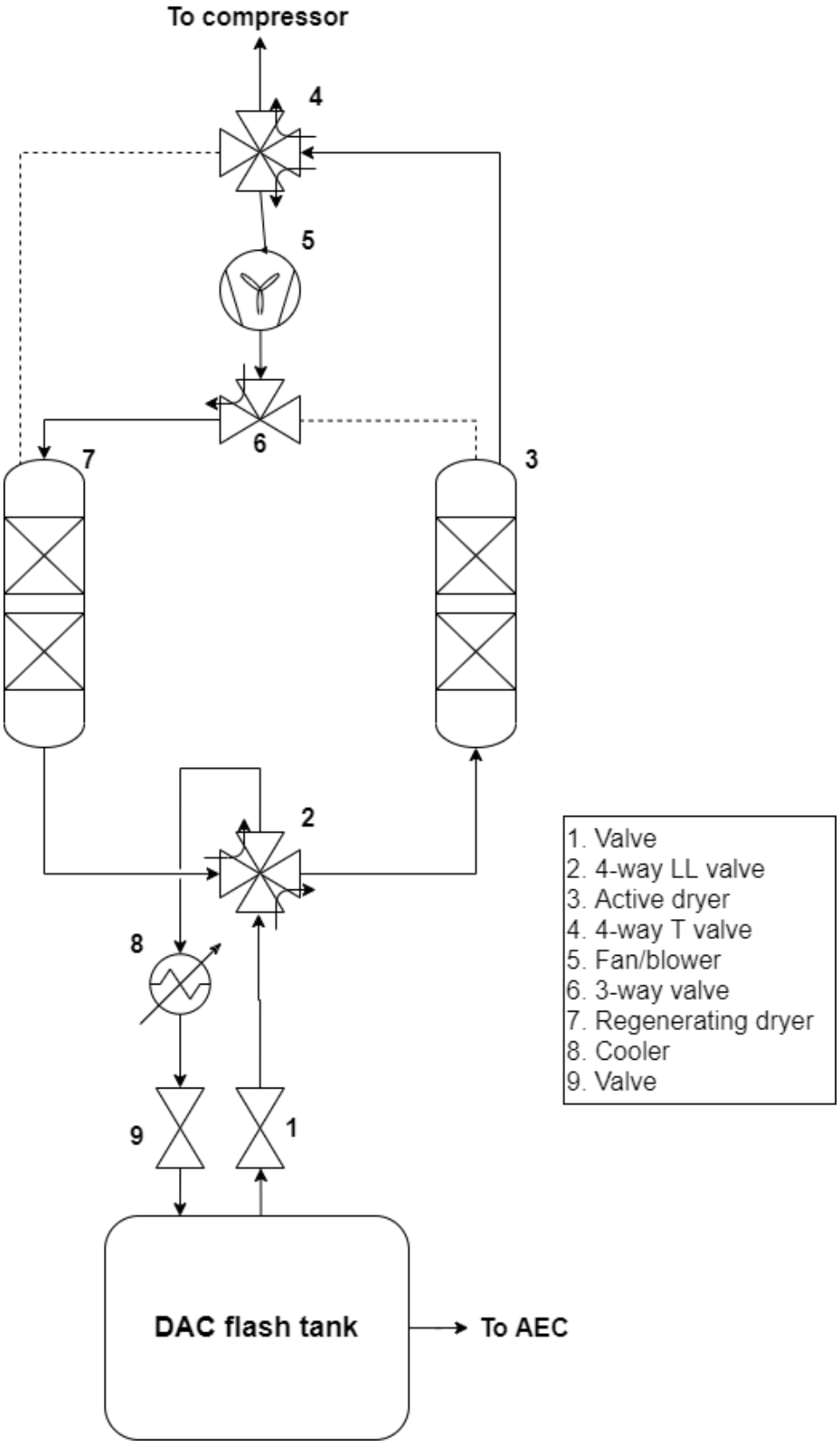

Figure A.2: PFD of the looped-column concept setup

B

Conceptualisation documentation

B.1. Function analysis

This subsection attempts to take inventory of the functions of the desired device, separated in main and sub-functions[13]. The sub-functions will be described as concerning either one or all types of separators. Then, potential solutions to these sub-functions will be discussed. In section B.2, these partial solutions will be combined to create several principle solutions [13] that will be investigated further.

It should be noted that this section has a significant overlap with the MoSCoW model presented in section 2.2 and chapter 4. The function analysis is not included in the main report for this reason, but might aid a reader to understand the thought process that translated the theoretical investigation of chapter 3 to the principal solutions that start chapter 4.

Main function: Separate water, oil and carbon dioxide in separate streams that are rich in one of these compounds, in accordance with the MoSCoW model.

Sub-functions: all types

- Provide an adequate cooling to comply with the inlet conditions of the next compression stage
- Feed separated oil to compressor(s)
- Feed separated carbon dioxide to next compression stage or reactor
- Feed separated water to purge
- Follow plant operation based on (solar) power availability

Sub-functions: dewatering-type

- Remove water from the direct air capture outlet stream (Dewatering-1 separator)
- Separate oil and CO2 from the compressor outlet stream (Dewatering-2 separator)

Sub-functions: degassing-type

- Remove CO2 from the compressor outlet stream (Degassing-1 separator)
- Separate oil and water from the degassing-1 outlet stream (Degassing-2 separator)

Sub-functions: deoiling-type

- Remove oil from the compressor outlet stream (Deoiling-1 separator)
- Separate CO2 and water from the deoiling-1 outlet stream. (Deoiling-2 separator)

B.2. Morphological table

This appendix will present partial solutions to each sub-function presented in section B.1 that is not a separation. This enables the combination of these solutions with a first and second separator of a single device type, as stated in table 3.2, into principal solutions [13] that serve as a starting point for concept analysis.

It must be stated that regarding the connections, the Swagelok tubing system is the preferred standard within ZEF. During design embodiment, it can be chosen to integrate several components in a single housing, eliminating the need for tubing. However, it is considered that this stage is too early for integration of parts.

Table B.1: Partial solutions per device function

Cooling duty	**Oil recycle**	**Plant operation**	**Feed CO_2 to next stage**	**Feed water to purge**
Plate fin heat exchanger (natural convection) Plate fin heat exchanger (forced convection) Shell & tube heat exchanger	Distributed per stage Centralised for all stages	Batch, during peak power availability Batch,during heating/cooling transients Batch, based on day/night cycle Continuous, synchronous with plant	Swagelok tubing system, pumped Swagelok tubing system, valve Swagelok tubing system, passive	Swagelok tubing system, pumped Swagelok tubing system, valve Swagelok tubing system, passive

B.3. Low potential principal solutions

The following principal solutions were considered, but deemed insufficiently promising to be included in the main document.

Concept 3: Centralized membranes (degassing-type)

- Separator 1: settling tank
- Separator 2: ultrafiltration membrane(s)
- Oil recycling: centralized
- Operation: based on heating/cooling (backup: based on power availability)
- Cooling configuration: after compressor

Short description: This concept collects the emulsion produced during the day across the entire compression train, and attempts to push this through a centralized filtration system in one batch per day to eliminate the need of multistage filtration systems after every compressor. This concept presents many opportunities to optimize the operation. For instance: the pressure and/or heat that is left in the plant during nightfall as an energy source. Alternatively, the oil can be filtered at night, to take advantage of the lower solubility of water in cold oil, removing more free water. It is also possible to filter the oil during day time when energy supply is highest.

Concept 4: Basic coalescer (degassing-type)

- Separator 1: settling tank
- Separator 2: structure/packed bed coalescer (backup: added (membrane) filter)
- Oil recycling: distributed
- Operation: based on peak power availability

Table B.2: Pros and cons of the desiccant dehumidifier concept

Pros	Cons
•Low pressure drop of gas stream •Low strain on plant-wide energy supply •Remove both free and dissolved water	•Complexity of system/many components needed. •Potential to require many filtration stages to reach desired purity •Many unknowns in overall system behaviour •Potentially high capital costs
Opportunities: •Energy integration with plant •Utilizing solubility changes with temperature	Dependencies: •Start/stop characteristics of plant •Availability of pumps to recycle oil to various stages

- Cooling configuration: after compressor

Short description: This concept collects the emulsion formed and allows the droplets to coalesce with the assistance of a structure or packed bed. Once peak power is available or when the liquid levels rise, the oil-rich and water-rich phases are pumped away. If needed, an additional (membrane) filter can be added to remove the droplets that are too small for the coalescer to remove.

Table B.3: Pros and cons of the basic coalescer concept

Pros	Cons
•Low pressure drop of gas stream •Low strain on plant-wide energy supply	•Difficulty/inability to remove droplets in the <10 micron range. [citeme dropletregimes]
Opportunities: •Incremental/iterative development	Dependencies: •Effect of micron-sized water particles on compressor life

When considering the four principle solutions that have been presented in section 4.1 and in this section, all four concepts seem viable. However, not all concepts appear to be equally viable. For instance, the centralized membrane concept will be eliminated due to the likelihood of high complexity and high capital costs. It is likely that many filtration stages will be needed to achieve the desired product quality, resulting in high costs. The membrane modules that are available on the market are also a lot larger than required, as the flowrates of the ZEF microplant are incredibly low (<0.001 m^3/day). This would require either unnecessarily large equipment to be purchased and used, or custom membrane modules to be developed that are suitable for mass production. This is deemed beyond the scope of this thesis.

The other concept that will be eliminated from consideration is the basic coalescer concept. Despite being the simplest and probably most low-cost of all concepts, it is also very unlikely that very small droplets of free water can be successfully separated [erdpel-citeme minimum droplet size]. Thus, (small quantities of) water would remain in the oil. This would require an investigation of the damage these small droplets can do to the equipment over time. This, while highly interesting, is considered out of the scope of this project which means this serious risk is wholly unaccounted for. Since the compression system is critical for further development of the plant and company, it is preferred to have an uncertainty in price, rather than an uncertainty in whether the working principle is effective. This concept could, however, be revisited when attempting a design iteration to reduce the microplant's cost price.

B.4. Harris profile elaboration

This section presents the more detailed elaboration that resulted into the creation of the Harris profile presented in section 4.3. These estimates are made based on the knowledge gained from chapters 2

and 3, as well as discussions with ZEF colleagues and undocumented experiences of the author. The concepts discussed are the delayed condensation (DC) and desiccant dehumidifier(DD) concepts.

•The concept device's energy consumption should be minimized.

As this is the most important of the criteria, it is discussed in the main document in section 4.3. However, some elaboration still applies, particularly in calculating the energy flows outside of the device scope.

Regarding the compressor savings, it was assumed that the energy use of a compressor scales linearly with the processed volume. When water is removed, this processed volume is reduced, thus saving energy. The effect of the reduced volume flow and altered flow composition on the lifetime of the compressor and its energy- and financial effects are considered to be well beyond the scope of this thesis.

It must also be noted that the compression system at ZEF is not yet at an advanced stage of development. Thus, estimating the energy usage of the compressor is fully based on a theoretical estimate. Current development suggests that compressors that are very well custom-engineered may reach that 50W estimate. It is also suggested that developing the (near) perfect compressor for the job is several years out of reach. With ZEF wanting to perform integration testing in 2021, it is considered that the energy savings in the compressor are even higher short- and medium-term development.

The heat of adsorption is very much an optional factor, as ZEF intends to leverage the ambient temperature in conjunction with passive heat exchangers, relying on the environment to create that cooling duty. However, it is considered unwise to discount the increased cooling duty as "free energy", since rarely anything really is for free. It is expected that this increased cooling duty increases the size of the required heat exchanger and thus capital cost of the plant. It is also conceivable that, in order to maintain a reasonable size, active cooling is required to force convection in windless ambient conditions. How to deal with this energy flow is not in the scope of this thesis, but it is mentioned here for the sake of a thorough and complete analysis and illustrates once more that the externalities are of equal or larger impact on the concept choice, than the concept itself.

A similar situation to the compressor system is true for the DAC system, in the sense that it too will change a lot over time in both product conditions and energy use. Furthermore, this "purge penalty" only applies when water is actually the limiting factor in methanol production. Early work assumed this was never the case, but recent work indicated that situations are conceivable where this is the case [27]. This makes the energy cost associated with the purge penalty an operational problem, more than a technical one, since most places in the world where the ZEF system can be deployed, do not face this problem. It also places this problem outside the scope of this thesis. It is conceivable that the dehumidifier concept allows the geographic boundaries where the ZEF system is viable to grow, but it is also conceivable that multiple versions of the ZEF system will exist further in development, based on varying climates. For the purposes of this work, the described dilemma is considered an addition to the argument for adding variation of knowledge to the company.

•The concept's dependencies should be reasonably solvable

DC – Examples of small coalescing filters are available on the market. Rated flowrates are still much higher than expected. A problem that needs to be solved however, is the temperature. The Parker Balston 9933-11 filter considered in the energy use calculation for instance, has a maximum operating temperature of 110 °C, which is lower than the compressor output and is close to the expected dewpoints after the compression stages. It is possible that metal mesh based filters can deal with higher temperatures though.

DD – A large range of desiccants can be found for many purposes. The selected desiccant should adsorb and desorb at relatively low temperatures and work well at high relative humidity. More work can be placed in the selection of desiccant family-group [citeme various families of desiccant] and specific type of desiccant [citeme various types of desiccant]. The day/night cycle appears to not affect desiccant performance much, while the temperature does [citeme desiccant temp]. Waste heat is not of very high temperature, but could play an assisting role in heating.

•The concept device should be make-able within thesis time constraints

DC – Should be very feasible. Many prototyping problems might already arise in the device of Jim Tomassen, colleague at ZEF, as it operates on the same working principles. This means they can be

avoided in this iteration, leaving time to ensure proper sensing methods for the resulting water and oil streams.

DD – Should be very feasible. Does not require the compressor in order to test. Adequate sensing should be easier to achieve via relative humidity and temperature. A major advantage can be found in the fact that the dehumidifier would operate at near-atmospheric pressure, greatly increasing the ease of prototyping since achieving a leak-tight system under pressure is a notorious time-sink within the company.

•The concept should be compatible with likely development of the ZEF system and design methodology in the coming years

DC –Ramon de Koning's work at ZEF considered the inclusion of a dry compressor as a first stage to be beneficial. Should this be implemented, the condensation can take place after the first compressor stage, where the results from this project will assist in finding good practices on the condensation and filtering of consecutive compressors. However, coalescing filters can still be very useful to prevent small liquid droplets from being gas stream "stowaways".

DD – The desiccant concept removes material from the input. Whereas water in vapour form in the compression train and/or reactor might not be harmful, it does not pose any benefits. Thus, compressed water vapour can be considered wasted energy. This means that the results from this project will provide insights in further projects aimed at operational optimization and overall plant efficiency.

•The concept device should maximize water removal from critical components

DC – Assume that the first-stage compressor compressed from **1** [bar] to **8** [bar], the partial pressure of saturated water vapour remains roughly equal in situations of equal temperature. Assuming that the mixture is cooled back to ambient temperature after compression, it is found that 7/8 of the water content condenses. This is due to the partial pressure increasing eightfold, while the saturation pressure hardly increases, indicating that only 1/8 of the water content of the compressed mixture can stay in. To generalise, it can be stated that the remaining water content is equal to one divided by the compression ratio.

DD – Desiccant dryers reach dewpoints of -40 [°C]. Most psychrometric tables do not have data on those temperatures, but literature states that between 95 and 99 percent of the water content can be removed [16]. For simplicity, it is assumed in the energy consumption criterion that all water is removed, as the energy use of the compressor is less accurately estimated than this number.

•The concept device's operation should be compatible with plant operation

DC – Due to the expected small size of the coalescing filter, it should not take a lot of energy to heat up the device. In fact, at the time of this project, the small available coalescing filters would be among the smallest actively heated components in the plant. Should the device be properly thermally insulated, it is suggested that it might even be feasible to maintain the device's temperature overnight, or reduce energy consumption when preparing the device for operation in early morning. This is based on heating up the device and its heat loss through the insulation walls being in the same order of magnitude.

DD – As the input of the absorber is directly connected to the output of the DAC system, it is expected that the device will easily be able to track plant operation. One of the desiccant towers might even be omitted if it turns out to be more efficient to purge the device at night when the plant is not active.

•The concept device's failure risks should be predictable and allow potential for mitigation

DC – If the composition of the device's output streams can be measured in situ, any problems should be picked up quickly, allowing maintenance crews to react before the plant is damaged. Replacement of the filter could also be remotely monitored by measuring for increased pressure drop across the filter. A potentially large problem is thermal control of the gas that goes into the coalescing filter, which needs to be warm enough to prevent condensation, but not exceed the filter's maximum operating temperature in order to prevent damage. Another problem is that there is no redundancy in this system. Should something fail, the plant must be shut down immediately to prevent damage to the compressors which may not always be possible in a way that still prevents condensation.

DD – This concept will likely consist of more parts and thus have more failure modes. However, by using low-cost humidity sensors, operation could be monitored easily. The fact that most parts can be

operated passively during operation will introduce a chance that a damaged system can still complete the day. This allows for replacement at night, removing the need for plant shutdown in case of some failures.

•The concept device's cost should be minimized and enable further reduction in future iterations

DC – As coalescing filters already exist on the market, this can be seen as a mainly business related problem, rather than a technical one. Deals can be made with manufacturers to reduce unit price when large quantities are purchased. Due to the ubiquity of pressure vessels and heat exchangers in the plant, those are not considered critical nor part of this project. Vertical integration by means of developing the filters in-house, might reduce the dependencies on other companies and reduce cost even further.

DD – While this concept will likely introduce more valves, it can be expected that the actual desiccant is relatively low-cost. Since there is no need for third-party devices from specific manufacturers such as the coalescing filter, this concept is considered to have a similar cost.

B.5. Energy consumption calculation details

Table B.4 presents the assumptions used for the energy calculations of section 4.2.1.

The DC concept is modelled after a Parker Balston 9933-11 coalescing filter, which is made out of nylon. The DD concept is modelled as silica gel that is capable of adsorbing **0.2** [g water/g desiccant]. For simplicity, the DC and DD concepts are modelled as a nylon and silica gel cylinder respectively that needs to be heated. A sketch depicting this setup can be found in figure B.4.

Table B.4: Parameters of the rough energy consumption calculations

Concept	Symbol	Parameter	Value	Unit
Both	T_{amb}	Ambient temperature	40	[°C]
Both	$m_{\mathrm{H_2O},daily}$	Daily water target	0.08	[kg/8h]
Both	$m_{\mathrm{CO_2},daily}$	Daily CO2 target	0.825	[kg/8h]
Both	t_{ins}	Insulation thickness	0.02	[m]
Both	k_{ins}	Insulation thermal conductivity	0.02	[W/m2K]
Both	L	Cylinder height	0.120	[m]
DD	D	Cylinder diameter	0.055	[m]
DD	c_p	Cylinder thermal capacity	1.6	[kJ/kgK]
DD	T_{op}	Operating temperature	120	[°C]
DD	X_w^*	Desiccant capacity	0.2	[kg/kg]
DD	ΔH	Heat of adsorption	3260	[kJ/kg]
DC	D	Cylinder diameter	0.036	[m]
DC	c_p	Cylinder thermal capacity	1.13	[kJ/kgK]
DC	T_{op}	Operating temperature	110	[°C]
Both	E_{warmup}	Energy to heat up cylinde	TBD	[kJ]
Both	$\dot{Q}_{walls}$	Average heat flux through walls	TBD	[kW]
Both	E_{walls}	Energy lost through walls	TBD	[kJ]
DD	E_{ads}	Heat of adsorption of $m_{\mathrm{H_2O},daily}$	TBD	[kJ/8h]

B.6. Ergun Equation

The Ergun equation as presented in equation B.1 can be used to estimate pressure drop in a packed bed. This pressure drop is then used to find the associated energy consumption.

$$\Delta p = \frac{150\mu L}{D_p^2}\frac{1-\epsilon^2}{\epsilon^3}v_s + \frac{1.75L\rho}{D_p}\frac{1-\epsilon}{\epsilon^3}v_s|v_s| \tag{B.1}$$

$$P_{losses} = \Delta p * Q \tag{B.2}$$

Δ p = Pressure drop in [Pa]

μ = Dynamic viscosity [Pa s]
L = Length of bed
D_p = Particle size [m]
ϵ = Void fraction [-]
v_s = Superficial velocity of the fluid [m/s]
ρ = density of the fluid[kg/m^3]
P_{losses} = Power consumption due to pressure drop [w]
Q = Volumetric flow rate [kg/s]

From equation B.2 it can be seen that, since the volumetric flow rate of the ZEF system is in the order of 1*10^{-5} [kg/s], power consumption due to pressure drop is 1[W] per 10^5 [Pa] or 1 [bar] pressure drop, which is very unlikely to occur in the setting of this work. For instance: pressure drop of the coarse material column with 100 [g] sorbent as used throughout chapter 6 6.5 is estimated to have a pressure drop of a mere 17[Pa]. When changed to the fine material described in section 6.5, this increases to 222[Pa], which is still considered negligible, especially when real pressure drop throughout the system is estimated in the 1-10 [kPa] range in section 6.4. Even readily available pressure drop calculators show higher pressure drops for the inlet connector alone, due to its 3mm diameter, than for the entire packed bed.

The pressure drop has been calculated at various points throughout this work, including the fine material used in chapter 7, and was not found to exceed 1 [kPa], leaving the power loss due to pressure drop at less than 0.01 [W] which is considered negligible. Therefore, the energy consumption due to pressure drop is not considered in this work.

Pressure drop is calculated nonetheless for each column that is designed, in order to ensure that fluidization does not occur.

C

Model appendix

C.1. Model equations and implementation

In Nastaj & Ambrozek (2009), time and space is made dimensionless with equations (C.1a and C.1b:

$$\tau = \frac{J_i t}{\rho_{i0} L} \tag{C.1a}$$

$$Z = \frac{z}{L} \tag{C.1b}$$

ρ_{i0} = Density of inert gas at column inlet [kg/m^3]
L = Column length [m]
z = Space coordinate [m]

As stated in section 5.2, a spatial discretization is applied to obtain equations C.2, C.3 and C.4. This is done in order to divide the bed into N sections, reducing the system of partial differential equations to ordinary differential equations in order to solve them using well-known tools. Note that in the 2009 paper, N = 50 and the dimensionless equations are valid for 2 ≤ n ≤ N+1.

$$\frac{\partial X_w}{\partial \tau} = \frac{\rho_{i0} L}{J_i} K_w (X_w^* - X_w) \tag{C.2}$$

$$\frac{\partial Y_w}{\partial \tau} = \frac{D_l \rho_{i0}}{J_i L \epsilon} \frac{Y_{n+1} - 2Y_n + Y_{n-1}}{\Delta Z^2} - \frac{\rho_{i0}}{\rho_i \epsilon} \frac{Y_{n+1} - Y_n}{\Delta Z} - \frac{\rho_b}{\rho_i \epsilon} \frac{\partial X_w}{\partial \tau} \tag{C.3}$$

$$\frac{\partial T_n}{\partial \tau} = \frac{k_e \rho_{i0}}{J_i \rho_b L c_\Sigma} \frac{T_{n+1} - 2T_n + T_{n-1}}{\Delta Z^2} - \frac{\rho_{i0} c_{p_g}}{c_\Sigma} \frac{T_{n+1} - T_n}{\Delta Z} + \frac{\Delta H_w}{c_\Sigma} \frac{\partial X_w}{\partial \tau} - \frac{\rho_{i0} L 4 k_w}{J_i \rho_b D c_\Sigma} (T - T_\infty) \tag{C.4}$$

The initial and boundary conditions that apply are described in equations C.5 and mainly imply that input conditions are dictated by a constant temperature and humidity, that the gas water content and temperature no longer change with respect to space beyond the column's domain and that initial conditions are pre-determined.

$$\begin{aligned}
Y_{w_{in}}, (0, \tau) &= Y_s \phi && \text{at Z = 0} \\
T(0, \tau) &= T_{in} && \text{at Z = 0} \\
\frac{\partial Y_{w_{N+1}}}{\partial Z} &= 0 && \text{at Z = 1} \\
\frac{\partial T_{N+1}}{\partial Z} &= 0 && \text{at Z = 1} \\
Y_w(Z, 0) &= Y_{w_0}(Z) && \text{at } \tau = 0 \\
X_w(Z, 0) &= X_{w_0}(Z) && \text{at } \tau = 0 \\
T(Z, 0) &= T_0(Z) && \text{at } \tau = 0
\end{aligned} \tag{C.5}$$

Y_s = Water content of gas phase at saturation pressure [kg/kg]
ϕ = Relative humidity [-]

Several additional variables are to be calculated. Formulae for the gas phase heat capacity and overall volumetric heat capacity are shown in equations C.7a and C.7b and are obtained from the 2009 paper, as is the two-site Dubinin-Radushkevich equation and the used parameters as shown in equation C.6a.

$$X_w^* = X_{0,1} exp\left[-\left(\frac{A}{E_{0,1}}\right)^2\right] + X_{0,2} exp\left[-\left(\frac{A}{E_{0,2}}\right)^2\right] \tag{C.6a}$$

$$A = RTln\left(\frac{p}{p_s}\right) \tag{C.6b}$$

$X_{0,1}$ = 0.27530 [kg/kg]
$X_{0,2}$ = 0.07302 [kg/kg]
E_1 = 3443.4 [J/mol]
E_2 = 10931.0 [J/mol]

$$c_{p_g} = (c_{p_i} + Y_w c_{p_{w,g}}) \tag{C.7a}$$

$$c_\Sigma = \rho_b (c_{p_s} + X_w c_{p_{w,l}}) + \epsilon \rho_i c_{p_i} \tag{C.7b}$$

c_{p_i} = Heat capacity of the inert gas [J/(kg K)]
$c_{p_{w,g}}$ = Heat capacity of water vapor [J/(kg K)]
c_{p_s} = heat capacity of desiccant [J/(kg K)]
$c_{p_{w,l}}$ = Heat capacity of liquid water [J/(kg K)]

The density of the gas is also obtained via the ideal gas law as described in equation C.8.

$$\rho_i = \frac{M_w P}{RT} \tag{C.8}$$

M_w = Molar weight [g/mol]
R = Universal gas constant[(L bar)/(K mol)]

Upon further inspection after implementation of the equation governing the heat of adsorption, it is found that Park & Knaebel use a slightly different method than the one used by Nastaj & Ambrozek and followed in this paper. Park & Knaebel substitute the Antoine equation(equation C.9a for water into an expression for the isosteric heat of adsorption, resulting in equation C.9b which results in an expression where the first term is the adsorption potential (equation C.6b) which is not accounted for in this work. The second term is the heat of vaporization of water, as obtained from the Clausius-Clapeyron equation, which is used in this work.

$$lnp^* = a - b/(T + c) \tag{C.9a}$$

$$\Delta H = -A - bRT^2/(T + c)^2 \tag{C.9b}$$

a, b, c = Antoine equations coefficients (for water)
A = Adsorpion potential described by C.6b

Solver selection MATLAB offers a diverse array of built-in solvers that are suitable to serve as temporal solver in this model, and building a custom solver might be helpful in various situations as well; choosing the correct solver is not trivial. Nastaj & Ambrozek state to use Adams-Moulton's or Gear's method in FORTRAN [58], the equivalent of which in MATLAB is ode15s. ode15s specialises in solving stiff differential equations: equations that turn unstable when using most common solvers, unless an unreasonably small step size is taken [91]. This is typically the case when rapidly transient behaviours are to be accommodated. As the average residence time of gas in the column described with the parameters in Nastaj & Ambrozek (2009)[58] is readily calculated to be in the order of magnitude of 0.1 second per node, while a run of this model can simulate upwards of 300000 [s], one can see how the system can be considered a stiff system.

It has been considered to circumvent the problem of the stiff system by implementing a method that observes a node in a column and allows that to iteratively settle to equilibrium before calculating the next node. However, this would imply that the water content of the gas and solid are always in equilibrium, thus bypassing the LDF approximation that equation C.2 is based upon. While this should be valid in a system in which it is assumed that equilibrium is instantly established, it seems to be irreconcilable with the assumptions made in this model. Therefore, this scheme is considered to be inferior to the MATLAB ode-based solvers.

Numerical errors and discretization When implementing the ode15s solver, some instabilities can be observed despite using the specialised solver. These instabilities are usually characterised by one node returning a complex value, which is then propagated throughout the column. This has been circumvented by forcing the ode15s function to return real values, which is not observed to have any adverse effects.

Another problem that was observed is a very slow propagation of moisture beyond the first node in both gas and solid. This is caused by the definition given in the Nastaj & Ambrozek 2009 paper that the spatially discretized versions of the equations that govern the main states only apply to 2 ≤ n ≤ N+1. This appears to be incompatible with the convection term, as this is based on a first-order forward differencing method, resulting in an inability of gas situated in the first node(which is determined by the boundary conditions for z = 0, which corresponds with n = 1), to reach the second node where convection does apply.

Two methods have been tested to resolve this issue. The first solution consists of the implementation of first-order central differencing to approximate the derivative with respect to space of the convection term in equations 5.2 and 5.3. The second solution is to implement the boundary conditions by defining Y_w and T outside of the column on the entry side, so that the second order terms at the first node can also be evaluated, thus including node 1 into the domain where the equations are valid.

While both methods appear to solve the problem, the latter is chosen in order to more accurately replicate the model as described in literature.

Improvements on calculation times While the equations appeared to be working, it has been observed that calculation times quickly increased with both simulation duration and node count. While FORTRAN is recommended over MATLAB for this application, MATLAB is not inherently inadequate for the task. This implied that the script required optimisation to reduce the run time. The most time-consuming step in calculations have been found to be the interpolation, which at that point was thoroughly used to calculate auxiliary states from lookup tables as described in section 5.2. Simply removing the interpolation in favour of a more finely meshed lookup table appeared to introduce instabilities at the transitions between values. In order to calculate these values in a continuous fashion, equations based on the Tetens and Clausius-Clapeyron equations are introduced as described in section 5.2. Another significant factor turned out to be the ode15s parameters. A limit on step size and tolerance was introduced to improve stability, the constraints of which could be significantly loosened to improve calculation speed without any visible deviation of results. The results of these improvements, and other small optimisations enable experiments with the same node count and duration as done by Nastaj & Ambrozek, with a maximum calculating time of approximately 15 seconds.

Mass transfer coefficient In order to verify the assumptions made in section 6.5, the empirical correlation of Petrovich & Thodos [68] can be used, as was done by Schork & Fair, who stated the correlation as equation C.10[77].

$$K_f = \frac{0.357}{\epsilon} Re^{0.64} Sc^{0.33} \frac{D_m}{2R_p} \qquad 3 < Re < 2000 \tag{C.10}$$

$$\frac{\partial X_w}{\partial \tau} \sim (K_f)\alpha \sim (R_p^{0.64} R_p^{-1}) R_p^{-1} \sim R_p^{-1.36} \tag{C.11}$$

K_f = Fluid-film mass transfer coefficient [m/s]
D_m = Molecular diffusivity [50]
R_p = Radius of sorbent particles[m]
Re = Reynolds number for packed beds
Sc = Schmidt number

α = Surface area to volume ratio

Equation C.11 describes the relation derived from the work of Schork & Fair, who use the Petrovich & Thodos correlation to establish a gas-based linear driving force model. While this work uses a different approach, the scaling with particle radius should be the same and thus scale inversely to the power of 1.36. This yields a 6.59 times increase in mass transfer coefficient as average particle size decreases by a factor 4 between materials. While this is not enough to explain the entirety of the difference between the fitted data of the two materials, it does show how fairly small changes to the material and experimental setup can result in large changes in mass transfer characteristics.

This theoretical approach can be argued to have several significant limitations which include but are not limited to the Reynolds number, as the values used are very close or under the lower boundary condition of equation C.10. The other limitation that should be stated is the fabrication of the sorbent, which plays an increasingly large role as the theoretical estimation comes ever nearer to reality. The exact size and shape of the particles plays a role on the scaling of α, and the material grade [36] also play a significant role on material performance that is not easily accounted for with neither the materials, nor the theoretical approaches used in this work. Therefore, this theoretical approach is considered to be supportive of experimental data at most. Section 7.1 presents a closer look at fitting the model to experimental data, which is expected to be an adequate and the best available approach for this work.

C.2. Additional data

C.3. Correspondence with prof. Nastaj

This section contains the correspondence with prof. Nastaj of the university of Szczecin, Poland. 2 e-mails were exchanged prior to the one presented here. The earlier e-mails were mainly intended to acquire an understanding of the model, and are not very relevant to this work. The e-mail exchange presented here is most relevant to section 5.3, as it concerns the discrepancies presented in that section.

The author would like to express his appreciation to prof. Nastaj and dr. Ambrozek for taking the time to answer these questions. While reaching different results, the answers to the questions both in this e-mail exchange and those prior have been critical for the understanding of the model.

Sent by Samir den Haan on 17-2-2021

> Dear prof. Nastaj,
>
> Thank you for your time in answering my previous e-mail. I have made a lot of progress since then: the model appears to be working quite well and runs within reasonable computing times. This did rais new questions when attempting to match my results to your 2009 or 2012 papers, or the 1992 Park and Knaebel paper you regularly refer to. I have some questions on three topics in particular that should help me match my model to the literature, and then my experiments to that model.
>
> 1) Did you use an equation of state to calculate the gas water content(Y_w)? If so, which one? The values I find are consistently higher than the values stated in the 2009 paper, for instance when trying to replicate figure 4. I used both the Tetens equation and steam tables to find the saturation pressure at a given temperature, as well as confirming my method to convert relative humidity to Y_w using the same equation used by Pesaran & Mills(1987). These methods all yielded the same results. When attempting to replicate the situation in CoCo simulator using an equation of state, I did notice that values could vary depending on the equation of state used. Since your method of finding this value is not stated in either paper, I hope that you'll be able to tell if this discrepancy is to be expected with the method used, or if i misunderstood the model.
>
> I tried both replicating your Y_w at the input as well as matching the stated relative humidity, with matching Y_w yielding results that are significantly closer to yours, as i tried to illustrate in image "Watercontentquestion", in which i attempt to replicate figure 3 of your 2009 paper by matching relative humidity or by matching Yw, both using the same temperatures as stated in the paper.

2) I noticed that the shapes of your temperature curves in figure 7(2009 paper) and figure 5(2012 paper) are different from the temperature curves in figure 7b and 7c of Park & Knaebel 1992's paper. Conditions in the 3 papers are roughly similar. While the equations I use are based on yours, my results are more similar to Park & Knaebel. I did notice that one of the prominent features that differentiate your model from Park & Knaebel's is the addition of gas diffusion and thermal conductivity. I used thermal conductivity(k_e) values found in papers such as Bjurström et al (1984). For simplicity i assumed it to be a constant 0.2 [W/(m*K)] for now. I tried to increase thermal conductivity to 15 [W/(m*K)] as an attempt to emphasise the differences in the models to get a better understanding of what happens, and i did note that my results looked a lot more like yours and I don't really know why this is the case. I tried to illustrate this in attached image "Thermalconductivityquestion". My question is: what value did you use for thermal conductivity(k_e)? Did i choose the wrong value, or do you think I may have implemented it in the wrong way? Or could there be another reason the shapes of the curves are different that i've not yet found?

3) In order to better understand the model and why my results are slightly different from yours, I did a unit analysis of the gas water content and temperature equations, as shown in attached images "Unit analysis gas watercontent" and "Unit analysis temperature".(Note: I used [J/kg] for delta H, instead of the listed [J/mol] in order to match the units. I converted the units in all my models and the values appear to be correct.) I noticed that your 2009 paper describes them in 3 ways: dimensioned non-discretized (eq. 1&2), dimensionless non-discretized (eq. 15&16) and dimensionless discretized (eq. 17&18). The gas water content did show the unit i expected ([(kg/kg)/s] and [(-/-)/s] for dimensioned, [kg/kg] or [-/-] for dimensionless). In the temperature equations, i expected to find a unit of [K/s] for the dimensioned version, which was also the case. However in the dimensionless case i expected to find units in [K], but instead found them to be in [(K*m³)/kg], and i'm not quite sure why. I expected the density of the solid to be somehow related to this, since it is not in the definition of dimensionless time, and appears in the dimensionless equations nonetheless. I tried to implement both the dimensioned and dimensionless versions hoping to find any discrepancies, and they do give the same results! I'm having a hard time understanding how this works, and I'm hoping you could elaborate. How come both versions of the equations are still equivalent, despite the apparant mismatch in units? What step might i have missed to introduce the density of the sorbent of the density into the equation?

I also have a smaller question in this topic. I noticed that the density of the sorbent in the convection term of eq. 16 was removed in eq. 19. Could this be a typo or is it related to my earlier question?

I understand that this is quite a bit of text, but I do hope you have an answer since I believe this to be the last barrier to fully understanding the subject to the extent where I could succesfully verify the results of my experiment and defend my thesis. Please let me know if any of the questions or attached images are unclear. Should it be easier to explain or answer these questions via a videocall, I'd be happy to do so.

Kind regards,

Samir den Haan

Delft University of Technology

Sent by Jozef Nastaj on 1-3-2021

Dear Samir den Haan,

It is our answer for your new questions:

Ad. 1. The Riedel or Antoine equations can be used to calculate the saturated water vapor pressure. The parameters of these equations for water can be found in the literature.

Ad. 2. The temperature distribution curves in our work (2009) and in the work of Park & Knaebel(1992) slightly differ, because the diameters of the bed differ (in our work D = 0.1 m, in the work of Park & Knaebel in Fig. 7 the results for D = 0.01339 m and D = 0.02362 m). The bed heights also vary. As can be seen from the heat balance equation, the diameter of the

bed exerts a great influence, especially at its low value, on the heat loss to the environment, and thus also on the temperature distribution along the bed.

In our simulation program (our own program developed in Fortran) the k_e coefficient was calculated using the thermal analogy to the Edwards and Richardson correlation, which is used to calculate the DL axial diffusion coefficient (Edwards & Richardson, 1968

Ad.3. In our work, we used dimensionless variables: dimensionless axial coordinate Z, and dimensionless time τ. We have not sought to obtain dimensionless equations. The heat of adsorption in equation (5) is expressed in [J / mol], while in equations (2), (16) and (19) in [J / kg].

The following typos crept during the editing of the article:

- Equations (15) and (18): unnecessary ε in the term containing D_L,
- Equations (16) and (19): unnecessary ρb in the first, second and fourth term on the right.
- Lack of ρ_b in the third term; this part should have the form:

$$\frac{\rho_b \Delta H}{C_\Sigma} \frac{\partial X_w}{\partial \tau}$$

Sincerely,

Józef Nastaj and Bogdan Ambrożek

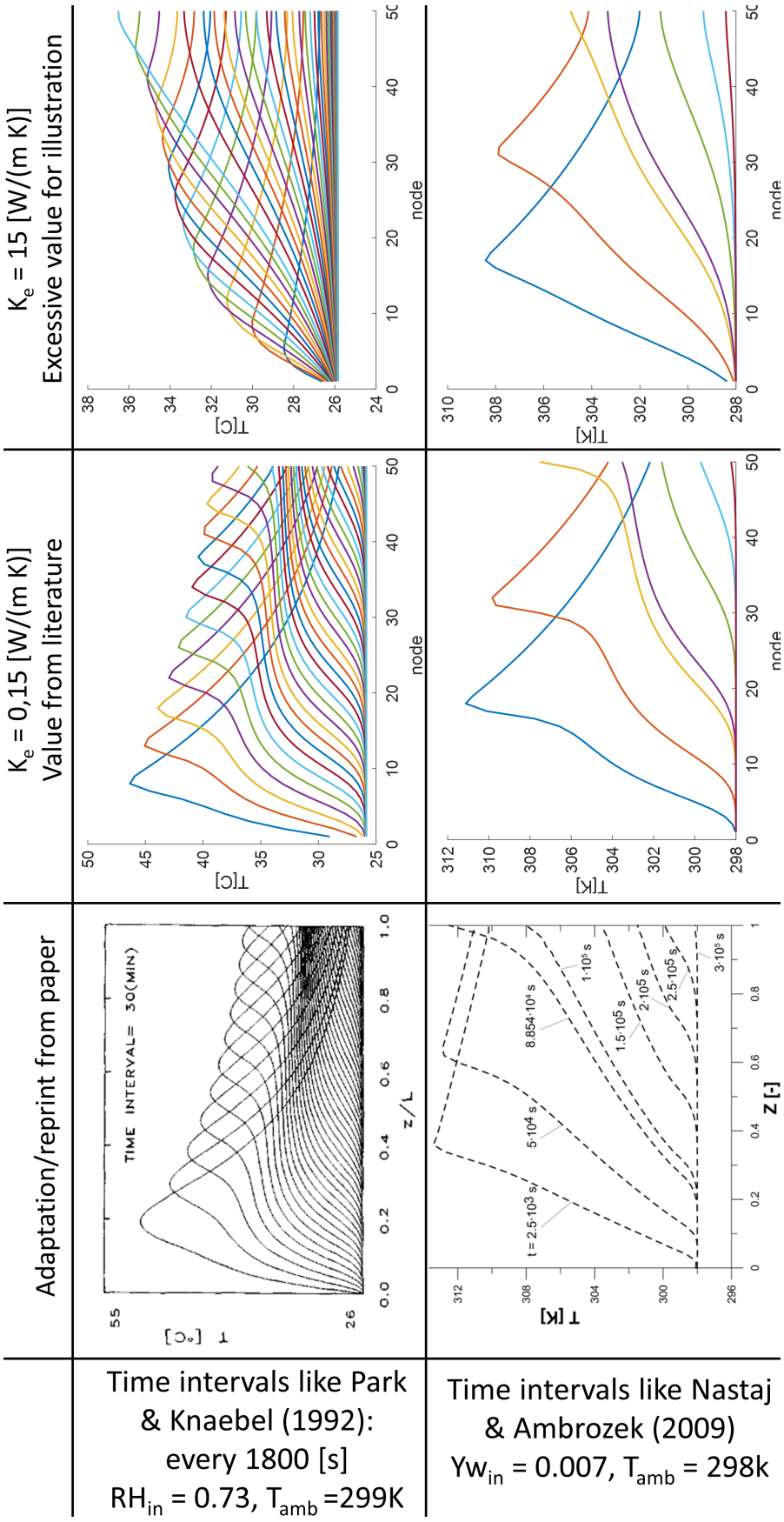

Figure C.1: Larger version of figure 5.4

$$-D_L \frac{\partial^2 Y_w}{\partial z^2} + \frac{\partial Y_w}{\partial t} + \frac{J_i}{\varepsilon \rho_i} \frac{\partial Y_w}{\partial z} + \frac{\rho_b}{\varepsilon \rho_i} \frac{\partial X_w}{\partial t} = 0 \qquad (1)$$ -/s

$$\frac{\partial Y_w}{\partial \tau} = D_L \frac{\rho_{i0}}{J_i L \varepsilon} \frac{\partial^2 Y_w}{\partial Z^2} - \frac{\rho_{i0}}{\rho_i \varepsilon} \frac{\partial Y_w}{\partial Z} - \frac{\rho_b}{\rho_i \varepsilon} \frac{\partial X_w}{\partial \tau} \qquad (15)$$ -/-

$$\frac{dY_{w_n}}{\partial \tau} = D_L \frac{\rho_{i0}}{J_i L \varepsilon} \frac{Y_{w_{n+1}} - 2Y_{w_n} + Y_{w_{n-1}}}{\Delta Z^2} - \frac{\rho_{i0}}{\rho_i \varepsilon} \frac{Y_{w_{n+1}} - Y_{w_n}}{\Delta Z} - \frac{\rho_b}{\rho_i \varepsilon} \frac{dX_{w_n}}{\partial \tau} \qquad (18)$$ -/-

Figure C.2: Unit analysis on the gas water content equations of the 2009 Nastaj & Ambrozek model. Contrary to figure 5.5, these equations did not contain unit discrepancies

D

Experiment appendix

This appendix presents additional rough data as extracted from the experiments performed in chapter 6.

D.1. Proof of concept experiment

This section will quickly present the first experiment that was conducted using the concept sketched in 6.2, why it was deemed insufficient, and what was learned to improve it. Note that this paragraph is not intended as a comprehensive experimental report, but rather to illustrate an iteration in the design process of the proper experiment that is presented in further sections.

In order to test the viability of the experimental concept, it was decided to first create a relatively simple setup to demonstrate the working principle. An image of the setup can be seen in figure D.1. A Bronckhorst F-232M-RAD-20-V mass flow controller is used to provide nitrogen as input gas. The input gas flows through a generic gas washing bottle (GWB). Nitrogen is chosen for practical and safety reasons, and it is not expected to yield significantly different results since Dalton's law applies and co-sorption of CO_2 was not expected to be a dominant factor [92].

Measurement of the water content was done with Amphenol ChipCap2 sensors, as this model is low-cost and can handle temperatures up to 125 °C. Temperature is measured with a standard issue 100k ohm NTC, as they too are low-cost and readily available. A ZEF prototyping PCB with an Arduino Nano was used to control all parts of the setup, excluding the mass flow controller. The I²C interface supporting various ADS1015 Analog-digital converters was extended to include the ChipCap sensors. NTCs are readily supported with this system, using the ADS1015 ADCs and resistors whose value was measured with a multimeter.

As for hardware, readily available silicone hose is used to connect the pieces. The sensors are placed in 3D printed casings, sealed with an O-ring. The glass columns are filled with 100g silica gel with coloured indicator. Glass spacer material and a stainless steel diffuser are added to place the material centred in the column with the NTC placed in the middle.

The experiment is conducted by switching on a flow of 0.6l/min. This is less than the target flow of the plant, and was reduced in order to investigate the behaviour of the experiment. In the most representative of runs, which is the only one that will be discussed in this section, the adsorption part of the experiment was left to fill up for 5 hours. Then, the columns are switched, the regenerating column is heated, and gas flows through both columns until the regenerating column appears to be dry.

Figure D.2 presents the measurements taken from of the runs of this experiment that performed well, showing the temperatures and relative humidities over time during the experiment. Data of all other runs can be found in appendix [erdpel]. The heater pre-heats from t=0 and the column is placed around t=20, indicated by the drop in heater temperature as the cold column is placed. The observation around t=40 is that as the regenerating column heats up, a lot of condensation occurs in the section after the heater. Judging from the temperature of the relative humidity sensors, the gas has a relatively quick heat exchange, being near ambient temperatures at all measurement points, even after passing through a hot heater. The regeneration appears to be faster than the adsorption process. However, it was deemed not possible to judge the regeneration progress on indicator colour alone as condensation

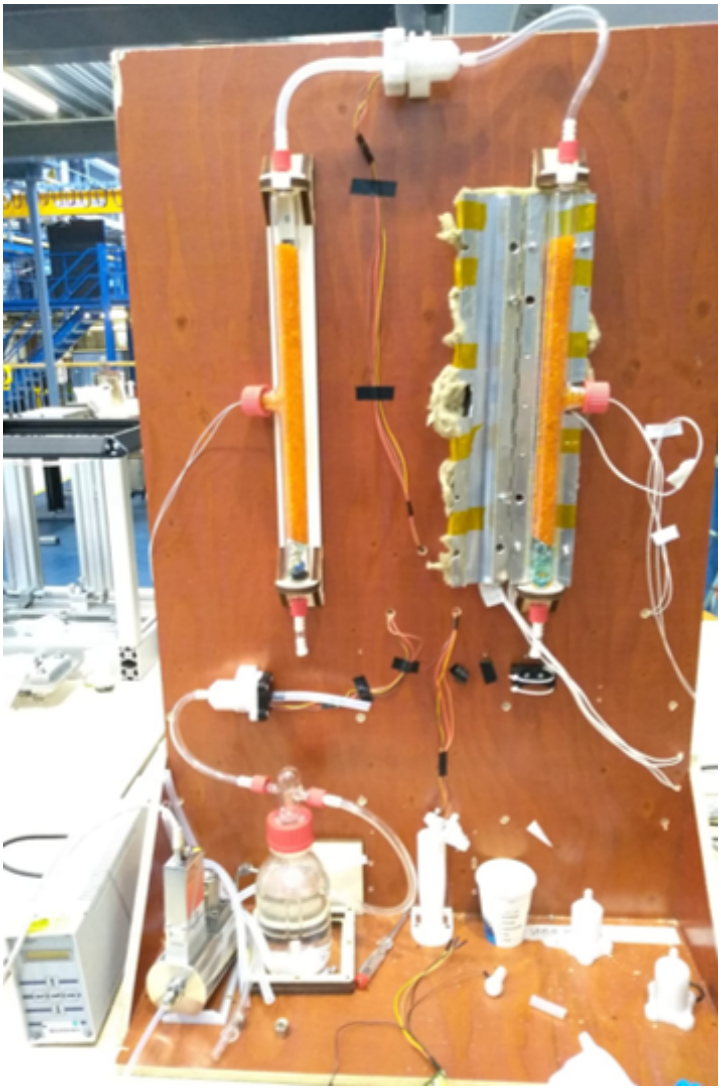

Figure D.1: The proof of concept setup

continued when all indicator returned to its original state. The output relative humidity sensor yielded no values, as it defaults to maximum values if liquid water is present on the sensor, which was the case due to the condensation. An attempt was made to clear the sensor of water around t=100 and a signal was restored, but this yielded no clear measurement on the process. What can be concluded from the condensation is that the gas leaving the column has a higher water content than the gas entering the system, but this experiment is not able to determine the gas composition leaving the system, rendering it invalid. While an invalid experiment, some lessons learned are the following:

- It is possible to regenerate the column at a faster rate than the adsorption rate. The condensation downstream from the regenerating column indicates that water content of the gas leaving the column exceeds that of the input gas, at least during some part of the process.
- The cooling of the regenerating gas happens very quickly. This caused condensation to form on the sensor, disabling it.
- A better definition is needed to describe the state of a dry column as the coloured indicator is unable to adequately describe the state of the desiccant.
- The I²C connection of the sensor caused the software to jam at irregular intervals in the order of magnitude of half an hour.
- The adsorption process is very slow: after several hours, the front of indicator turned dark green was only at roughly 25mm from the bottom of the bed. This is accredited to the low temperature

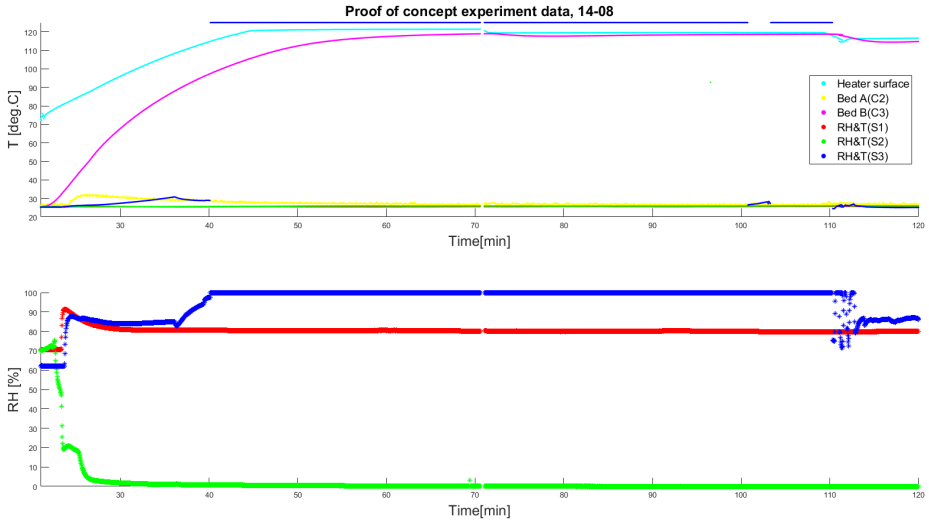

Figure D.2: Readings of the relative humidity and temperature sensors of the proof of concept experiment

of the lab environment relative to the ZEF micro-plant conditions, since the relative humidity of the input was deemed adequately high, but gas water content was not.

From these lessons learned, the decision was made to redesign the experiment in order to run experiments in a faster, more controlled manner. It should more closely resemble the ZEF use case and most importantly: yield data that can be compared to a model. This approach enables a path of progression that includes both prototyping and experimental experience to build a new system, suited for integration testing of several subsystems, as well as the creation of a model to increase the understanding of the process and to design and optimise variations of the Moisture Control System that will be used in a later stage of development.

This experiment, while invalid, has been useful to demonstrate the working principle. However, it is not a proper experiment with scientific value. It was decided to redesign the experiment in a way that allows proper measurements of the in- and output gas compositions and to better mimic the conditions the operating conditions of the device.

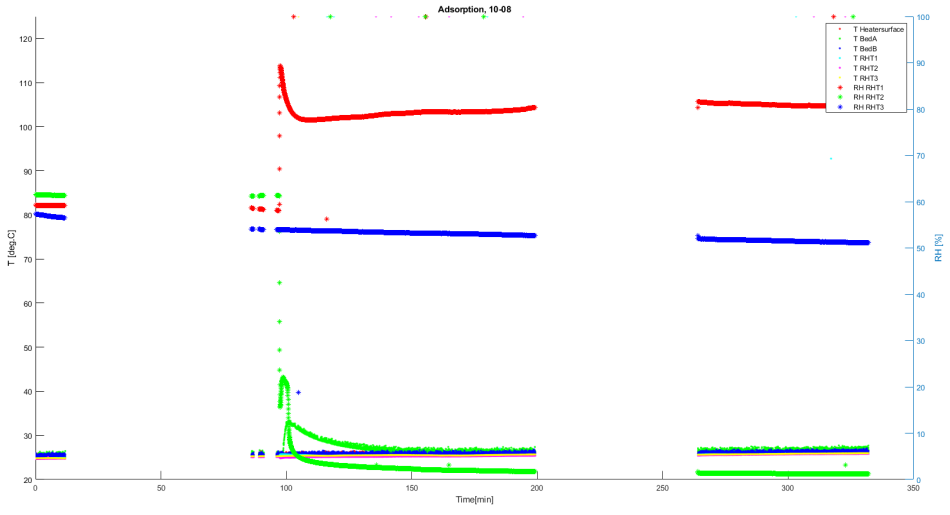

Figure D.3: Rough data of proof of concept experiment. The blank parts indicate a software failure, data has been placed back together via timestamps

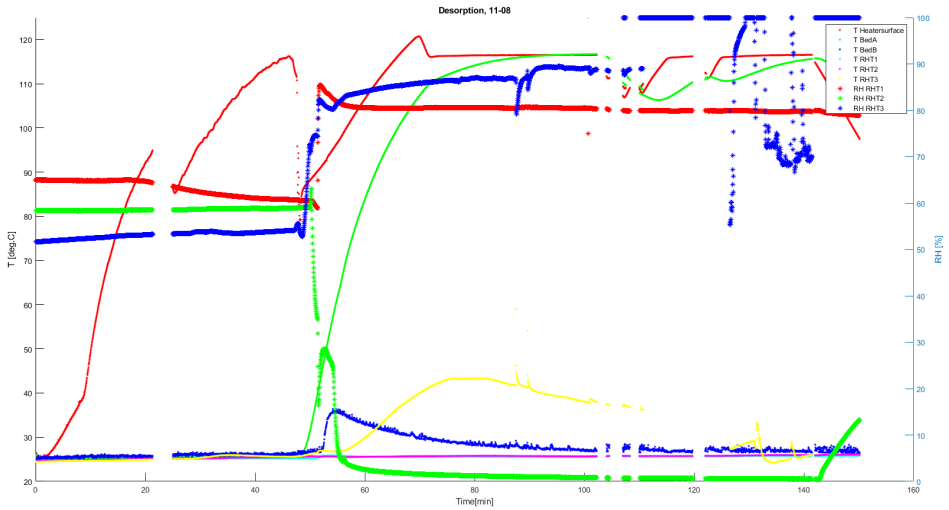

Figure D.4: Rough data of proof of concept experiment. The blank parts indicate a software failure, data has been placed back together via timestamps, note that the erratic behaviour of the RH RHT3 data is indicative of liquid water present on the sensor.

D.2. Experiment design sizing

In order to design an experiment, the correct sizing of the column and chamber is neccessary. It can be taken from the inlet conditions in section 2.2 that the mass flow of water in a plant with a **600**[g methanol/day] target is roughly **3**[g water/h].

The proof of concept experiment used **100**[g] of sorbent, based on a very rough estimation of an average loading of **0.1** [kg water/kg sorbent] at breakthrough, **1** [g water/h] at experimental conditions and experimental runs that last all day.

For the redesign, it is not deemed neccessary to perform these tests at full scale. Therefore, it is chosen that experimental runs of 2 hours each will allow for 2 to 3 tests to be performed per day, allowing to gather data of several cycles within reasonable time. When combined with the water mass flow increase from an estimated 1 to 3 grams per hour, this indicates that the **100**[g] sorbent used in the proof of concept experiment, is likely to be suitable for the redesigned experiment as well, albeit with a slightly different reason.

It is considered wise to design the column in such a way that it is possible to adjust the sorbent quantity as needed. Therfore, it is decided that a column should be able to hold **150**[g] of sorbent. At **720**[kg/m^3], this results in a volume of or **0.208** [dm^3]. Given that glass tubes with screw connections are only available in a few sizes, a tube with this volume of size GL25, GL32 and GL45 have minimum lengths of **0.78**[m], **0.46**[m] and **0.21**[m] respectively. With the GL25 tube being smaller than 8 times the particle diameter (recommended by Seader and Henley to develop the flow [78]), this is not considered a good choice. Both the GL25 and GL32 tubes result in unwieldy columns, which would require a very tall casing when implemented, resulting in a large surface area and thus heating and material requirements. Therefore, it is decided to make the column of a GL45 tube with a length of **250**[mm], in order to comfortably accommodate up to **150**[g] of sorbent and an RH&T sensor. This results in a more cubic shaped chamber design as shown in the CAD drawings of section 6.3.1, allowing for an easy to use setup, as well as lower material and heater costs.

D.3. Additional figures and data

D.4. Experiment equipment

The following is a list of equipment and materials used for the experimental setup.

Materials:

- Casing: 9mm poplar plywood, lasercut
- Windows: 3mm clear acryllic, lasercut

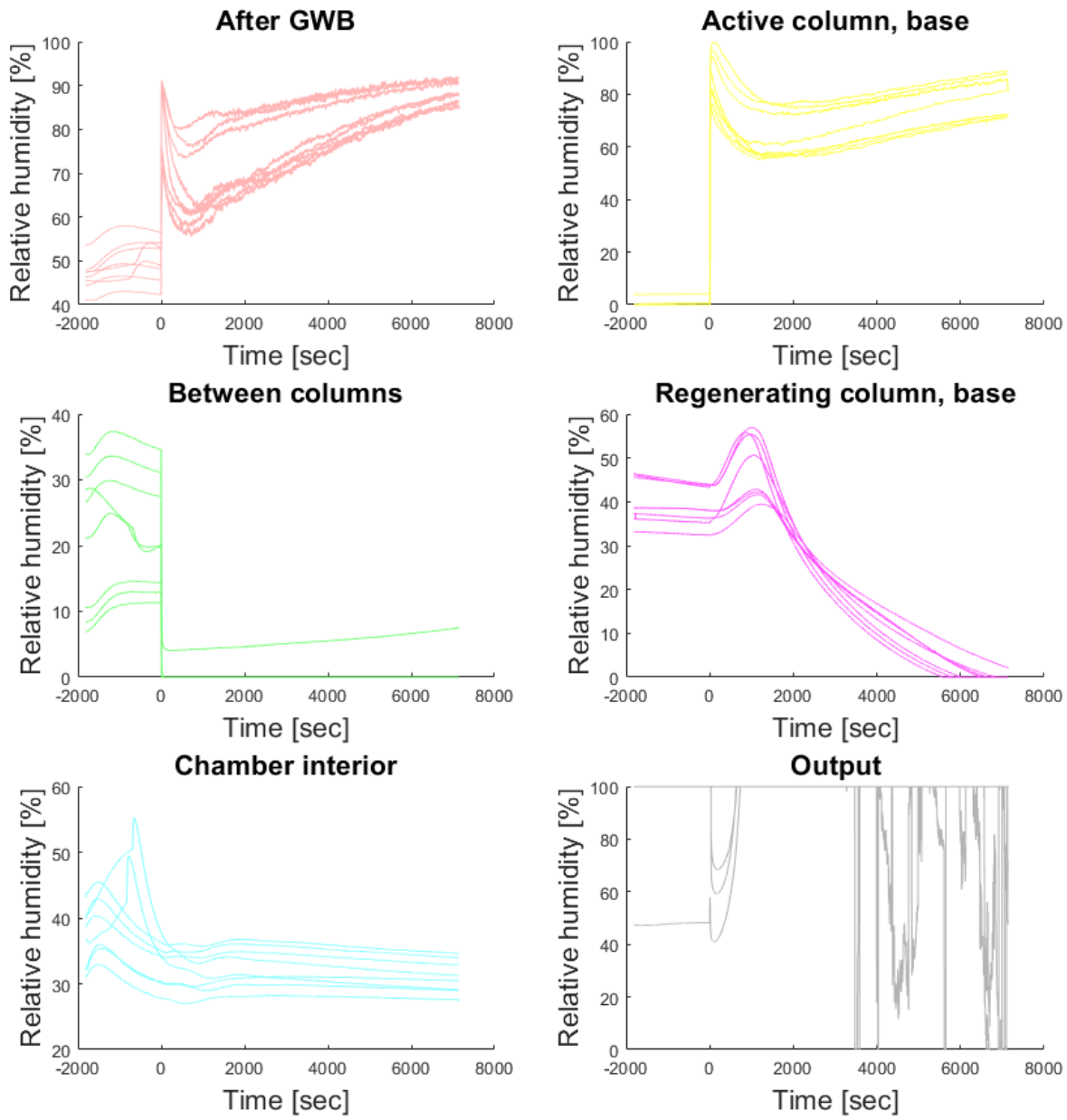

Figure D.5: Relative humidity at various positions during all desorption experiment runs

- 3D printed parts in red: 123-3D PETG, red
- 3D printed parts in white: 123-3D PLA, white
- 3D printed parts in black: Ultimaker polycarbonate, black
- Fasteners: generic steel machine screws, mainly in M3 and M4 sizes. Please refer to the CAD design for details.
- Coarse silica gel: silica-gel-shop.nl ”Silica Gel orange 3-5mm”
- Fine silica gel: xtrack.nl ”Silica gel zeer fijn (0,5 - 1,0 mm korrel)”
- Columns: GL45 borosilicate glass screw tube (LGS B.V.)
- Sensor housing in columns: stainless steel tube covered in fiberglass mesh
- Column connection ports: PTFE
- Heater: Aluminium tube, spray painted black. Wrapped in an 150W, 12V, 1200x12mm silicone pad heater. Insulated in a rockwool pipe wrap.

Equipment:

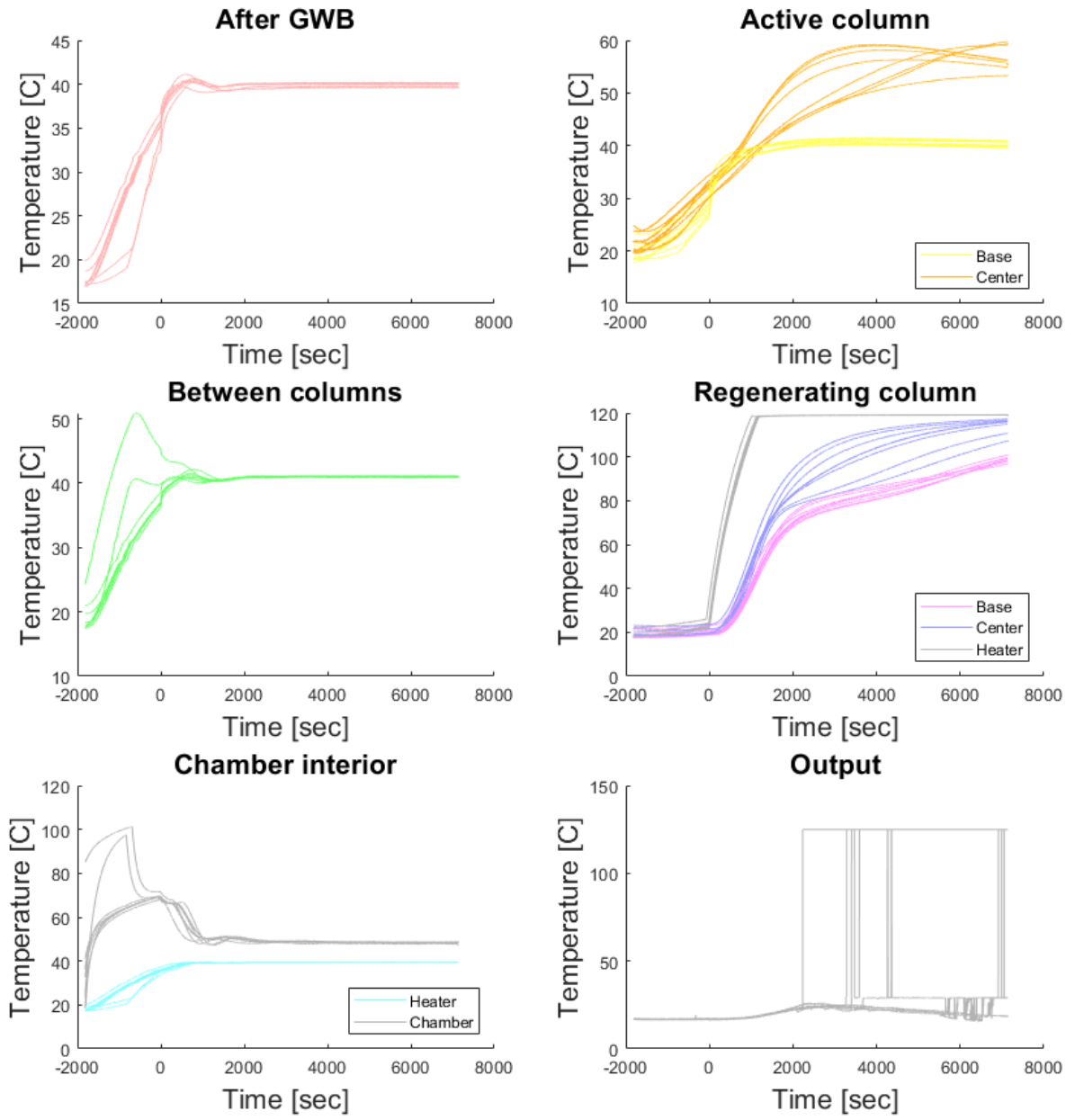

Figure D.6: Temperature at various positions during all desorption experiment runs

- Bronckhorst F-232M-RAD-20-V mass flow controller, with compatible peripherals
- ZEF prototyping board with arduino Nano
- PCE-BSK1100 weight scale
- Kiwi electronics RS232 to TTL converter
- Generic 100k ohm NTC resistors
- VOLTCRAFT PS-750 pocket weight scale
- Honeywell HIH6121 RH& T sensors
- Telaire ChipCap2 RH& T sensors
- Generic 12v aluminium heatplate for FDM 3D printers
- Generic 12v 120x120x20mm computer fan
- Generic 12V,40A power supply
- Duran 500ml borosilicate gaswashbottle (LGS B.V.)
- 9mm inner diameter silicone hose

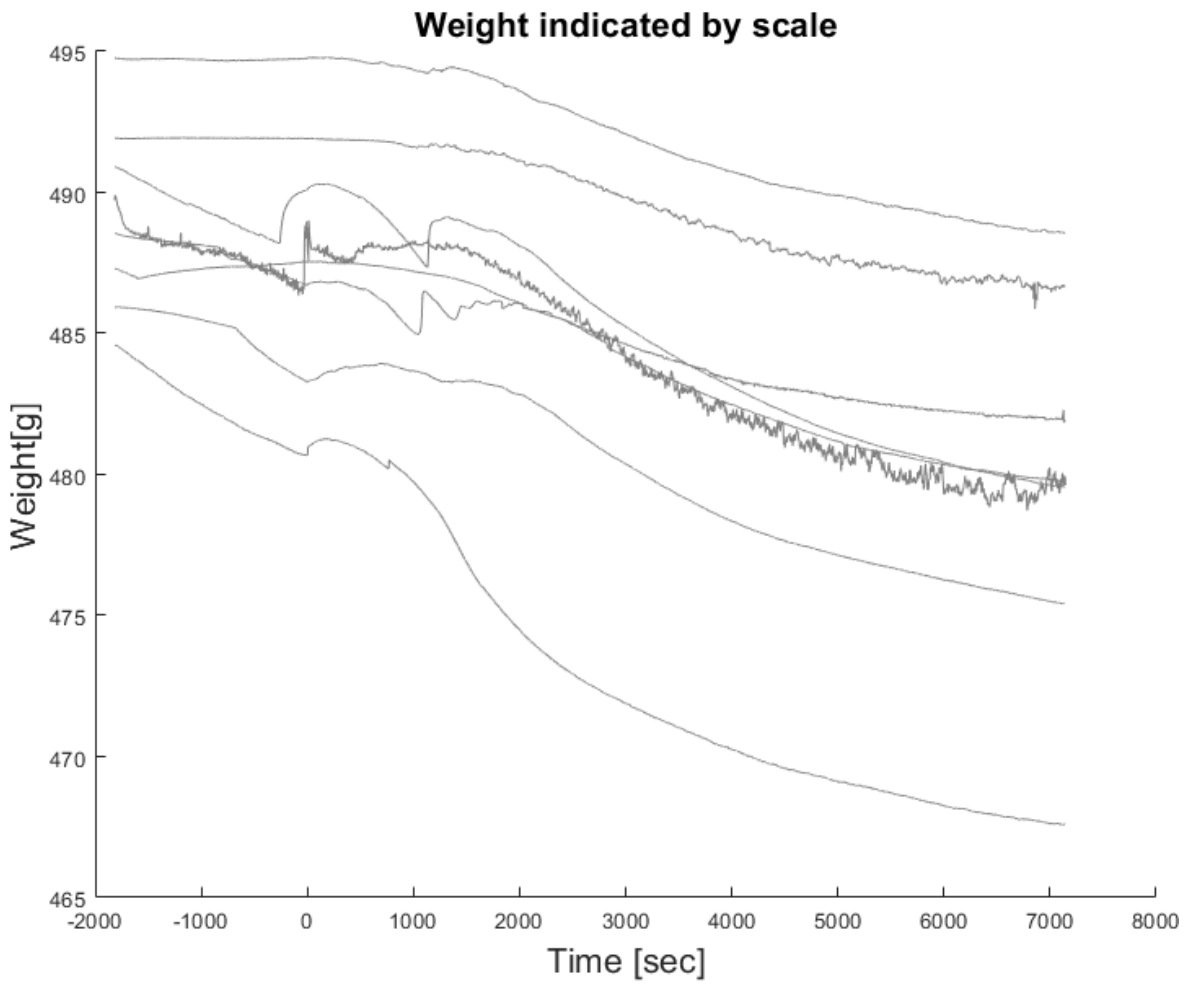

Figure D.7: Weight as indicated by the scale during all desorption experiment runs

D.5. Breakthrough model parameters

Run ID	Delta M GWB	Delta M Active column	Delta M Regenerating column	Notes
0	-6.3	5.3	-	Virgin dessicant
1	-5.5	4.9	-8.2	Virgin desiccant
2	-5.6	5.3	-8.0	
3	-5.7	5.5	-6.5	
4	-6.1	6.1	-6.1	
5	-5.6	5.4	-6.2	User error: fan switched on halfway through pre-hea
6	-6.1	6	-5.8	
7	-5.4	5.2	-6	
8	-6	5.7	-5.4	

Table D.1: Mass measurements using the VOLTCRAFT letter weighing scales of various elements before and after a run

Table D.2: Model parameters used for the breakthrough experiment

	Adsorption Initial model		Adsorption Adjusted model	
t_end	180000	[s]	180000	[s]
Xw_0	0	[kg/kg]	0.025	[kg/kg]
T_{in}	313	[K]	313	[K]
RH_{in}	0,99	[-]	0,99	[-]
J_i,ads	0.021*1	[kg/(m^2 s)]	0.021*1	[kg/(m^2 s)]
L	0.14	[m]	0.14	[m]
D	0.035	[m]	0.035	[m]
k_w	8.37	[W/(m^2 K)]	8.37	[W/(m^2 K)]
D_L	2,39E-05	[m^2/s]	2,39E-05	[m^2/s]
K_w	0.018	[1/s]	0.0036	[1/s]

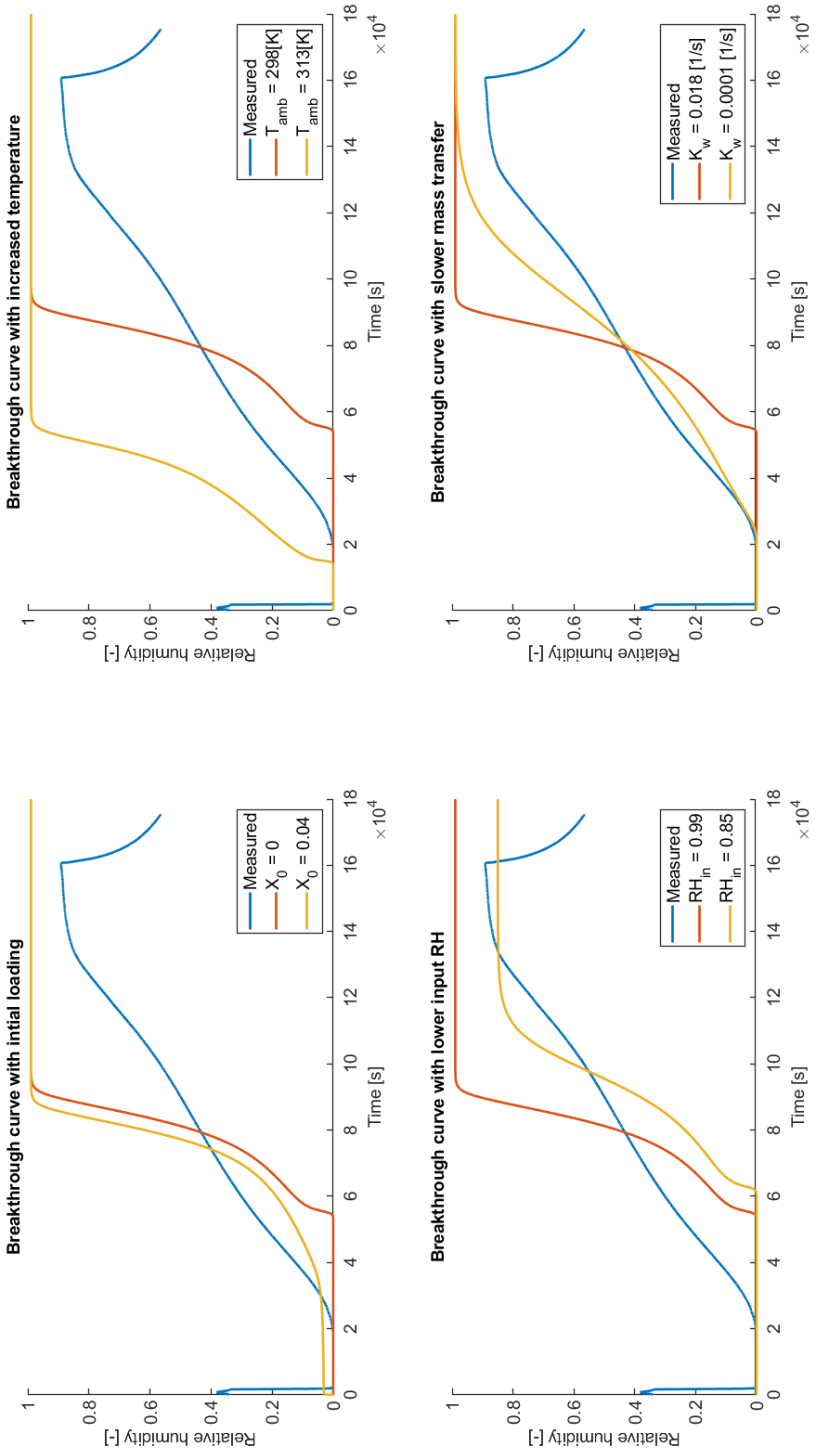

Figure D.8: Larger version of figure 6.17, breakthrough experiment

E

Design appendix

E.1. Model parameters

Table E.1: Adsorption parameters used to get initial conditions for the desorption done for the heat and mass transfer fit.

	Adsorption	
t_{end}	7200	[s]
T_{in}	313	[K]
T_{amb}	313	[K]
T_{init}	293	[K]
RH_{in}	0.85	[-]
J_i	0.021	[kg/(m^2 s)]
L	0.14	[m]
D	0.035	[m]
k_e	0.2	[W/(m K)]
k_w	8.37	[W/(m^2 K)]
D_L	2.39E-05	[m^2/s]
K_w	0.0001	[1/s]

Table E.2: Desorption parameters used for the desorption done for the heat and mass transfer fit.

	Desorption Heat transfer coefficient fit		Desorption Mass transfer coefficient fit		Desorption Demonstration with chosen values	
t_{end}	7200	[s]	7200	[s]	7200	[s]
T_{in}	313	[K]	313	[K]	313	[K]
T_{amb}	393	[K]	393	[K]	393	[K]
T_{init}	293	[K]	293	[K]	293	[K]
RH_{in}	0	[-]	0	[-]	0	[-]
J_i	0.021	[kg/(m^2 s)]	0.021	[kg/(m^2 s)]	0.021	[kg/(m^2 s)]
L	0.14	[m]	0.14	[m]	0.14	[m]
D	0.035	[m]	0.035	[m]	0.035	[m]
k_e	0.2	[W/(m K)]	0.2	[W/(m K)]	0.2	[W/(m K)]
k_w	Varies	[W/(m^2 K)]	8.37	[W/(m^2 K)]	8.37	[W/(m^2 K)]
D_L	2,39E-05	[m^2/s]	2,39E-05	[m^2/s]	2,39E-05	[m^2/s]
K_w	0.0001	[1/s]	Varies	[1/s]	4,74E-04	[1/s]

Table E.3: Adsorption parameters used to find average loading of rich sorbent to find the cyclic capacity

	Adsorption Base case		Adsorption Slim column		Adsorption Lower ambient		Adsorption Fine material	
t_{end}	14870	[s]	17245	[s]	26323	[s]	20728	[s]
T_{in}	313	[K]	313	[K]	313	[K]	313	[K]
T_{amb}	313	[K]	313	[K]	298	[K]	313	[K]
T_{init}	293	[K]	293	[K]	293	[K]	293	[K]
RH_{in}	0,8	[-]	0,8	[-]	0,8	[-]	0,8	[-]
J_i	0.021	[kg/(m^2 s)]	0.045	[kg/(m^2 s)]	0.021	[kg/(m^2 s)]	0.021	[kg/(m^2 s)]
L	0.14	[m]	0.298	[m]	0.14	[m]	0.14	[m]
D	0.035	[m]	0.024	[m]	0.035	[m]	0.035	[m]
k_w	8.37	[W/(m^2 K)]	8.37	[W/(m^2 K)]	8.37	[W/(m^2 K)]	8.37	[W/(m^2 K)]
D_L	2,39E-05	[m^2/s]	2,39E-05	[m^2/s]	2,39E-05	[m^2/s]	1,65E-05	[m^2/s]
K_w	4,74E-04	[1/s]	4,74E-04	[1/s]	4,74E-04	[1/s]	3,12E-03	[1/s]

Table E.4: Adsorption and desorption parameters used for the simulated energy use

	Ad/Desorption Coarse material		Ad/desorption Fine material	
$t_{end,ads}$	7200	[s]	7200	[s]
$t_{end,des}$	7200	[s]	7200	[s]
$T_{in,ads}$	313	[K]	313	[K]
$T_{in,des}$	313	[K]	313	[K]
$T_{amb,ads}$	313	[K]	313	[K]
$T_{amb,des}$	393	[K]	393	[K]
T_{init}	293	[K]	293	[K]
$RH_{in,ads}$	0,8	[-]	0,8	[-]
$RH_{in,des}$	0	[-]	0	[-]
J_i	0.021	[kg/(m^2 s)]	0.045	[kg/(m^2 s)]
L	0.14	[m]	0.298	[m]
D	0.035	[m]	0.024	[m]
k_w	8.37	[W/(m^2 K)]	8.37	[W/(m^2 K)]
D_L	2,39E-05	[m^2/s]	1,65E-05	[m^2/s]
K_w	4,74E-04	[1/s]	3,12E-03	[1/s]

Table E.5: Adsorption and desorption parameters used for the desorption rate scenarios

	Ad/Desorption Cool ambient, coarse		Ad/Desorption Cool ambient, fine		Ad/desorption Breakthrough, coarse		Ad/desorption Breakthrough, fine	
t_{end}	7200	[s]	7200	[s]	14869	[s]	20728	[s]
T_{in}	313	[K]	313	[K]	313	[K]	313	[K]
$T_{amb,ads}$	313	[K]	313	[K]	313	[K]	313	[K]
T_amb,des	393	[K]	393	[K]	393	[K]	393	[K]
T_{init}	293	[K]	293	[K]	293	[K]	293	[K]
$RH_{in,ads}$	0,8	[-]	0,8	[-]	0,8	[-]	0,8	[-]
J_i	0.021	[kg/(m^2 s)]	0.021	[kg/(m^2 s)]	0.021	[kg/(m^2 s)]	0.021	[kg/(m^2 s)]
L	0.14	[m]	0.14	[m]	0.14	[m]	0.14	[m]
D	0.035	[m]	0.035	[m]	0.035	[m]	0.035	[m]
k_w	8.37	[W/(m^2 K)]	8.37	[W/(m^2 K)]	8.37	[W/(m^2 K)]	8.37	[W/(m^2 K)]
D_L	2,39E-05	[m^2/s]	1,65E-05	[m^2/s]	2,39E-05	[m^2/s]	1,65E-05	[m^2/s]
K_w	4,74E-04	[1/s]	3,12E-03	[1/s]	4,74E-04	[1/s]	3,12E-03	[1/s]

Table E.6: Adsorption and desorption parameters used for the desorption rate scenarios

	Ad/Desorption Cool ambient, coarse		Ad/Desorption Cool ambient, fine		Ad/desorption Low flow, coarse		Ad/desorption Low flow, fine	
t_{end}	26323	[s]	31797	[s]	14869	[s]	20728	[s]
T_{in}	313	[K]	313	[K]	313	[K]	313	[K]
$T_{amb,ads}$	298	[K]	298	[K]	313	[K]	313	[K]
$T_{amb,des}$	393	[K]	393	[K]	393	[K]	393	[K]
T_{init}	293	[K]	293	[K]	293	[K]	293	[K]
$RH_{in,ads}$	0,8	[-]	0,8	[-]	0,8	[-]	0,8	[-]
$J_{i,ads}$	0.021	[kg/(m^2 s)]	0.021	[kg/(m^2 s)]	0.021	[kg/(m^2 s)]	0.021	[kg/(m^2 s)]
$J_{i,des}$	0.021	[kg/(m^2 s)]	0.021	[kg/(m^2 s)]	0.0105	[kg/(m^2 s)]	0.0105	[kg/(m^2 s)]
L	0.14	[m]	0.14	[m]	0.14	[m]	0.14	[m]
D	0.035	[m]	0.035	[m]	0.035	[m]	0.035	[m]
k_w	8.37	[W/(m^2 K)]	8.37	[W/(m^2 K)]	8.37	[W/(m^2 K)]	8.37	[W/(m^2 K)]
D_L	2,39E-05	[m^2/s]	1,65E-05	[m^2/s]	2,39E-05	[m^2/s]	1,65E-05	[m^2/s]
K_w	4,74E-04	[1/s]	3,12E-03	[1/s]	4,74E-04	[1/s]	3,12E-03	[1/s]

Table E.7: Adsorption and desorption parameters used for the desorption rate scenarios

	Ad/Desorption High temp, coarse		Ad/Desorption High temp, fine		Ad/desorption Slim column, coarse		Ad/desorption Slim column, fine	
t_{end}	14869	[s]	20728	[s]	17245	[s]	23778	[s]
T_{in}	313	[K]	313	[K]	313	[K]	313	[K]
$T_{amb,ads}$	313	[K]	313	[K]	313	[K]	313	[K]
$T_{amb,des}$	433	[K]	433	[K]	313	[K]	313	[K]
T_{init}	293	[K]	293	[K]	293	[K]	293	[K]
$RH_{in,ads}$	0,8	[-]	0,8	[-]	0,8	[-]	0,8	[-]
J_i	0.021*1	[kg/(m^2 s)]	0.021*1	[kg/(m^2 s)]	0.045	[kg/(m^2 s)]	0.045	[kg/(m^2 s)]
L	0.14	[m]	0.14	[m]	0.298	[m]	0.298	[m]
D	0.035	[m]	0.035	[m]	0.024	[m]	0.024	[m]
k_w	8.37	[W/(m^2 K)]	8.37	[W/(m^2 K)]	8.37	[W/(m^2 K)]	8.37	[W/(m^2 K)]
D_L	2,39E-05	[m^2/s]	1,65E-05	[m^2/s]	2,39E-05	[m^2/s]	1,65E-05	[m^2/s]
K_w	4,74E-04	[1/s]	3,12E-03	[1/s]	4,74E-04	[1/s]	3,12E-03	[1/s]

E.2. Additional figures

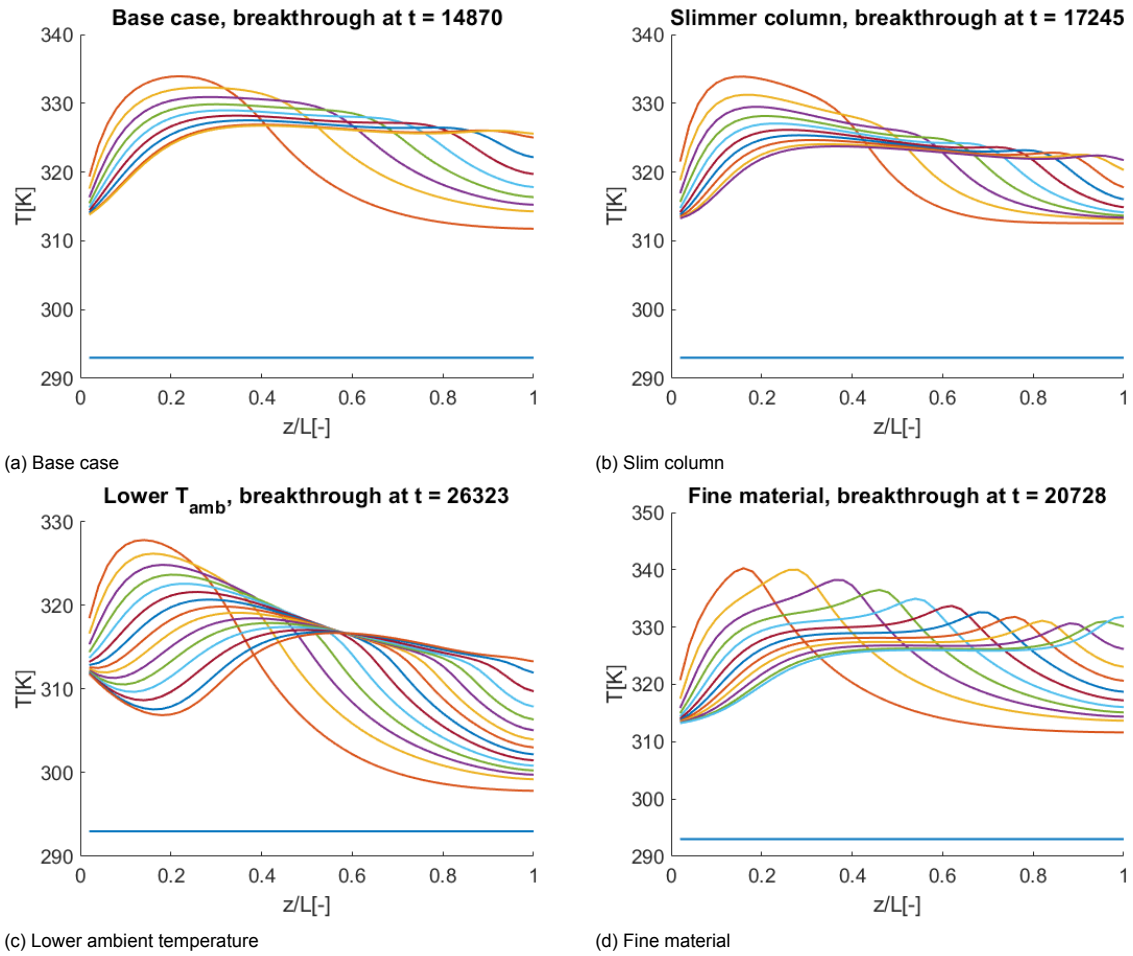

(a) Base case

(b) Slim column

(c) Lower ambient temperature

(d) Fine material

Figure E.1: Adsorption until breakthrough, space temperature curves of the scenarios sketched in figures 7.7, 7.8, 7.9. Lines with intervals of t=1800[s]

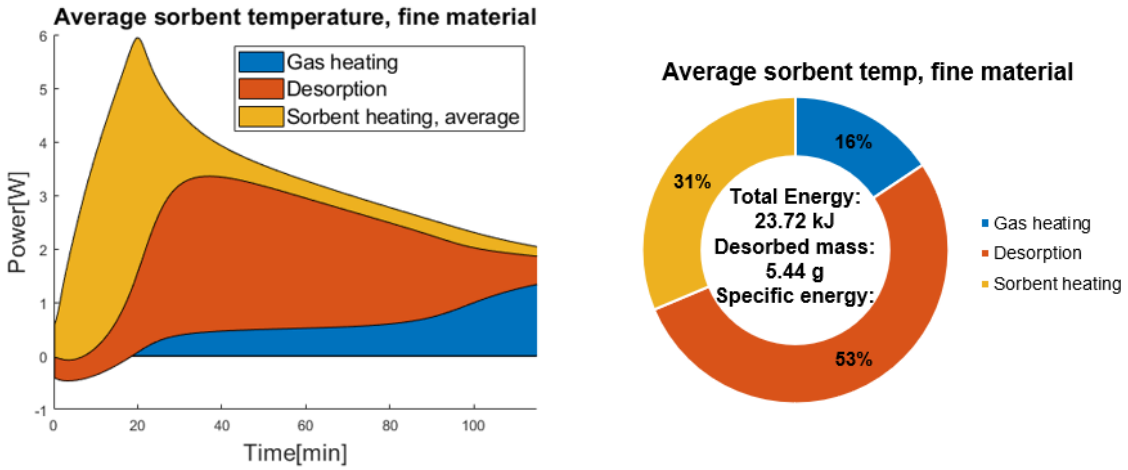

Figure E.2: Energy usage of simulated data when average temperature is used, instead of temperature measured at one node.

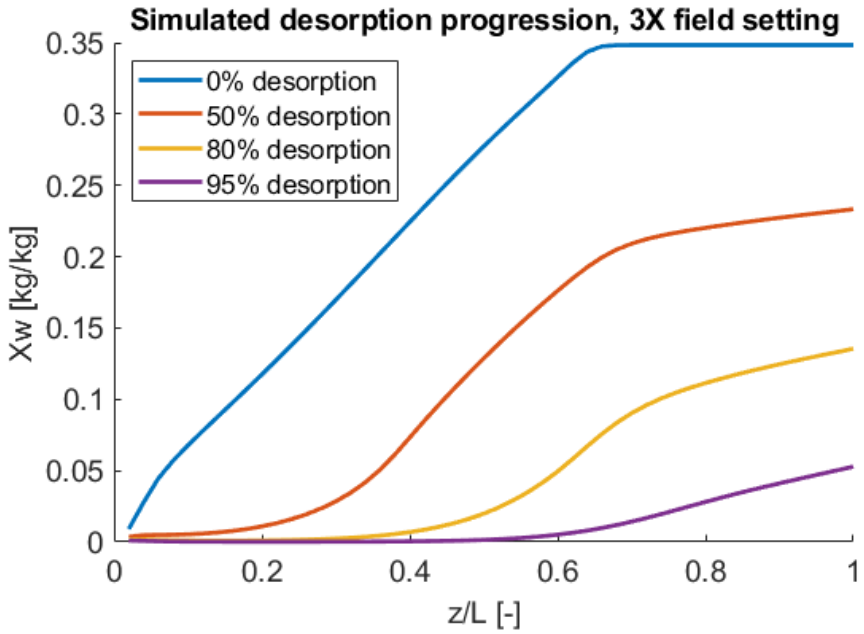

Figure E.3: Water distribution at various stages of desorption

E.3. Energy and heat transfer calculations

Preliminary data of power consumption of the desorption experiment as presented in section 6.4 is presented in figure E.4. It is measured by combining the duty cycle data with the voltage and maximum amperage. These are measured in advance using a multimeter and clamp-on current meter respectively while the heater is switched on at full power and are assumed to remain constant. Note that the line styles indicate the same runs as seen in figure 6.14, and t=0 is also set at identical times. It can be seen that for all runs, both heaters run at maximum power to increase the temperature to their setpoints. Note that the ambient heater starts at approx. t = **-30** [min] and the column heater at t = **0** [min] as described in section 6.3.2. Some variation is observed in the time required at full power to heat up the chamber. It can be seen that the most runs that are done as second run of the day require a somewhat shorter time to heat up the chamber as is expected from the hypothesis that the machine did not fully cool to ambient temperature between runs on the same day. The lack of obvious clustering such as the case in figure 6.14 make it difficult to discern any variations due to experimental conditions from variations due to a user error. It is observed that it is rather difficult to discern the exact processes presented in section 4.2.1 that utilise the energy emitted by the heaters. This has several reasons that can be summarised as the build quality not being optimized for efficiency. As stated in section 6.3.1, usability and versatility are leading in this design instead, resulting in an inadequate method for measuring heat transfer to and from the column and casing, which is not the goal of this experiment anyway. Section 7.2 presents a more thorough analysis where the energy consuption is built up from several partial processes rather than broken down from figure E.4 into said processes.

An attempt is done to derive an overall heat transfer coefficient from the heater to the column. In order to do this, equations E.1 are used to estimate the energy moved from the heater to the column. Energy used for gas heating is excluded from this equation in order to approximate the column as a closed system.

$$E_{transfer} = \int_{t1}^{t2} (E_{desorption} + E_{SH} - E_{HWH})dt \tag{E.1a}$$

$$UA = P_{transfer}/\Delta T \tag{E.1b}$$

From figure E.5 it can be seen that while estimated heat transfer and temperature difference between column and heater do follow the same trends, the correlation is not considered conclusive as the estimated overall heat transfer coefficient fluctuates between **0.2** and **0.6** [W/K]. However, a similar

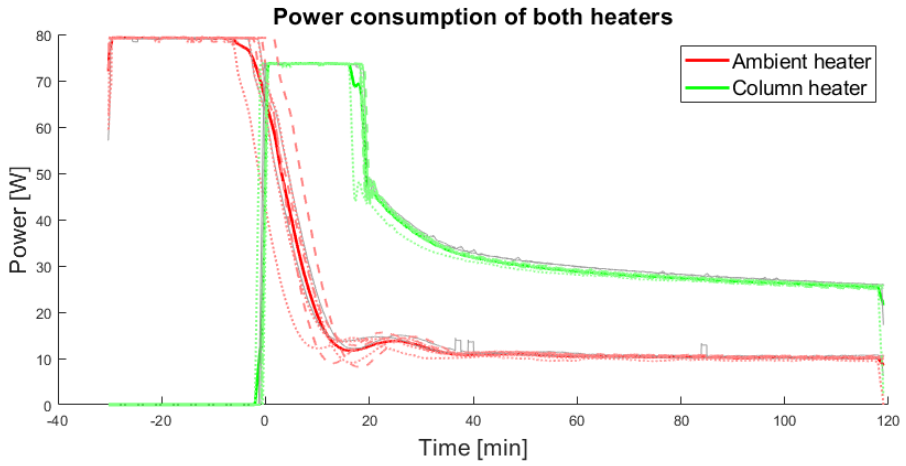

Figure E.4: Power consumption of the ambient and column heaters. Note that these figures are not representative of the actual process.

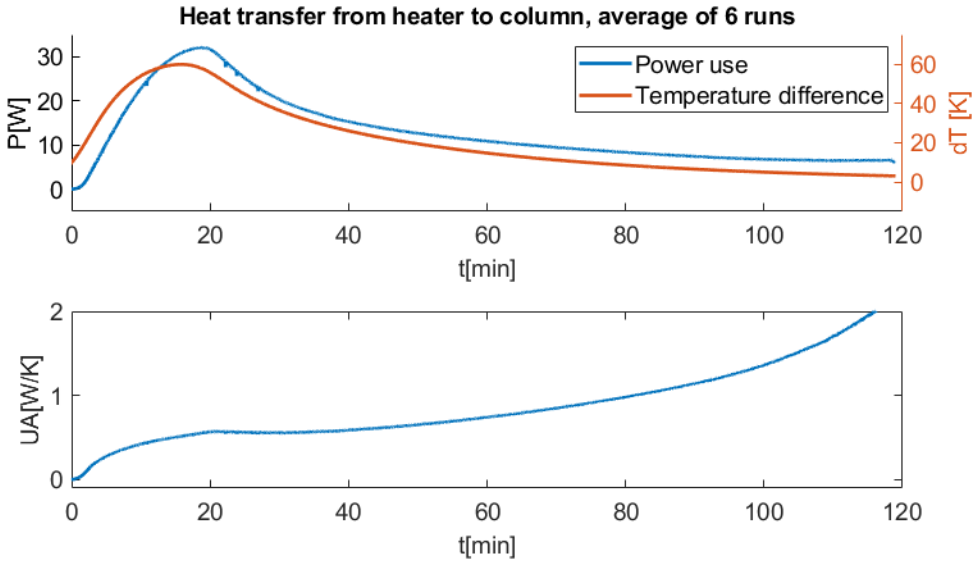

Figure E.5: Approximated heat transfer from the heater to the column.

analysis can be done in a later setup that is a closer approximation of a closed system. This may be useful to more accurately predict thermal requirements.

F

External documentation

F.1. Original assignment

Design and experimental characterization of an oil water system for a multistage CO2 compression system

1 Background

Two-thirds of all energy used is non-electric. Low cost synthetic fuels could disrupt this non-electric part of the energy market without the need of building new infrastructure. A major challenge in the production of low cost synthetic fuels is capital cost of the production unit. An approach to reduce the capital cost of the production unit is extreme integration of subsystems combined with system size reduction so that a plant can be designed as a product. Consequently mass manufacturing techniques become an option. A concept for such a highly integrated, mass manufactured methanol production unit is shown in Figure 1.

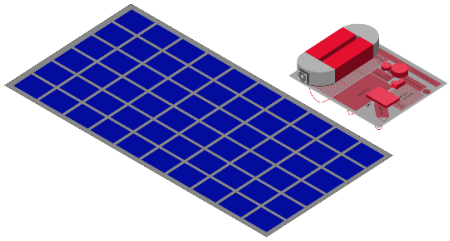

Figure 1 – Total methanol production unit, INCLUDING solar panel

2 Technology description

The unit shown in Figure 1 converts energy and air into methanol. The electrical energy needed to run the process is delivered by a 300 [W] solar panel. The air contains the feedstocks needed to produce methanol: CO2 and water. After the CO2 and water are filtered from the air the water is fed into an alkaline electrolyzer and is splitted into hydrogen and oxygen. Finally the CO2 and hydrogen are fed into a methanol reactor which converts the feedstock into a mixture of methanol and water. This mixture can be separated by using the concept of a heat pipe to distillate the mixture into a stream of water and high quality methanol. The aim is to design the system so that everything fits on the back of the solar panel.

3 State of the art and research scope

Initially the compressor used by ZEF was a multistage, non-lubricated, CO2-water compressor. Due to challenges in the system lifetime new methods for compressing the CO2 and water had to be researched. ZEF selected a method which employs a separate CO2 and water compressor. This has the advantage that the use of an off the shelf system becomes an option.

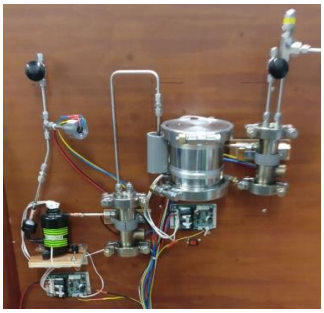

Currently ZEF is building a three stage system using three 250W capacity R134A compressors purchased from Hangzhou Purswave Technology Co., Ltd. Initial tests show promising results.

Oil water separation

One of the drawbacks of the use of the separate CO2 compressor is the fact that the system is oil-lubricated. The CO2 stream contains water and therefore the oil and water will form an emulsion which needs to be separated. This challenge is the topic of this thesis project.

Scope of work

Within this work first a thorough literature study will be done in order to map the different possibilities available for separating oil and water emulsions given the context of the ZEF system. Secondly the available test setup with the three stage compression system will be adjusted such that different oil-water separation systems can be tested. Several experiments will be done in order to show the performance of the different separation systems. Finally there will also be a modelling component which can be used to predict the performance of different systems.

Bibliography

[1] The Joy of Painting with Bob Ross - Season 9, Episode 5: Winter Oval, 1986. URL https://www.youtube.com/watch?v=pYWiLm_-sXw.

[2] Ailo Aasen, Morten Hammer, Geir Skaugen, Jana P. Jakobsen, and Wilhelmsen. Thermodynamic models to accurately describe the PVTxy-behavior of water / carbon dioxide mixtures. *Fluid Phase Equilibria*, 442:125–139, 2017. ISSN 03783812. doi: 10.1016/j.fluid.2017.02.006. URL http://dx.doi.org/10.1016/j.fluid.2017.02.006.

[3] Agile Business Consortium. Chapter 10: MoSCoW Prioritisation, 2014. URL https://www.agilebusiness.org/page/ProjectFramework_10_MoSCoWPrioritisation.

[4] M Alvarado. The changing face of the global methanol market. *IHS Chemical Week*, (March):10–11, 2016. URL http://www.metalbulletin.com/events/download.ashx/document/speaker/8479/a0ID000000ZP1j5MAD/Presentation%5Cnhttp://www.methanol.org/the-methanol-industry/.

[5] Bogdan Ambrożek and Józef Nastaj. Parametric study of pressure–temperature swing adsorption for gas dehumidification on two-layered bed of porous desiccants. *Drying Technology*, 38(1-2): 117–129, 2020. ISSN 15322300. doi: 10.1080/07373937.2019.1623247. URL https://doi.org/10.1080/07373937.2019.1623247.

[6] E.F. August. Ueber die Verdunflungskälte und deren Anwendung auf Hygrometrie. *Annalen der Phsysik*, 1825.

[7] Wilfried J. Bartz. Lubricants and the environment. In *Tribology International*, volume 31, pages 35–47, 1998. doi: 10.1016/S0301-679X(98)00006-1.

[8] A. Beerbower. Estimating the solubility of gases in petroleum and synthetic lubricants. *ASLE Transactions*, 23(4):335–342, 1980. ISSN 05698197. doi: 10.1080/05698198008982977.

[9] A. Beerbower and D. F. Greene. The behavior of lubricating oils in inert gas atmospheres. *ASLE Transactions*, 4(1):87–96, 1961. ISSN 05698197. doi: 10.1080/05698196108972422.

[10] D Daniel Bergmair. *Design of a system for humidity harvesting using water vapor selective membranes*. Number 2015. 2015. ISBN 9789038638171.

[11] A Bhatia and CED Engineering. Compressors and Compressed Air Systems. (877):1–24, 2006.

[12] Henrik Bjurström, Ernest Karawacki, and Bo Carlsson. Thermal conductivity of a microporous medium : moist silica gel. 1984.

[13] Annemiek van Boeijen, Jaap Daalhuizen, and Jelle Zijlstra. *Delft Design Guide*. 2020. ISBN 9788578110796.

[14] Shandil Bosch. Stage ZeroEmissionFuels Q1. *Zero Emission Fuels*, 2020.

[15] Francis B. Brown and John W. Erickson. Centrifugal separator. (19), 1976.

[16] G.W. Brundrett. *Handbook of Dehumidification Technology*. 1987.

[17] bse Engineering. Small scale Methanol Plants a chance for re-industrialisation. (May), 2017.

[18] Richard E. Cantley. The effect of water in lubricating oil on bearing fatigue life. *ASLE Transactions*, 20(3):244–248, 1977. ISSN 05698197. doi: 10.1080/05698197708982838.

[19] Carbon Engineering. Our Technology. URL https://carbonengineering.com/our-technology/.

[20] Munir Cheryan. *Ultrafiltration and Microfiltration*. 1998.

[21] Climate Analytics and New Climate Institute. Climate Action Tracker.

[22] Climeworks. The Climeworks story. URL https://www.climeworks.com/page/story-to-reverse-climate-change.

[23] Frederick Gardner Cottrell. PROCESS FOR SEPARATING AND COLLECTING PARTICLES OF ONE LIQUID SUSPENDED IN ANOTHER LIQUID. 12(522):343, 1911. URL https://patentimages.storage.googleapis.com/16/ab/f3/c4136401575e04/US987114.pdf.

[24] Francesco Dalena, Alessandro Senatore, Alessia Marino, Amalia Gordano, Marco Basile, and Angelo Basile. *Methanol Production and Applications: An Overview*. Elsevier B.V., 2018. ISBN 9780444640109. doi: 10.1016/B978-0-444-63903-5.00001-7. URL http://dx.doi.org/10.1016/B978-0-444-63903-5.00001-7.

[25] Mike Day and Christian Bauer. Water Contamination in Hydraulic and Lube Systems, 2007. URL https://www.machinerylubrication.com/Read/1084/water-contamination-lube.

[26] Design Council. Eleven lessons: managing design in eleven global brands. 2007.

[27] Rebecca Dowling. An experimental and computational study of CO2 absorption in aqueous solutions of tetraethylenepentamine. *Zero Emission Fuels*, 2020.

[28] Tim Dwyer. Rolling-piston rotary refrigerant compressors for air conditioning applications, 2020.

[29] Sherif El-Safty and Nguyen Duc Hoa. Organic–Inorganic Mesoporous Silica Nanotube Hybrid Anodic Alumina Membranes for Ultrafine Filtration of Noble Metal Nanoparticles. *Noble Metals*, (May), 2012. doi: 10.5772/33768.

[30] European Commission. 2030 climate & energy framework. URL https://ec.europa.eu/clima/policies/strategies/2030_en.

[31] FlyCarpet inc. Free Online Interactive Psychrometric Chart, 2020.

[32] Giebel GmbH. Regeneration of silica gel. 49(0):1–5, 2009.

[33] Global Carbon Project. Global Carbon Budget, 2019. URL https://www.globalcarbonproject.org/carbonbudget/index.htm.

[34] Global CCS Institute. Global Status of CCS 2019. 2019.

[35] Carlos Gomez, Juan Caldentey, Shoubo Wang, Luis Gomez, Ram Mohan, and Ovadia Shoham. Oil-Water Separation in Liquid-Liquid Hydrocyclones (LLHC) - Experiment and Modeling. *Proceedings - SPE Annual Technical Conference and Exhibition*, pages 1777–1794, 2001. doi: 10.2523/71538-ms.

[36] Grace Chemical co. Davisil brochure. pages 1–8, 2016.

[37] A.V. Guedes, R.C. Ferreira, F.N. Audenhove, and B.S. Marques. CO2 CORROSION ON NATURAL GAS COMPRESSORS: CRITERIA AND GUIDELINES Andre. *Forty-Second Turbomachinery Symposium*, pages 1–8, 2012. ISSN 1098-6596.

[38] J.M. Gurgel and R.P. Klüppel. Thermal conductivity of hydrated silica-gel. *The Chemical Engineering Journal*, 61, 1995.

[39] Yunrui Han, Limin He, Xiaoming Luo, Yuling Lü, Kaiyue Shi, Jianheng Chen, and Xin Huang. A review of the recent advances in design of corrugated plate packs applied for oil–water separation, 9 2017. ISSN 22345957.

[40] Lance G Hays. Multi-phase separator. (19):2–7, 1978.

[41] Honeywell. Honeywell HumidIcon Digital Humidity/Temperature Sensors HIH6100 Series. 2015. URL http://sensing.honeywell.com/honeywell-sensing-humidicon-hih6100-series-product-sheet-009059-6-en.pdf.

[42] IRENA. *The Power to Change: Solar and Wind Cost Reduction Potential to 2025*. Number June. 2016. ISBN 9789295111974.

[43] N Kharoua, L Khezzar, and H Saadawi. CFD Modelling of a Horizontal Three-Phase Separator: A Population Balance Approach. *American Journal of Fluid Dynamics*, 3(4):101–118, 2013. doi: 10.5923/j.ajfd.20130304.03.

[44] Tom Kleist. Internship report . Compressors for the Zero Emission Fuels. (May), 2020.

[45] A. B. Koltuniewicz, R. W. Field, and T. C. Arnot. Cross-flow and dead-end microfiltration of oily-water emulsion. Part I: Experimental study and analysis of flux decline. *Journal of Membrane Science*, 102(C):193–207, 1995. ISSN 03767388. doi: 10.1016/0376-7388(94)00320-X.

[46] Lawrence S Kubie. The Solubility of O2, CO2 and N2 in mineral oil and the transfer of carbon dioxide from oil to air. 124:65–85, 1927.

[47] Jingquan Li and Yongan Gu. Coalescence of oil-in-water emulsions in fibrous and granular beds. *Separation and Purification Technology*, 42(1):1–13, 2005. ISSN 13835866. doi: 10.1016/j.seppur.2004.05.006.

[48] Xin Mei Liu, G. Q. Lu, Zi Feng Yan, and Jorge Beltramini. Recent Advances in Catalysts for Methanol Synthesis via Hydrogenation of CO and CO2. *Industrial and Engineering Chemistry Research*, 42(25):6518–6530, 2003. ISSN 08885885. doi: 10.1021/ie020979s.

[49] M Scott; S Bell; M Bannister; K Cleaver; D Cridland; F Dadachanji; R Farley; P Greaves; R Harris; R Pragnell; M Wilkin; P Wortley. A guide to the Measurement of Humidity.

[50] W J Massman. A REVIEW OF THE MOLECULAR DIFFUSIVITIES OF H O , CO , CH , CO , O , SO , NH , N O , NO , AND NO IN AIR , O AND N NEAR STP. 32(6), 1998.

[51] Walter Meon, Wolfgang Rommel, and Eckhart Blass. Plate separators for dispersed liquid-liquid systems: hydrodynamic coalescence model. *Chemical Engineering Science*, 48(1):159–168, 1993. ISSN 00092509. doi: 10.1016/0009-2509(93)80292-X.

[52] Methanol Institute and Pieter 't Hart. Major Dutch Maritime Companies Join Green Maritime Methanol Project, 2019. URL https://www.einpresswire.com/article/477078882/major-dutch-maritime-companies-join-green-maritime-methanol-project.

[53] J. W. Miller. Synthetic lubricants and their industrial applications. (1):136–152, 1984. ISSN 0265-6582. doi: 10.1002/jsl.v1:2.

[54] Michael J. Moran, Howard N. Shapiro, Daisie D. Boettner, and Margaret B. Bailey. *Fundamentals of Engineering Thermodynamics*, volume 29. 2014. ISBN 9781118412930. doi: 10.7227/ijmee.29.1.2.

[55] Gijs Mulder. Characterization, Optimization and Design of the Sorbent System for a Continuous Direct Air Capture System. *Zero Emission Fuels*, 2021. ISSN 1098-6596.

[56] NASA Earth Observatory. The Carbon Cycle. 2011. URL https://earthobservatory.nasa.gov/features/CarbonCycle.

[57] J. Nastaj and B. Ambrozek. Modeling of Drying of Gaseous Mixtures in TSA System with Fixed Bed of Solid Desiccants. *Drying Technology*, 30(10):1062–1071, 2012. ISSN 07373937. doi: 10.1080/07373937.2012.685138.

[58] Józef Nastaj and Bogdan Ambrożek. Modeling of Drying of Gases Using Solid Desiccants. *Drying Technology*, 27(12):1344–1352, 2009. ISSN 0737-3937. doi: 10.1080/07373930903383679.

[59] Christine Noïk, Chen Jiaqing, and Christine Dalmazzone. Electrostatic demulsification on crude oil: A state-of-the-art review. *International Oil and Gas Conference and Exhibition in China 2006 - Sustainable Growth for oil and Gas*, 1(1):410–421, 2006. doi: 10.2523/103808-ms.

[60] Edward L. Nugent. BLOOD PHASE SEPARATOR DEVICE. (19), 1983.

[61] Khaled Okiel, Mona El-Sayed, and Mohamed Y. El-Kady. Treatment of oil–water emulsions by adsorption onto activated carbon, bentonite and deposited carbon. *Egyptian Journal of Petroleum*, 20(2):9–15, 6 2011. ISSN 20902468. doi: 10.1016/j.ejpe.2011.06.002.

[62] Illam Park and Kent S. Knaebel. Adsorption breakthrough behavior: Unusual effects and possible causes. *AIChE Journal*, 38(5):660–670, 1992. ISSN 15475905. doi: 10.1002/aic.690380504.

[63] Parker Hannifin Corporation. The Basics of Coalescing. 2004. ISSN 07452624.

[64] Herman Percopo. Reciprocating Compressor 1D Dynamic Simulation with Two-Phase Flow. *Zero Emission Fuels*, 2019.

[65] Ahmad A. Pesaran and Anthony F. Mills. Moisture transport in silica gel packed beds-I. Theoretical study. *International Journal of Heat and Mass Transfer*, 30(6):1051–1060, 1987. ISSN 00179310. doi: 10.1016/0017-9310(87)90035-4.

[66] Ahmad A. Pesaran and Anthony F. Mills. Moisture transport in silica gel packed beds-II. Experimental study. *International Journal of Heat and Mass Transfer*, 30(6):1051–1060, 1987. ISSN 00179310. doi: 10.1016/0017-9310(87)90035-4.

[67] Beldon A. Peters. Three-phase separator patent. (19), 1976.

[68] Louis J Petrovic and George Thodos. MASS TRANSFER IN THE FLOW OF GASES THROUGH PACKED BEDS. 1968.

[69] M. Polanyi. THEORIES OF THE ADSORPTION OF GASES. *Trans. Faraday Soc.*, 28:316–333, 1932.

[70] Hugo Gerardus Polderman. Three-phase Patent. 1(12), 2003.

[71] Project Drawdown. Drawdown Review.

[72] Hangzhou Purswave and Technology Co. ST Series DC Tiny Compressor User Manual.

[73] Maja Radetic, Vesna Ilic, Darinka Radojevic, Robert Miladinovic, Dragan Jocic, and Petar Jovancic. Efficiency of recycled wool-based nonwoven material for the removal of oils from water. *Chemosphere*, 70(3):525–530, 1 2008. ISSN 00456535. doi: 10.1016/j.chemosphere.2007.07.005.

[74] Wolfgang Rommel, Eckhart Blass, and Walter Meon. Plate separators for dispersed liquid-liquid systems: Multiphase flow, droplet coalescence, separation performance and design. *Chemical Engineering Science*, 47(3):555–564, 1992. ISSN 00092509. doi: 10.1016/0009-2509(92)80006-X.

[75] Wolfgang Rommel, Eckhart Blass, and Walter Meon. Plate separators for dispersed liquid-liquid systems: the role of partial coalescence. *Chemical Engineering Science*, 48(10):1735–1743, 1993. ISSN 00092509. doi: 10.1016/0009-2509(93)80343-O.

[76] Royal Dutch Shell. Shell opens solar park at Shell Moerdijk chemicals site in the Netherlands. URL https://www.shell.com/business-customers/chemicals/media-releases/2019-media-releases/shell-moerdijk-solar-farm.html.

[77] Joan M. Schork and James R. Fair. Parametric analysis of thermal regeneration of adsorption beds. *Industrial and Engineering Chemistry Research*, 27(3):457–469, 1988. ISSN 15205045. doi: 10.1021/ie00075a016.

[78] J.D. Seader, Ernest J. Henley, and D. Keith Roper. *Separation Process Principles*. Third edit edition, 2011. ISBN 9780470481837.

[79] Sigma-Aldrich. Particle Size Conversion Table. URL https://www.sigmaaldrich.com/chemistry/stockroom-reagents/learning-center/technical-library/particle-size-conversion.html.

[80] Mrigank Sinha. Direct Air Capture Characterization and Design of a Novel Absorption Process. *Zero Emission Fuels*, 2019.

[81] Solartron. Concentrated Solar Power for Petro Chemical Plants. URL https://www.solartronenergy.com/industry-sectors/petro-chemical-solar-concentrator/.

[82] S. Suni, A. L. Kosunen, M. Hautala, A. Pasila, and M. Romantschuk. Use of a by-product of peat excavation, cotton grass fibre, as a sorbent for oil-spills. *Marine Pollution Bulletin*, 49(11-12): 916–921, 12 2004. ISSN 0025326X. doi: 10.1016/j.marpolbul.2004.06.015.

[83] L Svarovsky. *Hydrocyclones*. Holt technology. Holt, Rinehart and Winston, 1984. ISBN 9780039105624. URL https://books.google.nl/books?id=NlcJQQAACAAJ.

[84] M.N. Syarhirah, A.N. Farhanah, and M.Z. Bahak. Friction and wear of bearing material under water contaminated compressor oil. *Jurnal Tribilogi*, 2015. ISSN 1098-6596.

[85] Telaire. Telaire ChipCap 2 humidity and temperature sensor. (February), 2018.

[86] Gavin Towler and Ray Sinnott. *Chemical Engineering Design: Principles, Practice and Economics of Plant and Process design*. 2013. ISBN 9780080966595. doi: 10.1016/c2017-0-01555-0.

[87] TU Delft E-refinery. e-Refinery initiative launched, 2018. URL https://www.tudelft.nl/en/2018/tu-delft/e-refinery-initiative-launched/.

[88] Jasper Van Baten, Richard Baur, Harry Kooijman, Ross Taylor, and William M. Barrett. Cape Open to Cape Open simulation environment. page https://www.cocosimulator.org/.

[89] Sjoerd Hubertus Jozef Vellinga. THREE-PHASE SEPARATOR AND INSTALLATION FOR BIOLOGICAL PURIFICATION OF EFFLUENT. 2(12), 2004.

[90] Paul Vroegindeweij. Design and implementation of the ZEF 6 continuous direct air capture system. *Zero Emission Fuels*, 2020.

[91] C Vuik, F.J. Vermolen, M.B. van Gijzen, and M.J. Vuik. *Numerical Methods for Ordinary Differential Equations*. Delft Academic Press, 2016.

[92] Yu Wang and M. Douglas LeVan. Adsorption equilibrium of carbon dioxide and water vapor on zeolites 5a and 13X and silica gel: Pure components. *Journal of Chemical and Engineering Data*, 54(10):2839–2844, 2009. ISSN 00219568. doi: 10.1021/je800900a.

[93] Quilitz Warmbrunn and Comp. August psychrometer, 1876.

[94] Stephen D. White, Mark Goldsworthy, Roger Reece, Thorsten Spillmann, Abdullah Gorur, and Dae Young Lee. Characterization of desiccant wheels with alternative materials at low regeneration temperatures. *International Journal of Refrigeration*, 34(8):1786–1791, 2011. ISSN 01407007. doi: 10.1016/j.ijrefrig.2011.06.012. URL http://dx.doi.org/10.1016/j.ijrefrig.2011.06.012.

[95] X. Zheng, T. S. Ge, and R. Z. Wang. Recent progress on desiccant materials for solid desiccant cooling systems. *Energy*, 74(1):280–294, 2014. ISSN 03605442. doi: 10.1016/j.energy.2014.07.027.

[96] Guofeng Zhu, Jong-leng Liow, and Andrew Neely. Compu tational Study of Flow in a Micro-Sized Hydrocyclone. (December), 2010.

[97] Guofeng Zhu, Jong Leng Liow, and Andrew Neely. Computational study of the flow characteristics and separation efficiency in a mini-hydrocyclone. *Chemical Engineering Research and Design*, 90(12):2135–2147, 2012. ISSN 02638762. doi: 10.1016/j.cherd.2012.05.020. URL http://dx.doi.org/10.1016/j.cherd.2012.05.020.


TU Delft


Z E F
ZERO EMISSION FUELS